Modeling host-pathogen interactions using zebrafish and *L. monocytogenes*

by

Simone Shen

A dissertation submitted in partial fulfillment of

the requirements for the degree of

Doctor of Philosophy

(Molecular and Cellular Pharmacology)

at the

UNIVERSITY OF WISCONSIN-MADISON

2024

Date of final oral examination: 07/02/2024

The dissertation is approved by the following members of the Final Oral Committee:

Anna Huttenlocher, Professor, Pediatrics and Medical Microbiology & Immunology

John-Demian Sauer, Associate Professor, Medical Microbiology & Immunology

Mark J. Mandel, Professor, Medical Microbiology & Immunology

Junsu Kang, Assistant Professor, Cell and Regenerative Biology

DISSERTATION ABSTRACT

This dissertation explores the intersection of infection, inflammation, and bacterial virulence mechanisms using innovative models and approaches to address critical challenges in wound healing and combating intracellular bacterial pathogens. Leveraging the optical transparency and high fecundity of zebrafish with the genetic tractability of *Listeria monocytogenes*, we investigated how microbe-induced inflammation influences tissue repair and identified virulence factors critical for infection. In Chapter 2, we focused on how inflammasome activation impacts wound healing utilizing genetically engineered *L. monocytogenes*. I demonstrated that IL-1β, downstream of inflammasome, is detrimental to wound healing and blocking IL-1R signaling improves the healing outcome. I futher highlighted a crucial window of microbial clearance necessary for efficient tissue repair. Although clearance of bacteria by antibiotics can be effective at promoting wound healing, there is a threat of escalating antibiotic-resistant bacteria. Therefore, in Chapter 3, I aimed to understand the bacterial virulence mechanisms to combat the antibiotic resistance crisis. I employed transposon mutagenesis and next generation sequencing (TIS) to perform a genome-wide analysis of *L. monocytogenes* in mouse bone marrow-derived macrophages (BMDMs) and zebrafish and identified genes important for survival under cell-intrinsic immune pressure *ex vivo* and innate immune defense *in vivo*. Taken together, our findings reveal that persistent inflammation, driven by IL-1β, due to infection disrupts wound healing, independent of bacterial load, and underscore the importance of timely bacterial clearance. Additionally, the identification of virulence factors provides novel targets for antibiotic development, offering potential strategies to combat intracellular bacterial infections. These insights highlight the utility of using zebrafish as a model for studying complex host-pathogen interactions and advancing therapeutic development.

ACKNOWLEDGMENTS

I was one of the lucky ones that did not have to go through a fourth rotation before landing in a lab. Too lucky in fact. I really enjoyed two out of my three rotations and could not decide which lab to join. I would like to thank my two wonderful PhD mentors, Dr. Anna Huttenlocher and Dr. JD Sauer, for making my decision easy or allowing me to not have to make the decision by taking me in as a co-mentored student. I feel privileged to say that I've had the best of both worlds. I came with no background in immunology or microbiology, so thank you for taking a chance on me and shaping me into the scientist I am today. Thank you both for your patience and guidance during my PhD.

To Anna: Thank you for your support over the past five years. Your respect in the scientific community is inspiring, and I am grateful to be mentored by you. Thank you also for being a caring mentor. You are like my American mom.

To JD: You have taught me so much. I didn't even know how to properly pronounce *L. monocytogenes* before I rotated in the lab. Your mentorship was invaluable, and your scientific ideas are inspiring. Thank you for challenging me and making me a better scientist.

Besides my PhD mentors, there are so many more people to thank for helping me get to where I am today. I thank my committee members for providing me helpful feedback and advice for my projects. To my labmates, current and former (Julie, Dave, Alex, Gayathri, Nayanna, Mallorie, Zhili, Yiran, Adam, Tanner, Veronika, Ashley, Morgan, Taylor, Kijeong, Kim, Matt, Grace, Delanie): Thank you all for hearing me complain when I have a long experiment day or when my experiments fail. You all have been a huge support during my PhD. Fish people, thanks for taking my feeding or switching feeding with me when I needed it. To Kim: I am so glad that we joined the lab at the same time and hey look now we're graduating at the same time, defending 4 days apart. You made being in the lab so much more fun. Thank you for being an amazing friend and a great writing buddy, I wouldn't be able to finish writing this dissertation without you. To Gayathri: Thank you for being one of my biggest cheerleaders. We've had so

many good memories from our various adventures, whether it's a trip to Java Den, a trip to Mackinac Island, or a trip to the Eras tour. You have definitely become one of my closest friends. I can't imagine getting through graduate school without you.

To my friends from badminton (Miranda, Dimuth, and Anusha especially): Thank you all for keeping me active and sane throughout my PhD. To Miranda: Thank you for getting me back into badminton. You are truly an amazing friend. You've been there through my ups and downs and I really appreciate your company. I will miss you tremendously.

To my godparents, Michael and Li-Fang, and their beautiful and talented daughter, Serena. You guys have become my second family and made Madison feel like home for me. Thank you so much for helping me settle down in Madison and helping me navigate and overcome difficult and challenging situations. I will miss you all!

Finally, to my family: Sorry for not going home as much as you would like. Thank you for being so understanding for me being so far away from home. I really appreciate your constant support not just throughout my PhD but throughout life.

TABLE OF CONTENTS

LIST OF FIGURES

LIST OF TABLES

CHAPTER 1: INTRODUCTION – Innate immune response and systemic damage caused by bacterial infections

Authors and their contributions:

Simone Shen: Planned, organized, and wrote this manuscript.

John-Demian Sauer: Supervised writing and editing of this manuscript.

Infectious disease and the antibiotic resistance crisis

Bacterial pathogens are a major cause of morbidity and mortality worldwide due to diseases ranging from tuberculosis and endocarditis to meningitis and dysentery (Ikuta et al., 2022). Diseases from bacterial infections can arise either from damage to our cells caused by pathogens or hyperactivation of our immune system as a response to pathogens, resulting in problems such as systemic inflammatory response syndrome (SIRS) which could lead to sepsis and death (Doron & Gorbach, 2008). In 1928, the discovery of penicillin started a new era known as the antibiotic revolution (A. Fleming, n.d.). The golden era for antibiotics discovery peaked in the mid-1950s and since then there have been a declined discovery rate for new classes of antibiotics (Adedeji, 2016; Hutchings et al., 2019). In the 20th century, antibiotics shifted the leading cause of death from transmissible diseases to non-transmissible diseases (Adedeji, 2016). However, the antibiotic resistance crisis represents a huge threat to the modern antibiotic era. According to the Centers for Disease Control and Prevention (CDC), in the most recent Antibiotics Resistance (AR) Threats report from 2019, over 2.8 million antimicrobial-resistant infections occur each year in the US, resulting in 35,000 deaths. Compared to the first published AR Threats report in 2013, within just a few years, the number of antimicrobial-resistant infections rose almost 50% from 2 million to 2.8 million (Centers for Disease Control and Prevention (U.S.), 2019). The drastic expansion and emergence of antibiotic-resistant bacteria has become a major public health crisis and highlights the necessity for us to understand the mechanism by which bacterial pathogens cause disease to drive the next generation of novel therapeutic development.

Listeria monocytogenes as a model pathogen for infectious disease

Bacterial pathogens have adapted a variety of virulence factors to facilitate their ability to colonize hosts, evade the immune system, and ultimately cause disease. These virulence factors often have conserved functions across different bacterial species due to their crucial role in pathogenicity. Some examples of common mechanisms of pathogenesis that bacterial utilize include entry into host cells via invasins, cell-to-cell spread via actin-based motility, environmental sensing and response via two-component systems, delivery of effector proteins via secretion systems, and nutrient acquisition via hijacking host metabolites (Wilson et al., 2002; Casadevall & Pirofski, 2009). In this dissertation, I utilized *L. monocytogenes* as a model pathogen to investigate both the mechanism by which pathogens cause disease as well as how infection can cause systemic damage to the host. *L. monocytogenes* was chosen for its tractable genetic systems, well-defined infectious cycle, and well-established infection models (Cossart, 2007).

L. monocytogenes is a zoonotic Gram-positive pathogen that not only survives in the environment as a saprophyte, but can also thrive and disseminate inside the host as an intracellular food-borne pathogen (Allerberger & Wagner, 2010; Freitag et al., 2009). *L. monocytogenes* can cause severe listeriosis, an infection with a high mortality rate of 20% in at-risk populations, including elderly, immunocompromised, and pregnant individuals, leading to deadly septicemia, meningitis, endocarditis, or spontaneous abortion.

L. monocytogenes lifecycle

Decades of research have identified the virulence factors that *L. monocytogenes* utilizes to invade host cells, survive in the host cytosolic environment, and disseminate into neighboring cells. First, *L. monocytogenes* enters professional phagocytes via phagocytosis or employs bacterial surface proteins internalin A (InlA) and internalin B (InlB) to facilitate receptor-mediated endocytosis to enter non-phagocytic cells (Mengaud et al., 1996; Y. Shen et al., 2000). After internalization, *L. monocytogenes* is engulfed in a host vacuole where it utilizes the cholesterol-dependent pore-forming toxin listeriolysin O (LLO) encoded by the gene *hly* to allow its escape into the host cytosol (Schnupf & Portnoy, 2007). Next, ActA promotes actin-based motility, enabling the bacterium's spread to an adjacent cell where it then gets encapsulated in a double-membrane host vacuole and again employs LLO and additional protein phospholipases PlcA and PlcB to promote escape into the cytosol (Brundage et al., 1993; Kocks et al., 1992; Tilney & Portnoy, 1989; G. A. Smith et al., 1995). All the virulence factors mentioned that establish *L. monocytogenes*' lifecycle are transcriptionally modulated by the master regulator PrfA (Chakraborty et al., 1992; Reniere et al., 2015). Following discoveries of these virulence factors in *L. monocytogenes*, similar mechanisms of pathogenesis were identified in other pathogens; such as, *Rickettsia* spp., *Shigella* spp., and *Burkholderia* spp., supporting *L. monocytogenes* as a powerful model organism (Ray et al., 2009).

Despite well-characterizations of these virulence factors, the antibiotic-resistant crisis is still a prominent issue. Identifying novel targets that can be disrupted without harming

human cells is challenging. Other than these well-characterized virulence factors in *L. monocytogenes*, as technologies in comparative genomics and transcriptomic advance, more and more virulence determinants have been revealed (Dussurget, 2008; Fischer et al., 2022a). *L. monocytogenes* requires these other virulence determinants to regulate oxidative stress, acquire nutrients, evade host immune response, and ultimately cause disease in the hostile host environment. For example, to protect against oxidative stress, the Fur family regulators are employed to modulate the expression of genes involved in reactive oxygen species defense (Rea et al., 2004; Rea et al., 2005; Dussurget, 2008). To acquire nutrients and facilitate multiplication, transporters are important for auxotrophs uptakes and genes involved in certain nucleotide and amino acid biosynthesis pathways are also indispensable (Stritzker et al., 2004; Schauer et al., 2010; Faith et al., 2012). To avoid detection by the host's immune system, *L. monocytogenes* modifies its pathogen-associated molecular pattern by deacetylating the N-acetylglucosamine residues on its cell wall peptidoglycan (Boneca et al., 2007). These are just examples of a few strategies that *L. monocytogenes* utilizes to contribute to its pathogenesis. To combat the antibiotic-resistant crisis, a more comprehensive understanding of how pathogens infect the host is needed. The focus of **Chapter 3** is to discover other unknown virulence determinants employed by *L. monocytogenes* through an unbiased comprehensive whole-genome-based approach to provide implications in potential antibiotic targets.

Innate immune responses induced by L. monocytogenes infections

While bacterial pathogens have adapted approaches to colonize and cause disease in the host, the host's immune system has also evolved methods to detect and defend against the bacteria. Inflammatory responses are triggered by bacteria through the activation of varying innate immune pathways in the host. *L. monocytogenes* stimulates nucleotide-binding oligomerization domain (NOD), MyD88-dependent, STING/IRF3-dependent, and caspase-1-dependent innate immune pathways (Witte et al., 2012). First, upon *L. monocytogenes* infection, Toll-like receptors (TLRs) localized to the host cell surface and vacuolar compartments, including TLR2 and TLR5, recognize *L. monocytogenes* lipoteichoic acid, lipoproteins, peptidoglycan, and flagellin, leading to downstream cascade activating MyD88 signaling (Hayashi et al., 2001; Torres et al., 2004). MyD88-dependent signaling leads to upregulation of inflammatory cytokines which plays an important role in host defense (Edelson & Unanue, 2002; Way et al., 2003). After *L. monocytogene*s' escape into the cytosol, the nucleotide-binding oligomerization domain (NOD) proteins detect *L. monocytogenes* cell wall peptidoglycan (D'Orazio, 2019). *L. monocytogenes* can evade activation of NOD1 through deacetylation of N-acetylglucosamine residues on peptidoglycan. However, NOD2 is still able to sense the cell wall fragments of *L. monocytogenes*, leading to NF-κB signaling and increased production of proinflammatory cytokines (Kobayashi et al., 2005). Inflammasome signaling is another cytosolic innate immune pathway triggered by *L. monocytogenes*, leading to caspase-1-dependent signaling. *L. monocytogenes* stimulates inflammasome signaling through Nlrp3, Nlrc4, and AIM2, which further activates IL-1β and IL-18 and leads to pyroptotic cell death (Kim et al., 2010; Warren et al., 2008; Sauer et al., 2010). Cytosolic STING/IRF3 signaling is also activated by *L.*

monocytogenes through secreted cyclic diadenosine monophosphate (c-di-AMP), resulting in robust IFN-β expression (Woodward et al., 2010; Sauer, Sotelo-Troha, et al., 2011; Barber, 2011). When these immune pathways are hyperactivated by infections, this could result in hyper-inflammation and potentially lead to systemic damage. For example, hyperactivation of the immune system by SARS-CoV-2 infection could lead to cytokine storms, causing organ failures even after the infection is cleared (Fajgenbaum & June, 2020). In **Chapter 2**, I focus on how inflammation caused by infection might be detrimental in the context of wound healing.

Zebrafish as a model system for studying infection and host response

The zebrafish has been a vital model organism in biomedical research for the last three decades due to its high fecundity, rapid development, and genetic tractability (Teame et al., 2019). Importantly, the zebrafish innate immune system is conserved compared to humans with >70% of human genes having at least one orthologue in zebrafish (Howe et al., 2013; Torraca & Mostowy, 2018). Moreover, all cell types of the human immune system have zebrafish equivalents (Meeker & Trede, 2008). Uniquely, the adaptive immune system in zebrafish is not fully formed until 4 weeks post-fertilization, and with its conserved innate immune system compared to humans, the zebrafish is a powerful animal model for studying innate immune responses to microbial infections *in vivo* (Lam et al., 2004).

Most innate immune signaling pathways are conserved in humans and zebrafish. Orthologs of mammalian TLRs have been found in zebrafish with additional zebrafish

specific TLRs due to the genome duplication event in the teleost lineage (Stein et al., 2007; Van Der Vaart et al., 2012). Homologs of adaptor proteins and transcription factors downstream of TLRs, such as MyD88 and NF-κB, have also been identified in zebrafish (Van Der Vaart et al., 2012). Canonical members of the Nod-like receptor (NLR) family, including NOD1, NOD2, and Nlrc3 are also conserved between humans and zebrafish (Van Der Vaart et al., 2012). However, most human NLRs associated with inflammasomes do not have a one-to-one ortholog in zebrafish. Despite the divergence in NLR-family sensors, downstream adaptors and pro-inflammatory caspases in inflammasome signaling have functional homologs in zebrafish (Forn-Cuní et al., 2019). Orthologues of the interferon response factors (IRFs), the signal transducers and activators of transcription (Stat2, Stat3, Stat4, and Stat6), and Tumor necrosis factor receptor-associated factors (TRAFs) have also been identified in zebrafish (Stein et al., 2007). However, many other components of the zebrafish immune system still require further investigation and characterization.

The availability of genetic tools in the zebrafish model, such as transcription activator-like effector nucleases (TALENs), CRISPR/Cas9, and morpholino oligonucleotides (MOs), enables mechanistic explorations of host-pathogen interactions (Varshney et al., 2015). Another unique advantage of zebrafish is that they are optically transparent during the larval stage and the availability of transgenic lines expressing fluorescent proteins in phagocytes allows for visualization of immune cell responses to pathogens in real-time (Gomes & Mostowy, 2020). Zebrafish has been used to model and investigate many various human infections, such as *Shigella flexneri*, *Mycobacterium tuberculosis*,

Burkholderia cepacian, *Pseudomonas aeruginosa*, and *Staphylococcus aureus*, which has provided a better understanding of microbial virulence mechanisms (Gomes & Mostowy, 2020; Torraca & Mostowy, 2018). In fact, zebrafish was one of the first animal models used to investigate bacterial autophagy (Gomes & Mostowy, 2020). Using imaging techniques, interactions between bacteria and host phagocytes can be observed *in vivo* in larval zebrafish and this led to the discovery that p62, a selective autophagy receptor that interacts with ubiquitin, is important for controlling *S. flexneri* infection (Mostowy et al., 2013). Utilizing the zebrafish model, other immune responses and processes have also been captured through live imaging; such as retrograde chemotaxis causing neutrophil reverse migration as a mechanism for inflammation resolution at the wound (Mathias et al., 2006). This phenomenon was not observed or described in mice until a decade later due to intra-vital imagining being challenging in mice (J. Wang et al., 2017). These examples highlight the valuable system zebrafish provide as a model organism.

In this dissertation, I utilized zebrafish as a model organism to understand the interactions between *L. monocytogenes* and the host's innate immune system. Specifically, in **Chapter 2**, I studied how the host's immune response to *L. monocytogenes* impacts the outcome of wound healing. Furthermore, in **Chapter 3**, I combined *ex vivo* infection models in macrophages with *in vivo* zebrafish models of infection to discover novel virulence determinants employed by *L. monocytogenes* to colonize and infect a host.

Wound healing

One of the primary functions of an intact skin is to protect from microorganisms. Without the skin barrier, the wound environment is conducive to microbial colonization and proliferation. When wounds are infected with microbes, this could lead to disruption in the healing process. Wound healing is a highly regulated and programmed process consisting of four overlapping phases: hemostasis, inflammation, proliferation, and remodeling (Guo & DiPietro, 2010). Hemostasis is the immediate response to injury, characterized by the constriction blood vessels to minimize bleeding, and the formation of a clot by platelets to seal the wound. This stage quickly transitions to inflammation, which lasts for a few days. Inflammation involves the migration of immune cells, specifically neutrophils and macrophages, to the site of the wound in order to combat infection and remove any debris. The proliferation or granulation phase follows inflammation and often lasts from a few days to many weeks. During this phase, new tissue forms as fibroblasts produce collagen and extracellular matrix, and angiogenesis occurs. An essential aspect of this stage is re-epithelialization, where epithelial cells migrate across the wound surface to restore the integrity of the skin. The healing then proceeds to the final stage, remodeling, which can last from weeks to years. During this final phase, the collagen fibers are reorganized, allowing the tissue to remodel and mature (Cañedo-Dorantes & Cañedo-Ayala, 2019; Naomi et al., 2021).

Zebrafish share similar wound healing features compared to humans except the healing phases happen in a different order and a faster manner. Upon injury, re-epithelialization is the first stage which occurs rapidly and lasts within hours. After the wound is sealed,

inflammation takes place where neutrophils and macrophages are recruited. Then neovascularization happens, collagen is deposited below the re-epithelialized site, and granulation tissue is formed. Finally, collagen reorganization and tissue regeneration complete the wound repair process (LeBert et al., 2018; Richardson, 2018; Naomi et al., 2021). While in mammals, the wound healing phases overlap one another, in zebrafish, each of the healing phases occurs sequentially, which enables us to study each healing process in isolation (Grada et al., 2018; Richardson, 2018). Additionally, optical transparency in larval zebrafish allows us to visualize the dynamics of immune cells and epithelial cells following injury, making it a powerful model for studying the wound repair processes.

It is important to understand the processes of wound healing since retrospective studies of Medicare found that from 2014 to 2019, over the 5 years, the number of Medicare beneficiaries affected by wounds rose from 8.2 million to 10.5 million (Carter et al., 2023). Wounds can be complicated to treat due to many factors, both local and systemic. Local factors; such as infections and oxygenation, can inhibit wound healing by directly affecting the characteristics of the wound itself. Whereas, systemic factors are the overall health or disease status of an individual, including age and metabolic disorders like diabetes (Guo & DiPietro, 2010). Surgical site infections (SSIs) contribute to a huge portion of the clinical and financial burden in wound care and treatment. According to the CDC healthcare-associated infection (HAI) prevalence survey, it was estimated that SSIs cost $3.3 billion annually. Infections also often affect diabetic wounds and increase the risk of the wounds becoming chronic (Dasari et al., 2021). A

better understanding of how microbes perturb the healing process is important for providing implications in therapeutic strategies for SSIs and infection-associated non-healing wounds.

Bacterial interference in wound healing

Our understanding of the impact of bacterial infections on wound healing has drastically progressed throughout the years. Hippocrates, the famous Greek physician of the fifth century BC wrote ‘if the pus is white, and not offensive, health will follow’. This belief led to the concept that pus, which builds up when an injury is infected, was beneficial for the repair process (Freiberg, 2017). Theodoric Bourgognoni was the first to challenge this theory in the 13th century and advocated the prevention of pus formation in wounds (Caldwell, 2020; Freiberg, 2017). Nevertheless, it was not until the 19th century that the discoveries made by Ignaz Semmelweis, Louis Pasteur, and Joseph Lister about germ theory and antiseptic techniques came into prominence (Alexander, 1985). It has been known for centuries that bacterial infections impair wound healing; however, even to this day, SSIs remain a major issue and a great financial burden in the healthcare system. A better understanding of how bacteria inhibit wound healing is necessary to relieve this clinical and financial burden from SSIs.

Microbial bioburden has been shown to predict healing outcomes of venous leg ulcers and diabetic wounds with the presence of a high bacterial load associated with non-healing wounds (Armstrong et al., 2023; Tuttle, 2015). Many other factors contribute to the healing outcomes of bacterial-infected wounds. For example, microbial virulence

factors involved in biofilm formation and toxins secretion can affect the susceptibility of antibiotic treatment and result in tissue damage at the wound, respectively (Orazi & O'Toole, 2019; Ovington, 2003; Shumba et al., 2019). Polymicrobial interactions also affect the healing outcome as microbial interactions can be synergistic, enhancing the colonization and pathogenesis of the microbes (Alves et al., 2018). Competition between interspecies can also impact healing, where one microbial species produces factors that make cells more susceptible to damage (Uberoi et al., 2024). Furthermore, the complex relationship between microbes and the wound microenvironment also greatly impacts the healing process (Uberoi et al., 2024). For instance, bacterial infections prolong the inflammation phase of wound healing, which is a highly regulated process. During the inflammation phase, damage-associated molecular patterns (DAMPs) are detected by pattern recognition receptors (PRRs), which then promote the recruitment of leukocytes to the wound site (Caldwell, 2020). Macrophages play an important role in wound healing. Pro-inflammatory M1 macrophages were first recruited to the wound to prevent infections (Miskolci et al., 2019). As healing progresses, to transition into the next phase of wound repair, anti-inflammatory M2 macrophages are required for inflammation resolution at the wound (Caldwell, 2020; Hesketh et al., 2017; Miskolci et al., 2019). When wounds are infected by bacteria, pathogen-associated molecular patterns (PAMPs) also activate the innate immune system, causing dysregulation in the inflammation phase of wound healing. Non-resolving inflammation triggered by pathogens could lead to chronic or non-healing wounds. However, how bacterial-derived inflammation impacts wound healing is not very well understood. In

Chapter 2, we further delve into the interplay between bacterial pathogens and the host immune response and its impact on wound healing.

Genome-wide approaches to virulence factor identification

Current treatment for bacterial-infected wounds focuses on reducing microbial load through antibiotic and antiseptic therapy (Hurlow & Bowler, 2022; Liu et al., 2022; X. Ding et al., 2022). However, it is important to note that approximately ~70% of wound-associated bacteria are resistant to at least one of the commonly used antibiotics (X. Ding et al., 2022). To combat the antibiotic resistance crisis and facilitate wound repair, there is a need to understand the mechanism by which bacteria inhibit wound healing. A better interpretation of how bacteria alter our immune response in the wound microenvironment could provide implications for therapeutic strategies for microbial-infected wounds. Additionally, a more comprehensive understanding of virulence determinants in bacteria is critical for developing novel antibiotics to facilitate the clearance of antibiotic-resistant bacteria from wounds.

To identify virulence determinants employed by bacteria, genome-wide genetic screens are powerful and helpful tools. The history of bacterial genetic screens has evolved drastically over the past few decades, owing to advancements in molecular biology, genetics, and computational technologies. Conventional genetic screens for identifying virulence determinants typically involved inducing mutations using chemical or physical agents, followed by in vitro phenotypic screening on a gene-by-gene basis, which could be laborious and time-consuming. In the 1990s, transposon mutagenesis revolutionized

genetic screening by enabling the random insertion of transposons into the bacterial genome, resulting in the disruption of genes and the generation of a library of mutants. The advent of signature-tagged mutagenesis (STM) in 1995, which entailed tagging different mutants with unique DNA sequences and monitoring their existence in a host after infection, allowed for the first time to conduct comprehensive and unbiased screenings for bacterial virulence determinants on a genome-wide scale *in vivo* (Hensel et al., 1995). However, STM approach is limited by the small size of mutant pools that can be tested in a screen. In 2001, a new genome-wide screening technique, transposon site hybridization (TraSH), was developed (Sassetti et al., 2001). TraSH utilizes microarray hybridization for clone detection and mutant mapping. One limitation of TraSH is that the resolution and sensitivity of the microarray can affect the identification of transposon insertions. Low sensitivity could fail to detect insertions, while poor resolution may not be able to differentiate between closely located insertion sites. Further advancements in DNA sequencing technologies led to the development of modern transposon-insertion sequencing (TIS) approaches, such as transposon sequencing (Tn-seq), transposon-directed insertion-site sequencing (TraDIS), insertion sequencing (INSeq), and high-throughput insertion tracking by deep sequencing (HITS), which allowed for high-throughput identification of transposon insertion sites (Cain et al., 2020).

Despite advances in clonal detection in technology, a challenge for performing TIS screens *in vivo* is the presence of narrow biological bottlenecks in an animal host (Chao et al., 2016). Under selective growth conditions, only mutants with reduced survival

should theoretically decrease in frequency. Nevertheless, transposon insertion mutants may be eliminated during selective growth as a result of fitness-independent stochastic events caused by bottlenecks. In an animal model, often only a small fraction of an inoculum can withstand the host barriers and effectively colonize a host (Barnes et al., 2006; Kaiser et al., 2013; Abel et al., 2015). The objective of TIS screens is to identify mutants whose representation in a population changes in response to selection pressure, but bottlenecks in *in vivo* infections can obscure these changes (Chao et al., 2016). Utilizing zebrafish as an *in vivo* animal model allows us to overcome this constraint by taking advantage of its high fecundity, cheap cost, and high-throughput infection method. We can easily increase the sample size, or the number of zebrafish, used in a TIS experiment to screen more transposon insertion mutants. In **Chapter 3**, I carried out TIS screens using a murine macrophage *ex vivo* infection model and a zebrafish *in vivo* infection model to identify genes in *L. monocytogenes* that are crucial for defending against cell-intrinsic immune response and *in vivo* intact immune response, respectively. Additionally, I identified *L. monocytogenes* genes important specifically for cell-intrinsic inflammasome defense using caspase-1 deficient murine macrophages. The identification of these genes has enhanced our understanding of the mechanisms by which pathogens cause diseases.

Altogether, this dissertation highlights the utility of employing zebrafish and *L. monocytogenes* as model organisms, which have allowed us to tease apart the intricate relationships between host and pathogen. Utilizing these models, we have gained a more comprehensive understanding of the host's immune responses to bacterial

infections and how these immune responses modify the milieu of a wound, ultimately affecting the process of wound healing. Additionally, identifications of virulence determinants in *L. monocytogenes* uncovered prospective targets that may be incorporated into antibiotic design and development. Targeting these virulence mechanisms has the potential to effectively eliminate bacteria and promote wound healing.

CHAPTER 2 – Infection-induced inflammation impairs wound healing through IL-1β signaling.

Authors and their contributions:

Simone Shen: Planned, designed, and conducted all experiments. Organized data and wrote this manuscript.

Veronika Miskolci: Assisted with statistical analysis and editing of this manuscript.

Colin N. Dewey: Analyzed transcriptomic data in Figure 2.2.

John-Demian Sauer: Supervised all research and contributed intellectually to the design of the experiments, edited this manuscript.

Anna Huttenlocher: Supervised all research and contributed intellectually to the design of the experiments, edited this manuscript.

This chapter was published in the following journal article:

Shen, S., Miskolci, V., Dewey, C.N., Sauer, J.D., Huttenlocher, A. (2024)

"Infection induced inflammation impairs wound healing through IL-1β signaling."

iScience

Abstract

Wound healing is impaired by infection; however, how microbe-induced inflammation modulates tissue repair remains unclear. We took advantage of the optical transparency of zebrafish and a genetically tractable microbe, *Listeria monocytogenes*, to probe the role of infection and inflammation in wound healing. Infection with bacteria engineered to activate the inflammasome, Lm-Pyro, induced persistent inflammation and impaired healing despite low bacterial burden. Inflammatory infections induced *il1b* expression and blocking IL-1R signaling partially rescued wound healing in the presence of persistent infection. We found a critical window of microbial clearance necessary to limit persistent inflammation and enable efficient wound repair. Taken together, our findings suggest that the dynamics of microbe-induced tissue inflammation impacts repair in complex tissue damage independent of bacterial load, with a critical early window for efficient tissue repair.

Graphical Abstract

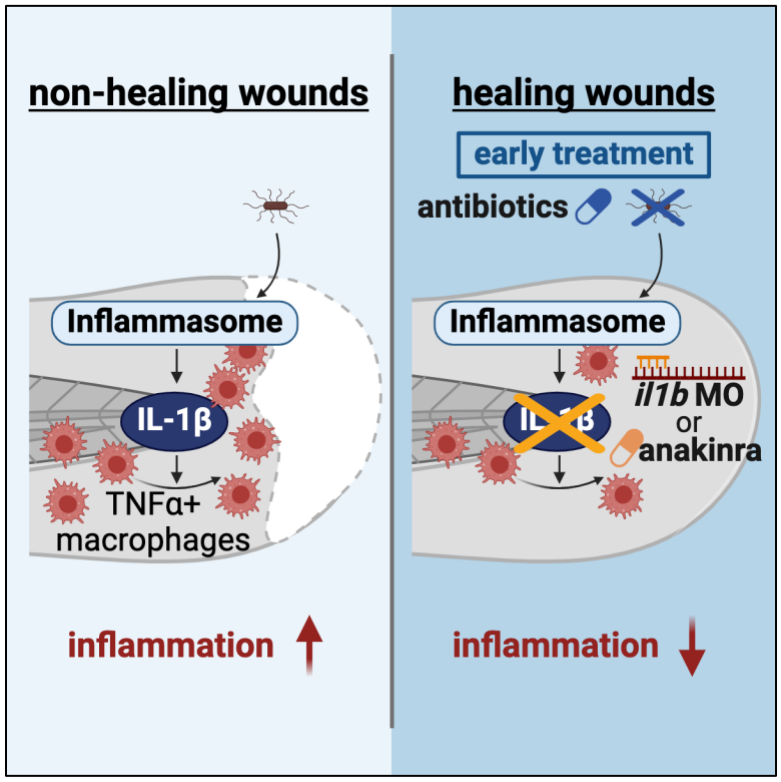

INTRODUCTION

Microbial infection is a common complication and leading cause of chronic non-healing wounds (Bessa et al., 2015; Leaper et al., 2015). Inflammatory responses are critical for pathogen detection and clearance, but when excessive or prolonged can also interfere with wound healing (Miskolci et al., 2019; Zhao et al., 2016). However, how immune responses triggered by microbes can impair wound healing remains unclear.

Caudal fin transection of larval zebrafish provides a powerful *in vivo* model to understand immune responses during infection and wound repair. When larval zebrafish transected wounds are infected with *Listeria monocytogenes* (*Lm*), there is an increase in neutrophil and macrophage infiltration at wounds compared to a sterile wound, and wound healing is impaired (Miskolci et al., 2019). In contrast, when transected wounds are infected with a Δ*hly* mutant, a *Lm* mutant unable to escape from the phagosome to the host cytosol due to loss of the gene encoding listeriolysin-O (LLO) (Jones & Portnoy, 1994), there is no defect in wound healing (Miskolci et al., 2019). Infection by Δ*hly* mutants is also associated with less inflammation and bacterial load at the wound site compared to wild-type (WT) *Lm* infection (Miskolci et al., 2019). This led us to hypothesize that infection-induced inflammation may drive the defect in wound healing in this model.

Lm stimulates inflammation through multiple pattern recognition receptors (PRRs), including toll-like receptor (TLR), stimulator of interferon genes (STING), and nucleotide oligomerization domain (NOD)-like receptors (NLRs) (Flo et al., 2000; Woodward et al.,

2010; Özören et al., 2006; Mariathasan et al., 2006; Meixenberger et al., 2010). Multiple NLRs, including NLRP3, and NLRC4 are induced by *Lm* (Mariathasan et al., 2006; Meixenberger et al., 2010; Sauer, Pereyre, et al., 2011). These NLRs, as well as AIM2 triggered by *Lm* DNA, form inflammasome complexes that activate caspase-1 (Sauer et al., 2010; Warren et al., 2008; J. Wu et al., 2010). Caspase-1 activation subsequently cleaves and activates IL-1β. A previous study from our group showed that Lm-Pyro, a *Lm* strain engineered to hyperactivate the inflammasome triggers robust inflammation and is attenuated in zebrafish (Vincent et al., 2016).

In this study, we demonstrate that inflammation associated with infection impairs wound healing of larval zebrafish. When transection wounds were infected with Lm-Pyro that triggers extensive inflammation through hyperactivation of the inflammasome, wound healing was impaired although there was an attenuation in bacteria virulence. Furthermore, RNA-seq identified an inflammatory profile, with increased expression of *il1b*. We utilized genetic and pharmacological approaches to demonstrate that IL-1β stimulated by *Lm* infection inhibits wound healing. Finally, we found that early eradication of infection is critical to prevent non-resolving inflammation and impaired wound healing. Taken together, our data establish that persistent inflammation associated with bacterial infection inhibits wound healing and that the use of clinically approved IL-1R antagonists, or early antibiotic intervention, can improve healing outcomes of infected wounds in zebrafish larvae.

Material and Methods

STAR Methods

RESOURCE AVAILABILITY

Data and code availability

Single-cell RNA-seq data have been deposited at GEO and are publicly available as of the date of publication. Accession numbers are listed in Table S2.2. Microscopy data reported in this paper will be shared by the lead contact upon request.

Experimental Model and Study Participant Details

Zebrafish Husbandry and Handling

All protocols using zebrafish in this study has been approved by the University of Wisconsin-Madison Research Animals Resource Center (protocol M005405-A02). Adult zebrafish were maintained on a 14 hr:10 hr light/dark schedule. Upon fertilization, embryos were transferred into E3 medium (4.96 µM NaCl, 0.18 µM KCl, 0.33 µM $CaCl_2$*$2H_2O$, 0.4 µM $MgCl_2$*$6H_2O$, 0.1% methylene blue) and maintained at 28.5°C. For wounding assays, 3 days post-fertilization (dpf) larvae were anesthetized in E3 medium containing 0.2 mg/mL Tricaine (ethyl 3-aminobenzoate; Sigma-Aldrich). Zebrafish strains utilized in this study are listed in Table S2.2. Larval zebrafish were used for all studies when sex cannot be determined.

Bacterial Strains

Listeria monocytogenes strain 10403S was used in this study. Strains used in this study are listed in Table S2.2.

METHOD DETAILS

Zebrafish wounding and infection

To prepare bacteria for wound infection, a streak plate from *L. monocytogenes* strain 10403S frozen stock was grown at 37°C. A fresh colony was picked and grown statically in 1 mL brain–heart infusion (BHI) medium (Becton, Dickinson and Company, Sparks, MD) overnight at 30°C to reach stationary phase. Bacteria were sub-cultured for ~1.5-2 hr in fresh BHI (4:1, BHI:overnight culture) to achieve growth to mid-logarithmic phase (OD600 ≈ 0.6–0.8). 1 mL of the mid-logarithmic phase bacterial culture were spun down and washed three times in sterile phosphate buffered saline (PBS) and resuspended in 100 µL of PBS. To infect and wound, zebrafish larvae were placed in 5 mL E3 medium containing Tricaine with 100 µL bacterial resuspension and caudal fins of larvae were transected using surgical blade (Feather no. 10) at the tip of the notochord without injury to the notochord. For controls, uninfected wounds, 100 µL sterile PBS was added in the medium instead of bacterial resuspension. After caudal fin transection, larvae were transferred to new tissue culture treated dishes and incubated for 1 hr on a horizontal orbital shaker at gentle speed (75-100 rpm). Larvae were then rinsed with E3 medium and maintained at 28.5°C until fixed or CFU plating at indicated time points as described.

Fixation

Zebrafish larvae were fixed in 1.5% formaldehyde (Polysciences, Wrrington, PA) containing 0.1 M Pipes (Sigma-Aldrich), 1.0 mM $MgSO_4$ (Sigma-Aldrich) and 2 mM

EGTA (Sigma-Aldrich) at 4°C overnight. Samples were washed with PBS and stored in PBS at 4°C until imaging.

Tissue regrowth area measurement

Fixed larvae at indicated timepoints were placed in Ibidi chamber in 0.1% Tween-20-PBS solution. A single-plane brightfield image is acquired using Zeiss Zoomscope (EMS3/SyCoP3; Zeiss, Oberkochen, Germany; Plan-NeoFluar Z objective; 112X magnification (0.7 μm resolution, 2.1 mm field of view, 9 μm depth of field) and Zen software (Zeiss). Tissue regrowth area was measured using FIJI using the polygon tool by outlining the tail fin tissue area distal to the notochord.

NF-κB quantification

Tg (NFκB:EGFP) zebrafish larvae were fixed at indicated timepoints post wounding. Fixed larvae were placed in Ibidi chamber in 0.1% Tween-20-PBS solution and 5-micron step z-stack images were collected using spinning disk confocal microscope (CSU-X, Yokogawa, Sugar Land, TX) with a confocal scanhead on a Zeiss Observer Z.1 inverted microscope, a Photometrics Evolve EMCCD camera and Zen Software (Zeiss). To quantify NF-κB signal, collected images were analyzed using FIJI (Schindelin et al., 2012). Sum-projections of the z-stacks were generated and the integrated density of NF-κB GFP signal was quantified in the caudal fin tissue extending from the caudal vein loop to the wound edge excluding the notochord using polygon tool. To adjust for background variation in each larva, a 48.7 x 48.7 micron box was drawn using the rectangle tool in FIJI and placed in region without NF-κB signal to measure integrated

density within the box. Background integrated density was then subtracted. To account for differences in tail fin area, NF-κB index was calculated by normalizing NF-κB integrated density to regrowth area in each zebrafish.

Macrophage and TNFα expression quantification

Double transgenic lines (*Tg(tnfa:GFP) x Tg(mpeg1:mCherry-CAAX)* larvae were fixed at indicated timepoints post wounding. Fixed samples were placed in Ibidi chamber in 0.1% Tween-20-PBS solution and 5-micron step z-stack images were collected using spinning disk confocal microscope (CSU-X, Yokogawa, Sugar Land, TX) with a confocal scanhead on a Zeiss Observer Z.1 inverted microscope, a Photometrics Evolve EMCCD camera and Zen Software (Zeiss). Macrophage recruitment and TNFα expression in macrophages were quantified in the caudal fin tissue area distal to the caudal vein loop by area thresholding of fluorescence intensity using Fiji, as previously (Miskolci et al., 2019). Polygon tool was used to outline the area of measurement in the brightfield image of caudal fin and the outlined area was then copied onto the sum z-projection of the z-stack from the corresponding macrophage (mCherry) channel. Macrophage within the outlined area was measured after thresholding fluorescence intensity and the measured macrophage area was outlined using region of interest (ROI) manager and copied onto the sum z-projection of the z-stack from the corresponding TNFα channel. To measure TNFα within the outlined macrophage area, the ROI were copied onto the sum z-projection of the z-stack from the corresponding GFP channel and fluorescence intensity was thresholded. Percentage of macrophage area colocalized with TNFα was calculated. To account for differences in tail fin area,

TNFα index was then computed by normalizing the percentage of TNFα+ macrophage to regrowth area in each zebrafish.

Bacterial burden quantification

To determine bacterial CFU counts, 10 zebrafish larvae were pooled from each treatment and each timepoint into 1.5 ml microcentrifuge tubes with 150 μl of 1x PBS. Pooled larvae were then homogenized using a mini bead beater for 15 seconds. Homogenates were subsequently serial diluted and plated on BHI agar containing 200 μg/mL streptomycin. Bacterial plates were incubated overnight at 37°C and CFUs were counted. To quantify bacterial burden using microscopy, mCherry-expressing WT *Lm* or Lm-Pyro were used, and infected larvae are fixed at indicated timepoints. Fixed samples were placed in Ibidi chamber in 0.1% Tween-20-PBS solution and 5-micron step z-stack images were collected using spinning disk confocal microscope (CSU-X, Yokogawa, Sugar Land, TX) with a confocal scanhead on a Zeiss Observer Z.1 inverted microscope, a Photometrics Evolve EMCCD camera and Zen Software (Zeiss). Fluorescent area of *Lm* at the tail fins was measured using area thresholding in FIJI.

RNA Sequencing

At 24 hpw, tail fins of 50 larvae were pooled and collected in ice cold PBS for each condition in each biological replicate. RNA was extracted from pooled tail fins using TRIzol reagent and RNAqueous Micro Kit (Invitrogen). Extracted RNA was submitted to GENEWIZ™ for library preparation and sequencing. The pooled RNA libraries were sequenced on an Illumina HiSeq to obtain 150-bp paired-end reads.

RNA sequencing analysis

RNA-seq reads were aligned to zebrafish reference genome GRCz11 using STAR v2.7.8a (Dobin et al., 2013) and the Ensembl release 95 transcript annotation. Default values were used for all STAR parameters except for outFilterMismatchNoverLmax (0.1), outFilterScoreMinOverLread (0.33), and outFilterMatchNminOverLread (0.33), following the standardized pipeline established for the GTEx project (GTEx Consortium, 2017). Transcript abundance was quantified from the resulting alignments using RSEM v1.3.3 (B. Li & Dewey, 2011) and differential expression between conditions was assessed using DESeq2 v1.32.0. (Love et al., 2014).

RT-qPCR

At specified time points (1 dpw, 3 dpw, or 5 dpw), tail fins of 18 to 23 larvae were pooled and collected in ice cold PBS for each condition in each biological replicate. RNA was extracted from pooled tail fins using TRIzol reagent and RNAqueous Micro Kit (Invitrogen). cDNA was then synthesized using SuperScript III RT and oligo-dT (Invitrogen). Using cDNA as a template, quantitative PCR (qPCR) was performed using FastStart Essential DNA (Roche) and a LightCycler96 (Roche). Fold changes in *il1b* expression over unwound control condition at 1dpw, normalized to *b-actin* were calculated from Cq values. Primers used for amplifying *il1b* and *b-actin* are listed in the Table S2.2.

Morpholino injections

Morpholino oligonucleotides targeting splice sites between intron 2 and exon 3 of *il1b* were obtained from Gene Tools, OR (López-Muñoz et al., 2011). The second intron of *il1b* is retained causing a frame shift resulting in a premature stop codon. 3nL of 350μM *il1b* antisense oligonucleotides or std MO were injected into one-cell stage embryos. To test for morpholino knockdown efficiency, RNA from std MO or *il1b* MO injected larvae was extracted using RNeasy Mini Kit (Qiagen) and RT-PCR was performed using OneStep RT-PCR Kit (Qiagen) with primers listed in Table S2.2.

Drug treatment

For anakinra experiments, the zebrafish embryos were dechorionated at 1 dpf and E3 medium without methylene blue (E3-) was supplemented with 10 μM anakinra (Kineret) and refreshed daily. For experiments depleting *Lm* infections, zebrafish E3- medium was supplemented with ampicillin (45 mg/ml, Fisher) and refreshed daily starting from 1 dpw, 2 dpw, or 3 dpw as indicated.

Quantification and Statistical Analysis

All experiments in the main figures in this study consist of at least three biological replicates and each biological replicate is defined as a separate clutch of larvae spawned on different days. All data were graphed using Prism (GraphPad Software, Inc, San Diego, CA) with statistical analysis performed using SAS/STAT 9.4 (SAS Institute Inc, Cary, NC). SAS proc mixed procedure was used for variance analysis to account for the variation due to fixed effects and random effects from samples, as previously (Miskolci et al., 2022). If the normality assumptions of errors failed, a non-

parametric analysis was performed using the ranks. When rank analysis was performed, it is indicated in the figure legends. For RNA sequencing analysis, statistical testing for differential expression between each treatment group was performed using the Wald test implemented in the DESeq2 package and genes with a Benjamini–Hochberg corrected P value (FDR) ≤ 0.05 were considered statistically significant (Love et al., 2014). For RT-qPCRs, reactions were performed in three technical replicates and two-way ANOVA (Prism) was used to determine statistical significance by comparing the calculated ΔCq derived from subtraction of cycle numbers for gene of interest from cycle numbers for housekeeping control gene. p values are displayed as *<0.05, **<0.01, ***<0.001 and ****<0.0001 in the figures. Statistical details of experiments can be found in the figure legends.

RESULTS

L. monocytogenes that hyperactivates the inflammasome impairs wound healing despite rapid clearance

Microbes stimulate inflammation through multiple PRRs including TLRs and NLRs that lead to activation of different innate immune signaling pathways (Flo et al., 2000; Opitz et al., 2009; Takeuchi & Akira, 2010). We previously demonstrated that Δ*hly Lm* mutant that fails to escape the phagosome into the host cell cytosol and has attenuated virulence, does not inhibit wound healing in zebrafish larvae (Jones & Portnoy, 1994; Miskolci et al., 2019). This led to the hypothesis that the cytosolic innate immune signaling activated by *Lm* may impair wound healing. An important inflammatory response dependent on *Lm* access to the cytosol is activation of the inflammasome

(Mariathasan et al., 2006; Meixenberger et al., 2010; Sauer et al., 2010; Warren et al., 2008; J. Wu et al., 2010). To address how inflammasome activation may affect wound healing, we took advantage of a *Lm* mutant, Lm-Pyro, that hyperactivates the inflammasome via ectopic secretion of flagellin but also has reduced virulence (Figure 2.1A) (Sauer, Pereyre, et al., 2011; Theisen & Sauer, 2017; Vincent et al., 2016). In accordance with prior reports, Lm-Pyro was attenuated in the zebrafish wound model with decreased bacterial burden compared to WT *Lm* infection (Figure 2.1D) (Vincent et al., 2016). Early on during infection, WT *Lm* and Lm-Pyro started off at similar burden at 1 day-post-wound (dpw). Over time, at 3 dpw, we observed significantly reduced bacterial burden in Lm-Pyro-infected compared to WT *Lm*-infected larvae, indicating attenuation in virulence as expected. At 5 dpw, we saw a similar trend, but the difference was not statistically significant (Figure 2.1D). Although wound healing was slightly improved compared to WT *Lm*-infected larvae, it was still severely impaired in Lm-Pyro-infected compared to uninfected larvae despite Lm-Pyro having a lower bacterial burden (Figure 2.1B, C). To determine if hyperactivation of the inflammasome, despite the attenuation in Lm-Pyro infection, still triggers hyperinflammation at the wound site, we quantified NF-κB expression at the wound microenvironment using *Tg(NFκB:EGFP)* zebrafish (Kanther et al., 2011). In this study, we define the wound microenvironment or wound site as the caudal fin tissue area distal to the caudal vein loop excluding the notochord (Miskolci et al., 2019). To visualize spread of infection, we utilized WT *Lm* and Lm-Pyro expressing red fluorescent protein, mCherry. We found at 3 and 5 dpw, there was less burden of Lm-Pyro compared to WT *Lm* at the tail fins, as suggested by the smaller mCherry fluorescent area, which is consistent with the results

obtained by CFU plating (Figure 2.1D, F). At early-stage infection, 1 dpw, there was a higher level of NF-κB at the wound site in Lm-Pyro-infected wounds compared to WT *Lm*-infected and uninfected wounds, suggesting Lm-Pyro triggered hyperinflammation early after infection. At 3 and 5 dpw, when there was a lower burden of Lm-Pyro at the infected tail wounds, both WT *Lm* and Lm-Pyro highly induced NF-κB at the wound site, suggesting that both types of infections stimulated extensive and prolonged inflammation independent of bacterial load (Figure 2.1E, G). We have previously shown that *Lm* infection increases recruitment of pro-inflammatory macrophages to the wound site (Miskolci et al., 2019). To further assess if hyperactivation of the inflammasome affects the inflammatory state of the macrophages at the wound, pro-inflammatory wound-associated macrophages were identified using a transgenic reporter line for TNFα expression crossed to a line that labels all macrophages (*Tg(tnfa:GFP) x Tg(mpeg1.1:mCherry-CAAX)*) (Miskolci et al., 2019; Marjoram et al., 2015; Bojarczuk et al., 2016; Nguyen-Chi et al., 2015). We found that more macrophages were recruited to the wound sites in WT *Lm*-infected and Lm-Pyro-infected wounds at 1, 3, and 5 dpw compared to uninfected wounds (Figure S2.1A). The macrophages at the wound site in WT *Lm*-infected and Lm-Pyro-infected wounds both persistently expressed TNFα, indicating that both WT *Lm* and Lm-Pyro triggered hyperinflammation early and the inflammation was persistent even after the bacteria started to clear (Figure 2.1H, I; Figure S2.1B). These findings suggest that extensive inflammation stimulated by infection, and particularly inflammasome activation, can impair wound healing independent of bacterial burden.

L. monocytogenes upregulates *il1b* at zebrafish tail wounds

Our findings suggest that *Lm*-stimulated inflammation correlates with impaired wound healing. We therefore hypothesized that a specific signature of inflammation may be associated with infected wounds. To identify the signature, we performed bulk RNA-sequencing on uninfected, WT *Lm*-infected, or Lm-Pyro-infected tail wounds. We identified *il1b* as one of the top upregulated genes in both WT *Lm* infection and Lm-Pyro infection (Figure 2.2A, B, E; Table S2.1). Indeed, the change in gene signature induced by WT *Lm* and Lm-Pyro were surprisingly similar (Figure 2.2C). We found that there were 22 genes that were upregulated more than 2-fold in WT *Lm*-infected tail wounds compared to uninfected tail wounds, and all 22 genes were also upregulated more than 2-fold with Lm-Pyro infection (Figure 2.2D). Among the 22 genes that were induced by both WT *Lm* and Lm-Pyro infections, *il1b* was the fifth most upregulated gene (Figure 2.2D, E; Table S2.1). Other top candidates were less well characterized in zebrafish and included acod1 and chemokine ligand 35. To validate RNA-sequencing results, we focused on *il1b* and confirmed the upregulation of *il1b* expression in zebrafish tail wounds infected with both WT *Lm* and Lm-Pyro infections compared to uninfected wounds (Figure 2.2F). In contrast, Δ*hly,* which does not induce hyperinflammation or affect wound healing, had no effect on *il1b* expression of infected tail wounds (Figure 2.2F) (Miskolci et al., 2019). These findings suggest that increased IL-1β induced by infection may be detrimental to wound healing.

L. monocytogenes infection inhibits wound healing through IL-1β signaling

To test the hypothesis that *Lm*-induced *il1b* expression impairs wound healing, we tested the effects of inhibition of IL-1β using both genetic and pharmacological approaches. *il1b* was depleted using an antisense morpholino oligonucleotide (MO) that was confirmed by changes in *il1b* mRNA splicing (Figure 2.3B) (López-Muñoz et al., 2011). To determine if knocking down *il1b* affects bacterial clearance in the zebrafish, mCherry-expressing *Lm* were used, and we found no difference in bacterial burden between standard control MO (std MO) and *il1b* MO injections in either WT *Lm*-infected or Lm-Pyro-infected larvae (Figure 2.3C). In both WT *Lm*-infected and Lm-Pyro-infected zebrafish, when *il1b* was knocked down, there was improved wound healing compared to std MO injected larvae (Figure 2.3D). There was also reduced inflammation in the IL-1β-deficient larvae, as suggested by the decreased NF-κB expression upon depletion of *il1b* (Figure 2.3E). To complement gene depletion, we took a pharmacological approach to inhibit IL-1β signaling using anakinra, an antagonist of interleukin-1 receptor (IL-1Ra). Blocking IL-1 signaling with anakinra did not affect wound healing in uninfected zebrafish; however, it improved wound healing in *Lm*-infected tail wounds (Figure 2.3F). Anakinra treatment also dampened inflammation at the wound site in *Lm*-infected wounds *as* suggested by the decreased abundance of pro-inflammatory (TNFα+) macrophages at the tail wounds (Figure S2.2). Importantly, anakinra was able to improve wound healing without affecting bacterial clearance (Figure 2.3G). Taken together, these findings suggest that *Lm*-induced inflammation impairs wound healing, at least in part, via IL-1β signaling.

Early clearance of *L. monocytogenes* is necessary to prevent persistent inflammation and enable wound healing

To determine if clearance of bacteria would resolve inflammation and restore wound healing, we tested the effects of antibiotic treatment with ampicillin. In addition, to investigate if the timing of antibiotics administration is critical, we treated *Lm*-infected larvae with ampicillin starting at 1, 2, or 3 dpw (Figure 2.4A). Under all conditions, ampicillin treatment effectively cleared infection completely by 5 dpw (Figure 2.4B). Surprisingly, only early treatment with ampicillin starting at 1 dpw rescued wound healing by 5 dpw (Figure 2.4D). Even at 6 and 7 dpw, *Lm*-infected larvae treated with ampicillin at a later timepoint, at either 2 or 3 dpw, still displayed impaired wound healing (Figure 2.4C, D). To assess if inflammation is altered by ampicillin treatment, pro-inflammatory (TNFα+) macrophages at the wound sites were quantified. Ampicillin treatment starting at any stage of infection reduced TNFα-expressing macrophages; however, only treatment starting at 1 dpw dampened inflammation to uninfected levels (Figure 2.4C, E). This provides further support for the idea that resolution of inflammation at the wound site correlates with improved wound healing in the early ampicillin treatment group. At 6 and 7 dpw, later treatment with ampicillin still did not resolve the presence of TNFα-expressing macrophages at the wound site, indicating non-resolving inflammation (Figure 2.4C, E). Our findings suggest that there is a critical window for bacterial clearance necessary to limit prolonged inflammation and promote tissue repair.

DISCUSSION

Bacterial infection has long been associated with defects in wound healing, however the mechanisms remain unclear (Zhao et al., 2016). In humans, wound healing involves four distinct phases: hemostasis, inflammation, proliferation, and resolution (Gosain & DiPietro, 2004). Zebrafish larvae share similar wound healing characteristics although lack the blood-clotting step during the initial hemostasis phase (Naomi et al., 2021). Accordingly, re-epithelization is an early wound healing phase in larval zebrafish and in general, zebrafish tissue regenerates after inflammation resolves (Naomi et al., 2021).

Taking advantage of this simplified wound healing model in zebrafish larvae, here we show that infection-induced inflammation impairs wound healing independent of bacterial burden. We demonstrate that non-resolving inflammation triggered by infection leads to dysregulation of the inflammation phase of wound healing resulting in impaired tissue repair. We provide evidence that there is a critical window during which bacterial clearance can abrogate chronic tissue inflammation. Interestingly, clearance of infection after this critical window is not sufficient to improve tissue repair. However, resolving inflammation by knocking down *il1b* or by blocking IL-1 signaling with anakinra, an IL-1R antagonist, was able to partly rescue the defect in wound healing even in the presence of persistent bacterial burden. Taken together, our findings suggest that persistent inflammation induced by infection is sufficient to limit tissue repair even after the infection is cleared.

Our gene expression analysis demonstrated that *il1b* expression was induced by both WT *Lm* and Lm-Pyro. Our findings suggest that *il1b* expression is a common signature of infected and inflammatory non-healing wounds, independent of bacterial load. In diabetic fibroblast *ex vivo* models, high levels of IL-1β inhibits cell proliferation (Dai et al., 2021). Additionally, in diabetic mice, treatment with IL-1β-neutralizing antibody shifted the macrophage phenotype from a pro-inflammatory state to a pro-healing state and improved wound healing (Mirza et al., 2013). Infected wounds share similar characteristics as diabetic chronic wounds where both types of non-healing wounds often exhibit polymicrobial infections and prolonged inflammatory responses (Holl et al., 2021). In this study, we demonstrated that IL-1β signaling triggered by infection inhibits wound healing and that IL-1R blockade with anakinra improved wound healing in *Lm*-infected zebrafish tail wounds. Importantly, anakinra treatment did not affect bacterial burden. This suggests that IL-1β could serve as a potential therapeutic target for treating infected wounds.

Additionally, our RNA-seq analysis suggested that there were other inflammatory profiles that were highly upregulated by infections, such as immune-responsive gene 1 (*irg1*), also known as aconitate decarboxylase (*acod1)*, which could potentially serve as an alternative target for dampening inflammation during wound healing. However, inhibiting inflammation in the setting of infection can pose a significant challenge since inflammation plays an essential role in host defense against infections. Studies have shown *irg1* to be essential for clearance of *Mycobacterium tuberculosis* (*Mtb*) infection (Nair et al., 2018). In contrast, there is an attenuation in *S. aureus* virulence in *irg1*-

deficient mice (Tomlinson et al., 2023). Future studies are needed to further examine the role of *irg1* in wound healing and host defense against infection to determine if *irg1* could be a potential target for treating infected wounds. It is critical to identify inflammatory targets that do not link to host defense.

Treatment of infected wounds typically involves the use of antimicrobial agents to reduce bacterial colonization at the wound and promote wound healing (Negut et al., 2018; Ye et al., 2018; Rădulescu et al., 2016). Indeed, current treatments for infected wounds focus on killing the bacteria with antibiotics (Mirhaj et al., 2022; Seidelman & Anderson, 2021). Our findings suggest that post-infection, there is a narrow therapeutic window for antibiotic treatment before chronic inflammation is established. It will be interesting to determine if a similar critical window is also true for humans with infected wounds. Overall, our findings suggest that future therapeutics for infected wounds, including surgical site infections, could combine antibiotic treatment with anti-inflammatory agents that limit inflammation triggered by infections to further facilitate wound healing.

Limitations of the study

However, one limitation in our experimental setup was that the absolute bacterial burden at different timepoints pre-ampicillin treatment was different; therefore, we cannot rule out that the extent of infection was not driving the differences observed in wound healing between zebrafish larvae treated with ampicillin at varying timepoints. In addition, the application of these findings to human wounds remains unknown.

In conclusion, our data demonstrate that sustained inflammation induced by infection limits tissue repair in zebrafish larvae. This study supports our prior work which showed a correlation between the presence of inflammatory macrophages (TNFα positive) and impaired wound healing (Miskolci et al., 2022). Here, we show that inflammasome activation and induction of *il1b* is associated with impaired wound healing independent of bacterial burden. Early events during infection induced inflammation appear to influence long-term healing outcome, since only early antibiotics treatment facilitated repair. This work raises the interesting question about the combined use of antibiotics and anti-inflammatory agents such as an IL-1 receptor antagonist to treat infected wounds.

ACKNOWLEDGEMENTS

We thank Dr. Warren Rose at University of Wisconsin-Madison School of Pharmacy for access to anakinra. Figure diagrams and graphical abstract were made with biorender.com. This work was supported by GM118027 (A.H.), 1R01AI137070 and 1R21AI173738 (J.D.S.), and NIH K99GM138699 and AHA 17POST33410970 (V.M.).

Figures

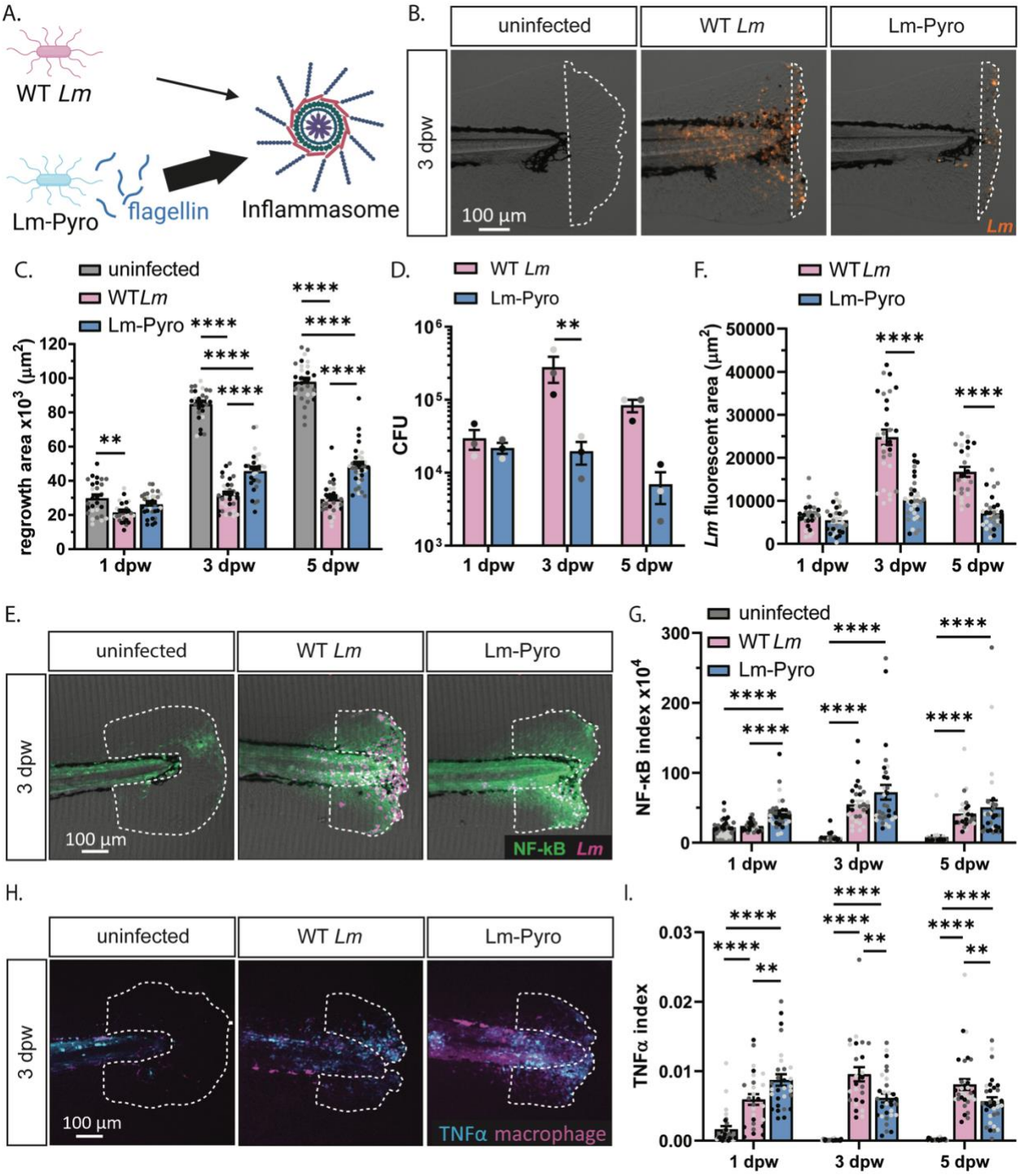

Figure 2.1. Inflammation stimulated by inflammasome signaling impairs wound healing in *Lm*-infected zebrafish larvae.

(A) Lm-Pyro hyperactivates the inflammasome through secretion of flagellin. (B) Representative merged images of single-plane brightfield and fluorescent images of the caudal fin of zebrafish larvae in response to WT *Lm* or Lm-Pyro infection over time using mCherry-expressing *Lm*, and the corresponding quantification of tissue regrowth from three biological replicates are shown in (C). White dashed line in (B) outlines regrowth area. N = 28-32 larvae per treatment per timepoint. (D) CFU of *Lm* was determined at indicated timepoints by pooling 10 zebrafish larvae per condition per timepoint. (E) Representative sum-projections of z-stacks of the caudal fin acquired by laser scanning confocal microscope using *Tg(NFκB:EGFP)* larvae and mCherry-expressing *Lm* fixed at indicated timepoints. NF-κB is shown in green and *Lm* is shown in magenta. White dashed line denotes the wound sites, where NF-κB was quantified. The corresponding quantification of *Lm* fluorescent area at the tail fins quantified by area thresholding is shown in (F) and NF-κB index showing NF-κB integrated intensity normalized to regrowth area is plotted in (G). (E-G) N = 24-33 larvae per treatment per time point. (H) Representative sum-projections of z-stacks acquired by laser scanning confocal microscope using double transgenic larvae (*Tg(tnfa:GFP) x Tg(mpeg1:mCherry-CAAX)*) over time in response to uninfected, WT *Lm*-infected, or Lm-Pyro-infected wounds. TNFα is shown in cyan and macrophages are shown in magenta. White dashed line denotes area measured for TNFα+ macrophages area. Corresponding quantification is plotted in (I) with TNFα index showing percentage of TNFα positive macrophages quantified by area thresholding and normalized by regrowth fin area.(H-I) N= 25-32 larvae per treatment per timepoint. Values in (C), (D), (F), (G), and (I) are arithmetic means and SE with associated p values obtained by least

square mean analysis in (C), two-way ANOVA in (D), and rank analysis due to residuals not being normally distributed in (F), (G) and (I). Three biological replicates were performed with data points from different biological replicates displayed in different shades of gray. *p<0.05, **p<0.01, ***p<0.001, ****p<0.0001. See also Figure S1.

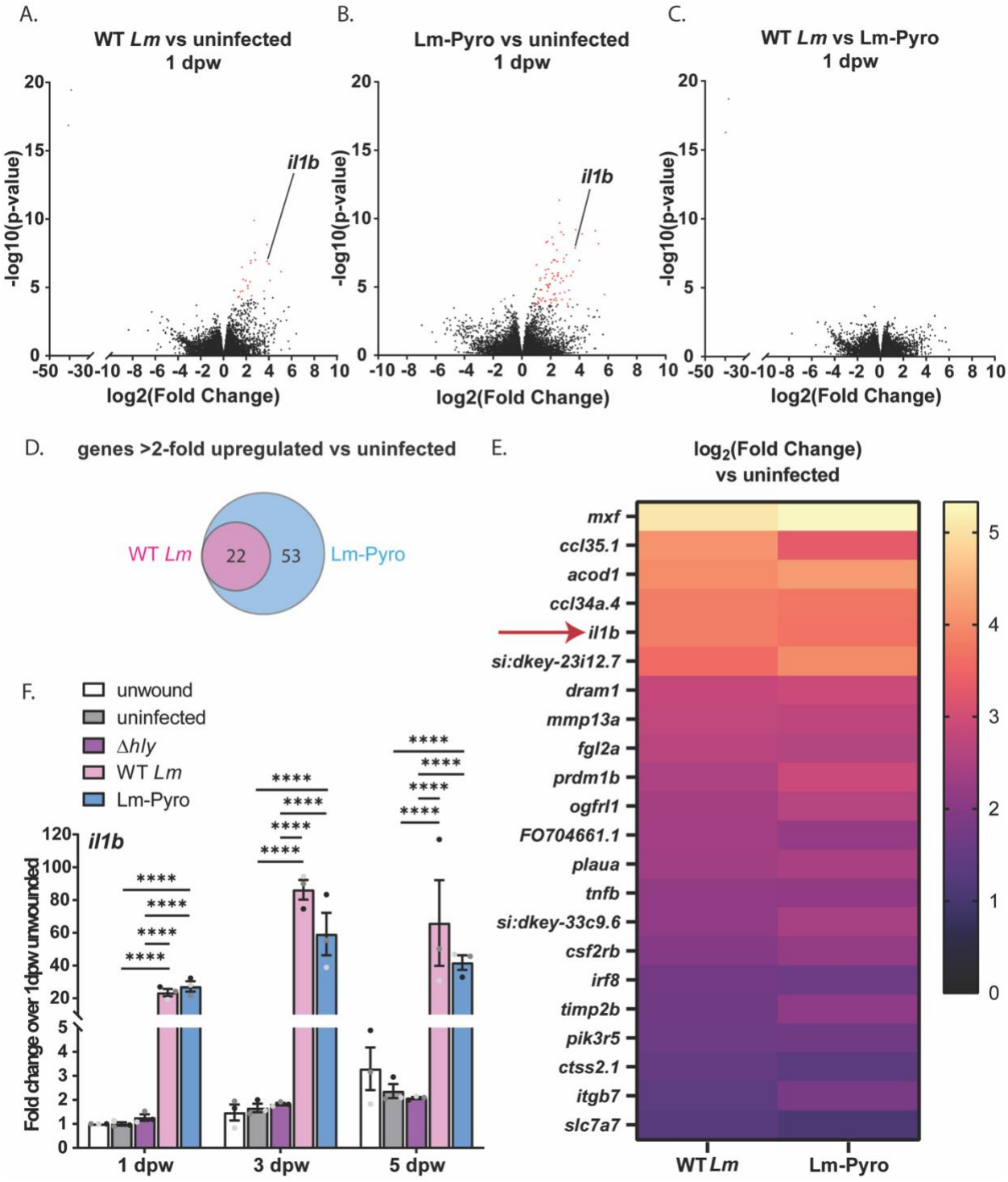

Figure 2.2. Transcriptomic analysis identifies *il1b* as an inflammatory marker in *Lm*-infected wounds.

(A) Volcano plot for gene expression comparison between (A) uninfected and WT *Lm*-infected, (B) uninfected and Lm-Pyro infected, and (C) WT *Lm*-infected and Lm-Pyro-infected tail fins at 1 dpw obtained by RNA-sequencing. (A-C) Red dots depict more than 2-fold upregulated genes and blue dots depict more than 2-fold downregulated genes for with Benjamini-Hochberg corrected p value <0.05 for each comparison. (D) Venn diagram depicting genes that are more than 2-fold upregulated compared to uninfected condition in WT *Lm*-infected and Lm-Pyro-infected tail wounds, with the overlapping gene lists shown in a heat map in (E). (A-E) n = 50 per treatment per biological replicate with three biological replicates. (F) *il1b* expression normalized to fold change over 1 dpw unwounded condition in pooled tail fin tissue collected from larvae from each treatment at indicated timepoints measured by RT-qPCR from three biological replicates with N = 18-25 larvae per treatment per timepoint per biological replicate. (F) is showing arithmetic means and SE with associated p values obtained by two-way ANOVA performed on RT-qPCR ΔCq values. Data points from different biological replicates are displayed in different shades of gray. ****p<0.0001. See Table S2.1 for detailed information on upregulated genes shown in (E).

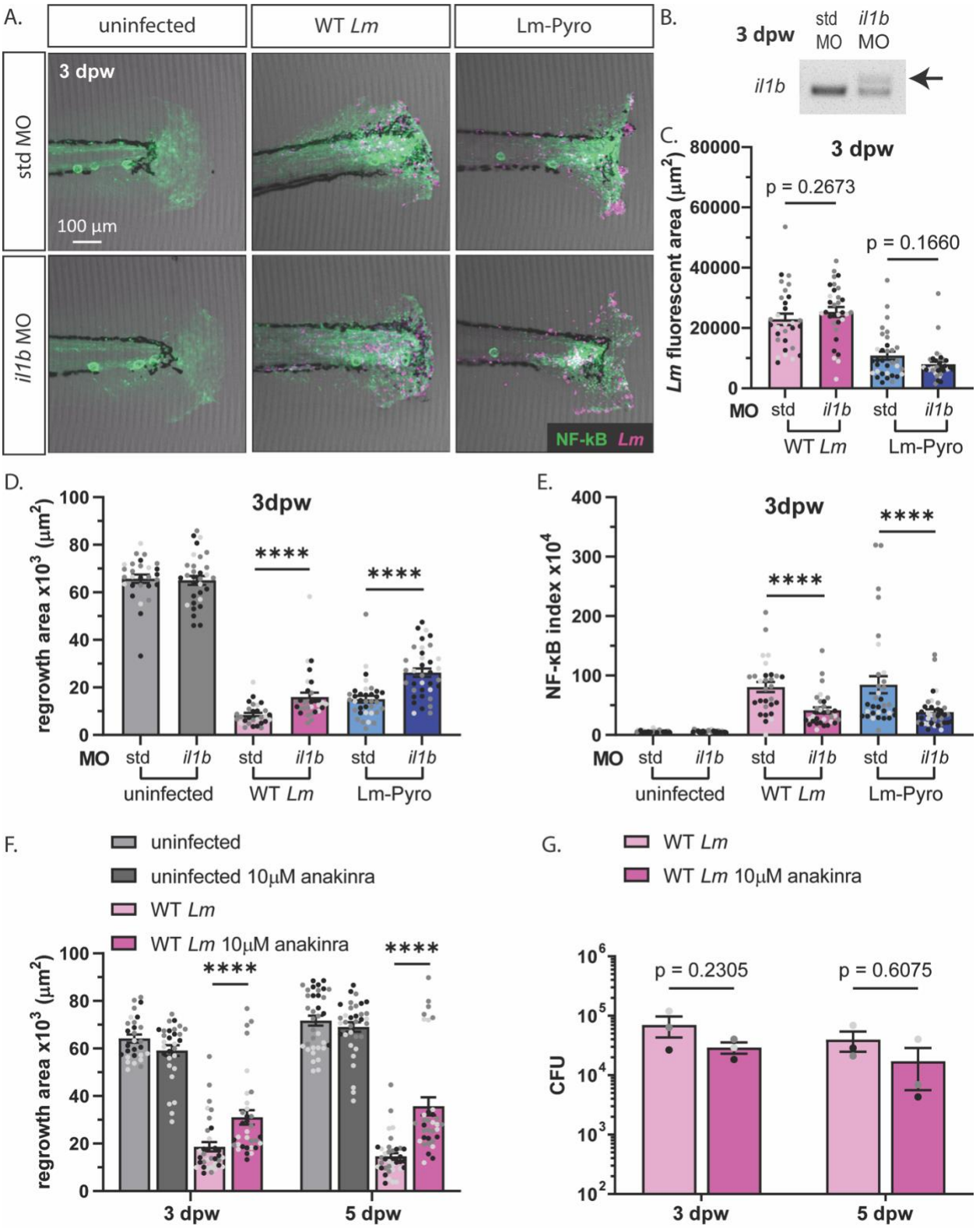

Figure 2.3. *Lm* inhibits wound healing through IL-1β signaling.

(A) Representative images for sum-projections of z-stacks acquired by laser scanning confocal microscope using std MO- or *il1b* MO-injected *Tg(NFκB:EGFP)* zebrafish larvae and mCherry-expressing *Lm* fixed at 3 dpw. NF-κB signal is shown in green and *Lm* shown in magenta. Scale bar is 100 microns. (B) PCR amplification of *il1b* cDNA from std MO- or *il1b* MO-injected larvae at 3 dpw. Quantification of (C) *Lm* fluorescent area at the tail fins using area thresholding, (D) regrowth area of the tail fins and (E) integrated intensity for background-corrected NF-κB normalized to regrowth area shown as NF-κB index from images in (A). (F) and (G) 1 day-post-fertilization larvae were treated with 10 μM anakinra with quantification of regrowth area over time in (F). (G) CFU of *Lm* was determined at indicated timepoints by pooling 10 larvae per condition per timepoint from three biological replicates. (F) regrowth area was quantified from three biological replicates with N = 28-36 larvae per treatment per timepoint. (C-G) are arithmetic means and SE with associated p values obtained by least square mean analysis in (C), rank analysis due to residuals not being normally distributed in (D-F), and two-way ANOVA in (G). Data points from different biological replicates are displayed in different shades of gray. *p<0.05, **p<0.01, ***p<0.001, ****p<0.0001. See also Figure S2.

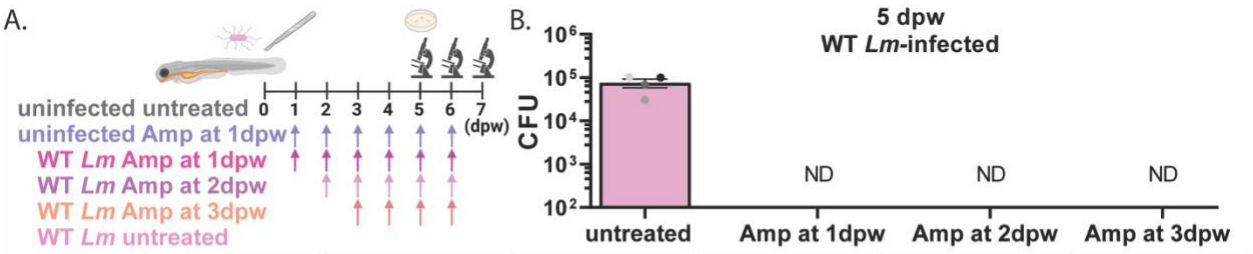

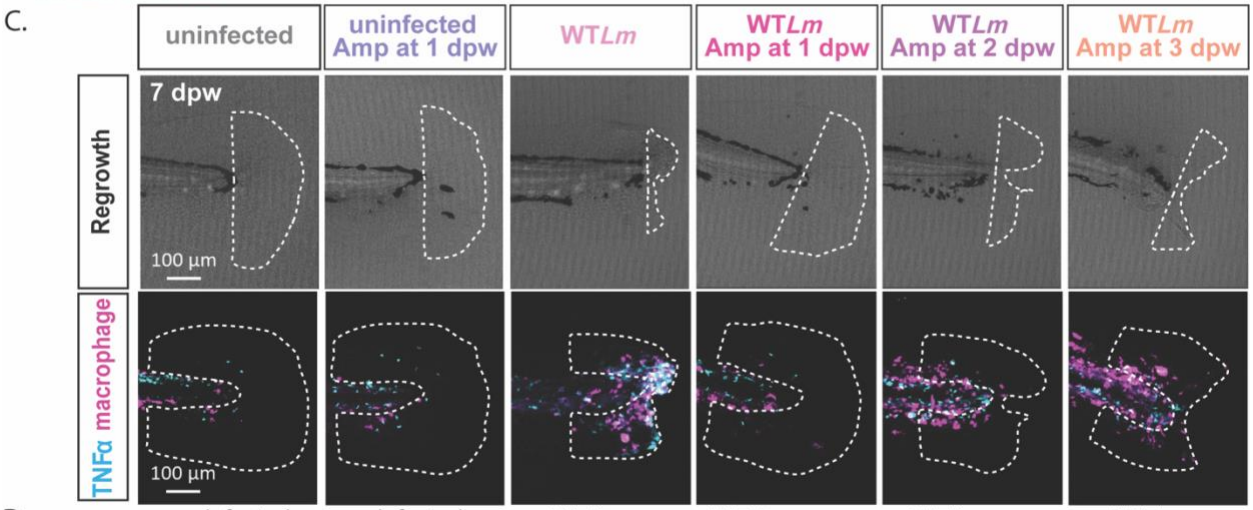

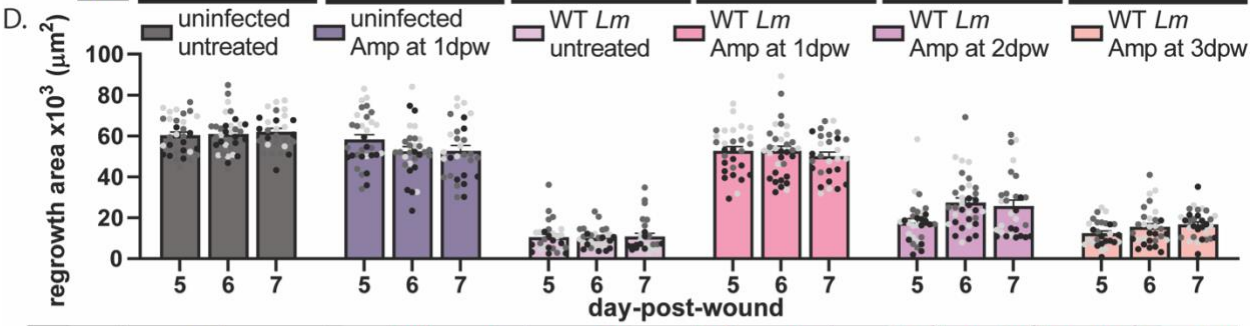

p-value	un. vs un. 1d	un. vs Lm	un. vs Lm 1d	un. vs Lm 2d	un. vs Lm 3d	Lm vs Lm 1d	Lm vs Lm 2d	Lm vs Lm 3d	Lm 1d vs Lm 2d	Lm 1d vs Lm 3d	Lm 2d vs Lm 3d
5 dpw	ns	****	ns	****	****	****	**	ns	****	****	ns
6 dpw	*	****	*	****	****	****	****	ns	****	****	***
7 dpw	*	****	**	****	****	****	****	*	****	****	*

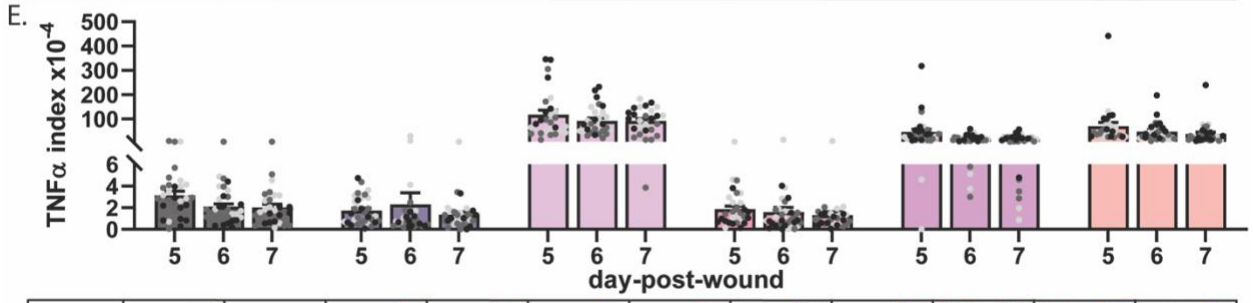

p-value	un. vs un. 1d	un. vs Lm	un. vs Lm 1d	un. vs Lm 2d	un. vs Lm 3d	Lm vs Lm 1d	Lm vs Lm 2d	Lm vs Lm 3d	Lm 1d vs Lm 2d	Lm 1d vs Lm 3d	Lm 2d vs Lm 3d
5 dpw	ns	****	ns	****	****	****	**	ns	****	****	ns
6 dpw	ns	****	ns	****	****	****	****	*	****	****	**
7 dpw	ns	****	ns	****	****	****	****	**	****	****	*

Figure 2.4. Early eradication of *Lm* infection is required for inflammation resolution and wound healing.

(A) Experimental setup is shown. Double transgenic WT larvae (*Tg(tnfa:GFP) x Tg(mpeg1:mCherry-CAAX)*) fixed and imaged at indicated timepoints (5-7 dpw) following uninfected, WT *Lm*-infected, or WT *Lm*-infected tail transection at 3 dpf that were treated with ampicillin starting at 1 , 2, or 3 dpw. (B) CFU of *Lm* at 5 dpw was determined by pooling 10 zebrafish larvae per condition per timepoint from four biological replicates. (C) Representative sum-projections of z-stack images at 7 dpw acquired by laser scanning confocal microscope are shown. Tail wounds were also imaged at 5 and 6 dpw, but only the 7 dpw time point is shown. White dashed line on top row outlines regrowth area and on bottom row denotes area for TNFα+ macrophage quantification. TNFα is shown in cyan and macrophages are shown in magenta. Scale bar is 100 microns. (D) Corresponding quantification of regrowth area of larvae at 5, 6, and 7 dpw using data set in (C), and in (E) corresponding quantification of TNFα index showing TNFα+ macrophages were quantified by area thresholding and normalized to regrowth area. (C-E) from three biological replicates with total N = 27-34 larvae per treatment per time point. (B), (D), and (E) are arithmetic means and SE with associated p values obtained by two-way ANOVA in (B) and rank analysis in (D) and (E). Data points from different biological replicates are displayed in different shades of gray. **p<0.01, ****p<0.0001. Amp, ampicillin; un., uninfected; un. 1d, uninfected Amp at 1 dpw; *Lm* 1d, *Lm*-infected Amp at 1 dpw; *Lm* 2d, *Lm*-infected Amp at 2 dpw; *Lm* 3d, *Lm*-infected Amp at 3 dpw.

Supplementary Figures

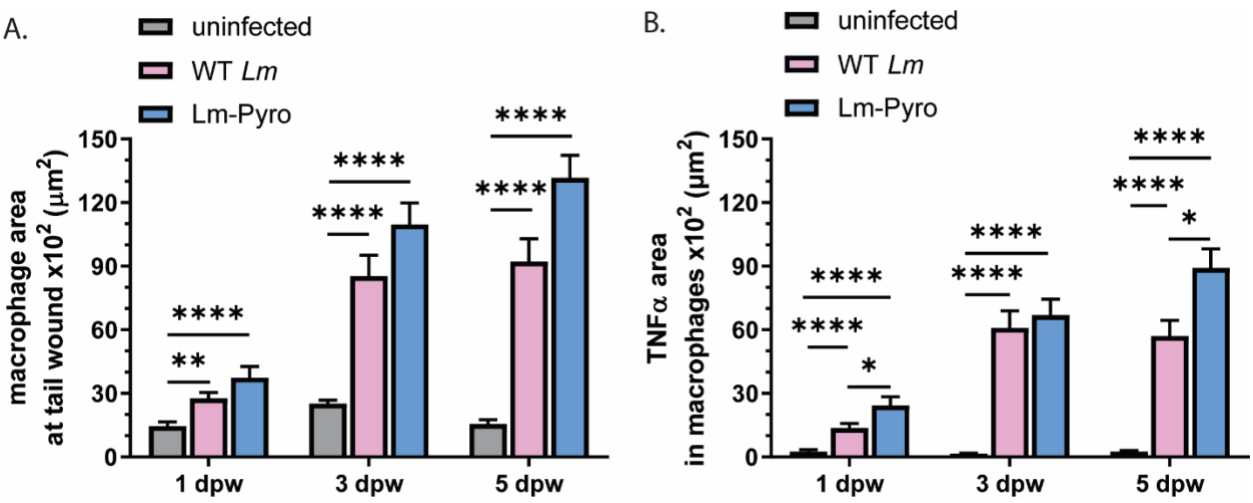

Figure S2.1. Both WT *Lm* and Lm-Pyro induce hyperinflammation, related to Figure 2.1.

The corresponding quantification of the data set in Figure 1H. (A) quantification of raw macrophage area in the caudal fin tissue area distal to the caudal vein loop, and (B) TNFα expression in the macrophage area was quantified by area thresholding of fluorescence intensity. N= 25-32 larvae per treatment per timepoint. Values are arithmetic means and SE from three biological replicates with associated p values obtained by rank analysis due to residuals not being normally distributed. *p<0.05, **p<0.01, ***p<0.001, ****p<0.0001.

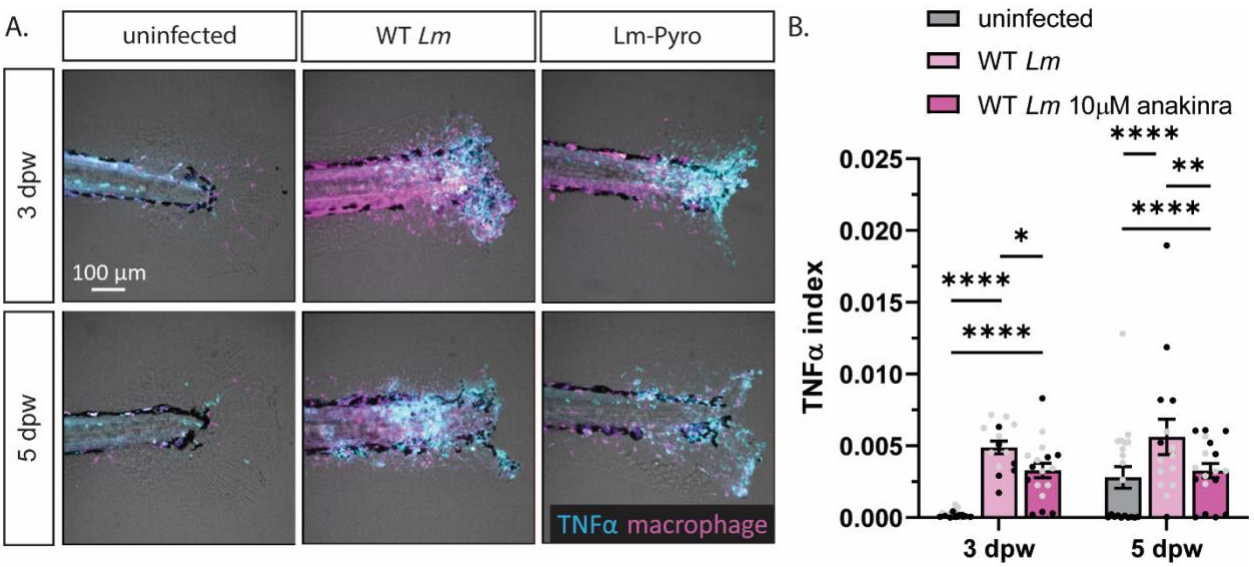

Figure S2.2. Anakinra treatment dampens inflammation in *Lm*-infected wounds, related to Figure 2.3.

(A) Representative sum-projections of z-stacks acquired by laser scanning confocal microscope using double transgenic WT larvae (*Tg(tnfa:GFP) x Tg(mpeg1:mCherry-CAAX)*) over time following uninfected, WT *Lm*-infected, or WT *Lm*-infected anakinra treated tail transections, and in (B) the corresponding quantification of TNFα index showing percentage of macrophage area expressing TNFα at the wound using area thresholding of fluorescence intensity normalized to regrowth area. Anakinra treated larvae were bathed in 10 μM anakinra starting at 1 day-post-fertilization. Scale bar in (A) is 100 microns. TNFα is shown in cyan and macrophages are shown in magenta in (A). Two biological replicates were performed with a total of N= 14-20 larvae per treatment per timepoint. Values are arithmetic means and SE from three biological replicates with associated p values obtained by rank analysis due to residuals not being normally distributed. Data points from different biological replicates are displayed in different shades of gray. *p<0.05, **p<0.01, ****p<0.0001.

Supplementary Tables

Table S2.1. Genes that are more than 2-fold upregulated by both WT *Lm* and Lm-Pyro, related to Figure 2.2.

Gene Name	Description	log_2(FC) compared to uninfected	
		WT *Lm*	Lm-Pyro
mxf	myxovirus (influenza virus) resistance F	5.07	5.33
ccl35.1	chemokine (C-C motif) ligand 35, duplicate 1	4.10	3.33
acod1	aconitate decarboxylase 1	4.01	4.19
ccl34a.4	chemokine (C-C motif) ligand 34a, duplicate 4	3.85	3.74
il1b	interleukin 1, beta	3.84	3.71
si:dkey-23i12.7	si:dkey-23i12.7	3.58	4.00
dram1	DNA-damage regulated autophagy modulator 1	2.82	2.89
mmp13a	matrix metallopeptidase 13a	2.77	2.39
fgl2a	fibrinogen-like 2a	2.69	2.61
prdm1b	PR domain containing 1b, with ZNF domain	2.51	2.91
ogfrl1	opioid growth factor receptor-like 1	2.41	2.62
FO704661.1	gamma-glutamyl hydrolase	2.40	2.20
plaua	plasminogen activator, urokinase a	2.36	2.46
tnfb	tumor necrosis factor b (TNF superfamily, member 2)	2.15	2.13
si:dkey-33c9.6	si:dkey-33c9.6	2.14	2.44
csf2rb	colony stimulating factor 2 receptor, beta, low-affinity (granulocyte-macrophage)	1.96	2.18
irf8	interferon regulatory factor 8	1.73	1.65
timp2b	TIMP metallopeptidase inhibitor 2b	1.69	2.11
pik3r5	phosphoinositide-3-kinase, regulatory subunit 5	1.63	1.68
ctss2.1	cathepsin S, ortholog2, tandem duplicate 1	1.50	1.36
itgb7	integrin, beta 7	1.39	1.78
slc7a7	solute carrier family 7 (amino acid transporter light chain, y+L system), member 7	1.29	1.07

RNA-seq was performed on tail fins of uninfected, WT *Lm*-infected, and Lm-Pyro-infected transected tail wounds at 1 dpw. n = 50 per treatment per biological replicate with three biological replicates.

Table S2.2. Key resource table.

Bacterial and virus strains		
10403S, *L. monocytogenes* WT strain	Edman et al.	N/A
10403S, *L. monocytogenes* WT strain-mCherry	Vincent et al.	N/A
10403S, Lm-Pyro	Sauer et al.	N/A
10403S, Lm-Pyro mCherry	Vincent et al.	N/A
10403S, *Δhly*	Jones and Portnoy	N/A
Chemicals, peptides, and recombinant proteins		
Phosphate buffered saline (PBS)	Sigma-Aldrich	Cat# P3813
TWEEN-20	Sigma	Cat# P1379
Difco Brain Heart Infusion (BHI)	Becton Dickinson	REF# 237500
streptomycin	Fisher	Cat#BP910-50
Agar	Fisher	Cat# BP1423
TRIzol	Ambion	Cat#15596-026
chloroform	Fisher	Cat#C298-500
anakinra	Kineret	CAS# 143090-92-0
ampicillin	thermofisher	Cat#BP176025
Critical commercial assays		
RNAqueous Micro Kit	Invitrogen	Cat# AM1931
SuperScript™ III First-Strand Synthesis System	Invitrogen	Cat# 18080051
FastStart Essential DNA Green Master	Roche	Cat# 6402712001
RNeasy Mini Kit	Qiagen	Cat#74104
OneStep RT-PCR Kit	Qiagen	Cat#210212
Deposited data		
RNA-seq data	This paper	GEO: GSE237265
Experimental models: Organisms/strains		
D. Rerio WT (AB)	ZIRC	ZL1
Zebrafish Tg(NF-κB:GFP)	Kanther et al.	ZDB-TGCONSTRCT-120409-6
Zebrafish Tg(tnfa:GFP)	Marjoram et al.	ZDB-TGCONSTRCT-150603-6
Zebrafish Tg(mpeg1.1:mCherry-CAAX)	Bojarczuk et al.	ZDB-TGCONSTRCT-160414-8
Oligonucleotides		
Forward primer for *il1b* qPCR: ATGGCGAACGTCATCCAAGA	Tsarouchas et al.	N/A
Reverse primer for *il1b* qPCR: GAGACCCGCTGATCTCCTTG	Tsarouchas et al.	N/A
Forward primer for *b-actin* qPCR: CACTGAGGCTCCCCTGAATCCC	Tsarouchas et al.	N/A
Reverse primer for *b-actin* qPCR: CGTACAGAGAGAGCACAGCCTGG	Tsarouchas et al.	N/A
il1b MO1 Sequence: CCCACAAACTGCAAAATATCAGCTT	López-Muñoz et al.	ZBD-MRPHLNO-110620-2
Standard control morpholino Sequence: CCTCTTACCTCAGTTACAATTTATA	Gene Tools	N/A
Forward primer for checking *il1b* MO altered splicing: ATGGCATGCGGGCAATATGAA	López-Muñoz et al.	N/A
Reverse primer for checking *il1b* MO altered splicing: CACTTCACGCTCTTGGATGA	López-Muñoz et al.	N/A

Recombinant DNA		
pPL2(mCherry)	Vincent et al.	N/A
pPL2e(pActA-mCherry)	Vincent et al.	N/A
Software and algorithms		
FIJI, Image J	Schindelin et al.	RRID:SCR_002285
GraphPad Prism		RRID:SCR_002798
SAS		RRID:SCR_008567
Spliced Transcripts Alignment to a Reference (STAR)	Dobin et al.	https://github.com/alexdobin/STAR
RSEM v1.3.3	Li and Dewey	https://deweylab.github.io/RSEM/
DESeq2 v1.32.0	Love et al.	https://bioconductor.org/packages/release/bioc/html/DESeq2.html

CHAPTER 3 – Genome-wide screen reveals fitness determinants of bacterial pathogen for intracellular survival and *in vivo* virulence

Authors and their contributions:

Simone Shen: Planned and conducted experiments. Organized data and wrote this manuscript.

Ian Humphrey: Performed deep learning protein-protein interaction prediction experiment for Figure 3.6A

Anna Huttenlocher: Supervised all research and contributed intellectually to the design of the experiments.

John-Demian Sauer: Supervised all research and contributed intellectually to the design of the experiments, edited this manuscript.

Abstract

Intracellular bacterial pathogens are major contributors to global morbidity and mortality. Furthermore, with escalating antibiotic resistance threats, there is an increasing need to understand bacterial virulence mechanisms to develop novel anti-virulence targeting therapeutics. Combining transposon mutagenesis and next generation sequencing (TIS) allows us to obtain a global understanding of bacterial virulence strategies utilized on a genome-wide scale. Current murine models present obstacles for identifying *in vivo* virulence genes through TIS screens due to infection bottlenecks and high costs. To overcome these hurdles, we utilize zebrafish as a model host, due to their high fecundity and low cost. *Listeria monocytogenes*, an intracellular pathogen that causes listeriosis, is an ideal model pathogen due to its well-characterized infectious cycle and tractable genetic systems. Nevertheless, knowledge on how *L. monocytogenes* evades the immune system to cause infection remains limited. In this study, we performed *L. monocytogenes* TIS screen in mouse bone marrow-derived macrophages (BMDMs) to identify genes required for cytosolic growth in the absence of immune selective pressure. Additionally, we identified genes critical for inflammasome immune evasion utilizing caspase-1 deficient BMDMs. To further identify genes required for *in vivo* infection in the presence of an intact innate immune system, we executed the TIS screen in zebrafish. With the comprehensive identification of virulence factors and their functions may lead to discovery of novel therapeutic targets and new strategies in combating intracellular bacterial infections.

INTRODUCTION

Intracellular pathogens are among the leading causes of morbidity and mortality worldwide (Ikuta et al., 2022). To survive in the host, bacterial pathogens have evolved virulence factors that help them avoid detection and subsequent clearance from the host (Hornef et al., 2002; Van Avondt et al., 2015). To spread and cause disease in the host, pathogens require different virulence factors to manipulate the host and adapt to different host-imposed stressors; such as cell wall stress, nutritional stress, and oxidative stress (Eisenreich et al., 2015; Janakiraman & Lesser, 2017; Ribet & Cossart, 2015). Understanding specific mechanisms by which pathogens avoid clearance by the host will provide insights into novel targets for new antibiotic development strategies.

Listeria monocytogenes is a Gram-positive, facultative intracellular foodborne pathogen and the causative agent of listeriosis (Vázquez-Boland et al., 2001). Robust genetic tools and well-characterized infection models have made *L. monocytogenes* a powerful model organism to study bacterial pathogenesis (Cossart, 2007; Hamon et al., 2006). Using well-defined infection models, including *ex vivo* mammalian cell culture and *in vivo* mouse models, studies have identified factors clustered in the Listeria Pathogenicity Island-1 (LIPI-1) that *L. monocytogenes* utilizes to survive and replicate in the host cells. For example, *L. monocytogenes* uses internalin proteins to invade non-phagocytic cells (Mengaud et al., 1996; Y. Shen et al., 2000), the pore-forming cytolysin listeriolysin O (LLO) to avoid oxidative, proteolytic, and pH stress by facilitating escape from the phagosome into the cytosol (Schnupf & Portnoy, 2007), and finally, ActA to promote spreading into neighboring cells through actin-based motility (Brundage et al.,

1993; Kocks et al., 1992; Tilney & Portnoy, 1989). After invasion into neighboring cells, *L. monocytogenes* uses LLO and phospholipase Cs to escape the double membrane vacuole into the cytosol and reinitiate the infection cycle (G. A. Smith et al., 1995). All of these virulence factors are transcriptionally controlled by the master regulator, PrfA, whose expression is tightly regulated by environmental stressors (Chakraborty et al., 1992; Reniere et al., 2015). Besides these well-characterized virulence factors in the LIPI-1, many other virulence determinants are required to support *L. monocytogenes*' growth and dissemination in the restricted environment in the host (G. Y. Chen, Pensinger, et al., 2017). For example, to regulate cell wall stress, genes involved in peptidoglycan synthesis such as *prkA*, *reoM*, and *glmR* are required (Kelliher et al., 2021; Pensinger et al., 2023). To modulate nutritional stress, genes involved in nucleotide and aromatic amino acid biosynthesis are crucial for replication when resources are limited in the host cell (Faith et al., 2012; Schauer et al., 2010; Stritzker et al., 2004). *L. monocytogenes* can also hijack nutrients from the host through genes that encode transporters to import essential amino acids and other nutrients for which *L. monocytogenes* is auxotrophic, which are also critical for pathogenesis (Schauer et al., 2010). To resist oxidative stress, superoxide dismutase (SOD) can neutralize reactive oxygen species (ROS) (Welch et al., 1979). Additionally, to maintain redox balance, genes involved in the synthesis of DHNA, an intermediate of menaquinone biosynthesis, are also important along with NADH dehydrogenase (Ndh2) (Smith et al., 2023). *Listeria monocytogenes* serves as an excellent model for studying the pathogenesis, immune responses, and intracellular survival of various other bacterial pathogens. Its ability to mimic aspects of infection biology common to many pathogens

makes it a valuable tool in studying infectious diseases. For example, similary to *L. monocytogenes*, *Shigella flexneri*, *Rickettsia spp*., and *Burkholderia pseudomalle* all can also hijack host actin to facilitate cell-to-cell spread through actin-based motility (Durand et al., 1997; Reed et al., 2014; Srinon et al., 2019). The discovery of additional novel virulence genes *L. monocytogenes* could improve our understanding of the mechanism by which pathogens cause disease and could facilitate novel approaches for therapeutic development. Targeting virulence factors can attenuate the pathogen without necessarily killing it, which may reduce the likelihood of resistance (Lee et al., 2020).

Forward genetic screens utilizing transposon insertion sequencing (TIS) approaches, which combine the technology of transposon mutagenesis and next-generation sequencing, have been used to identify virulence genes in many bacterial pathogens. Recently, the first TIS screen in *L. monocytogenes* has been described using a murine macrophage cell line as a surrogate to identify genes important for intracellular survival (Fischer et al., 2022). However, one limitation of the study is that macrophages were infected by *L. monocytogenes* for 24 hours which could lead to macrophage cell deaths, confounding the results of their study. This prompted us to perform another *ex vivo L. monocytogenes* TIS screen with a shorter infection time by identifying genes important for intracellular growth at 6-hour post-infection. Additionally, instead of using a mouse macrophage cell line, we chose to use mouse bone-marrow-derived primary macrophages, which is more physiologically relevant. While *ex vivo* cell culture models are invaluable tools for understanding bacterial pathogenesis, several limitations exist in these models, particularly when it comes to modeling complex *in vivo* environments

(Disson & Lecuit, 2013). The lack of tissue complexity and the absence of an intact immune system inhibit *ex vivo* models from encapsulating all of the physiological conditions pathogens encounter during infection (Shi et al., 2019). Therefore, it is important to explore virulence determinants in *L. monocytogenes* in an *in vivo* model. However, one hurdle of performing a TIS screen *in vivo* is the substantial bottleneck present in the murine model of listeriosis where only 1000 unique bacteria colonize a given host even when administered intravenously (Zhang et al., 2017). To overcome *in vivo* infection bottlenecks, we adopted zebrafish as our model host, taking advantage of its high fecundity and cheap cost.

In this study, using *L. monocytogenes* as a model pathogen, we identified genes important for fitness *ex vivo* using BMDMs. Additionally, we demonstrated the utility of knockout host cells and identified genes involved in inflammasome defense using caspase-1 deficient BMDMs. Furthermore, utilizing zebrafish as a model organism, we identified 909 genes in *L. monocytogenes* that are important for fitness *in vivo* through a TIS screen. Additionally, we coupled the TIS screen with a deep learning-based genome-wide prediction of protein-protein interactions (PPI) (Cong et al., 2019; Humphreys et al., 2021) , which generated a novel list of 3316 putative PPIs in *L. monocytogenes*. Overlaying the TIS data, the PPI predictions and existing *in vivo* transcriptomic data we identified 9 putative PPI pairs where both genes were both transcriptionally upregulated in vivo and predicted to be important for virulence by our TIS screen. Future studies verifying interactions between putative PPI pairs and confirming their role in *L. monocytogenes* pathogenesis *in vivo* in a murine model of

listeriosis are needed to validate the deep learning PPI approach and to further demonstrate zebrafish as a viable model for studying bacteria pathogenesis. Additionally, verification of a role in virulence for these genes could unveil novel targets for antibiotic development.

RESULTS

Identification of genes essential for growth in *L. monocytogenes* through TIS screen

To generate pools of *L. monocytogenes* mutants for carrying out the TIS screens using transposon mutagenesis, the *L. monocytogenes* transposon library was constructed through mariner-based transposon delivery plasmid, pJZ037, resulting in a highly saturated library containing around 10^9 individual mutant clones for each library (Zemansky et al., 2009). To determine *L. monocytogenes* essential genes, genes that are indispensable for survival even in the absence of a host selective pressure, we cultivated ~5 x 10^6–5 x 10^7 CFU from our transposon library in BHI broth at 37°C for 5 hours, allowing for ~6 generations of replication (Figure 3.1A). After 5 hours of cultivation, we extracted genomic DNA and libraries were prepared for Illumina sequencing (see Materials and Methods). Illumina paired-end sequencing was performed on prepared libraries using NovaSeq 6000 at the University of Wisconsin-Madison Biotechnology Center with the request of ~7–20 million reads per replicate to identify transposon insertion sites. Sequenced reads FASTQ files were then uploaded to Galaxy where sequenced reads were trimmed, filtered, and mapped to the *L. monocytogenes* 10403s genome (The Galaxy Community et al., 2022) (see Materials

and Methods). Tn-seq Explorer was then utilized to count the number of unique transposon insertions for each gene (see Materials and Methods) (Solaimanpour et al., 2015). Sequenced reads from our libraries revealed an average of ~73,000 unique transposon insertion sites in each library, corresponding to approximately 25x coverage of the *L. monocytogenes* genome. To determine the limit of detection (LOD) for each sample, the sliding window method on Tn-seq Explorer was employed, which counts the number of unique transposon insertions in overlapping windows of a fixed size (Solaimanpour et al., 2015). The appropriate sliding window length is automatically determined by Tn-seq Explorer for each sample, resulting in a bimodal distribution for the number of insertions within a given window, where the left peak consists of putative essential genes with low unique insertion counts and the trough that separates the two modes is determined as LOD (Solaimanpour et al., 2015). We found 391 genes with the number of unique transposon insertions below LOD across all 9 replicates and claimed these genes as essential genes in *L. monocytogenes*, corresponding to a similar number of essential genes in *L. monocytogenes* suggested in the literature (Fischer et al., 2022). A closer comparison found 300 genes overlap between ours and Fischer et al.'s essential gene list (Figure S3.1; Table S3.1). Genes that are uniquely identified as essential in this study or in the previously published screen are highlighted in Table S3.1 (Fischer et al., 2022b). As expected, most genes that encode for tRNAs or rRNAs were found to be essential (Figure 3.1B, ring 1 and 2 from the innermost ring). Furthermore, KEGG orthology mapping uncovered that most essential genes are involved in translation and metabolism (Figure 3.1C). Taken together, this data demonstrates that a subset of genes is essential for general survival in *L.*

monocytogenes and the remaining genes in the *L. monocytogenes* could contribute to virulence in some manner.

Identification of *L. monocytogenes* genes important for intracellular fitness

An *ex vivo L. monocytogenes* TIS screen through J774 mouse macrophages has been previously described, where macrophages were infected for 24 hours and 42 genes were identified to be required for macrophage infection (Fischer et al., 2022). However, with a 40-minute doubling time of *L. monocytogenes*, the long 24-hour replication period most likely led to cell deaths of the macrophages, which could be a limitation for assessing *L. monocytogenes*' intracellular survival. To determine genes important for intracellular survival and replication, we infected mouse bone marrow-derived macrophages (BMDMs) with the transposon library at a low multiplicity of infection (MOI) of 0.5 and collected samples at a much earlier time point, 6-hour post-infection (hpi) since in our preliminary study, we observed around 10-fold replication of *L. monocytogenes* at 6 hpi (Figure 3.2A). We infected 10 million BMDMs, screening approximately 5 x 10^6 transposon mutants in each biological replicate, which is around 2000-fold coverage of the *L. monocytogenes* genome. Prior to infection, the transposon library was recovered by cultivation in BHI broth at 37°C 250 rpm for 30 minutes. After recovery of the library, we took a subpopulation, approximately 5 x 10^6 CFU, from the library as our reference "input" population, corresponding to the number of transposon mutants used for infection (Figure 3.2B). Our ultimate goal is to identify genes important *in vivo* under intact immune selection pressure, which is described later on in this study. One challenge in *in vivo* TIS screening is that in an animal host, during DNA extraction,

there is a high percentage of host DNA contaminant. Therefore, an outgrowth process for *L. monocytogenes* is needed to enrich for *L. monocytogenes* genomic DNA (gDNA). To be able to compare the results from our *ex vivo* and *in vivo* TIS screens, we followed the same procedure post-infection after extracting the transposon mutants from the host, where we cultivated the mutants in BHI+200 µg/mL streptomycin at 37°C shaking for 5 hours (~6 generations), resulting in our "output". The inputs also went through the same cultivation process as the outputs.

Tn-seq Explorer was used to calculate unique transposon insertion counts and total read counts for each gene and to determine LOD. Total read counts for each gene was then adjusted and normalized to sequencing depth and gene size (see Materials and Methods). Genes with the number of unique insertions below LOD in any individual input sample were eliminated from the analysis, resulting in the exclusion of 611 genes which includes the previously identified 391 essential genes. A comparison of the normalized read counts for each gene between the inputs and outputs indicated that 96 genes in *L. monocytogenes* were more than 2-fold negatively selected and statistically significant (p-value < 0.05) during BMDM infection (Figure 3.2C; Table 3.2); whereas only 42 genes were discovered as important in previously published screen (Fischer et al., 2022). A closer comparison between the genes we found to be important and the genes Fischer et al. identified, revealed that only 19 genes overlap the two lists (Figure S3.2; Table S3.2). To validate our screening approach, we assessed the selection of known virulence genes that form the *Listeria* pathogenicity island LIPI-1, including *actA*, *hly*, *mpl*, *plcA*, *plcB*, and *prfA*. Importantly, *hly* and *prfA* mutants were found to be highly

attenuated (>10-fold) in our TIS screen, which provided confidence in our screening approach (Portnoy et al., 1988; Freitag et al., 1993). *plcA* showed a little over a 2-fold reduction in the output compared to the input, and deletion of which have also been to have limited growth in BMDMs starting from 3 hpi (Camilli et al., 1993). *mpl* was excluded from our analysis due to low transposon insertions in the inputs. *actA* and *plcB* were not required for intracellular growth. However, this is not surprising since *actA* is required for cell-to-cell spread and *plcB* is employed for escaping secondary vacuole after spreading into a neighboring cell, which are dispensable under our screening condition within 6 hours of infection (Portnoy et al., 2002; G. A. Smith et al., 1995). Additionally, genes associated with cell division that have been shown to contribute to virulence, including *divIVA, secA2, ftsK* were determined to be essential for intracellular fitness in both our TIS screen and in the published screen (Halbedel et al., 2012; Lenz et al., 2003; Fischer et al., 2022). Some examples of genes that were only negatively selected for fitness in BMDMs in our screen but were found dispensable in the published screen include *yjbH* and genes encoding for galactitol-specific PTS system (*LMRG_00184, LMRG_02211*, *LMRG_01248*) (Table S3.2) *yjbH* has been described to affect intracellular growth and alter the expression of virulence and phosphotransferase system (PTS) genes under oxidative stress, including genes that encode for the galactitol-specific PTS system (C. Cheng et al., 2021).

KEGG orthology functional analysis further revealed that most genes required for intracellular fitness are involved in metabolism, including genes that have previously been linked to virulence; such as genes involved in purine biosynthesis (*purA, purB*),

menaquinone biosynthesis (*aroA*, *aroB, aroE, aroF, menB, menC, menD, menE, menF, menI*), and TCA cycle (*pdhA, pdhB, pdhC, pdhD*) (Figure 3.2D) (Faith et al., 2012; G. Y. Chen, McDougal, et al., 2017; H. B. Smith et al., 2021; Rivera-Lugo et al., 2022; H. B. Smith et al., 2023). Genes involved in purine biosynthesis and a subset of genes required for menaquinone biosynthesis (*aroE, aroF, menB, menC, menF, menI*) were also shown to be important by Fischer et al. Genes that have not been implicated with a role in intracellular survival or virulence that act in pantothenate and CoA biosynthesis (*panB, panC, LMRG_01195*) and serine and threonine metabolism (*hom, thrB, thrC*) were also identified in our screen. *thrC* was also implicated a role in intracellular survival but further testing with clean deletion of *thrC* did not show a defect in intracellular replication (Fischer et al., 2022b). However, the data was not shown in the previous study, and the identification of multiple genes involved in the pathway in our screen suggests a potential role for serine and threonine metabolism in regulating intracellular replication. Genes with putative role in cell wall metabolism (*walK, yycH*) and genes that encode for ATP synthase (*atpA, atpB, atpC, atpD, atpE, atpF, atpH, atpI*) were also found to be critical for macrophage replication. Taken together, our TIS screen using BMDMs revealed known and unknown mechanisms that *L. monocytogenes* utilize to survive and replicate *ex vivo*.

Identification of *L. monocytogenes* genes important for inflammasome immune defense

In previous non-TIS based screens we have identified *L. monocytogenes* genes critical for defense against cell-intrinsic immune defenses (G. Y. Chen, McDougal, et al., 2017).

When *L. monocytogenes* is in the host cytosol, multiple innate immune signaling pathways are employed by the host to defend against the infection. One example of which is inflammasome signaling, which can be activated through the detection of LLO, flagellin, or bacterial DNA (Mariathasan et al., 2006; Sauer et al., 2010; Theisen & Sauer, 2016). Inflammasome signaling results in caspase-1 activation which is a protective mechanism by the host as it has been shown that inflammasome activation attenuates *L. monocytogenes* virulence (Sauer et al., 2010; Sauer, Pereyre, et al., 2011). Therefore, to survive in the cytosol and promote virulence, it is crucial for *L. monocytogenes* to avoid detection by the inflammasome through mechanisms such as avoiding cytosolic lysis (Sauer et al., 2010). We hypothesized that some *L. monocytogenes* virulence determinants essential for replication in WT macrophages might be dispensable in caspase-1 deficient macrophages due to their critical role for evading inflammasome-mediated immunity. To explore virulence determinants *L. monocytogenes* utilizes to defend against inflammasome-mediated immune response, we performed a TIS screen through caspase-1 deficient BMDMs. 552 genes were eliminated from the analysis of the caspase-1 deficient BMDM TIS screen due to unique insertions for any individual input sample falling below LOD. A comparison of WT BMDM and caspase-1 deficient BMDM TIS screens revealed 41 genes that are uniquely negatively selected in WT BMDMs and 29 genes that are uniquely negatively selected in caspase-1 deficient BMDMs (Figure 3.3A; Table 3.2). 14 out of the 29 genes that were found to be important only in caspase-1 deficient BMDM had low unique transposon insertion counts in the inputs and therefore were excluded from the analysis in our WT BMDM TIS screen. Among the remaining 15 genes that were uniquely

negatively selected in caspase-1 deficient BMDM, 12 of them also had similar fold reduction in WT BMDM but were not identified due to loss of statistical significance, and 3 of which were right below the cutoff of 2-fold reduction (Table 3.2). 5 out of the 41 genes that were only required in WT BMDM were eliminated from the analysis in our caspase-1 deficient BMDM screen due to low unique transposon insertion counts in the input, leaving 36 genes that are important only under WT BMDM immune selection pressure but are dispensable in the absence of caspase-1 signaling (Figure 3.3A,B).

KEGG module mapping demonstrated that most of the genes that are required in WT BMDMs but dispensable in the absence of Caspase-1 BMDMs are involved in shikimate and menaquinone biosynthesis (Figure 3.3C). Interestingly, these pathways are interconnected. The shikimate pathway generates chorismite, which further feeds into menaquinone biosynthesis pathways. Our findings suggested a link between these metabolic pathways and caspase-1-dependent defense in *L. monocytogenes*. Previous studies have demonstrated that DHNA-deficient *L. monocytogenes* strains exhibited increased bacteriolysis in the macrophage, which suggests that their defect for intracellular survival may be due to increased activation of the inflammasome (G. Y. Chen, McDougal, et al., 2017; H. B. Smith et al., 2021). Genes with a putative role in cell wall metabolism (*pbp1A* and *walK*) were highly attenuated in WT BMDMs but not non-essential in caspase-1 deficient macrophages, suggesting that these genes may play an important role in cell wall synthesis to prevent lysis in the host cells to further avoid detection by the inflammasome. Genes that encode for the galactitol-specific PTS system (*LMRG_00184*, *LMRG_01248*, *LMRG_02211*) also became dispensable in

caspase-1 BMDMs, suggesting a novel link between galactitol utilization and inflammasome evasion. Altogether, we demonstrated the utility of using knockout host models to identify bacterial genes associated with specific functions through TIS screens. Here, we discovered genes important for *L. monocytogenes* to evade inflammasome-mediated immune defense in the host.

Establishment of zebrafish tail wound infection model for TIS screen

Our ex vivo TIS selections have identified genes essential for virulence in primary bone marrow-derived macrophages as well as genes involved in avoiding caspase-1-dependent immune defenses ex vivo. To further discover *L. monocytogenes* genes that are important under selection pressure from an intact innate immune system *in vivo*, we utilized zebrafish as a host for a novel TIS screen. We previously demonstrated that the zebrafish tail wound infection model is a powerful model for studying host immune response to *L. monocytogenes* infections (Miskolci et al., 2019; S. Shen et al., 2024). To further characterize the zebrafish tail wound infection method for performing *in vivo* TIS screens, we first determined the optimal *L. monocytogenes* dose for infection. We infected 3 day-post-fertilization (dpf) zebrafish larvae with a low (5×10^8 CFU) and a high (5×10^9 CFU) inoculum. We found that more *L. monocytogenes* were able to colonize the zebrafish tail fin when infected with the higher inoculum, and with either inoculum, *L. monocytogenes* replicated robustly from 2 to 48 hours post-infection (hpi) (Figure 3.4A). At a 5×10^9 CFU inoculum, approximately 400-500 bacteria *L. monocytogenes* invaded and colonized the tail wound in each zebrafish larvae by 2 hours and these bacteria expanded around 50-fold from 2 to 48 hpi, reaching ~2×10^4

CFU/fish with a leveling out of bacterial burdens between 48-72 hpi. This led us to perform the TIS screen using the higher dose, 5 x 10^9 CFU, as our inoculum and evaluate genes that are negatively selected at 48 hpi to identify genes important for fitness *in vivo*. *hly*, the gene encoding for listeriolysin O is an essential virulence factor ex vivo and in murine models of infection and has been previously suggested to be important for virulence in the zebrafish tail wound infection model (Miskolci et al., 2019). To further validate the zebrafish tail wound model we infected zebrafish with 1:1 mixed ratio of WT and Δ*hly* at a total CFU of 5 x 10^9. In this competitive index model that mimics our proposed TIS selection conditions, Δ*hly* mutants displayed a significant fitness defect while WT was able to replicate robustly, suggesting that the zebrafish tail wound infection model is a suitable system to identify virulence determinants employed by *L. monocytogenes* in a TIS screen (Figure 3.4B). Finally, it is necessary to determine the bottleneck during infection since we are only interested in genes that are negatively selected due to immune selective pressure and not by stochastic processes, and *in vivo* animal infection models often exhibit a large bottleneck (Cain et al., 2020; Chao et al., 2016). Our initial colonization experiments demonstrated that ~400 bacteria infect a tail wound by 2 hpi, therefore, to test for infection bottleneck, zebrafish were infected with a 1:400 mixture of erythromycin-resistant (Erm^R) and kanamycin-resistance (Kan^R) *L. monocytogenes* at a total CFU of 5 x 10^9 (Figure 3.4C). At 2 hpi, Erm^R and Kan^R *L. monocytogenes* colonized the zebrafish tail wounds at an approximately 1:400 ratio and stayed at around this ratio at 48 hpi (Figure 3.4C). This suggests that given a mixed population of 400 random transposon mutants, which is around the number of *L. monocytogenes* that invade each fish, our TIS screen can detect any mutant in the

population with a fitness defect at 48 hpi. This indicates that genes negatively selected from our TIS screen are likely are biologically relevant and due to immune selective pressure.

Zebrafish TIS screen identified genes important for *in vivo* virulence in *L. monocytogenes*

To discover genes important for *in vivo* virulence in *L. monocytogenes*, we infected 490 zebrafish/replicate and performed three biological replicates screening approximately 196,000 transposon mutants for each biological replicate, which is around 75-fold coverage of the non-essential genes in the *L. monocytogenes* genome. After recovery of the transposon library, we took a subpopulation, approximately 5 x 10^7 CFU, from the library as our reference “input” population, corresponding to a roughly equal number of *L. monocytogenes* that we harvested at 48 hpi. 1 x 10^9 CFU/mL inoculum was prepared from the recovered library and used for TIS infection. At 48 hpi, 490 infected zebrafish larvae were pooled, and *L. monocytogenes* was extracted through homogenization (Figure 3.5A).

Despite our previous results suggesting minimal bottleneck in our zebrafish infection model, we found a 50-80% loss of unique transposon insertions in our outputs. Therefore, instead of automatically determining sliding window size by Tn-seq Explorer, we manually adjusted the window size for our outputs. We identified the smallest window length that results in bimodal peaks in each of our outputs and set that as our sliding window size. 587 genes were eliminated from our analysis due to unique

insertions for any individual input sample falling below LOD. After the elimination of these genes, we identified 909 genes that were more than 10-fold negatively selected in zebrafish and were statistically significant (Figure 3.5B). Importantly, there is an over 10-fold reduction for genes in the LIPI-1, including *prfA*, *hly*, *plcA*, *plcB*, and *actA*, in the output compared to input, which provided confidence in the results of our screen, suggesting that the zebrafish model was able to capture genes that contribute to virulence (Figure 3.5B). Like in our WT BMDM TIS screen, *mpl* in the LIPI-1 was also eliminated from the analysis of our zebrafish TIS screen due to not having sufficient transposon insertions in the input. Genes associated with metabolism and transporters, including PTS systems, were the most enriched among the virulence genes *in vivo* (Figure 3.5C). 33 genes encoding for the PTS system were identified to contribute to fitness *in vivo*, while only 5 genes in the PTS system were found to be important *ex vivo* for intracellular survival (Figure 3.2C, 3.5C).

To further examine the differences under cell-intrinsic and intact immune selection pressure, we overlaid genes identified from WT BMDM and zebrafish screens. As expected, most genes found to be essential for intracellular survival and replication were also identified to be crucial *in vivo* (Figure 3.5D). 31 genes were uniquely negatively selected in WT BMDM compared to zebrafish. Out of the 31 genes, 9 genes were not identified in zebrafish due to being below the LOD in the input pools for the *in vivo* screen, and an additional 19 genes were found to be negatively selected *in vivo* but did not meet statistical significance criteria. After excluding these genes, 3 genes remained from the list, *LMRG_01774*, *LMRG_01617*, and *LMRG_01618* (Table 3.3). A

closer examination of these genes discovered that *LMRG_01774* still exhibited a more than 5-fold fitness defect in zebrafish but was less than the 10-fold cutoff. Interestingly, *LMRG_01617* and *LMRG_01618* both encode for ABC transporter and *LMRG_01618* was also found to be important in previously published *L. monocytogenes* Tn-seq screen (Fischer et al., 2022b). 844 additional genes were identified to contribute to virulence *in vivo* compared to *ex vivo*. Out of the 844 genes, 37 genes were excluded from the BMDM TIS screen analysis due to input samples being below the LOD (Figure 3.5D). KEGG orthology mapping further revealed that most genes that were only negatively selected *in vivo* but not *ex vivo* are involved in carbohydrate metabolism and amino acid metabolism, which could be due to the higher nutritional stress present in an animal host compared to a cell culture mode (Figure 3.5El. Overall, this suggests that in an intact animal host, bacterial pathogens are under very different immune-mediated stress compared to an *ex vivo* environment. Taken together, the overwhelming number of virulence leads require additional approaches to prioritize these leads.

Evaluation of TIS screen virulent candidates filtered by in-silico protein-protein interaction (PPI) predictions combined with published upregulated gene list *in vivo*

Our zebrafish TIS selection suggests a very large number of genes that contribute to *L. monocytogenes* virulence *in vivo*. To prioritize the selection of candidate genes derived from the TIS screen for further study, we performed in-silico protein-protein interaction prediction by applying deep learning algorithms, AlphaFold and RoseTTaFold2-Light, to the *L. monocytogenes* genome (Humphreys et al., 2021). RoseTTaFold2-Light

predicted de novo protein-protein interactions (PPIs) by aligning *L. monocytogenes* genes to orthologues of other bacterial species and utilizing information on co-evolving proteins. AlphaFold then provided a secondary stringent reevaluation and was used to model complex structures, revealing a list of 3316 PPI pairs (Figure 3.6A). By overlaying the virulence candidates from the zebrafish TIS screen with the predicted PPI gene list, we found 614 virulence candidates with at least one interacting partner predicted by deep learning (Figure 3.6B). Furthermore, we identified 431 PPI pairs consisting of two virulence genes since if two genes that interact with each other are both suggested to be important for fitness *in vivo*, this would suggest these genes may work in pairs to contribute to pathogenicity. These 431 PPI pairs consist of 393 unique genes (Figure 3.6B). Focusing on these genes would provide higher confidence for these refined candidates to indeed be critical for virulence rather than choosing any TIS screen candidates at random. Next, to further strengthen the confidence in our virulence candidates, we eliminated any genes that are predicted to have more than 5 interacting partners under the assumption that these proteins may be sticky in nature and interactions predicted for these proteins could be false positives (Figure 3.6B).

To further narrow down the candidates, we applied an additional filter, focusing on genes that are also upregulated *in vivo*. Camejo et al. identified 457 genes in *L. monocytogenes* that are upregulated *in vivo* in mice spleen throughout the time course of 24–72 hpi, and we found that 437 of these *in vivo* upregulated genes are crucial for survival in zebrafish (Figure 3.6B). When we applied all the described filters to our list, this resulted in our final list of refined virulence candidates: 9 PPI pairs, containing 18

unique genes (Figure 3.6B; Table 3.4). 3 out of the 9 PPI pairs, *oppB*/*oppC*, *dltA*/*dltC*, and *fur*/*perR*, have previously been shown to contribute to virulence (Abachin et al., 2002; Krypotou et al., 2019; Berude et al., 2024). Opps are ABC oligopeptide transporters that import cysteine-containing peptides, which have been implicated in controlling the master virulence regulator, PrfA, to promote intracellular growth and *in vivo* virulence (Borezee et al., 2000; Krypotou et al., 2019; Berude et al., 2024). The *dlt* operon plays a role in modifying the net charge of cell wall and deletion *dltA* in *L. monocytogenes* has been shown to be attenuated *in vivo* (Abachin et al., 2002; D'Onofrio et al., 2023). Deletion of *fur* or *perR* in *L. monocytogenes* have both been demonstrated to increase sensitivity to oxidative stress and decrease virulence *in vivo* (Rea et al., 2004; Rea et al., 2005). LLO made up of one of the other PPI pairs; however, its interacting partner is a hypothetical protein.

All the other virulence candidates from the 9 PPI pairs have not been linked to virulence in *L. monocytogenes.* Some of these candidates however have been implicated a role in virulence in other bacterial species. For example, pyruvate formate lyase (PFL) has been shown to promote virulence in *Streptococcus pneumoniae* (Yesilkaya et al., 2009). Genes involved in tRNA post-transcriptional modifications were also identified, including TrmB and MiaA. TrmB is important for regulating oxidative stress in *Pseudomonas aeruginosa* and is critical for stress response and pathogenesis in *Acinetobacter baumannii* (Thongdee et al., 2019; McGuffey et al., 2023). The well-conserved tRNA modifying enzyme MiaA has been described to contribute to virulence in *Shigella flexneri* and extraintestinal pathogenic *Escherichia coli* (ExPEC) (Durand et al., 1997; B.

A. Fleming et al., 2022). However, neither TrmB's nor MiaA's interacting partner, RimP (LMRG_00771/lmo1321) and PhnA (LMRG_00062/lmo0370), respectively, have been linked to virulence. Taken together, combining the approaches of TIS, deep learning PPI prediction, and transcriptomics technologies, we have identified putative PPI pairs involved in pathogenesis. Further investigation of virulence and interactions for these PPI pairs is needed to confirm the validity of our screening approaches. Validation in virulence for these genes would provide insights into potential targets for antibiotic development.

Discussion

Many virulence determinants are required for intracellular pathogens to survive in a cell, defend against a host's immune response, and replicate in a host. Here we performed genome-wide *L. monocytogenes* TIS screens in different contexts, using WT BMDMs, caspase-1-deficient BMDMs, and zebrafish, to identify genes in *L. monocytogenes* important for intracellular survival and replication, inflammasome defense, and infection *in vivo*.

Identifications of genes in *L. monocytogenes* important for standard growth in BHI and intracellular growth in macrophages through TIS screens have previously been described in *L. monocytogenes* (Fischer et al., 2022b). We found 391 genes to be essential in *L. monocytogenes*, closely corroborating to the number of essential genes found in their study (402 genes). However, a closer comparison discovered that only 300 of our essential genes overlap (Table S3.1). A major difference between the two

studies is that we cultivated our library for ~6 generations, but Fischer et al. cultivated their library for ~15 generations before isolating genomic DNA from *L. monocytogenes* and subsequently processing for sequencing, which may result in the discrepancy in the essential genes identified between the two studies. The genes identified in our screen are likely to more closely represent genes that affect *L. monocytogenes*' viability and disruption of which may be lethal in *L. monocytogenes*, while the genes identified in the published screen represent genes important for *in vitro* growth in BHI broth (Fischer et al., 2022b). The variation may also be due to the different methods for constructing the transposon library as a different transposon delivery system, pJZ037, was used to generate our transposon library compared to the published study, pKRMIT. After the transformation of the transposon plasmid into *L. monocytogenes*, mutants were grown on BHI agar plates as monoclonal individual colonies; whereas transposon mutants were cultivated in BHI broth in the published study, which may introduce competition, resulting in the inability to generate certain mutants with growth defects. Additionally, while 10403S was used in our study, EGD-e was used in the published work and there may be a difference between the two *L. monocytogenes* background strains (Fischer et al., 2022b). The information on sequencing depth was not provided in the previous study but it is possible that sequencing was performed at a deeper depth in our study and thus we are capturing more genes and finding fewer genes to be essential for viability in *L. monocytogenes.* Different methods were also used for data analysis between the two studies, which may also result in the discrepancy observed. In this study, we determined the LOD in each replicate using the sliding window approach on Tn-seq Explorer and further identified genes with unique transposon insertions below

the LOD across all nine replicates (Solaimanpour et al., 2015). Whereas, in the previously published study, they calculated the insertion density for each gene and identified the genes with an insertion density below 0.01 (Fischer et al., 2022b). Despite the differences between the two screens, there is a ~75% overlap between the two lists, which provided confidence that the genes we identified are essential in *L. monocytogenes*.

Among the 391 essential genes identified in this study, most genes are associated with translation, including 42 genes encoding for ribosomal proteins and 42 genes encoding for aminoacyl-tRNAs. Enzymes in the fatty acid biosynthesis pathway, except for FabK and FabL, were all found to be essential. Central carbohydrate metabolism (glycolysis, TCA cycle, and pentose phosphate pathway), with 16 genes identified in this pathway, is also important for general growth in *L. monocytogenes.* Although identifications of essential genes provided a better understanding of the general survival of bacteria, antibiotics targeting these factors may lead to suppressor mutants and resistance may emerge (Otoupal et al., 2021). Thus, the identification of conditionally essential genes in bacterial pathogens is important. Targeting genes that are essential for infection but not viability could represent better novel antibiotic targets (Gadar & McCarthy, 2023).

Fischer et al. have also described the first *L. monocytogenes* TIS screen *ex vivo*, utilizing J774 macrophages and sampling *L. monocytogenes* at 24 hpi. While they found 43 genes important for intracellular growth, we identified 96 genes that are important with 19 genes overlapping the two lists. One explanation for the variations could be that

in the published study, the long infection period may lead to macrophage cell death, which could convolute the interpretation of their results. Another major difference is that we utilized primary BMDMs, whereas Fischer et al. used J774 immortalized cell lines, which is not as physiologically relevant. Out of the 77 genes that are only negatively selected for fitness in macrophages from our screen but not from the published screen, 19 of them were identified to be essential for growth in BHI broth in the published study (Fischer et al., 2022b). There have been other studies that reported disruption in 7 out of these 19 genes, including *rbfA*, *era*, *panB*, *panC*, *atpA*, *atpB*, and *pdhC* in *L. monocytogenes*, indicating that loss of these genes is not lethal in *L. monocytogenes* (Auvray et al., 2007; Müller-Herbst et al., 2014; Schauer et al., 2010; van der Veen et al., 2009). Furthermore, *era* mutant has been demonstrated to have a growth defect in broth and *rbfA* mutant has been reported to have a growth defect in broth at a high temperature (42°C) (Auvray et al., 2007; van der Veen et al., 2009). However, no reports have tested the effect of the loss of these genes on *L. monocytogenes*' growth during an infection. Since the transposon mutants go through a much longer cultivation time in BHI broth in the previous study when determining essential genes in *L. monocytogenes*, these mutants may be less fit in BHI broth after 15 generations of growth but not after only 6 generations of replication, which is when we sample our mutants in our study. It is possible that when undergoing a higher selection pressure in the macrophages, we picked up the fitness defect of these mutants *ex vivo*. Therefore, some of the genes we identified to be important for survival and replication in macrophages may be somewhat important but not necessary for growth and replication in general. However, *atpA* and *atpB*, which encode subunits of two ATP synthases have

been reported a role in intracellular replication in *L. monocytogenes*. Furthermore, we also discovered other subunits of ATP synthases, including *atpC*, *atpD atpE*, *atpF*, *atpH*, and *atpI* to be crucial for replication *ex vivo*. While *atpE*, *atpF*, and *atpH* were found required for growth in BHI by Fischer et al., *atpC*, *atpD, atpI* were neither determined to be necessary for growth in BHI nor in macrophages in that study. It has been shown that ATP synthase is important for virulence in *Francisella novicida* (Kraemer et al., 2009). These findings together suggest that ATP synthase plays a prominent role in virulence. However, the exact mechanism by which ATP synthase contributes to virulence in *L. monocytogenes* is not very well understood. ATP synthase is required for the production of ATP, which is important in many physiological processes. Further characterization of why it is necessary for survival in the host can be valuable. *phdC*, which encodes for one of the components of the pyruvate dehydrogenase complex, has also been demonstrated to be crucial for intracellular replication, survival in the host cytosol, cell-to-cell spread, and virulence (G. Y. Chen, McDougal, et al., 2017). Additional to *pdhC*, we also found the rest of the genes that encode the pyruvate dehydrogenase complex, namely *pdhA, pdhB,* and *pdhD*, to be important for intracellular growth in macrophages, which suggests that the pyruvate dehydrogenase complex is likely indispensable during an infection. The mechanism by which PDH contributes to virulence in *L. monocytogenes* is not very well understood. However, it has been reported in *Streptococcus suis* that PDH is important for modulating temperature and oxidative stress (Y. Wang et al., 2019). Importantly, consistent with our finding, deletion of *pdh* in *Streptococcus suis* does not affect *in vitro* growth in broth but is attenuated in macrophages (Y. Wang et al., 2019). Future studies

investigating if PDH regulates stress response in *L. monocytogenes* may provide a better understanding of how *L. monocytogenes* regulate stress in the host.

Both our screen and the published screen found that several genes associated with cell wall synthesis (*secA2, ftsK, divIVA*) are critical for survival and replication *ex vivo*, and all of these genes are known to be involved in virulence (Fischer et al., 2022b; Halbedel et al., 2012; Lenz et al., 2003). In addition to these genes, we have also identified other genes involved in cell wall synthesis that were not found to be important by Fischer et al., such as *sepF*, *pgdA,* and *pbpA1*. Notably, *pgdA* has been shown to catalyze the deacetylation of N-acetylglucosamine (GlcNAc) residue in peptidoglycan and is important for evading the host innate immune response by avoiding detection by the nucleotide-binding oligomerization domain 1 (NOD1) (D'Orazio, 2019). Corroborated with previous findings, all genes involved in the steps of the synthesis of 1,4-dihydroxy-2-naphthoyl acid (DHNA) from chorismite except for *menH* were identified to be important for intracellular survival (*menF, menD, menC, menE, menB, menI*) while *menA* and *menG*, which are involved in the synthesis of the full-length menaquinone are dispensable (G. Y. Chen, McDougal, et al., 2017; H. B. Smith et al., 2021). We also found the enzymes, LMRG_02522, AroE, and AroF, which facilitate chorismite synthesis from shikimate to be crucial. *menB, menC*, *menF*, *aroE*, and *aroF* were also identified important for intracellular growth in macrophages by Fischer et al. Altogether, findings from previous studies further provided validation and confidence in our screening approach.

In this study, to further identify genes that are required for defending against inflammasome-mediated immune response, we performed a TIS screen using caspase-1-deficient BMDMs. Interestingly, genes involved in the synthesis of DHNA from shikimate (*LMRG_02522, aroE, aroF, menF, menD, menC, menE, menB, menI*) all became dispensable in the absence of caspase-1 BMDMs (G. Y. Chen, McDougal, et al., 2017; H. B. Smith et al., 2021). Further studies validating that the deletion of enzymes involved in the synthesis of DHNA in *L. monocytogenes* leads to attenuation in WT BMDMs that are primed, to ensure activation of the inflammasome, and that their growth is rescued in caspase-1 deficient BMDMs is required. Altogether, our findings suggest that DHNA, the precursor of menaquinone, may regulate inflammasome signaling.

Interestingly, studies have identified DHNA as an agonist of the aryl hydrocarbon receptor (AhR) (Fukumoto et al., 2014; Y. Cheng et al., 2017). Additionally, activation of AhR has been shown to inhibit NLRP3 transcription and suppress NLRP3 inflammasome signaling (Huai et al., 2014). We hypothesize that DHNA synthesized by *L. monocytogenes* could activate AhR signaling and further dampens inflammasome signaling. While other pathogens; such as *Yersinia spp*. and *Pseudomonas aeruginosa*, have evolved ways to inhibit inflammasome activations, there is little evidence of inflammasome inhibition by *L. monocytogenes* (Theisen & Sauer, 2016). To determine if DHNA may act through NLRP3 inflammasome, future studies can examine if the growth of DHNA mutants is rescued in NLRP3 deficient macrophages. Measuring caspase-1, IL-1β, and IL-18 activation through Western blot and ELISA, and quantification of

pyroptosis through lactate dehydrogenase (LDH) release assay in WT macrophages and AhR deficient macrophages by WT or DHNA *L. monocytogenes* mutants could further provide better insight into the correlation of DHNA and inflammasome signaling.

Additionally, genes that encode for the galactitol-specific PTS system (*LMRG_00184, LMRG_02211*, *LMRG_01248*) were also only negatively selected for fitness in WT BMDMs but not in caspase-1 deficient BMDMs. Further validation that clean deletions of these mutants are attenuated in WT BMDMs but have no effect on growth in caspase-1 deficient macrophages would suggest that *L. monocytogenes* may preferentially utilize galactitol as a carbon source to avoid activation of the inflammasome. The galactitol-specific PTS system is not very well studied. Galactitol is formed when there is a galactose buildup and galactitol can cause excessive stress to the host cell (Succoio et al., 2022). We hypothesize that *L. monocytogenes* might uptake galactitol to prevent oxidative stress in the host cell to avoid detection by the host and prevent inflammasome activation. Future studies exploring genes that may be regulated by galactitol-specific PTS systems during infection through RNA-sequencing and identifying genes that are differentially expressed in galactitol-PTS specific mutants may provide a better insight on why the galactitol-specific PTS systems may be important for intracellular growth and survival and why it might play a role in regulating inflammasome defense. A better characterization of the galactitol-specific PTS system and the mechanism by which galactitol usage promotes virulence will provide a better understanding of the pathogenesis of *L. monocytogenes*. Confirmation that the genes we identified are critical for survival in WT BMDM and play a part in avoiding or reducing

inflammasome activation could further support the validity and the utility of using genetic knockout hosts for TIS screens.

In this study, we also identified genes in *L. monocytogenes* that contribute to *in vivo* virulence. The factors that contribute to *L. monocytogenes* virulence in the host have not been thoroughly investigated at a genome-wide level. Due to bottlenecks in animal hosts, *in vivo* TIS screens have been challenging. The very first *L. monocytogenes in vivo* TIS screen was recently described using the RECON$^{-/-}$ murine infection model (Stamm et al., 2024). RECON$^{-/-}$, an immune-deficient mouse model, allows for a higher dose of *L. monocytogenes* to colonize and infect the host, which has revealed unknown virulence determinants in *L. monocytogenes* that are dispensable *ex vivo*. However, the low transposon insertion density of their transposon library may have prevented them from capturing smaller-size genes that are also important for survival in the host. Additionally, the small number of mice used in the study may have also obscured the identification of other virulence determinants. Contrary to what have been demonstrated in the literatures, they identified a lot of genes with tissue-specific phenotypes in the spleen compared to the liver, which is not a norm in *L. monocytogenes* pathogenesis. Therefore, a more comprehensive *L. monocytogenes* genome-wide screen *in vivo* is needed for a better global understanding of *L. monocytogenes*' pathogenesis. Here to overcome the bottleneck in animal models, we employed larval zebrafish as our model host, which enables us to have a much bigger sample size. Studies have demonstrated zebrafish as a viable model for performing bacterial genetic screens (Stoop et al., 2011; Wiles et al., 2013). We previously demonstrated that *L. monocytogenes* can colonize

zebrafish transected tail wounds (Miskolci et al., 2019; S. Shen et al., 2024). Utilizing the high fecundity and cheap cost of zebrafish and the high-throughput infection method, we were able to infect 490 larval zebrafish, screening approximately 196,000 transposon mutants in each of three biological replicates, which is difficult to achieve using other animal models.

Although our preliminary studies, where we infected a mixed population of two different antibiotic-resisting WT *L. monocytogenes*, suggested minimal effects from the bottleneck in our infection model, we found around 50-80% loss of unique transposon insertions in the outputs compared to inputs in our zebrafish TIS screen, indicating the possibility of bottleneck selection. A potential way to mitigate the impact of bottlenecks from the zebrafish model is to increase more biological replicates to increase statistical power. Despite the loss of statistical significance potentially due to bottlenecks in some of the genes in our zebrafish TIS screen, we still identified 909 genes that are important for fitness *in vivo*. Many more genes were found to be important for fitness *in vivo* compared to *ex vivo*, demonstrating the discrepancy between *in vivo* and *ex vivo* models. However, due to the bottleneck observed, the likelihood of false positives identified from our TIS screen could be high. Future studies verifying the role of these genes in virulence is necessary.

Surprisingly, 2 genes that are dispensable for fitness *in vivo* in zebrafish were required for intracellular growth in BMDMs. Interestingly, both of these genes, *LMRG_01617* and *LMRG_01618*, are in the same operon and associated with the ABC transport system.

Both of these genes were also identified to be required for intracellular growth by Fischer et al. However, little is known about these genes in *L. monocytogenes*. Further characterizations of these genes may uncover differences in nutrient sources in a host cell compared to an intact host. On the other hand, 807 genes were important for fitness only *in vivo* but not *ex vivo*. Among those genes, 11 genes (*fliP, flhA, flgG, motA, fliM, flgL, fliD, fliS, fliG, fliH, sigL*) are associated with flagellar assembly. However, this may be a result of an artifact from our infection method. *L. monocytogenes* that expresses flagella may be more fit to swim to the wound to colonize the zebrafish. We also identified 78 genes involved in amino acid metabolism which were not negatively selected *ex vivo.* These genes were likely not found to be important *ex vivo* due to the amino acids being supplemented in the cell culture medium masking the importance of these genes, which is a limitation in cell culture models. Interestingly, multiple genes encoding for the fructose PTS system (*LMRG_00092, LMRG_00118, LMRG_00120, LMRG_02803*) and involved in the fructose metabolism (*LMRG_00187, LMRG_00224, LMRG_00225, LMRG_01246, LMRG_02784, LMRG_02803, LMRG_02807*) were also found, suggesting that fructose may be an important energy source for *L. monocytogenes in vivo*.

Since approximately one-third of the genes in the *L. monocytogenes* genome were identified as virulence genes in our zebrafish TIS screen, to prioritize the selection of virulence candidates for future studies, we predicted de novo protein-protein interactions through proteome coevolution utilizing deep learning methods and identified PPI pairs constitute of two *in vivo* virulence proteins (Cong et al., 2019; Humphreys et

al., 2021). Additionally, we prioritized the genes in those PPI pairs that have been shown to be upregulated in vivo using published transcriptomic data and selected those PPI pairs as our final virulence candidates (Camejo et al., 2009). This final list consists of 9 PPI pairs (18 genes). 3 out of the 9 PPI pairs have been shown to contribute to virulence (OppB/OppC, DltA/DltC, Fur/PerR). Future studies verifying the interactions between the other 6 PPI pairs (LLO/LMRG_02629, MiaA/LMRG_00062, TrmB/RimP, PflA/FliS, MrsA/LMRG_00459, LMRG_00751/LMRG_00563) predicted by deep learning using the bacterial two-hybrid (Bacterial Adenylate Cyclase-Based Two-Hybrid (BATCH)) system are necessary to support the validity of our protein-protein interaction approach (Karimova et al., 2017). Additionally, generating clean deletions of these 12 genes in *L. monocytogenes* and validating the virulence defects of these mutants in a murine model of listeriosis is important. Validation of virulence in the murine model would strengthen the confidence and utility of using zebrafish as an infection model for *L. monocytogenes*. There are many different reasons that a gene may be important for virulence, one of which is the regulation of cell-to-cell spread. To test if these mutants are attenuated due to a defect in phagosomal escape, replication, or cell-to-cell spread, a plaque assay can be employed in future studies. Since a plaque assay encompasses evaluation for all these important processes required for *L. monocytogenes* to sustain infection *ex vivo*, it will be interesting to identify mutants that are not attenuated in a plaque assay but are confirmed for attenuation *in vivo*. This would suggest that cell culture models might not be capable of encapsulating the immune selective pressures *in vivo*. We hypothesize that proteins in a pair likely work together through the same mechanism to promote virulence. LLO contributes to virulence by facilitating the escape

of *L. monocytogenes* from the phagosome. Therefore, future studies could test if LLO's predicted partner, LMRG_02629, may also be involved in this process. MiaA, TrmB, RimP, and MsrA have all been demonstrated to be involved in regulating stress responses in other bacterial species, but little is known about the role of these proteins in *L. monocytogenes* (Dhandayuthapani et al., 2001; B. A. Fleming et al., 2022; McGuffey et al., 2023; Poonam et al., 2019). The interacting partner of MiaA and MsrA, LMRG_00062 and LMRG_00459, respectively, are not very well studied. Future studies investigating the growth of these PPI *L. monocytogenes* mutants and elucidating their involvement in stress modulation *in vivo* can be valuable for comprehending some of the virulence strategies employed by bacteria.

Overall, our findings provided a comprehensive understanding of the genetic factors crucial for *L. monocytogenes*' pathogenesis. Here, we highlighted the importance of using multiple models to capture a complete picture of bacterial virulence and demonstrated the potential of using zebrafish as a model for TIS screens. Future work should focus on validating these findings in more physiologically relevant models and exploring the mechanisms underlying the identified genes' roles in virulence and immune evasion. Better characterization of the functions of these genes could shed light on potential antibiotic targets.

MATERIALS AND METHODS

L. monocytogenes strains and growth conditions

All *L. monocytogenes* strains used in this study were in the 10403s background (Edman et al., 1968). Erythromycin-resistant *L. monocytogenes* (Erm^R) was made by integration of pPL2e, derived from pPL2 with chloramphenicol resistance cassette replaced by erythromycin resistance cassette (Lauer et al., 2002). Kanamycin-resistant *L. monocytogenes* (Kan^R) was made by integration of pIMK, a kanamycin-resistant vector (Monk et al., 2008). *L. monocytogenes* was grown at 30°C or 37°C in brain–heart infusion (BHI) broth (Becton, Dickinson and Company, Sparks, MD). Antibiotics were used at concentrations of 200 µg/mL streptomycin (BP910-50; Fisher Scientific), 30 µg/mL kanamycin (BP906-5; Fisher Scientific), and 2 µg/ml erythromycin (227330050; Acros Organics).

L. monocytogenes transposon library construction

Transposon delivery plasmid, pJZ032, was prepped (Zemansky et al., 2009). Plasmid was cleaned up through 3 rounds of phenol/chloroform extraction 3. Electrocompetent *L. monocytogenes* were generated as previously described (Park & Stewart, 1990) with the exception that vegetable peptone broth was used in place of BHI to increase electroporation efficiency (Zemansky et al., 2009). ~2 µg pJZ032 was electroporated into ~50 µL electrocompetent *L. monocytogenes* and recovered in 1 mL of vegetable peptone broth + 0.5 M sucrose at 30°C for 1 hour. Recovered *Lm* were then plated on BHI Erm plates for 48 hours at 30°C. Then plates were incubated at 41.5°C for 24 hours to cure the plasmid. Colonies were replica plated onto fresh BHI Erm plates and grown at 41.5°C for an additional 24 hours. Finally, colonies were harvested in PBS using a

sterile cell scraper and resuspended in BHI + 40% glycerol for storage at -80°C with ~10^9 CFU in ~100 μL in each frozen transposon insertion library cryogenic vial.

Library preparation for sequencing

L. monocytogenes was pelleted from input or output BHI cultures. Genomic DNA was then purified using the MasterPure Gram-positive DNA purification kit (Lucigen) according to the manufacturer's protocol with the exception that 5 U/μl mutanolysin was used in place of lysozyme. Extracted DNA was sheared by Covaris by the University of Wisconsin-Madison Biotechnology Center followed by end-repair using NEBNext® End Repair Module (New England Biolabs). After end-repair, DNA was purified with Qiagen MiniElute PCR cleanup kit and 1 μg of cleaned-up end-repaired DNA was then used in C-tailing reaction where a poly-(C)-tail was added to the 3' end of DNA sequences using terminal deoxynucleotidyl transferase (Promega) and 9.5 mM dCTP + 0.5 mM ddCTP (Sigma). C-tailed DNA was then purified using a DTR gel filtration column (EdgeBiosystem). Finally, to amplify *L. monocytogenes* gDNA and attach sequencing adaptors for Illumina sequencing, PCR was performed using a forward primer that binds to the transposon sequence with a sequencing adaptor linked to the 5' end and a reverse primer containing a poly-(G) chain that binds to the poly-(C)-tails with sequencing adaptor attached to the 3' end (see Table S3.4 for primer sequences). Prepared libraries were then submitted to University of Wisconsin-Madison Biotechnology Center for Illumina paired-end NovaSeq 6000 sequencing at a depth of 7 to 20 million reads per sample.

TIS data analysis

Galaxy was used to process sequenced reads (The Galaxy Community et al., 2022). *L. monocytogenes* 10403s genome from the NCBI database (NCBI RefSeq assembly GCF_000168695.2) and sequencing results FASTQ files were uploaded to Galaxy. First, “FASTQ Trimmer” was run to trim sequenced reads to 20 bp from the transposon insertion start site, removing all non-genomic sequences, including sequencing adaptors and transposon, from the sequenced reads with truncated *L. monocytogenes* genomic DNA (gDNA) remaining. truncated down to 20 bp from the transposon insertion site. Next, we removed any bad sequenced reads by running “Filter by quality” and “Remove sequencing artifacts”. We then map the cleaned-up sequenced reads to the *L. monocytogenes* genome using “Bowtie2”. Finally, we utilized Tn-seq Explorer to calculate the number of total transposon insertion counts and unique transposon insertion counts in each gene across the *L. monocytogenes* genome excluding insertion counts located in the first 5% (from 5’ end) or last 20% (from 3’ end) of each gene (Solaimanpour et al., 2015). The sliding window method was used to determine the limit of detection. Appropriate sliding window lengths were determined automatically by Tn-seq Explorer except for zebrafish output samples, where sliding window lengths were manually adjusted to generate proper bimodal peaks. Genes in input samples with unique insertion counts below LOD in any replicate were excluded from our analysis. We accounted for variation in sequencing depth by normalizing the transposon insertion counts to per million sequenced reads that are mapped to the genome. Additionally, we normalized our insertion counts per million reads by gene size, resulting in our final “normalized read counts”. To determine the LOD for normalized read counts for output

samples, we found the lowest normalized read counts among the genes with unique insertion counts above LOD in the outputs. Next, we converted normalized read counts to LOD for genes with unique insertions below LOD in the outputs. Finally, fold change $(\frac{\text{Input}}{\text{Output}})$ of final normalized read counts was calculated.

L. monocytogenes essential gene determination

To identify essential genes in *L. monocytogenes*, 9 input samples from different biological replicates were prepared and sequenced. Essential genes were determined by identification of genes with unique transposon insertion counts below LOD across all 9 replicates.

Testing intracellular growth in bone marrow-derived macrophages (BMDMs)

Bone marrow-derived macrophages (BMDMs) were extracted and differentiated from C57BL/6 mice or caspase-1 deficient C57BL/6 mice as previously described (Jones & Portnoy, 1994). BMDMs were seeded at $5x10^5$ cells/well in a 24 plate overnight. WT *L. monocytogenes* was grown overnight (16–18 hours) at 30°C in BHI on a slant. BMDMs were infected at an MOI of 0.5. Spin-infection was performed to increase infection efficiency by spinning the cells at 500 xg for 10 minutes at 4°C after inoculation. At 30 minutes post-infection, BMDMs were washed with pre-warmed BMDM medium three times and treated with 50 μg/mL gentamicin. At 2 hpi, medium containing gentamicin was removed and replaced with pre-warmed BMDM medium. To determine number of bacterial cells, BMDMs were lysed with 1% saponin and plated on LB plates to quantify

for CFU at indicated time points post-infection. 8 biological replicates were performed with 3 technical replicates in each biological replicate.

BMDM TIS screen

For each biological replicate, BMDMs were seeded at $5x10^5$ cells/well in 20 wells a 24-well plate overnight. One vial of *L. monocytogenes* transposon library with approximately $1x10^9$ transposon mutants was thawed and washed with PBS for each replicate. Transposon libraries were recovered by culturing in 3 mL BHI at 37°C at 240 rpm for 30 minutes. BMDMs were infected with recovered transposon mutants at a MOI of 0.5. Spin-infection was performed to increase infection efficiency by spinning the cells at 500 xg for 10 minutes at 4°C after inoculation. 1-hour post-infection (hpi), BMDMs were washed with pre-warmed BMDM medium three times and treated with 50 μg/mL gentamicin for 1 hour. Medium containing gentamicin was then removed and replaced with fresh pre-warmed medium. At 6hpi, “output” samples were collected by lysing BMDMs with 1% saponin. Lysed cells containing *L. monocytogenes* were pelleted and washed with PBS and resuspended in 25 mL 200 μg/mL streptomycin BHI. Cultures were then incubated at 37°C at 250 rpm for 5 hours. We define our “input” as pooled ~5 x 10^6 transposon mutants from the recovered transposon library, similarly, cultured in 25 mL BHI containing 200 μg/mL streptomycin at 37°C at 250 rpm for 5 hours. Three biological replicates were performed.

Zebrafish husbandry and handling

All protocols using zebrafish in this study has been approved by the University of Wisconsin-Madison Research Animals Resource Center (protocol M005405-A02). Adult zebrafish were maintained on a 14 hr:10 hr light/dark schedule. Upon fertilization, embryos were transferred into E3 medium (4.96 μM NaCl, 0.18 μM KCl, 0.33 μM CaCl2∗2H2O, 0.4 μM MgCl2∗6H2O, 0.1% methylene blue) and maintained at 28.5°C. Larval WT AB zebrafish strain was used in this study when sex cannot be determined.

Zebrafish tail wound transection infection

L. monocytogenes strains were grown overnight in BHI slanted at 30°C. Bacteria were sub-cultured for ~1.5-2 hours in fresh BHI (4:1, BHI:overnight culture) to achieve growth to OD_{600} ≈ 0.6–0.8). 1 mL of the mid-logarithmic phase bacterial culture was spun down and washed three twice in sterile phosphate-buffered saline (PBS). 3 day-post-fertilization (dpf) larvae were anesthetized in E3 medium containing 0.2 mg/mL tricaine (ethyl 3-aminobenzoate; Sigma-Aldrich) and *L. monocytogenes* resuspension with respective doses indicated in the figure legends. To infect, caudal fins of larvae were transected using a surgical blade (Feather no. 10) at the tip of the notochord without injury to the notochord. After caudal fin transection, larvae with tricaine E3 medium containing *L. monocytogenes* were transferred to new tissue culture-treated dishes and incubated for 1 hour on a horizontal orbital shaker at a gentle speed (75-100 rpm). Larvae were then rinsed with E3 medium and maintained at 28.5°C until CFU plating at indicated time points. 10 larvae were pooled for each condition at each time point and homogenized in 150 μL PBS and homogenates were plated for CFU quantification.

In vivo zebrafish bottleneck testing

Two marked WT *L. monocytogenes* strains were utilized, one carrying pPL2e plasmid and the other carrying pIMK plasmid, conferring resistance to 2 µg/ml erythromycin and 30 µg/mL kanamycin respectively (Lauer et al., 2002; Monk et al., 2008). Since ~400-500 *L. monocytogenes* get into the transection wound and colonize the zebrafish tail fin in each larva (Figure 3.4A), inoculum containing WT pPL2e and WT pIMK *L. monocytogenes* at an approximately 1:400 ratio at a total CFU of 5×10^9 was prepared. 10 larvae were pooled and CFUs were quantified at indicated time points.

In vivo zebrafish TIS infections

For the zebrafish TIS screen, for each replicate, one vial of *L. monocytogenes* transposon library with approximately $1x10^9$ transposon mutants was thawed and washed with PBS. Transposon libraries were recovered by culturing in 3 mL BHI at 37°C at 240 rpm for 30 minutes. 70 3 dpf zebrafish larvae were placed in 5 mL $5x10^9$ CFU *L. monocytogenes* tricaine E3 resuspension in a 60 mm dish. For each biological replicate, 7 dishes of 70 larvae each were infected. At 48 hour-post-infection (hpi), these 490 larvae were pooled and homogenized in 0.1% Nonidet P-40 (NP-40) in PBS. Homogenates were then cultured in 12.5 mL BHI containing 200 µg/mL streptomycin at 37°C for 5 hours, which is defined as our “output”. We define our “input” as pooled ~$5x10^7$ transposon mutants from the transposon library similarly cultured in 12.5 mL BHI containing 200 µg/mL streptomycin at 37°C for 5 hours. Three biological replicates were performed.

Protein-protein interaction prediction

To predict proteome-wide physically interacting PPIs in L. monocytogenes, we developed and applied a bioinformatic and deep learning pipeline. This pipeline is a modification to previous work (Cong et al., 2019; Humphreys et al., 2021), and integrates RoseTTAFold2-Lite (RF2-Lite), a rapid structure prediction tool for interaction prediction (Humphreys et al., 2024).

To curate our L. monocytogenes protein alignments, we created a genomic sequence database with 44,871 representative bacterial proteomes (one per species) from NCBI and JGI selected based on either the reference proteome or the proteome with the largest number of proteins and we include all unlabeled species (May, 2021). Each protein in L. monocytogenes (EGD-e) was used as a query to search for orthologues in our representative proteome database using reciprocal best hit (rbh) criterion to minimize error (Cong et al., 2019; Wall et al., 2003). We applied Hmmer (Eddy, 2011) to create a local ‘seed’ alignment from the previously identified orthologues followed by Hmmsearch to align the sequences. Sequences were filtered following our previous protocol for identity, gap ratio, and possible multiple alignments (Humphreys et al., 2024). We paired each of the 2844 proteins in L. monocytogenes (4,042,746 pairs) based on their genomic IDs such that each paired MSA contains a single orthologue per proteome from our bacterial sequence database. We filtered paired MSAs based on concatenated protein length (<2400 amino acids) and screened 4,036,043 pairs of possible interactions with RF2-Lite. The 533,000 pairs above a 0.05 RF2-Lite interaction score threshold were subjected to interaction prediction with AlphaFold2 (AF2) (Jumper et al., 2021). For RF2-Lite and AF2, we compute an interaction score based on the

highest summed predicted residue-residue distance probability < 12Å between the two proteins.

Figures

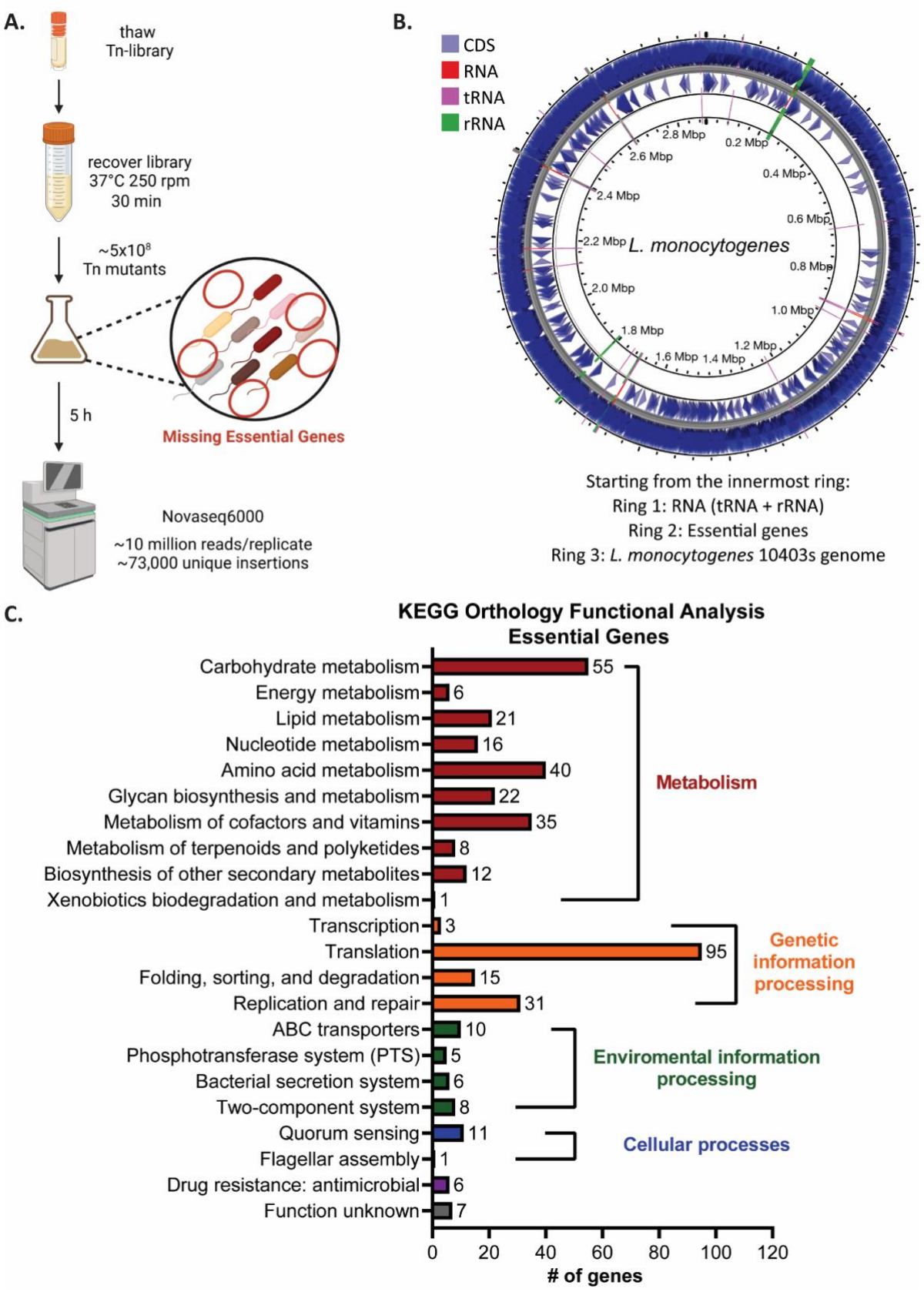
A.
thaw
Tn-library
recover library
37°C 250 rpm
30 min
~5x10^8
Tn mutants
5 h
Missing Essential Genes
Novaseq6000
~10 million reads/replicate
~73,000 unique insertions
B.
CDS
RNA
tRNA
rRNA
L. monocytogenes
Starting from the innermost ring:
Ring 1: RNA (tRNA + rRNA)
Ring 2: Essential genes
Ring 3: L. monocytogenes 10403s genome
C.
KEGG Orthology Functional Analysis
Essential Genes
Carbohydrate metabolism 55
Energy metabolism 6
Lipid metabolism 21
Nucleotide metabolism 16
Amino acid metabolism 40
Glycan biosynthesis and metabolism 22
Metabolism of cofactors and vitamins 35
Metabolism of terpenoids and polyketides 8
Biosynthesis of other secondary metabolites 12
Xenobiotics biodegradation and metabolism 1
Transcription 3
Translation 95
Folding, sorting, and degradation 15
Replication and repair 31
ABC transporters 10
Phosphotransferase system (PTS) 5
Bacterial secretion system 6
Two-component system 8
Quorum sensing 11
Flagellar assembly 1
Drug resistance: antimicrobial 6
Function unknown 7
Metabolism
Genetic information processing
Enviromental information processing
Cellular processes
0 20 40 60 80 100 120
# of genes

Figure 3.1. Identification of essential genes in *L. monocytogenes*. (A) Schematic for essential gene determination. (B) A map of *L. monocytogenes* genome and distribution of essential genes (determined by unique insertion counts <LOD in all biological replicates) across the genome generated by CGView Server. Coding regions of genes (CDS) are shown in blue, tRNAs are shown in purple, rRNAs are shown in green, and RNAs are shown in red in ring 2. (C) KEGG orthology mapping of essential genes in *L. monocytogenes*. Data are from nine biological replicates.

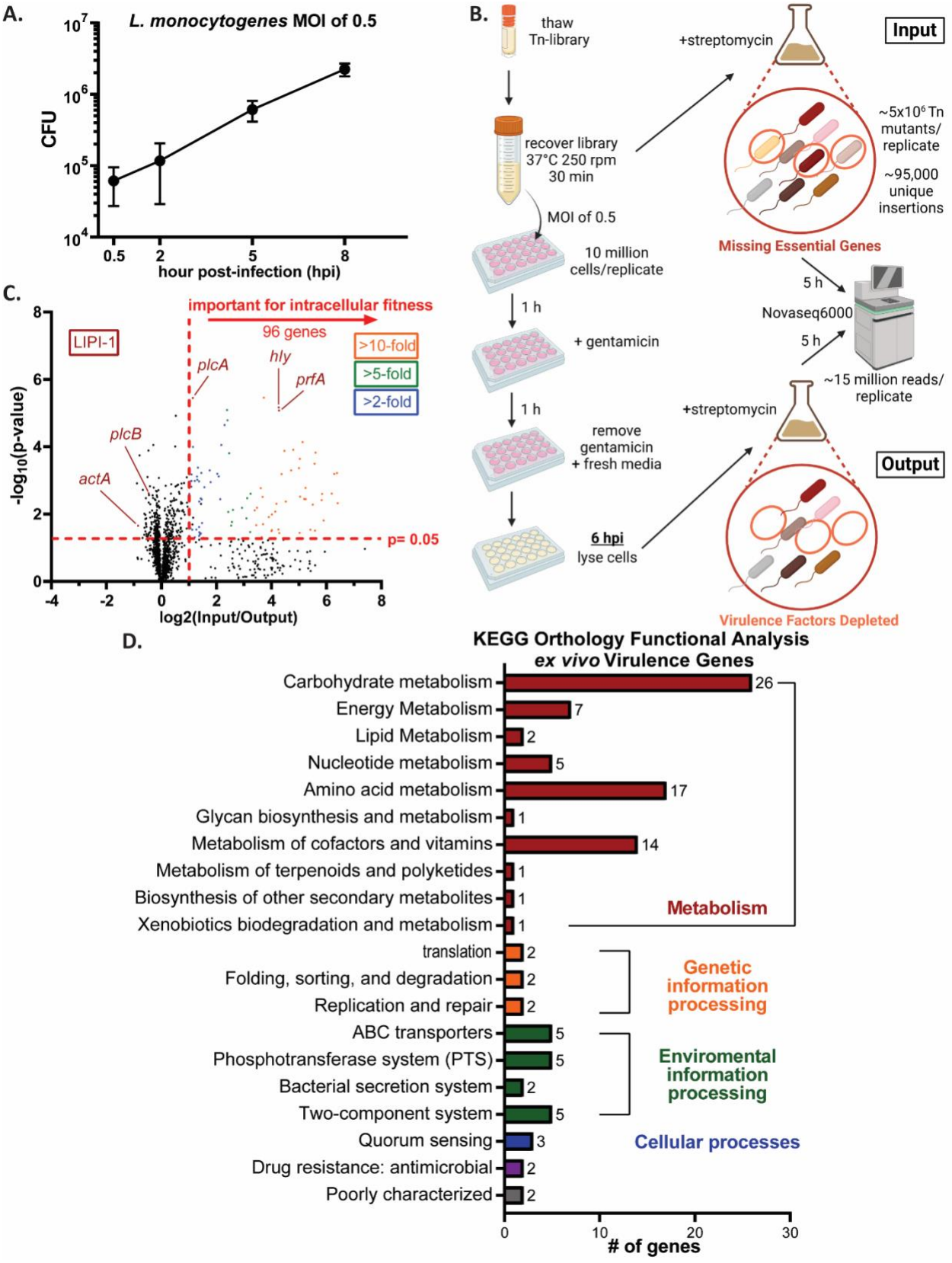
A.
L. monocytogenes MOI of 0.5
CFU
hour post-infection (hpi)
B.
thaw Tn-library
recover library 37°C 250 rpm 30 min
MOI of 0.5
10 million cells/replicate
1 h
+ gentamicin
1 h
remove gentamicin + fresh media
6 hpi
lyse cells
+streptomycin
Input
~5x10⁶ Tn mutants/ replicate
~95,000 unique insertions
Missing Essential Genes
5 h
Novaseq6000
5 h
~15 million reads/ replicate
+streptomycin
Output
Virulence Factors Depleted
C.
important for intracellular fitness
96 genes
LIPI-1
>10-fold
>5-fold
>2-fold
plcA
hly
prfA
plcB
actA
p= 0.05
-log10(p-value)
log2(Input/Output)
D.
KEGG Orthology Functional Analysis
ex vivo Virulence Genes
Carbohydrate metabolism 26
Energy Metabolism 7
Lipid Metabolism 2
Nucleotide metabolism 5
Amino acid metabolism 17
Glycan biosynthesis and metabolism 1
Metabolism of cofactors and vitamins 14
Metabolism of terpenoids and polyketides 1
Biosynthesis of other secondary metabolites 1
Xenobiotics biodegradation and metabolism 1
Metabolism
translation 2
Folding, sorting, and degradation 2
Replication and repair 2
Genetic information processing
ABC transporters 5
Phosphotransferase system (PTS) 5
Bacterial secretion system 2
Two-component system 5
Enviromental information processing
Quorum sensing 3
Drug resistance: antimicrobial 2
Cellular processes
Poorly characterized 2
# of genes

Figure 3.2. Identification of *L. monocytogenes* genes important for intracellular survival. (A) Bone marrow-derived macrophages (BMDMs) were infected with WT *L. monocytogenes* at an MOI of 0.5. Data represents mean ± SEM from 8 biological replicates. (B) Schematic showing the experimental workflow of bone marrow-derived macrophage TIS screen. A volcano plot displaying *L. monocytogenes* genes important for fitness during intracellular growth identified from the screen is shown in (C). (D) KEGG orthology functional analysis of genes important for intracellular fitness. Three biological replicates were performed.

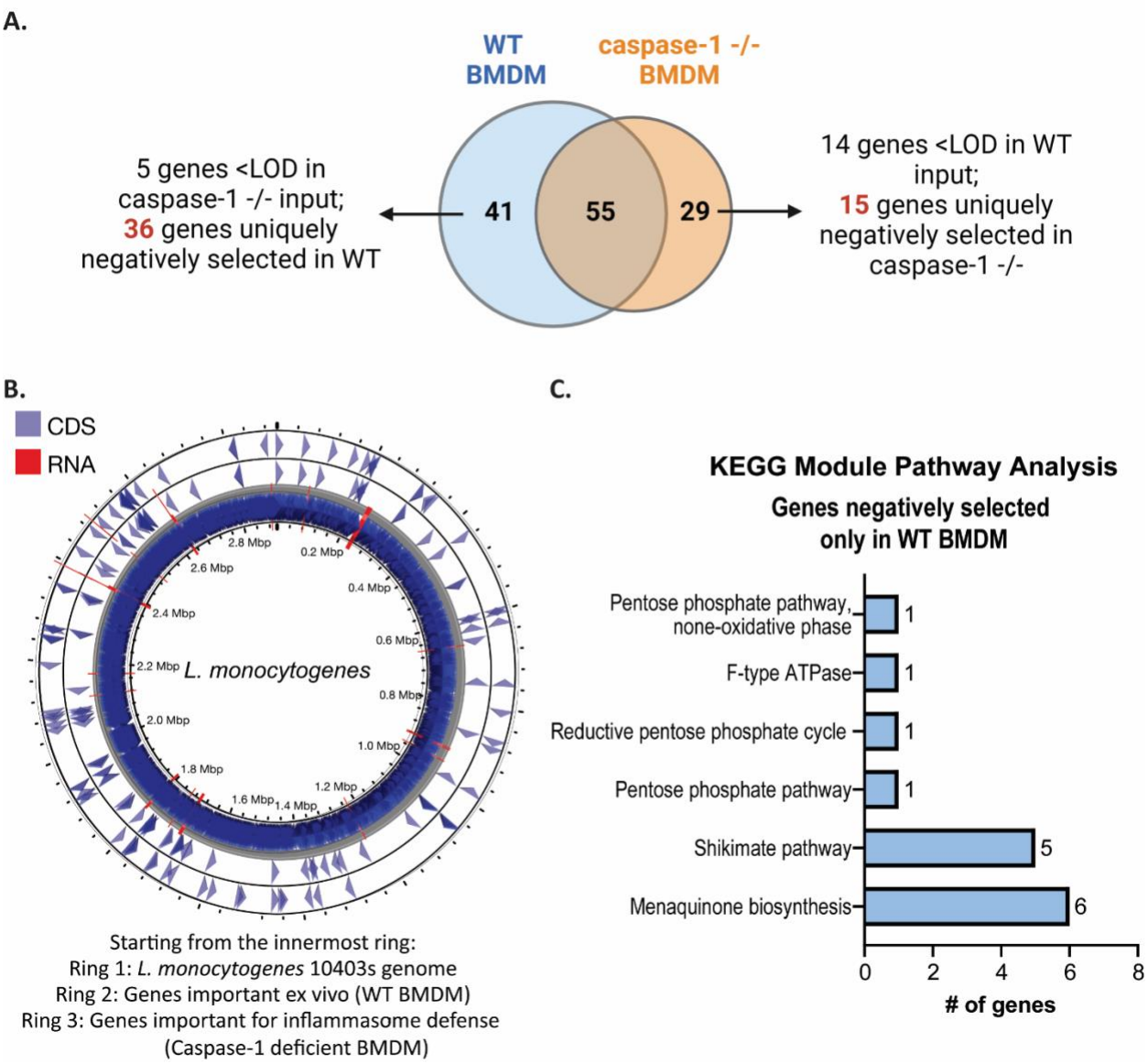

Figure 3.3. Identification of *L. monocytogenes* genes important for inflammasome defense. TIS screen was performed using caspase-1 deficient BMDMs. (A) A Venn diagram comparing genes that are negatively selected in WT and caspase-1 deficient BMDM. (B) A map of *L. monocytogenes* genome and distribution of genes important for intracellular growth in WT BMDM (second innermost ring) and inflammasome defense. (C) KEGG module pathway analysis of genes important for fitness in WT BMDM but dispensable in caspase-1 deficient BMDM. Three biological replicates were performed.

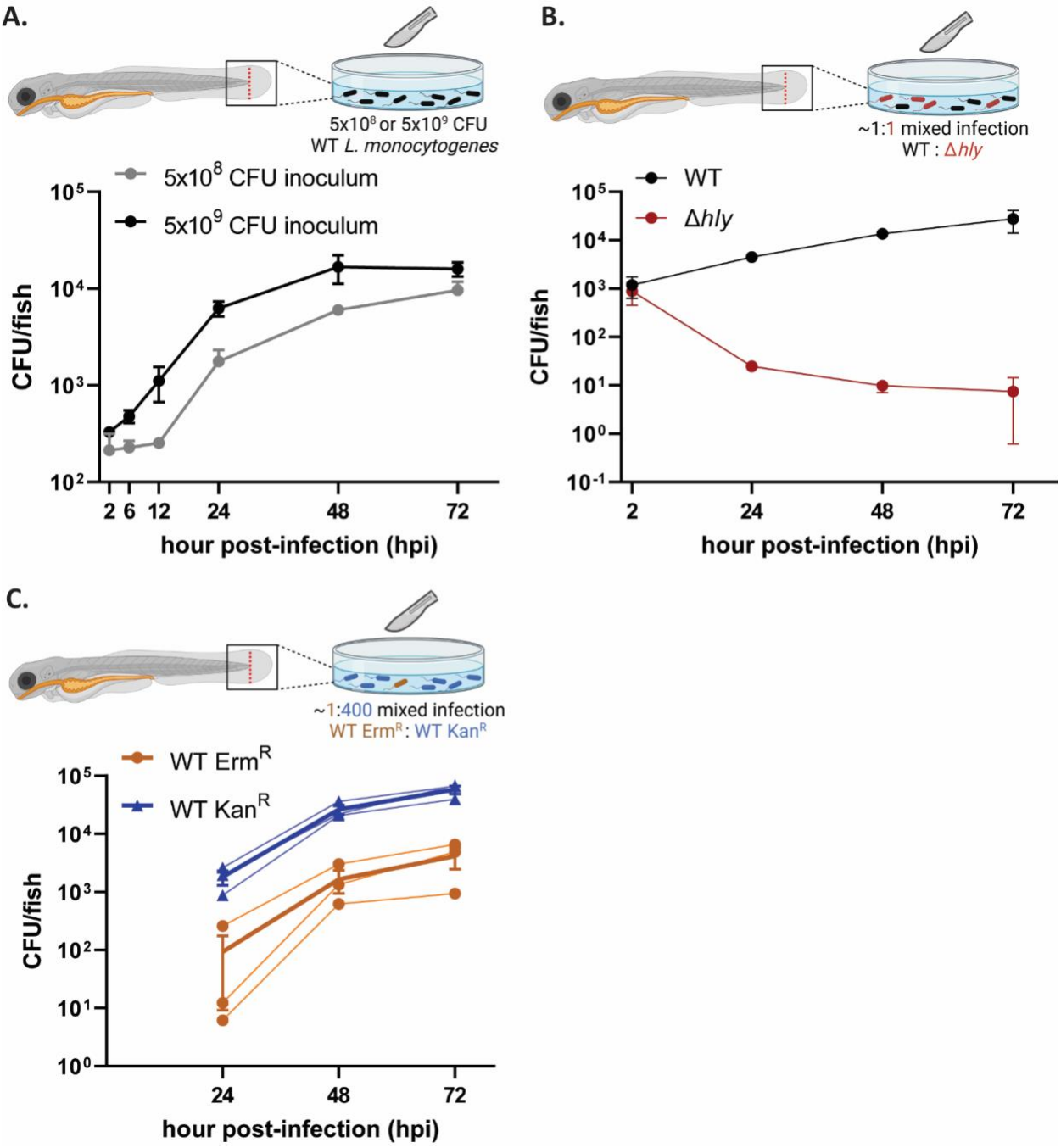

Figure 3.4. Characterization of the zebrafish tail wound infection model. Zebrafish larvae were infected by inducing a wound at the tail with (A) 5 x 10^8 or 5 x 10^9 CFU *Lm* in the medium, or (B) a total of 5 x 10^9 CFU *L. monocytogenes*, containing Δ*hly* and WT at a 1:1 ratio in the medium, or (C) a total of 5 x 10^9 CFU *L. monocytogenes*, containing WT Erm^R and WT Kan^R at an approximately 1:400 ratio, in the medium. To plate for

CFU, 10 zebrafish larvae were pooled for each condition at each time point. Data represent mean ± SEM from three biological replicates. In (C) data from each biological replicate were also displayed.

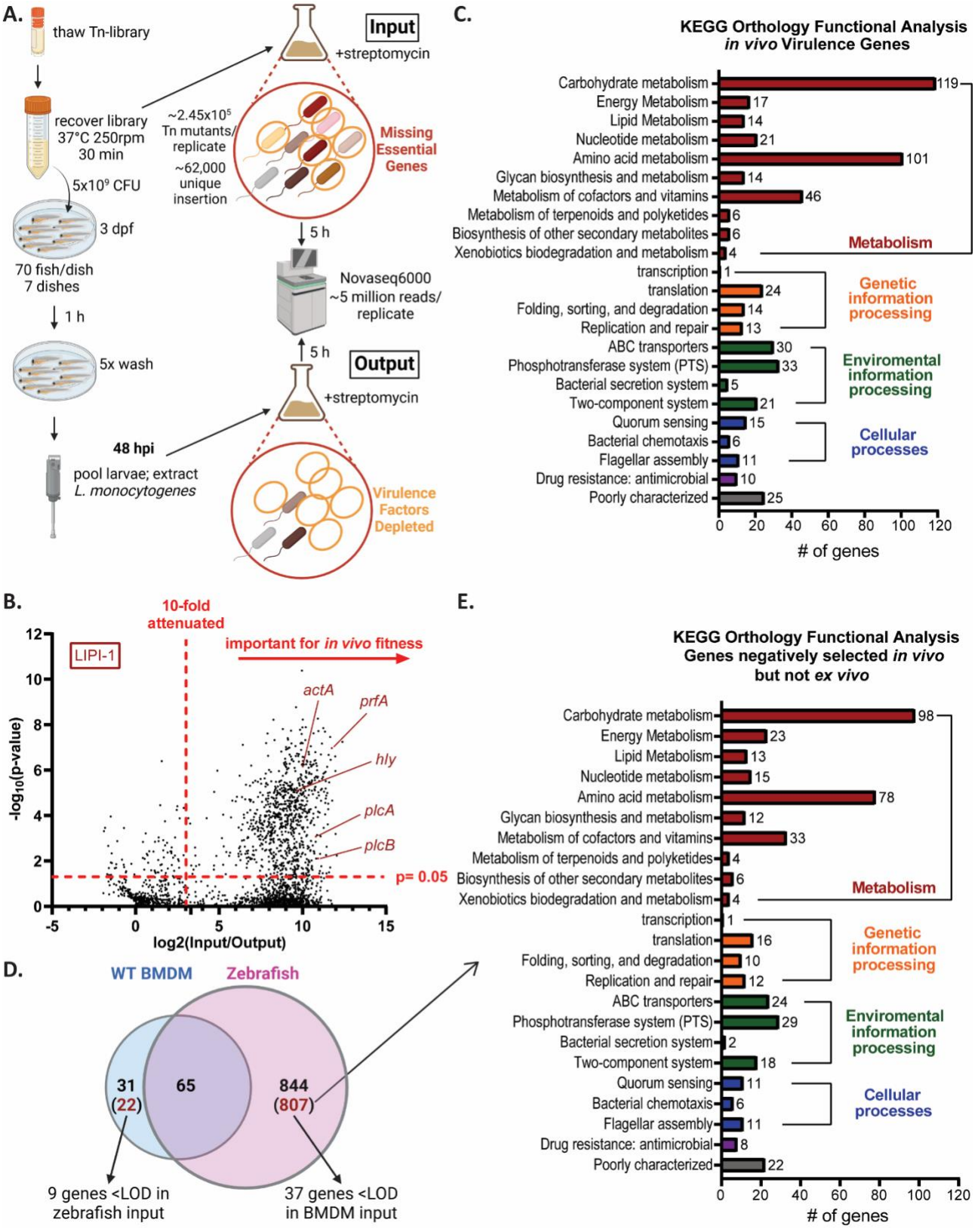
A.
thaw Tn-library
recover library
37°C 250rpm
30 min
5x10⁹ CFU
3 dpf
70 fish/dish
7 dishes
1 h
5x wash
48 hpi
pool larvae; extract
L. monocytogenes
Input
+streptomycin
~2.45x10⁵
Tn mutants/
replicate
~62,000
unique
insertion
Missing
Essential
Genes
5 h
Novaseq6000
~5 million reads/
replicate
5 h
Output
+streptomycin
Virulence
Factors
Depleted
B.
10-fold
attenuated
important for in vivo fitness
LIPI-1
actA
prfA
hly
plcA
plcB
p= 0.05
-log10(p-value)
log2(Input/Output)
C.
KEGG Orthology Functional Analysis
in vivo Virulence Genes
Carbohydrate metabolism 119
Energy Metabolism 17
Lipid Metabolism 14
Nucleotide metabolism 21
Amino acid metabolism 101
Glycan biosynthesis and metabolism 14
Metabolism of cofactors and vitamins 46
Metabolism of terpenoids and polyketides 6
Biosynthesis of other secondary metabolites 6
Xenobiotics biodegradation and metabolism 4
Metabolism
transcription 1
translation 24
Folding, sorting, and degradation 14
Replication and repair 13
Genetic information processing
ABC transporters 30
Phosphotransferase system (PTS) 33
Bacterial secretion system 5
Two-component system 21
Enviromental information processing
Quorum sensing 15
Bacterial chemotaxis 6
Flagellar assembly 11
Cellular processes
Drug resistance: antimicrobial 10
Poorly characterized 25
0 20 40 60 80 100 120
# of genes
D.
WT BMDM
Zebrafish
31
(22)
65
844
(807)
9 genes <LOD in
zebrafish input
37 genes <LOD
in BMDM input
E.
KEGG Orthology Functional Analysis
Genes negatively selected in vivo
but not ex vivo
Carbohydrate metabolism 98
Energy Metabolism 23
Lipid Metabolism 13
Nucleotide metabolism 15
Amino acid metabolism 78
Glycan biosynthesis and metabolism 12
Metabolism of cofactors and vitamins 33
Metabolism of terpenoids and polyketides 4
Biosynthesis of other secondary metabolites 6
Xenobiotics biodegradation and metabolism 4
Metabolism
transcription 1
translation 16
Folding, sorting, and degradation 10
Replication and repair 12
Genetic information processing
ABC transporters 24
Phosphotransferase system (PTS) 29
Bacterial secretion system 2
Two-component system 18
Enviromental information processing
Quorum sensing 11
Bacterial chemotaxis 6
Flagellar assembly 11
Cellular processes
Drug resistance: antimicrobial 8
Poorly characterized 22
0 20 40 60 80 100 120
# of genes

Figure 3.5. Identification of essential genes and virulent genes through TIS screen. (A) Schematic of experimental workflow for zebrafish TIS screen. A volcano plot displaying *L. monocytogenes* genes important for fitness during intracellular growth identified from the screen is shown in (B). (C) KEGG orthology functional analysis of genes important for fitness *in vivo*. A comparison of *L. monocytogenes* genes critical for fitness *ex vivo* and *in vivo* is shown in a Venn diagram in (D). (E) KEGG orthology mapping on the 807 genes that are only negatively selected for fitness *in vivo* but not *ex vivo.* 3 biological replicates were performed.

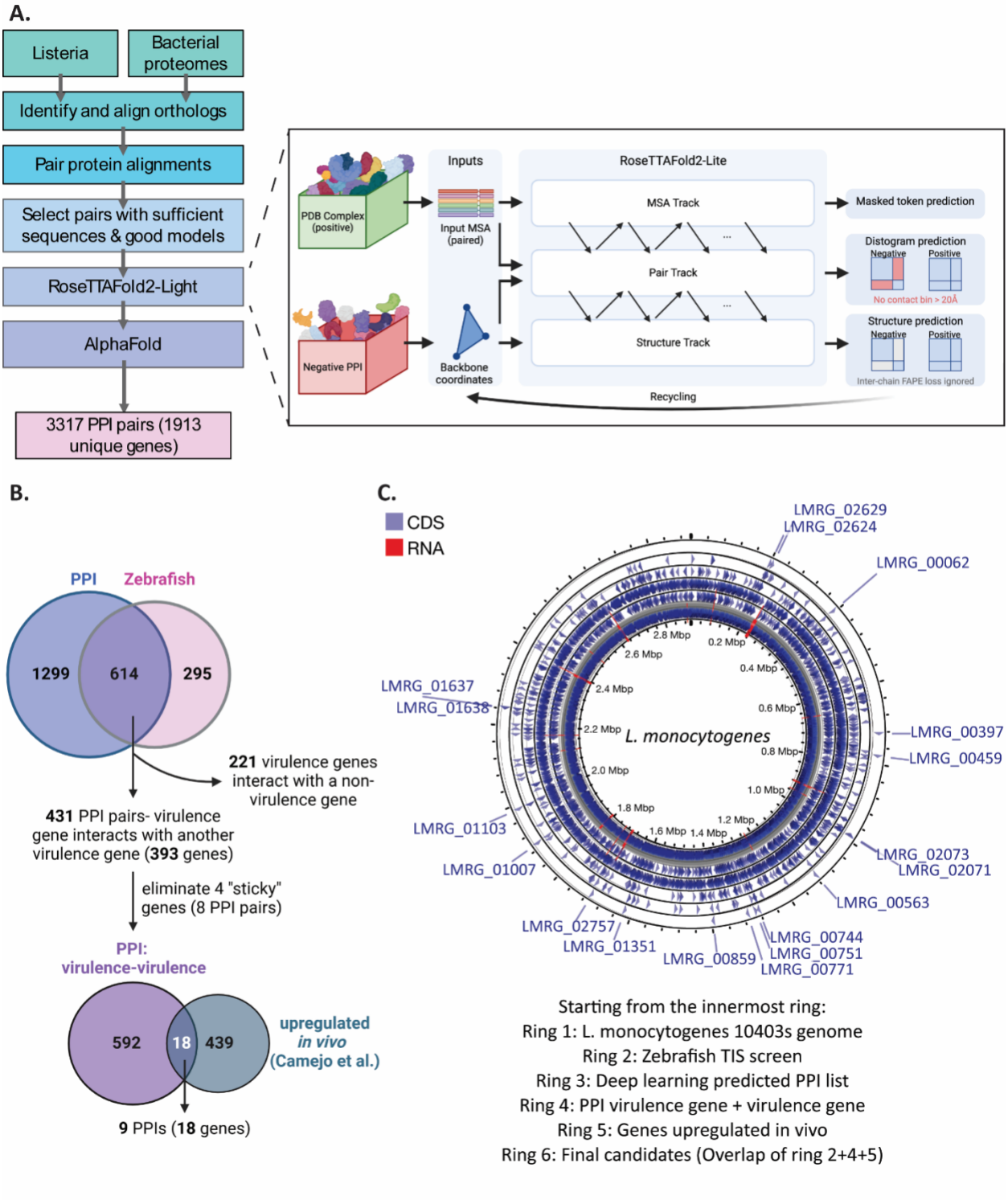

Figure 3.6. Use of deep learning PPI predictions to prioritize genes of interest. (A) Schematic showing deep learning PPI prediction pipeline. (B) Workflow for prioritizing virulence leads by overlaying PPI predicted genes with zebrafish TIS screen determined

virulence genes, and further overlaying genes known to be upregulated *in vivo*. (C) A map showing from the innermost to outermost ring: *L. monocytogenes* genome (ring 1), TIS screen identified *in vivo* virulence genes (ring 2), deep learning PPI predictions (ring 3), virulent gene interacting with another virulent gene from the PPI list (ring 4), genes upregulated *in vivo* (ring 5), and the genes that are overlapped between ring 2, 4, and 5 (ring 6).

Supplementary Figures

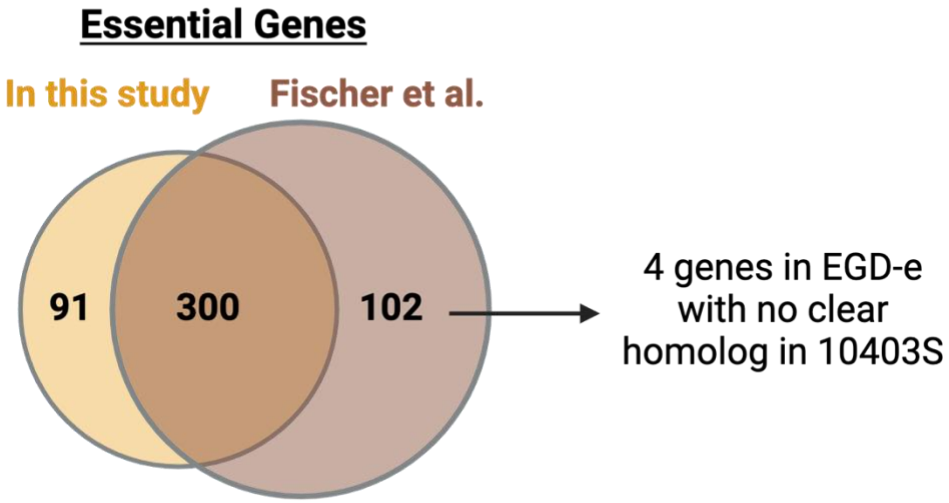

Figure S3.1. Venn diagram showing essential gene comparison between this study and Fischer et al.

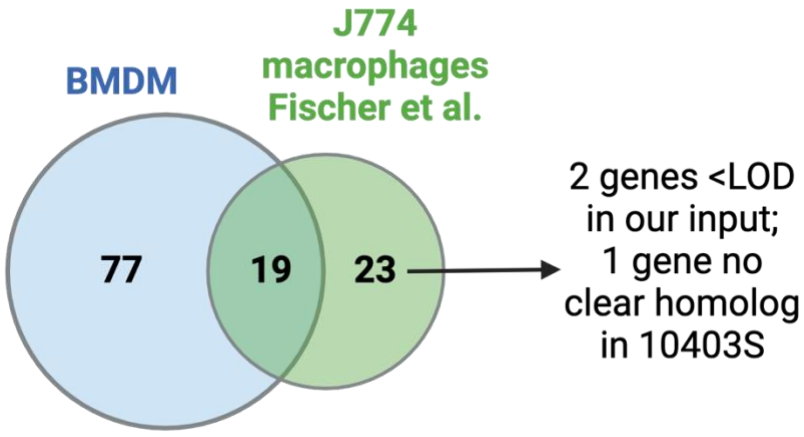

Figure S3.2 Venn diagram showing comparison of genes negatively selected for fitness in BMDMs and in J774 macrophages by Fischer et al.

Tables

Table 3.1 *L. monocytogenes* genes required for intracellular fitness in BMDMs.

locus_tag	description	Fold Reduction	p-value
LMRG_00265	protein translocase subunit secA 2	85.12	0.005
LMRG_02498	adenylosuccinate lyase	83.50	0.001
LMRG_00514	pyruvate dehydrogenase E1 component	77.76	0.001
LMRG_00809	transcription antitermination factor NusB	73.39	0.002
LMRG_01178	YggT family protein	59.60	0.016
LMRG_00516	pyruvate dehydrogenase E2 component	57.41	0.003
LMRG_00515	pyruvate dehydrogenase E1 component subunit beta	56.83	0.004
LMRG_05516	5S ribosomal RNA	48.55	1.50E-04
LMRG_01038	recombination protein U	48.00	0.031
LMRG_00517	dihydrolipoyl dehydrogenase	47.54	3.20E-04
LMRG_01048	pantoate-beta-alanine ligase	45.40	0.005
LMRG_00914	GTP-binding protein Era	42.86	0.029
LMRG_02532	polar amino acid transport system ATP-binding protein	37.96	0.004
LMRG_01190	methylase MraW	37.75	0.002
LMRG_01070	3-phosphoshikimate 1-carboxyvinyltransferase	36.60	0.004
LMRG_01039	penicillin binding protein 1A	35.12	7.31E-05
LMRG_00561	hypothetical protein	32.94	0.003
LMRG_01719	ATP synthase F1 beta subunit	32.81	2.30E-04
LMRG_00314	hypothetical protein	32.60	0.036
LMRG_01313	cellsurface protein	32.07	4.33E-04
LMRG_02583	sensor histidine kinase VicK	27.77	1.24E-04
LMRG_01049	3-methyl-2-oxobutanoate hydroxymethyltransferase	26.29	0.001
LMRG_01532	phage terminase large subunit	23.05	0.004
LMRG_01716	ATP synthase F1 delta subunit	22.23	1.33E-04
LMRG_02531	polar amino acid transport system permease	20.70	0.001
LMRG_00712	transcriptional regulator	19.58	0.037
LMRG_02622	listeriolysin regulatory protein	19.41	8.37E-06
LMRG_02624	listeriolysin O	19.24	6.84E-06
LMRG_00184	galactitol-specific PTS system IIA component	19.12	0.029
LMRG_02211	galactitol-specific PTS system IIB component	18.17	0.005
LMRG_01775	hypothetical protein	17.62	0.008
LMRG_05513	5S ribosomal RNA	16.23	0.030
LMRG_02433	DNA replication and repair protein recF	16.22	0.010
LMRG_02582	YycH protein	16.01	0.032

LMRG_01720	ATP synthase F1 epsilon subunit	14.97	0.012
LMRG_02485	adenylosuccinate synthetase	13.25	3.51E-06
LMRG_00965	ribulose-phosphate 3-epimerase	12.97	0.020
LMRG_00853	hypothetical protein	12.81	0.003
LMRG_02063	hypothetical protein	12.53	0.049
LMRG_01169	cell division initiation protein	12.24	0.002
LMRG_01294	naphthoate synthase	11.11	0.006
LMRG_01248	galactitol-specific PTS system IIB component	10.93	0.022
LMRG_01199	hypothetical protein	10.50	0.008
LMRG_00264	invasion associated secreted endopeptidase	9.49	0.003
LMRG_00777	ribosome-binding factor A	9.39	0.034
LMRG_01075	chorismate synthase	8.70	0.003
LMRG_00057	high-affinity iron transporter	8.52	0.013
LMRG_00956	fatty acid/phospholipid synthesis protein PlsX	7.63	0.007
LMRG_02765	dUTP pyrophosphatase	6.08	0.008
LMRG_00833	acylphosphatase	5.91	0.017
LMRG_02274	hypothetical protein	5.80	0.022
LMRG_01714	F-type H+-transporting ATPase subunit C	5.52	1.57E-04
LMRG_00186	ribulose-phosphate 3-epimerase	5.40	0.009
LMRG_01713	ATP synthase F0 A subunit	5.29	1.65E-05
LMRG_01715	ATP synthase F0 B subunit	5.24	8.13E-06
LMRG_01717	ATP synthase F1 alpha subunit	4.93	2.27E-05
LMRG_01195	2-dehydropantoate 2-reductase	4.53	8.90E-05
LMRG_00838	DNA translocase ftsK	4.40	0.004
LMRG_00281	biotin biosynthesis protein BioY	4.24	0.001
LMRG_01797	preprotein translocase SecG subunit	4.10	0.001
LMRG_01774	hypothetical protein	3.46	0.001
LMRG_02753	dimethyladenosine transferase	3.38	0.001
LMRG_01927	hypothetical protein	2.95	0.002
LMRG_02730	ComA operon protein 2	2.79	0.018
LMRG_01926	antibiotic transport system ATP-binding protein	2.76	0.004
LMRG_02769	hypothetical protein	2.74	0.001
LMRG_01291	menaquinone-specific isochorismate synthase	2.72	0.005
LMRG_02530	hypothetical protein	2.71	0.038
LMRG_01701	threonine synthase	2.69	0.003
LMRG_01292	2-succinyl-5-enolpyruvyl-6-hydroxy-3-cyclohexene-1-carboxylate synthase	2.64	0.040
LMRG_02522	shikimate kinase	2.61	0.035
LMRG_00422	LacI family transcriptional regulator	2.59	0.004
LMRG_01702	homoserine kinase	2.59	0.001
LMRG_01295	O-succinylbenzoate-CoA ligase	2.59	0.024

LMRG_02525	hypothetical protein	2.58	0.045
LMRG_01700	homoserine dehydrogenase	2.51	4.18E-04
LMRG_01712	ATP synthase I	2.47	0.001
LMRG_01745	cardiolipin synthase	2.46	0.001
LMRG_00107	peptidoglycan N-acetylglucosamine deacetylase	2.41	0.029
LMRG_01525	recombination protein RecT	2.33	0.001
LMRG_02524	hypothetical protein	2.33	0.049
LMRG_00958	ATP-dependent DNA helicase RecG	2.23	0.013
LMRG_00768	RIP metalloprotease RseP	2.22	1.02E-04
LMRG_02623	1-phosphatidylinositol phosphodiesterase	2.21	3.58E-06
LMRG_01524	gp47	2.18	0.020
LMRG_01074	3-dehydroquinate synthase	2.18	0.029
LMRG_02136	CRISPR-associated protein cas2	2.14	0.001
LMRG_01617	ABC-2 type transport system ATP-binding protein	2.14	0.001
LMRG_01728	O-succinylbenzoic acid synthetase	2.13	0.002
LMRG_02346	mannose-specific PTS system IIC component	2.12	0.001
LMRG_01367	bifunctional 3-deoxy-7-phosphoheptulonate synthase/chorismate mutase	2.08	0.026
LMRG_01618	ABC-2 type transport system permease	2.06	0.001
LMRG_01302	hypothetical protein	2.04	0.004
LMRG_02523	hypothetical protein	2.03	0.002
LMRG_01179	cell division protein sepF	2.02	0.003
LMRG_01846	hypothetical protein	2.00	0.003

Table 3.2. Comparisons of *L. monocytogenes* genes uniquely negatively selected in WT or caspase-1 deficient BMDM.

	locus_tag	Gene Symbol	description	WT FC	WT p-value	Caspase-1 -/- FC	Caspase-1 -/- p-value
Only negatively selected in WT BMDM	LMRG_01178		YggT family protein	59.60	0.016	1.31	0.006
	LMRG_05516		5S ribosomal RNA	48.55	1.50E-04	1.17	0.155
	LMRG_01070	aroE	3-phosphoshikimate 1-carboxyvinyltransferase	36.60	0.004	1.16	0.386
	LMRG_01039	pbpA1	penicillin binding protein 1A	35.12	0.000	1.78	6.75E-05
	LMRG_00314		hypothetical protein	32.60	0.036	0.99	0.857
	LMRG_01313		cellsurface protein	32.07	0.000	0.92	0.553
	LMRG_02583	walK	sensor histidine kinase VicK	27.77	0.000	1.61	0.092
	LMRG_00712		transcriptional regulator	19.58	0.037	0.61	0.009
	LMRG_00184		galactitol-specific PTS system IIA component	19.12	0.029	1.20	0.219
	LMRG_02433	recF	DNA replication and repair protein recF	16.22	0.010	1.86	0.005
	LMRG_00965	rpeA	ribulose-phosphate 3-epimerase	12.97	0.020	1.34	0.227
	LMRG_01199		hypothetical protein	10.50	0.008	1.36	0.059
	LMRG_01075	aroF	chorismate synthase	8.70	0.003	1.52	0.045
	LMRG_00833		acylphosphatase	5.91	0.017	2.84	0.121
	LMRG_01774	yvcJ	hypothetical protein	3.46	0.001	1.63	4.97E-04
	LMRG_02730	menI	ComA operon protein 2	2.79	0.018	0.96	0.499
	LMRG_01291	menF	menaquinone-specific isochorismate synthase	2.72	0.005	0.92	0.205
	LMRG_01292	menD	2-succinyl-5-enolpyruvyl-6-hydroxy-3-cyclohexene-1-carboxylate synthase	2.64	0.040	0.96	0.649
	LMRG_02522		shikimate kinase	2.61	0.035	0.87	0.454
	LMRG_01295	menE	O-succinylbenzoate-CoA ligase	2.59	0.024	0.90	0.118

Only negatively selected in WT BMDM	LMRG_02524	virB	hypothetical protein	2.33	0.049	1.96	4.42E-04
	LMRG_00958	recG	ATP-dependent DNA helicase RecG	2.23	0.013	1.55	0.009
	LMRG_01074	aroB	3-dehydroquinate synthase	2.18	0.029	0.99	0.798
	LMRG_02136		CRISPR-associated protein cas2	2.14	0.001	1.72	0.003
	LMRG_01728	menC	O-succinylbenzoic acid synthetase	2.13	0.002	1.03	0.937
	LMRG_02346		mannose-specific PTS system IIC component	2.12	0.001	1.83	3.05E-05
	LMRG_01367	aroA	bifunctional 3-deoxy-7-phosphoheptulonate synthase/chorismate mutase	2.08	0.026	0.93	0.593
	LMRG_02523		hypothetical protein	2.03	0.002	1.84	0.001
	LMRG_00561		hypothetical protein	32.94	0.003	11.16	0.090
	LMRG_01532		phage terminase large subunit	23.05	0.004	5.64	0.368
	LMRG_02211		galactitol-specific PTS system IIB component	18.17	0.005	3.03	0.777
	LMRG_05513		5S ribosomal RNA	16.23	0.030	8.86	0.229
	LMRG_01720	atpC	ATP synthase F1 epsilon subunit	14.97	0.012	7.78	0.983
	LMRG_01294	menB	naphthoate synthase	11.11	0.006	5.34	0.301
	LMRG_01248		galactitol-specific PTS system IIB component	10.93	0.022	6.20	0.149
	LMRG_00057	efeU	high-affinity iron transporter	8.52	0.013	7.20	0.095
	LMRG_02532		polar amino acid transport system ATP-binding protein	37.96	0.00	1.88	0.003
	LMRG_00186		ribulose-phosphate 3-epimerase	5.40	0.01	2.38	0.006
	LMRG_00809	nusB	transcription antitermination factor NusB	73.39	0.00	12.69	0.025
	LMRG_00777	rbfA	ribosome-binding factor A	9.39	0.03	11.02	0.004
	LMRG_00956	plsX	fatty acid/phospholipid synthesis protein PlsX	7.63	0.01	1.79	0.089

Only negatively Selected in caspase-1 -/- BMDM	LMRG_01204	ylbG	hypothetical protein	1.91	0.005	2.53	0.001
	LMRG_01613	prsA2	foldase prsA 2	1.89	0.027	2.27	0.001
	LMRG_02412	yabC	hypothetical protein	1.41	0.010	2.06	0.002
	LMRG_00489		hypothetical protein	12.50	0.164	13.41	0.048
	LMRG_02581		hypothetical protein	5.82	0.065	10.29	0.001
	LMRG_01638	oppC	peptide/nickel transport system permease	7.49	0.080	3.60	0.001
	LMRG_02526	virR	response regulator	2.60	0.058	3.10	1.27E-05
	LMRG_01636	oppA	peptide/nickel transport system substrate-binding protein	9.96	0.076	2.73	0.004
	LMRG_01368	ccpA	catabolite control protein A	3.48	0.085	2.58	2.66E-04
	LMRG_02432		hypothetical protein	2.75	0.093	4.71	0.038
	LMRG_02360	pdeD	hypothetical protein	13.91	0.781	4.51	0.046
	LMRG_02153	rpmJ	50S ribosomal protein L36	9.12	0.095	3.89	0.033
	LMRG_02569		cellobiose-specific PTS system IIB component	12.54	0.985	3.14	0.007
	LMRG_02703	lipL	hypothetical protein	4.11	0.052	2.85	1.26E-05
	LMRG_01637	oppB	peptide/nickel transport system permease	8.97	0.085	2.72	0.001
	LMRG_01867		beta-phosphoglucomutase	53.07	1.15E-04	30.05	5.52E-05
	LMRG_00897	zurR	transcriptional regulator ZurR	33.92	0.176	19.33	3.06E-05
	LMRG_05052		Tyr tRNA	16.94	0.019	15.05	0.001
	LMRG_01385		site-specific DNA-methyltransferase	31.84	0.040	13.51	0.002
	LMRG_02289	cshA	ATP-dependent RNA helicase DeaD	25.67	0.077	11.64	9.36E-05
	LMRG_01026	cspD	cold shock protein	12.46	0.225	9.00	0.011
	LMRG_00902	cshB	DEAD-box ATP-dependent RNA helicase cshB	15.94	0.128	5.28	3.44E-04
	LMRG_01025		hypothetical protein	50.49	0.011	22.63	0.042
	LMRG_01300		L-lactate dehydrogenase	12.71	0.096	20.44	3.08E-07
	LMRG_05062		Arg tRNA	38.01	0.009	17.64	0.017

	LMRG_01687		nicotinate-regulated transporter	30.64	2.34E-04	13.15	0.045
	LMRG_01437	ruvA	Holliday junction DNA helicase RuvA	28.03	0.002	11.07	0.005
	LMRG_01443	secDF	bifunctional preprotein translocase subunit SecD/SecF	22.78	0.004	9.41	1.58E-04
	LMRG_00003		hypothetical protein	2.57	0.986	5.00	0.023

Cells shaded in light gray are genes not identified due to not meeting statistical significance.

Cells shaded in dark gray are genes eliminated from analysis due to input <LOD.

Fold change (Input/Output) is abbreviated as FC.

>2-fold is considered to be important.

Table 3.3 *L. monocytogenes* genes that are negatively selected for fitness in WT BMDM but not in zebrafish.

	locus_tag	Description	Zebrafish Fold Reduction	Zebrafish p-value
Dispensable *in vivo*	LMRG_01774	hypothetical protein	5.55	5.69E-05
	LMRG_01617	ABC-2 type transport system ATP-binding protein	1.69	0.012
	LMRG_01618	ABC-2 type transport system permease	0.50	0.345
Eliminated due to loss of statistical significance	LMRG_00107	peptidoglycan N-acetylglucosamine deacetylase	1058.16	0.897
	LMRG_00768	RIP metalloprotease RseP	856.85	0.890
	LMRG_00833	acylphosphatase	12.34	0.083
	LMRG_00958	ATP-dependent DNA helicase RecG	152.59	0.742
	LMRG_01524	gp47	260.33	0.433
	LMRG_01712	ATP synthase I	882.97	0.857
	LMRG_01713	ATP synthase F0 A subunit	403.64	0.890
	LMRG_01714	F-type H+-transporting ATPase subunit C	623.54	0.382
	LMRG_01715	ATP synthase F0 B subunit	184.66	0.081
	LMRG_01717	ATP synthase F1 alpha subunit	662.35	0.969
	LMRG_01719	ATP synthase F1 beta subunit	244.22	0.476
	LMRG_01846	hypothetical protein	1916.31	0.095
	LMRG_01926	antibiotic transport system ATP-binding protein	2143.72	0.440
	LMRG_02346	mannose-specific PTS system IIC component	842.33	0.114
	LMRG_02523	hypothetical protein	269.29	0.809
	LMRG_02525	hypothetical protein	295.38	0.137
	LMRG_02530	hypothetical protein	1420.04	0.073
	LMRG_02769	hypothetical protein	850.36	0.160
	LMRG_05513	5S ribosomal RNA	31.35	0.337
Eliminated due to Input <LOD	LMRG_00186	ribulose-phosphate 3-epimerase	17.20	0.062
	LMRG_00561	hypothetical protein	50.55	0.014
	LMRG_00809	transcription antitermination factor NusB	180.13	0.001
	LMRG_00956	fatty acid/phospholipid synthesis protein PlsX	13.14	0.041
	LMRG_01294	naphthoate synthase	71.22	8.48E-05

Eliminated due to Input <LOD	LMRG_01313	cellsurface protein	73.54	2.40E-05
	LMRG_02063	hypothetical protein	86.65	2.07E-04
	LMRG_02532	polar amino acid transport system ATP-binding protein	324.94	3.31E-05
	LMRG_05516	5S ribosomal RNA	37.33	0.339

Table 3.4. *L. monocytogenes* PPI pairs consist of genes that are upregulated and important for virulence *in vivo.*

Gene 1	Gene 2	Gene 1 Description	Gene 2 Description	Gene 1 FC	Gene 2 FC	af
LMRG_01637 lmo2195 oppB	LMRG_01638 lmo2194 oppC	Peptide/nickel transport system permease	Peptide/nickel transport system permease	615.7	387.0	1.00
LMRG_02073 lmo0974 dltA	LMRG_02071 lmo0972 dltC	D-alanine-poly(phosphoribitol) ligase subunit 1	D-alanine-poly(phosphoribitol) ligase subunit 2	227.3	64.8	0.94
LMRG_01103 lmo1956 fur	LMRG_02757 lmo1683 perR	fur family transcriptional regulator	fur family transcriptional regulator	247.2	987.5	1.00
LMRG_02624 lmo0202 hly	LMRG_02629 lmo0207	listeriolysin O	hypothetical protein	818.5	109.5	0.96
LMRG_00744 lmo1294 miaA	LMRG_00062 lmo0370	tRNA delta(2)-isopentenylpyrophosphate transferase	alkylphosphonate utilization operon protein PhnA	890.1	469.6	0.96
LMRG_01351 lmo1615 trmB	LMRG_00771 lmo1321 ylxS	tRNA (guanine-N(7)-)-methyltransferase	Ribosome maturation factor RimP	485.9	873.4	0.94
LMRG_00859 lmo1407 pflA	LMRG_00397 lmo0708	pyruvate formate-lyase 1-activating enzyme	flagellar biosynthesis protein fliS	444.9	1030.9	0.92
LMRG_01007 lmo1860 msrA	LMRG_00459 lmo0771	peptide-methionine (S)-S-oxide reductase	hypothetical protein	779.2	1328.2	0.96
LMRG_00751 lmo1301	LMRG_00563 lmo1121	N-acetyltransferase domain-containing protein	hypothetical protein	468.1	409.2	0.96

Input/Ouput fold reduction in zebrafish abbreviated as FC.
AlphaFold predicted interaction score abbreviated as af.

Supplementary Table

Table S3.1 Essential genes in *L. monocytogenes.*

	locus_tag	description
Essential genes in both studies	LMRG_00415	glutamine-fructose-6-phosphate transaminase
	LMRG_00512	polypeptide deformylase
	LMRG_00533	cell division protein FtsW
	LMRG_00534	pyruvate carboxylase
	LMRG_00536	teichoic acid transport system permease
	LMRG_00539	hypothetical protein
	LMRG_00547	CDP-ribitol:poly(ribitol phosphate) ribitol phosphotransferase
	LMRG_00548	2-C-methyl-D-erythritol 4-phosphate cytidylyltransferase
	LMRG_00549	alcohol dehydrogenase
	LMRG_00550	hypothetical protein
	LMRG_00551	glycerol-3-phosphate cytidylyltransferase
	LMRG_00552	hypothetical protein
	LMRG_00553	hypothetical protein
	LMRG_00554	nicotinate phosphoribosyltransferase
	LMRG_00555	NAD+ synthetase
	LMRG_00558	GMP synthase
	LMRG_00667	phenylalanyl-tRNA synthetase alpha subunit
	LMRG_00668	phenylalanyl-tRNA synthetase beta subunit
	LMRG_00674	ribonuclease HIII
	LMRG_00679	thioredoxin
	LMRG_00683	glutamate racemase
	LMRG_00722	ribosome biogenesis GTP-binding protein YlqF
	LMRG_00725	DNA topoisomerase I
	LMRG_00734	hypothetical protein
	LMRG_00736	DNA topoisomerase IV B subunit
	LMRG_00737	DNA topoisomerase IV A subunit
	LMRG_00749	glutamine synthetase type I
	LMRG_00752	LexA repressor
	LMRG_00756	hypothetical protein
	LMRG_00763	UMP kinase
	LMRG_00764	ribosome recycling factor
	LMRG_00765	di-trans,poly-cis-decaprenylcistransferase
	LMRG_00766	phosphatidate cytidylyltransferase
	LMRG_00769	prolyl-tRNA synthetase

Essential genes in both studies

LMRG_00770	DNA polymerase III alpha subunit
LMRG_00772	transcription termination factor NusA
LMRG_00774	hypothetical protein
LMRG_00781	polyribonucleotide nucleotidyltransferase
LMRG_00806	acetyl-CoA carboxylase
LMRG_00807	acetyl-CoA carboxylase
LMRG_00828	6-phosphogluconate dehydrogenase
LMRG_00835	isopentenyl-diphosphate delta-isomerase type 2
LMRG_00848	CDP-diacylglycerol-glycerol-3-phosphate 3-phosphatidyltransferase
LMRG_00850	RecA protein
LMRG_00851	hypothetical protein
LMRG_00866	acetyl-CoA C-acetyltransferase
LMRG_00867	hydroxymethylglutaryl-CoA synthase
LMRG_00872	UDP-N-acetylenolpyruvoylglucosamine reductase
LMRG_00887	dihydrodipicolinate synthase
LMRG_00888	aspartate kinase
LMRG_00889	aspartate-semialdehyde dehydrogenase
LMRG_00890	hypothetical protein
LMRG_00900	manganese-dependent inorganic pyrophosphatase
LMRG_00905	hypothetical protein
LMRG_00906	RNA polymerase sigma factor rpoD
LMRG_00907	DNA primase
LMRG_00910	glycyl-tRNA synthetase beta subunit
LMRG_00911	glycyl-tRNA synthetase alpha subunit
LMRG_00912	DNA repair protein RecO
LMRG_00917	metalloprotease
LMRG_00922	30S ribosomal protein S21
LMRG_00925	chaperone DnaJ
LMRG_00926	chaperone DnaK
LMRG_00927	co-chaperone GrpE
LMRG_00934	DNA polymerase III delta subunit
LMRG_00941	nicotinate nucleotide adenylyltransferase
LMRG_00944	ribosome biogenesis GTPase YqeH
LMRG_00945	HAD superfamily phosphatase
LMRG_00948	signal recognition particle protein
LMRG_00950	signal recognition particle-docking protein FtsY
LMRG_00951	chromosome segregation protein SMC
LMRG_00953	acyl carrier protein

Essential genes in both studies	LMRG_00954	3-oxoacyl-[acyl-carrier-protein] reductase
	LMRG_00955	malonyl CoA-acyl carrier protein transacylase
	LMRG_00970	methionyl-tRNA formyltransferase
	LMRG_00971	primosomal protein N'
	LMRG_00972	phosphopantothenoylcysteine decarboxylase/phosphopantothenate-cysteine ligase
	LMRG_00974	guanylate kinase
	LMRG_01020	dihydrofolate reductase
	LMRG_01021	thymidylate synthase
	LMRG_01035	cell cycle protein gpsB
	LMRG_01042	DNA replication protein
	LMRG_01044	aspartate aminotransferase
	LMRG_01051	hypothetical protein
	LMRG_01052	CCA-adding enzyme
	LMRG_01054	dihydrodipicolinate reductase
	LMRG_01080	GTP cyclohydrolase I
	LMRG_01081	DNA-binding protein HU-beta
	LMRG_01083	glycerol-3-phosphate dehydrogenase, NAD-dependent
	LMRG_01084	ribosome-associated GTPase EngA
	LMRG_01086	cytidylate kinase
	LMRG_01124	ribonuclease Z
	LMRG_01166	hypothetical protein
	LMRG_01167	diaminopimelate epimerase
	LMRG_01168	isoleucyl-tRNA synthetase
	LMRG_01181	cell division protein FtsZ
	LMRG_01182	cell division protein FtsA
	LMRG_01183	cell division protein FtsQ
	LMRG_01184	undecaprenyldiphospho-muramoylpentapeptide beta-N-acetylglucosaminyltransferase
	LMRG_01185	UDP-N-acetylmuramoylalanine-D-glutamate ligase
	LMRG_01186	phospho-N-acetylmuramoyl-pentapeptide-transferase
	LMRG_01187	UDP-N-acetylmuramoyl-L-alanyl-D-glutamate-2
	LMRG_01188	penicillin binding protein 2B
	LMRG_01189	cell division protein FtsL
	LMRG_01202	pantetheine-phosphate adenylyltransferase
	LMRG_01218	chaperonin GroL
	LMRG_01219	chaperonin GroS
	LMRG_01226	O-sialoglycoprotein endopeptidase
	LMRG_01228	hypothetical protein

Essential genes in both studies	LMRG_01229	hypothetical protein
	LMRG_01272	phosphoglucosamine mutase
	LMRG_01274	hypothetical protein
	LMRG_01303	methionine adenosyltransferase
	LMRG_01307	leucyl-tRNA synthetase
	LMRG_01309	30S ribosomal protein S2
	LMRG_01310	translation elongation factor Ts
	LMRG_01319	1-acyl-sn-glycerol-3-phosphate acyltransferase
	LMRG_01361	UDP-N-acetylmuramate-alanine ligase
	LMRG_01365	hypothetical protein
	LMRG_01369	tyrosyl-tRNA synthetase
	LMRG_01371	30S ribosomal protein S4
	LMRG_01373	septation ring formation regulator EzrA
	LMRG_01394	acetyl-CoA carboxylase carboxyl transferase beta subunit
	LMRG_01395	acetyl-CoA carboxylase carboxyl transferase alpha subunit
	LMRG_01396	6-phosphofructokinase
	LMRG_01404	dephospho-CoA kinase
	LMRG_01406	replication initiation and membrane attachment protein
	LMRG_01407	primosomal protein DnaI
	LMRG_01408	threonyl-tRNA synthetase
	LMRG_01412	porphobilinogen deaminase
	LMRG_01413	uroporphyrinogen-III synthase
	LMRG_01414	delta-aminolevulinic acid dehydratase
	LMRG_01416	valyl-tRNA synthetase
	LMRG_01417	folylpolyglutamate synthase
	LMRG_01422	rod shape-determining protein mreB
	LMRG_01423	rod shape-determining protein MreC
	LMRG_01424	rod shape-determining protein MreD
	LMRG_01427	hypothetical protein
	LMRG_01428	50S ribosomal protein L21
	LMRG_01429	hypothetical protein
	LMRG_01430	50S ribosomal protein L27
	LMRG_01433	GTP-binding protein
	LMRG_01441	hypothetical protein
	LMRG_01447	GTP pyrophosphokinase
	LMRG_01450	histidyl-tRNA synthetase
	LMRG_01451	aspartyl-tRNA synthetase
	LMRG_01457	cysteine desulfurase
	LMRG_01458	tRNA methyl transferase

Essential genes in both studies	LMRG_01466	alanyl-tRNA synthetase
	LMRG_01468	hypothetical protein
	LMRG_01474	transcription elongation factor greA
	LMRG_01562	ATP-dependent nuclease subunit B
	LMRG_01630	3-oxoacyl-[acyl-carrier-protein] synthase 3
	LMRG_01631	3-oxoacyl-[acyl-carrier-protein] synthase 2
	LMRG_01634	tryptophanyl-tRNA synthetase
	LMRG_01639	peptide/nickel transport system ATP-binding protein
	LMRG_01640	oligopeptide transport ATP-binding protein oppF
	LMRG_01641	arsenate reductase
	LMRG_01677	ribonucleoside-diphosphate reductase subunit alpha
	LMRG_01678	ribonucleoside-diphosphate reductase
	LMRG_01679	ribonucleotide reductase-associated flavodoxin
	LMRG_01680	thioredoxin
	LMRG_01691	fructose-16-bisphosphate aldolase class II
	LMRG_01704	peptide chain release factor 1
	LMRG_01706	translation factor
	LMRG_01710	UDP-N-acetylglucosamine 2-epimerase
	LMRG_01722	UDP-N-acetylglucosamine 1-carboxyvinyltransferase
	LMRG_01724	beta-hydroxyacyl-(acyl-carrier-protein) dehydratase FabZ
	LMRG_01727	N-acetylglucosaminyldiphosphoundecaprenol
	LMRG_01738	preprotein translocase SecA subunit
	LMRG_01739	peptide chain release factor 2
	LMRG_01741	cell division ATP-binding protein FtsE
	LMRG_01742	cell division transport system permease
	LMRG_01761	hypothetical protein
	LMRG_01765	HPr(Ser) kinase/phosphatase
	LMRG_01770	thioredoxin-disulfide reductase
	LMRG_01773	phosphoglucomutase/phosphomannomutase
	LMRG_01776	hypothetical protein
	LMRG_01780	Clp protease
	LMRG_01789	glyceraldehyde-3-phosphate dehydrogenase
	LMRG_01790	phosphoglycerate kinase
	LMRG_01791	triosephosphate isomerase
	LMRG_01793	phosphopyruvate hydratase
	LMRG_01800	SsrA-binding protein
	LMRG_01833	FeS assembly ATPase SufC
	LMRG_01834	FeS assembly protein SufD
	LMRG_01835	selenocysteine lyase

Essential genes in noth studies	LMRG_01836	NifU family SUF system FeS assembly protein
	LMRG_01837	FeS assembly protein SufB
	LMRG_01907	ParB family chromosome partitioning protein
	LMRG_01908	hypothetical protein
	LMRG_01949	seryl-tRNA synthetase
	LMRG_01993	DNA polymerase III subunit gamma/tau
	LMRG_01994	hypothetical protein
	LMRG_02026	phosphoglycerol transferase
	LMRG_02067	inorganic polyphosphate/ATP-NAD kinase 1
	LMRG_02069	enoyl-[acyl-carrier protein] reductase I
	LMRG_02103	phosphoenolpyruvate-protein phosphotransferase
	LMRG_02106	aminotransferase
	LMRG_02111	2,3,4,5-tetrahydropyridine-2,6-dicarboxylate N-acetyltransferase
	LMRG_02112	N-acetyl-L,L-diaminopimelate deacetylase
	LMRG_02127	hypothetical protein
	LMRG_02128	hypothetical protein
	LMRG_02140	30S ribosomal protein S9
	LMRG_02144	cobalt/nickel transport system ATP-binding protein
	LMRG_02145	cobalt import ATP-binding protein cbiO 2
	LMRG_02149	50S ribosomal protein L17
	LMRG_02150	DNA-directed RNA polymerase alpha subunit
	LMRG_02151	30S ribosomal protein S11
	LMRG_02152	30S ribosomal protein S13
	LMRG_02155	adenylate kinase
	LMRG_02156	preprotein translocase SecY subunit
	LMRG_02157	50S ribosomal protein L15
	LMRG_02158	50S ribosomal protein L30
	LMRG_02159	30S ribosomal protein S5
	LMRG_02160	50S ribosomal protein L18
	LMRG_02161	50S ribosomal protein L6
	LMRG_02162	30S ribosomal protein S8
	LMRG_02163	30S ribosomal protein S14p/S29e
	LMRG_02164	large subunit ribosomal protein L5
	LMRG_02165	50S ribosomal protein L24
	LMRG_02166	50S ribosomal protein L14
	LMRG_02167	30S ribosomal protein S17
	LMRG_02168	50S ribosomal protein L29
	LMRG_02169	50S ribosomal protein L16
	LMRG_02170	30S ribosomal protein S3

Essential genes in both studies	LMRG_02171	50S ribosomal protein L22
	LMRG_02172	30S ribosomal protein S19
	LMRG_02173	50S ribosomal protein L2
	LMRG_02174	50S ribosomal protein L23
	LMRG_02175	50S ribosomal protein L4/L1
	LMRG_02176	50S ribosomal protein L3
	LMRG_02177	small subunit ribosomal protein S10
	LMRG_02198	translation elongation factor Tu
	LMRG_02199	translation elongation factor G
	LMRG_02200	30S ribosomal protein S7
	LMRG_02201	30S ribosomal protein S12
	LMRG_02240	thymidylate kinase
	LMRG_02250	hydroxymethylglutaryl-CoA reductase
	LMRG_02278	D-alanine-D-alanine ligase
	LMRG_02279	UDP-N-acetylmuramoylalanyl-D-glutamyl-2
	LMRG_02309	holo-(acyl-carrier-protein) synthase
	LMRG_02384	peptide/nickel transport system substrate-binding protein
	LMRG_02385	peptide/nickel transport system permease
	LMRG_02386	peptide/nickel transport system permease
	LMRG_02407	DNA polymerase III subunit delta
	LMRG_02426	ribonuclease P
	LMRG_02429	chromosomal replication initiator protein DnaA
	LMRG_02430	DNA polymerase III beta subunit
	LMRG_02434	DNA gyrase, B subunit
	LMRG_02435	DNA gyrase subunit A
	LMRG_02439	mevalonate kinase
	LMRG_02440	diphosphomevalonate decarboxylase
	LMRG_02441	phosphomevalonate kinase
	LMRG_02474	single-strand DNA-binding protein
	LMRG_02483	replicative DNA helicase
	LMRG_02513	DNA ligase
	LMRG_02515	aspartyl-tRNA(Asn)/glutamyl-tRNA amidotransferase subunit C
	LMRG_02516	glutamyl-tRNA(Gln) amidotransferase subunit A
	LMRG_02517	aspartyl/glutamyl-tRNA(Asn/Gln) amidotransferase subunit B
	LMRG_02561	methionine aminopeptidase type I
	LMRG_02584	response regulator VicR
	LMRG_02620	UDP-N-acetylglucosamine diphosphorylase/glucosamine-1-phosphate N-acetyltransferase
	LMRG_02621	ribose-phosphate pyrophosphokinase 1

Essential genes in both studies	LMRG_02635	peptidyl-tRNA hydrolase
	LMRG_02641	tRNA(Ile)-lysidine synthetase
	LMRG_02642	cell division protease FtsH
	LMRG_02650	DNA-directed RNA polymerase beta' subunit
	LMRG_02651	DNA-directed RNA polymerase beta subunit
	LMRG_02655	50S ribosomal protein L7/L12
	LMRG_02656	large subunit ribosomal protein L10
	LMRG_02657	50S ribosomal protein L1
	LMRG_02658	50S ribosomal protein L11
	LMRG_02667	cysteinyl-tRNA synthetase
	LMRG_02669	glutamyl-tRNA synthetase
	LMRG_02707	hypothetical protein
	LMRG_02708	arginyl-tRNA synthetase
	LMRG_02710	CTP synthase
	LMRG_02712	glucose-6-phosphate isomerase
	LMRG_02723	multicomponent Na+:H+ antiporter subunit A
	LMRG_02724	multicomponent Na+:H+ antiporter subunit B
	LMRG_02725	multicomponent Na+:H+ antiporter subunit C
	LMRG_02726	multicomponent Na+:H+ antiporter subunit D
	LMRG_02727	multicomponent Na+:H+ antiporter subunit E
	LMRG_02728	multicomponent Na+:H+ antiporter subunit F
	LMRG_02735	hypothetical protein
	LMRG_02742	methionyl-tRNA synthetase
	LMRG_02786	carbonic anhydrase
	LMRG_02811	50S ribosomal protein L19
	LMRG_02816	tRNA (guanine-N1)-methyltransferase
	LMRG_02817	16S rRNA processing protein RimM
	LMRG_02821	30S ribosomal protein S16
	LMRG_02827	translation initiation factor IF-3
	LMRG_02829	50S ribosomal protein L20
	LMRG_02836	lysyl-tRNA synthetase
	LMRG_02839	dihydroneopterin aldolase
	LMRG_02922	recombination helicase AddA
	LMRG_02938	serine O-acetyltransferase
	LMRG_02943	DNA polymerase III subunit alpha
	LMRG_02980	glucose-6-phosphate dehydrogenase
Essential only in this study	LMRG_00005	hypothetical protein
	LMRG_00008	TENA/THI-4 family protein
	LMRG_00048	fructose-specific PTS system IIA component
	LMRG_00138	hypothetical protein
	LMRG_00185	hypothetical protein
	LMRG_00215	ACT domain-containing protein
	LMRG_00230	hypothetical protein

Essential only in this study	LMRG_00423	ribulose-phosphate 3-epimerase
	LMRG_00424	ribose 5-phosphate isomerase B
	LMRG_00453	hypothetical protein
	LMRG_00587	propanediol utilization protein pduU
	LMRG_00589	alpha-ribazole-5-phosphate synthase CblS
	LMRG_00591	cobalamin-5-phosphate synthase
	LMRG_00592	alpha-ribazole phosphatase
	LMRG_00597	propanediol dehydratase medium subunit
	LMRG_00601	hypothetical protein
	LMRG_00639	precorrin-8X methylmutase
	LMRG_00640	cobalamin biosynthesis protein CbiD
	LMRG_00642	precorrin-8W decarboxylase
	LMRG_00643	precorrin-4 C11-methyltransferase
	LMRG_00644	cobalamin biosynthesis protein CbiG
	LMRG_00645	precorrin-3B C17-methyltransferase
	LMRG_00658	hypothetical protein
	LMRG_00775	translation initiation factor IF-2
	LMRG_00796	competence protein ComGB
	LMRG_00797	competence protein ComGA
	LMRG_00805	translation elongation factor P
	LMRG_00870	nucleotide pyrophosphatase
	LMRG_00921	hypothetical protein
	LMRG_00933	30S ribosomal protein S20
	LMRG_01019	rRNA (guanine-N1-)-methyltransferase
	LMRG_01069	hypothetical protein
	LMRG_01150	mannose-specific PTS system IIB component
	LMRG_01157	multiple sugar transport system permease
	LMRG_01158	response regulator YesN
	LMRG_01159	sensor histidine kinase YesM
	LMRG_01165	cold shock protein
	LMRG_01197	50S ribosomal protein L32
	LMRG_01252	pyridoxine biosynthesis protein
	LMRG_01336	indole-3-glycerol phosphate synthase
	LMRG_01453	nitrogen regulatory protein P-II
	LMRG_01496	polar amino acid transport system permease
	LMRG_01507	1-phosphofructokinase
	LMRG_01518	gp41
	LMRG_01522	gp44
	LMRG_01620	uroporphyrinogen decarboxylase

Essential only in this study	LMRG_01743	D-glutamyl-L-m-Dpm peptidase P45
	LMRG_01811	hypothetical protein
	LMRG_01816	hypothetical protein
	LMRG_01893	hypothetical protein
	LMRG_02057	GntR family transcriptional regulator
	LMRG_02086	methionine ABC transporter ATP-binding protein
	LMRG_02120	hypothetical protein
	LMRG_02141	50S ribosomal protein L13
	LMRG_02297	hypothetical protein
	LMRG_02363	bacteriophage-type repressor
	LMRG_02394	hypothetical protein
	LMRG_02395	hypothetical protein
	LMRG_02450	mannose-specific PTS system IIA component
	LMRG_02661	preprotein translocase SecE subunit
	LMRG_02802	DNA-binding/PRD domain-containing protein
	LMRG_02981	hypothetical protein
	LMRG_05003	Thr tRNA
	LMRG_05005	Leu tRNA
	LMRG_05007	Leu tRNA
	LMRG_05009	Pro tRNA
	LMRG_05012	Asn tRNA
	LMRG_05015	Asp tRNA
	LMRG_05020	Asn tRNA
	LMRG_05023	His tRNA
	LMRG_05024	Phe tRNA
	LMRG_05025	Asp tRNA
	LMRG_05026	Met tRNA
	LMRG_05027	Ser tRNA
	LMRG_05029	Met tRNA
	LMRG_05031	Pro tRNA
	LMRG_05033	Leu tRNA
	LMRG_05037	Thr tRNA
	LMRG_05040	Leu tRNA
	LMRG_05044	Gln tRNA
	LMRG_05046	Leu tRNA
	LMRG_05047	Cys tRNA
	LMRG_05049	Gln tRNA
	LMRG_05050	His tRNA
	LMRG_05051	Trp tRNA
	LMRG_05053	Phe tRNA
	LMRG_05054	Asp tRNA
	LMRG_05055	Met tRNA
	LMRG_05059	Asn tRNA

	LMRG_05063	Thr tRNA
	LMRG_05064	Asn tRNA
Essential only in Fischer et al.	LMRG_00327	cadmium-translocating P-type ATPase
	LMRG_00358	hypothetical protein
	LMRG_00514	pyruvate dehydrogenase E1 component
	LMRG_00515	pyruvate dehydrogenase E1 component subunit beta
	LMRG_00516	pyruvate dehydrogenase E2 component
	LMRG_00537	teichoic acids export ATP-binding protein tagH
	LMRG_00540	UTP-glucose-1-phosphate uridylyltransferase
	LMRG_02906	translation initiation factor IF-1
	LMRG_00721	signal peptidase I
	LMRG_00727	tyrosine recombinase XerC
	LMRG_00730	GTP-sensing transcriptional pleiotropic repressor CodY
	LMRG_02940	glutamyl-tRNA reductase
	LMRG_00744	tRNA delta(2)-isopentenylpyrophosphate transferase
	LMRG_00773	hypothetical protein
	LMRG_00776	hypothetical protein
	LMRG_00777	ribosome-binding factor A
	LMRG_00780	30S ribosomal protein S15
	LMRG_00810	hypothetical protein
	LMRG_00813	geranyltranstransferase
	LMRG_00891	superoxide dismutase
	LMRG_00902	DEAD-box ATP-dependent RNA helicase cshB
	LMRG_00914	GTP-binding protein Era
	LMRG_00952	ribonuclease III
	LMRG_00956	fatty acid/phospholipid synthesis protein PlsX
	LMRG_00963	50S ribosomal protein L28
	LMRG_00965	ribulose-phosphate 3-epimerase
	LMRG_00966	ribosome small subunit-dependent GTPase A
	LMRG_00968	serine/threonine phosphatase stp
	LMRG_00979	orotidine 5'-phosphate decarboxylase
	LMRG_01026	cold shock protein
	LMRG_01038	recombination protein U
	LMRG_01047	aspartate 1-decarboxylase
	LMRG_01048	pantoate-beta-alanine ligase
	LMRG_01049	3-methyl-2-oxobutanoate hydroxymethyltransferase
	LMRG_01077	heptaprenyl diphosphate synthase component II
	LMRG_01079	trans-hexaprenyltranstransferase
	LMRG_01092	hypothetical protein

Essential only in Fischer et al.	LMRG_01097	segregation and condensation protein B
	LMRG_01098	ScpA/B protein
	LMRG_01102	tyrosine recombinase XerD
	LMRG_01170	transcriptional repressor
	LMRG_01195	2-dehydropantoate 2-reductase
	LMRG_01267	heme peroxidase
	LMRG_01290	1,4-dihydroxy-2-naphthoate octaprenyltransferase
	LMRG_01304	asparagine synthase
	LMRG_01346	succinyl-diaminopimelate desuccinylase
	LMRG_01386	acetate kinase
	LMRG_01409	ribosome biogenesis GTP-binding protein YsxC
	LMRG_01415	glutamate-1-semialdehyde-2,1-aminomutase
	LMRG_01437	Holliday junction DNA helicase RuvA
	LMRG_01438	Holliday junction DNA helicase RuvB
	LMRG_01443	bifunctional preprotein translocase subunit SecD/SecF
	LMRG_01514	transcriptional regulator, Cro/CI family
	LMRG_01570	hypothetical protein
	LMRG_01613	foldase prsA 2
	LMRG_01615	hypothetical protein
	LMRG_01627	phosphoglycerate mutase
	LMRG_01699	50S ribosomal protein L31
	LMRG_01713	ATP synthase F0 A subunit
	LMRG_01714	F-type H+-transporting ATPase subunit C
	LMRG_01715	ATP synthase F0 B subunit
	LMRG_01716	ATP synthase F1 delta subunit
	LMRG_01717	ATP synthase F1 alpha subunit
	LMRG_01792	2,3-bisphosphoglycerate-independent phosphoglycerate mutase
	LMRG_01972	DNA binding 3-demethylubiquinone-9 3-methyltransferase domain-containing protein
	LMRG_01977	tRNA-adenosine deaminase
	LMRG_01995	recombination protein RecR
	LMRG_02045	hypothetical protein
	LMRG_02070	D-alanine transfer protein
	LMRG_02071	D-alanine-poly(phosphoribitol) ligase subunit 2
	LMRG_02072	membrane protein
	LMRG_02073	D-alanine-poly(phosphoribitol) ligase subunit 1
	LMRG_02102	phosphocarrier protein HPr
	LMRG_02153	50S ribosomal protein L36

Essentail only in Fischer et al.	LMRG_02289	ATP-dependent RNA helicase DeaD
	LMRG_02308	protoporphyrinogen oxidase
	LMRG_02383	hypothetical protein
	LMRG_02427	50S ribosomal protein L34
	LMRG_02432	hypothetical protein
	LMRG_02433	DNA replication and repair protein recF
	LMRG_02473	30S ribosomal protein S6
	LMRG_02475	30S ribosomal protein S18
	LMRG_02512	ATP-dependent DNA helicase PcrA
	LMRG_02583	sensor histidine kinase VicK
	LMRG_02618	stage V sporulation protein G
	LMRG_02639	DivIC protein
	LMRG_02660	transcription termination/antitermination factor NusG
	LMRG_02705	4-oxalocrotonate tautomerase
	LMRG_02762	enoyl-[acyl carrier protein] reductase III
	LMRG_02765	dUTP pyrophosphatase
	LMRG_02785	GTP pyrophosphokinase
	LMRG_02828	50S ribosomal protein L35
	LMRG_02838	7,8-dihydro-6-hydroxymethylpterin-pyrophosphokinase
	LMRG_02982	hypothetical protein
	LMRG_02983	hypothetical protein

Table S3.2. Comparison of *L. monocytogenes* virulence genes in BMDM from this study and in J774 macrophages by Fischer et al.

Catergory	Genes	Description
Genes negatively selected in both screen	LMRG_00265	protein translocase subunit secA 2
	LMRG_00838	DNA translocase ftsK
	LMRG_01070	3-phosphoshikimate 1-carboxyvinyltransferase
	LMRG_01075	chorismate synthase
	LMRG_01169	cell division initiation protein
	LMRG_01291	menaquinone-specific isochorismate synthase
	LMRG_01294	naphthoate synthase
	LMRG_01617	ABC-2 type transport system ATP-binding protein
	LMRG_01618	ABC-2 type transport system permease
	LMRG_01618	ABC-2 type transport system permease
	LMRG_01701	threonine synthase
	LMRG_01728	O-succinylbenzoic acid synthetase
	LMRG_01775	hypothetical protein
	LMRG_02485	adenylosuccinate synthetase
	LMRG_02498	adenylosuccinate lyase
	LMRG_02622	listeriolysin regulatory protein
	LMRG_02623	1-phosphatidylinositol phosphodiesterase
	LMRG_02624	listeriolysin O
	LMRG_02730	ComA operon protein 2
	LMRG_02753	dimethyladenosine transferase
Only negatively selected in this study	LMRG_00057	high-affinity iron transporter
	LMRG_00107	peptidoglycan N-acetylglucosamine deacetylase
	LMRG_00184	galactitol-specific PTS system IIA component
	LMRG_00186	ribulose-phosphate 3-epimerase
	LMRG_00264	invasion associated secreted endopeptidase
	LMRG_00281	biotin biosynthesis protein BioY
	LMRG_00314	hypothetical protein
	LMRG_00422	LacI family transcriptional regulator
	LMRG_00514	pyruvate dehydrogenase E1 component
	LMRG_00515	pyruvate dehydrogenase E1 component subunit beta
	LMRG_00516	pyruvate dehydrogenase E2 component
	LMRG_00517	dihydrolipoyl dehydrogenase
	LMRG_00561	hypothetical protein
	LMRG_00712	transcriptional regulator
	LMRG_00768	RIP metalloprotease RseP

Only negatively selected in this study	LMRG_00777	ribosome-binding factor A
	LMRG_00809	transcription antitermination factor NusB
	LMRG_00833	acylphosphatase
	LMRG_00853	hypothetical protein
	LMRG_00914	GTP-binding protein Era
	LMRG_00956	fatty acid/phospholipid synthesis protein PlsX
	LMRG_00958	ATP-dependent DNA helicase RecG
	LMRG_00965	ribulose-phosphate 3-epimerase
	LMRG_01038	recombination protein U
	LMRG_01039	penicillin binding protein 1A
	LMRG_01048	pantoate-beta-alanine ligase
	LMRG_01049	3-methyl-2-oxobutanoate hydroxymethyltransferase
	LMRG_01074	3-dehydroquinate synthase
	LMRG_01178	YggT family protein
	LMRG_01179	cell division protein sepF
	LMRG_01190	methylase MraW
	LMRG_01195	2-dehydropantoate 2-reductase
	LMRG_01199	hypothetical protein
	LMRG_01248	galactitol-specific PTS system IIB component
	LMRG_01292	2-succinyl-5-enolpyruvyl-6-hydroxy-3-cyclohexene-1-carboxylate synthase
	LMRG_01295	O-succinylbenzoate-CoA ligase
	LMRG_01302	hypothetical protein
	LMRG_01313	cellsurface protein
	LMRG_01367	bifunctional 3-deoxy-7-phosphoheptulonate synthase/chorismate mutase
	LMRG_01524	gp47
	LMRG_01525	recombination protein RecT
	LMRG_01532	phage terminase large subunit
	LMRG_01700	homoserine dehydrogenase
	LMRG_01702	homoserine kinase
	LMRG_01712	ATP synthase I
	LMRG_01713	ATP synthase F0 A subunit
	LMRG_01714	F-type H+-transporting ATPase subunit C
	LMRG_01715	ATP synthase F0 B subunit
	LMRG_01716	ATP synthase F1 delta subunit
	LMRG_01717	ATP synthase F1 alpha subunit
	LMRG_01719	ATP synthase F1 beta subunit
	LMRG_01720	ATP synthase F1 epsilon subunit

Only negatively selected in this study	LMRG_01745	cardiolipin synthase
	LMRG_01774	hypothetical protein
	LMRG_01797	preprotein translocase SecG subunit
	LMRG_01846	hypothetical protein
	LMRG_01926	antibiotic transport system ATP-binding protein
	LMRG_01927	hypothetical protein
	LMRG_02063	hypothetical protein
	LMRG_02136	CRISPR-associated protein cas2
	LMRG_02211	galactitol-specific PTS system IIB component
	LMRG_02274	hypothetical protein
	LMRG_02346	mannose-specific PTS system IIC component
	LMRG_02433	DNA replication and repair protein recF
	LMRG_02522	shikimate kinase
	LMRG_02523	hypothetical protein
	LMRG_02524	hypothetical protein
	LMRG_02525	hypothetical protein
	LMRG_02530	hypothetical protein
	LMRG_02531	polar amino acid transport system permease
	LMRG_02532	polar amino acid transport system ATP-binding protein
	LMRG_02582	YycH protein
	LMRG_02583	sensor histidine kinase VicK
	LMRG_02765	dUTP pyrophosphatase
	LMRG_02769	hypothetical protein
	LMRG_05513	5S ribosomal RNA
	LMRG_05516	5S ribosomal RNA
Only negatively selected in Fischer et al.	LMRG_00266	hypothetical protein
	LMRG_00362	motility repressor mogR
	LMRG_00408	PadR family transcriptional regulator
	LMRG_00799	glycine cleavage system P-protein
	LMRG_00800	glycine dehydrogenase subunit 2
	LMRG_00822	2-oxoisovalerate dehydrogenase E1 component
	LMRG_00823	2-oxoisovalerate dehydrogenase E1 component
	LMRG_00980	dihydroorotate oxidase
	LMRG_01347	D-amino acid aminotransferase
	LMRG_01392	hypothetical protein
	LMRG_01636	peptide/nickel transport system substrate-binding protein
	LMRG_01906	chromosome partitioning protein
	LMRG_01946	hypothetical protein
	LMRG_01978	cytochrome bd-I oxidase subunit I

	LMRG_01981	ABC transporter CydDC cysteine exporter CydC
	LMRG_02030	lipoate-protein ligase A
	LMRG_02107	hypothetical protein
	LMRG_02373	hypothetical protein
	LMRG_02580	ribonuclease Z
	LMRG_02627	phospholipase C
	LMRG_02703	hypothetical protein
	LMRG_02974	hypothetical protein

Table S3.3. *L. monocytogenes* genes important for *in vivo* fitness in zebrafish.

locus_tag	description	Input/Output	P-value
LMRG_00002	threonine aldolase	678.65	7.1E-03
LMRG_00006	hypothetical protein	667.61	1.4E-05
LMRG_00009	hydroxyethylthiazole kinase	775.61	7.7E-06
LMRG_00010	phosphomethylpyrimidine kinase	226.06	1.8E-05
LMRG_00014	hypothetical protein	865.39	2.3E-06
LMRG_00015	hypothetical protein	582.23	4.3E-02
LMRG_00016	lipoprotein	764.99	3.6E-05
LMRG_00019	transcriptional regulator	257.78	2.2E-04
LMRG_00022	hypothetical protein	438.83	6.1E-03
LMRG_00024	hypothetical protein	1422.98	3.6E-03
LMRG_00027	hypothetical protein	973.80	2.6E-06
LMRG_00028	hypothetical protein	501.54	3.1E-04
LMRG_00029	hypothetical protein	331.28	3.9E-05
LMRG_00030	inorganic pyrophosphatase	892.78	8.7E-05
LMRG_00032	hypothetical protein	312.07	4.2E-03
LMRG_00036	ribose 5-phosphate isomerase B	843.27	2.6E-04
LMRG_00038	dihydroxyacetone kinase L subunit	827.03	5.1E-03
LMRG_00040	hypothetical protein	715.48	2.7E-03
LMRG_00041	hypothetical protein	760.83	1.1E-06
LMRG_00042	dihydroxyacetone kinase	72.39	3.4E-04
LMRG_00044	hypothetical protein	1935.82	2.0E-06
LMRG_00051	transcriptional regulator	90.25	1.2E-03
LMRG_00053	twin arginine-targeting protein translocase TatC	1020.91	3.5E-05
LMRG_00054	sec-independent protein translocase tatAy	2278.72	6.7E-06
LMRG_00055	dipeptidase E	1340.17	2.5E-03
LMRG_00057	high-affinity iron transporter	85.40	2.4E-04
LMRG_00061	hypothetical protein	414.61	3.8E-02
LMRG_00062	alkylphosphonate utilization operon protein PhnA	469.62	1.4E-05
LMRG_00066	cellobiose-specific phosphotransferase enzyme IIB component	3248.31	3.5E-08
LMRG_00069	hypothetical protein	1008.86	1.2E-05
LMRG_00075	DeoR family transcriptional regulator	1038.87	2.2E-05
LMRG_00077	5-deoxy-glucuronate isomerase	363.35	1.2E-05

LMRG_00080	hypothetical protein	428.44	1.6E-02
LMRG_00081	hypothetical protein	1371.03	4.1E-02
LMRG_00082	low temperature requirement protein LtrA	413.74	3.1E-05
LMRG_00083	uracil-DNA glycosylase	191.55	2.5E-05
LMRG_00084	hypothetical protein	2195.67	7.4E-06
LMRG_00086	hypothetical protein	227.49	4.0E-06
LMRG_00091	fructose-specific PTS system IIA component	980.26	6.2E-08
LMRG_00092	fructose-specific PTS system IIB component	468.84	1.6E-05
LMRG_00096	hypothetical protein	652.54	1.9E-04
LMRG_00098	PiT family inorganic phosphate transporter	118.24	2.4E-05
LMRG_00099	lactoylglutathione lyase	321.92	1.1E-04
LMRG_00100	hypothetical protein	832.30	1.7E-05
LMRG_00101	hypothetical protein	464.01	4.8E-05
LMRG_00105	hypothetical protein	1343.79	2.0E-07
LMRG_00106	zinc transporter	657.51	4.7E-06
LMRG_00108	transcriptional regulator	43.38	4.0E-03
LMRG_00110	hypothetical protein	328.77	1.3E-04
LMRG_00111	hypothetical protein	346.91	1.3E-05
LMRG_00114	lineage-specific thermal regulator protein	988.86	2.6E-08
LMRG_00117	PRD/PTS system IIA 2 domain-containing regulatory protein	837.53	2.1E-05
LMRG_00118	fructose-specific PTS system IIA component	741.83	4.3E-05
LMRG_00120	fructose-specific PTS system IIC component	510.67	2.1E-02
LMRG_00123	hypothetical protein	899.03	3.9E-06
LMRG_00124	hypothetical protein	345.97	4.6E-02
LMRG_00128	hypothetical protein	1478.44	7.1E-07
LMRG_00137	hypothetical protein	854.89	1.0E-02
LMRG_00139	glutamate decarboxylase	1335.03	1.1E-02
LMRG_00142	hypothetical protein	271.90	3.3E-04
LMRG_00149	hypothetical protein	1158.90	1.2E-02
LMRG_00150	hypothetical protein	802.23	2.8E-03
LMRG_00151	hypothetical protein	574.92	2.3E-05

LMRG_00157	hypothetical protein	407.78	8.3E-05
LMRG_00165	heme-degrading monooxygenase IsdG	877.93	1.4E-05
LMRG_00166	hypothetical protein	2318.79	2.4E-06
LMRG_00172	3-dehydroquinate dehydratase type I	202.31	1.2E-03
LMRG_00177	hypothetical protein	372.44	1.0E-04
LMRG_00180	ribulose-phosphate 3-epimerase	199.68	2.6E-04
LMRG_00182	transcription antiterminator	64.94	1.5E-02
LMRG_00183	hypothetical protein	284.72	6.7E-04
LMRG_00184	galactitol-specific PTS system IIA component	417.87	1.2E-05
LMRG_00187	L-iditol 2-dehydrogenase	1774.81	1.4E-03
LMRG_00192	hypothetical protein	969.00	1.3E-07
LMRG_00193	hypothetical protein	523.67	3.8E-06
LMRG_00196	universal stress protein	727.53	1.6E-05
LMRG_00204	hypothetical protein	507.40	7.9E-03
LMRG_00214	hypothetical protein	82.92	1.5E-05
LMRG_00216	hypothetical protein	567.74	1.2E-03
LMRG_00220	N-acyl-L-amino acid amidohydrolase	853.35	8.2E-06
LMRG_00224	hypothetical protein	2852.75	7.2E-07
LMRG_00225	hypothetical protein	628.49	4.2E-02
LMRG_00234	hypothetical protein	803.58	1.5E-03
LMRG_00239	phosphoglycerate mutase	224.09	1.5E-03
LMRG_00240	6-phosphogluconolactonase	189.37	8.8E-03
LMRG_00241	hypothetical protein	845.97	8.4E-03
LMRG_00243	phosphoribosyl-ATP pyrophosphohydrolase	950.35	1.7E-04
LMRG_00244	phosphoribosyl-AMP cyclohydrolase	1905.25	2.2E-06
LMRG_00247	imidazole glycerol phosphate synthase	1033.58	2.6E-07
LMRG_00252	histidinol-phosphatase	175.12	1.5E-04
LMRG_00259	integral membrane protein	1130.49	5.1E-05
LMRG_00262	hypothetical protein	593.68	3.0E-05
LMRG_00264	invasion associated secreted endopeptidase	1934.88	1.2E-04
LMRG_00265	protein translocase subunit secA 2	992.66	3.3E-04
LMRG_00268	hypothetical protein	280.27	3.1E-06
LMRG_00276	homoserine O-acetyltransferase	1204.84	8.1E-04
LMRG_00278	hypothetical protein	11.98	5.8E-03
LMRG_00280	transcription regulator CRP/FNR family protein	1701.70	2.2E-06

LMRG_00281	biotin biosynthesis protein BioY	2134.31	4.8E-03
LMRG_00283	hypothetical protein	1287.02	1.4E-02
LMRG_00284	hypothetical protein	1175.17	1.3E-08
LMRG_00292	hypothetical protein	1175.36	6.6E-05
LMRG_00295	hypothetical protein	1291.21	1.6E-02
LMRG_00298	hypothetical protein	227.36	2.1E-05
LMRG_00302	hypothetical protein	363.31	1.7E-02
LMRG_00303	hypothetical protein	1335.47	6.2E-05
LMRG_00306	hypothetical protein	1327.95	1.6E-07
LMRG_00314	hypothetical protein	339.65	2.8E-05
LMRG_00318	2-haloalkanoic acid dehalogenase	1452.34	1.3E-03
LMRG_00323	hypothetical protein	105.38	4.7E-03
LMRG_00325	transcription regulator	685.36	3.4E-04
LMRG_00327	cadmium-translocating P-type ATPase	570.27	1.1E-02
LMRG_00331	hypothetical protein	252.64	6.6E-03
LMRG_00334	hypothetical protein	1027.29	7.6E-05
LMRG_00336	hypothetical protein	888.20	4.6E-05
LMRG_00337	membrane protein	195.12	3.0E-03
LMRG_00344	hypothetical protein	1327.57	9.3E-03
LMRG_00346	hypothetical protein	355.53	2.6E-05
LMRG_00347	transposase	628.97	4.8E-02
LMRG_00351	maltose O-acetyltransferase	4043.03	6.5E-04
LMRG_00352	hypothetical protein	1027.48	5.3E-07
LMRG_00362	motility repressor mogR	386.33	1.1E-06
LMRG_00364	flagellar biosynthetic protein FliP	28.57	6.1E-03
LMRG_00368	flagellar biosynthesis protein FlhA	190.63	2.2E-04
LMRG_00370	flagellar basal-body rod protein FlgG	443.72	1.5E-05
LMRG_00371	chemotaxis protein methyltransferase	305.66	3.1E-05
LMRG_00372	hypothetical protein	988.05	1.1E-04
LMRG_00373	chemotaxis protein MotA	1278.26	5.0E-06
LMRG_00379	chemotaxis protein cheY	1218.72	4.3E-02
LMRG_00380	chemotaxis protein cheA	831.25	5.5E-05
LMRG_00384	hypothetical protein	546.08	5.9E-03
LMRG_00388	flagellar motor switch protein FliM	740.88	6.2E-03
LMRG_00392	hypothetical protein	475.77	6.0E-06
LMRG_00395	flagellar hook-associated protein 3	784.12	4.4E-03
LMRG_00396	flagellar hook-associated protein 2	432.88	1.3E-02
LMRG_00397	flagellar biosynthesis protein fliS	1030.91	6.6E-08
LMRG_00403	flagellar motor switch protein FliG	525.36	1.9E-04

LMRG_00404	flagellar assembly protein H	520.51	4.9E-03
LMRG_00407	hypothetical protein	725.31	6.1E-05
LMRG_00408	PadR family transcriptional regulator	185.46	3.5E-04
LMRG_00414	peptidoglycan binding protein	415.60	2.0E-03
LMRG_00421	transcriptional regulator	1333.88	2.6E-02
LMRG_00422	LacI family transcriptional regulator	421.77	3.0E-04
LMRG_00431	hypothetical protein	679.07	2.4E-05
LMRG_00432	hypothetical protein	852.96	2.3E-05
LMRG_00433	hypothetical protein	1194.58	5.5E-07
LMRG_00435	hypothetical protein	308.01	2.0E-04
LMRG_00436	hypothetical protein	756.43	1.2E-04
LMRG_00442	hypothetical protein	10.62	3.7E-02
LMRG_00447	glyoxylase	776.93	2.4E-07
LMRG_00448	hypothetical protein	550.53	1.2E-07
LMRG_00452	lipoate-protein ligase A	361.61	3.1E-02
LMRG_00459	hypothetical protein	1328.21	7.9E-07
LMRG_00462	hypothetical protein	705.57	9.4E-06
LMRG_00463	hypothetical protein	594.00	5.0E-06
LMRG_00464	hypothetical protein	1807.01	7.9E-03
LMRG_00468	hypothetical protein	681.06	4.6E-04
LMRG_00469	mannose-specific PTS system IID component	1327.20	1.3E-05
LMRG_00478	YbaK/EbsC family protein	733.61	1.1E-03
LMRG_00484	YceI like family protein	874.34	1.7E-02
LMRG_00495	glycerol kinase	248.52	1.3E-05
LMRG_00498	hypothetical protein	1275.20	2.2E-03
LMRG_00500	molybdate transport system ATP-binding protein	264.90	4.1E-05
LMRG_00501	molybdate transport system permease	241.55	4.4E-06
LMRG_00502	molybdate ABC transporter periplasmic molybdate-binding protein	141.82	8.1E-05
LMRG_00504	molybdopterin-guanine dinucleotide biosynthesis protein B	48.80	6.0E-03
LMRG_00506	molybdopterin converting factor	392.75	1.2E-04
LMRG_00507	molybdenum cofactor biosynthesis protein C	363.40	9.7E-06
LMRG_00510	molybdopterin biosynthesis protein MoeB	633.64	2.5E-07
LMRG_00511	hypothetical protein	1214.94	1.7E-05

LMRG_00514	pyruvate dehydrogenase E1 component	221.00	5.3E-06
LMRG_00515	pyruvate dehydrogenase E1 component subunit beta	171.78	2.0E-04
LMRG_00516	pyruvate dehydrogenase E2 component	162.22	4.9E-04
LMRG_00517	dihydrolipoyl dehydrogenase	284.30	1.6E-05
LMRG_00518	hypothetical protein	567.15	2.5E-03
LMRG_00520	hypothetical protein	605.94	8.8E-05
LMRG_00522	hypothetical protein	953.28	7.3E-06
LMRG_00524	hypothetical protein	716.89	3.1E-02
LMRG_00535	iron complex transport system substrate-binding protein	388.83	8.7E-05
LMRG_00542	hypothetical protein	652.33	9.5E-05
LMRG_00545	dTDP-glucose 4,6-dehydratase	273.46	1.2E-03
LMRG_00556	monooxygenase	1964.55	6.7E-05
LMRG_00557	cellobiose-specific PTS system IIB component	1236.33	7.2E-04
LMRG_00563	hypothetical protein	409.18	3.2E-04
LMRG_00564	hypothetical protein	179.69	1.0E-04
LMRG_00565	hypothetical protein	339.80	5.1E-03
LMRG_00566	hypothetical protein	566.67	4.8E-06
LMRG_00568	acetyltransferase	451.61	1.8E-06
LMRG_00571	hypothetical protein	25.94	2.4E-02
LMRG_00575	hypothetical protein	669.86	4.1E-06
LMRG_00576	regulatory protein	80.77	5.1E-03
LMRG_00577	hypothetical protein	222.01	1.4E-06
LMRG_00582	hypothetical protein	920.03	1.2E-04
LMRG_00583	hypothetical protein	402.67	1.1E-05
LMRG_00584	hypothetical protein	966.19	8.0E-06
LMRG_00595	propanediol utilization protein pduB	330.67	2.0E-02
LMRG_00598	propanediol dehydratase small subunit	230.72	6.8E-05
LMRG_00600	hypothetical protein	363.40	7.5E-04
LMRG_00602	propanediol utilization polyhedral body protein PduJ	275.42	3.1E-03
LMRG_00603	hypothetical protein	530.32	4.2E-03
LMRG_00604	ethanolamine utilization protein EutJ	352.00	9.0E-05
LMRG_00605	propanediol utilization protein PduM	704.87	4.1E-07
LMRG_00607	ATP:Cob(I)alamin adenosyltransferase	273.55	4.4E-03
LMRG_00612	threonine-phosphate decarboxylase	566.26	1.0E-05

LMRG_00617	iron-containing alcohol dehydrogenase pduQ	254.24	2.4E-02
LMRG_00620	ethanolamine utilization protein EutA	247.11	3.2E-05
LMRG_00621	ethanolamine ammonia-lyase large subunit	518.13	9.7E-08
LMRG_00623	ethanolamine utilization protein EutL	423.51	6.0E-03
LMRG_00624	ethanolamine utilization polyhedral-body-like protein EutM	217.94	1.1E-04
LMRG_00628	ethanolamine utilization protein	410.17	1.2E-05
LMRG_00629	ethanolamine utilization protein	330.95	5.3E-06
LMRG_00630	ethanolamine utilization protein EutN	650.71	6.7E-04
LMRG_00631	ethanolamine utilization protein PduT	331.11	4.4E-05
LMRG_00632	ethanolamine transporter	1036.13	4.5E-06
LMRG_00633	ethanolamine utilization protein EutQ	115.69	4.9E-06
LMRG_00636	hypothetical protein	287.01	3.2E-04
LMRG_00649	precorrin-2 C20-methyltransferase	157.92	3.1E-04
LMRG_00650	cobalamin biosynthesis protein CbiM	67.45	1.5E-05
LMRG_00651	cobalt transporter	142.60	3.8E-04
LMRG_00653	ABC transporter ATP-binding protein	95.78	4.8E-03
LMRG_00659	hypothetical protein	418.93	1.4E-03
LMRG_00660	hypothetical protein	307.15	3.6E-04
LMRG_00665	hypothetical protein	215.03	1.1E-04
LMRG_00666	hypothetical protein	378.82	9.9E-06
LMRG_00669	ABC transporter ATP-binding protein	621.90	4.9E-06
LMRG_00675	hypothetical protein	140.02	8.5E-03
LMRG_00680	excinuclease ABC subunit C	418.39	1.4E-03
LMRG_00689	hypothetical protein	464.14	7.3E-03
LMRG_00692	ATP-dependent RNA helicase dbpA	268.78	7.6E-04
LMRG_00693	hypothetical protein	582.56	7.0E-06
LMRG_00695	hypothetical protein	1581.74	1.2E-05
LMRG_00699	hypothetical protein	514.20	9.0E-06
LMRG_00701	hypothetical protein	4001.96	2.5E-07
LMRG_00702	trehalose operon repressor	288.41	5.0E-02
LMRG_00706	hypothetical protein	495.33	2.4E-05
LMRG_00712	transcriptional regulator	194.58	1.9E-03
LMRG_00713	hypothetical protein	730.38	1.7E-03
LMRG_00715	hypothetical protein	943.59	1.1E-04
LMRG_00719	signal peptidase I	910.53	4.6E-05
LMRG_00721	signal peptidase I	226.12	6.5E-08

LMRG_00724	DNA processing protein	307.90	6.1E-09
LMRG_00728	ATP-dependent HslUV protease	1243.31	7.5E-05
LMRG_00735	hypothetical protein	969.82	3.2E-05
LMRG_00738	S-ribosylhomocysteinase LuxS	321.05	4.8E-08
LMRG_00740	internalin	834.24	5.7E-03
LMRG_00741	hypothetical protein	292.91	6.0E-04
LMRG_00742	hypothetical protein	166.55	3.6E-04
LMRG_00743	glycerol-3-phosphate dehydrogenase	624.06	5.6E-06
LMRG_00744	tRNA delta(2)-isopentenylpyrophosphate transferase	890.08	3.8E-06
LMRG_00745	host factor-I protein	314.45	1.0E-05
LMRG_00751	hypothetical protein	468.05	6.2E-05
LMRG_00753	cell division suppressor protein yneA	1027.26	1.1E-05
LMRG_00754	hypothetical protein	253.57	2.7E-04
LMRG_00755	transketolase	136.74	1.2E-04
LMRG_00759	hypothetical protein	76.79	2.3E-03
LMRG_00762	hypothetical protein	499.78	3.2E-07
LMRG_00771	hypothetical protein	873.37	4.8E-03
LMRG_00776	hypothetical protein	464.05	6.1E-05
LMRG_00777	ribosome-binding factor A	72.28	6.3E-03
LMRG_00783	hypothetical protein	64.13	2.4E-05
LMRG_00786	5-formyltetrahydrofolate cyclo-ligase	382.08	2.1E-02
LMRG_00787	rhomboid family protein	1150.13	5.2E-03
LMRG_00788	hypothetical protein	279.92	1.2E-04
LMRG_00790	hypothetical protein	321.25	2.4E-02
LMRG_00795	competence protein ComGC	104.12	9.8E-04
LMRG_00800	glycine dehydrogenase subunit 2	727.56	9.2E-03
LMRG_00802	hypothetical protein	514.40	2.5E-04
LMRG_00804	X-Pro aminopeptidase	1687.50	3.9E-07
LMRG_00808	hypothetical protein	448.31	3.0E-04
LMRG_00812	exodeoxyribonuclease VII small subunit	407.45	5.2E-05
LMRG_00813	geranyltranstransferase	117.02	3.0E-04
LMRG_00814	cold shock-like protein cspLA	102.74	1.3E-02
LMRG_00816	hemolysin	1247.61	2.3E-05
LMRG_00817	arginine repressor	711.45	8.5E-03
LMRG_00819	phosphate butyryltransferase	731.35	4.0E-05
LMRG_00821	dihydrolipoyl dehydrogenase	489.84	9.2E-06
LMRG_00822	2-oxoisovalerate dehydrogenase E1 component	473.89	4.6E-06

LMRG_00823	2-oxoisovalerate dehydrogenase E1 component	586.17	2.2E-05
LMRG_00824	2-oxoisovalerate dehydrogenase E2 component	366.33	9.4E-06
LMRG_00829	KDP operon response regulator KdpE	613.58	3.4E-06
LMRG_00830	sensor histidine kinase	426.19	1.5E-04
LMRG_00832	hypothetical protein	371.44	1.2E-04
LMRG_00834	hypothetical protein	295.75	4.0E-04
LMRG_00838	DNA translocase ftsK	210.69	4.3E-05
LMRG_00852	acetyltransferase	183.40	3.9E-06
LMRG_00853	hypothetical protein	176.57	9.6E-06
LMRG_00854	hypothetical protein	369.00	4.1E-05
LMRG_00859	pyruvate formate-lyase 1-activating enzyme	444.87	5.5E-05
LMRG_00863	transcriptional regulator	384.82	3.8E-03
LMRG_00865	peptidoglycan bound protein	11.83	2.6E-03
LMRG_00869	MFS transporter	256.54	1.4E-04
LMRG_00874	hypothetical protein	648.10	6.7E-08
LMRG_00875	hypothetical protein	808.15	5.9E-03
LMRG_00878	osmoprotectant transport system substrate-binding protein	613.54	3.1E-03
LMRG_00879	osmoprotectant transport system permease	514.41	1.4E-06
LMRG_00880	osmoprotectant transport system ATP-binding protein	283.55	5.2E-04
LMRG_00881	proton-coupled thiamine transporter YuaJ	2869.75	1.0E-05
LMRG_00884	hypothetical protein	256.50	1.1E-02
LMRG_00891	superoxide dismutase	147.41	2.2E-04
LMRG_00895	hypothetical protein	515.49	3.5E-04
LMRG_00902	DEAD-box ATP-dependent RNA helicase cshB	26.16	9.1E-06
LMRG_00914	GTP-binding protein Era	410.28	9.0E-05
LMRG_00915	cytidine deaminase	715.69	8.7E-03
LMRG_00916	diacylglycerol kinase	106.40	8.8E-04
LMRG_00919	phosphate starvation-inducible protein PhoH	1059.76	3.4E-02
LMRG_00928	heat-inducible transcription repressor HrcA	261.17	1.1E-02

LMRG_00937	competence protein ComEA	73.68	2.7E-03
LMRG_00939	iojap protein 155	330.43	1.5E-02
LMRG_00942	hypothetical protein	711.05	1.0E-02
LMRG_00952	ribonuclease III	639.74	1.8E-08
LMRG_00961	hypothetical protein	344.85	1.9E-02
LMRG_00964	thiamine pyrophosphokinase	36.15	9.8E-04
LMRG_00965	ribulose-phosphate 3-epimerase	103.57	2.1E-04
LMRG_00969	ribosomal RNA small subunit methyltransferase B	747.32	2.2E-05
LMRG_00981	dihydroorotate dehydrogenase electron transfer subunit	156.34	5.6E-05
LMRG_00983	carbamoyl-phosphate synthase small subunit	120.87	1.6E-04
LMRG_00992	AGZA family MFS transporter xanthine/uracil permease	471.20	1.2E-03
LMRG_00996	manganese/iron transport system ATP-binding protein	504.49	4.4E-07
LMRG_00997	hypothetical protein	225.90	3.5E-05
LMRG_01001	hypothetical protein	490.71	3.1E-05
LMRG_01005	hypothetical protein	594.19	4.5E-03
LMRG_01007	peptide-methionine (S)-S-oxide reductase	779.18	4.7E-05
LMRG_01010	hypothetical protein	424.85	2.2E-03
LMRG_01015	lactoylglutathione lyase	1153.66	4.8E-08
LMRG_01024	transcriptional regulator mntR	594.77	9.6E-05
LMRG_01026	cold shock protein	72.08	4.8E-03
LMRG_01027	ribonuclease HI	466.99	1.7E-02
LMRG_01029	30S ribosomal protein S14	100.91	3.7E-03
LMRG_01030	chitinase	542.05	9.4E-07
LMRG_01032	xanthine phosphoribosyltransferase	186.49	1.7E-03
LMRG_01033	carboxypeptidase Taq	525.38	7.4E-07
LMRG_01034	N6-adenine-specific DNA methylase	434.39	6.1E-06
LMRG_01036	hypothetical protein	531.04	1.3E-06
LMRG_01037	hypothetical protein	2545.12	1.3E-06
LMRG_01038	recombination protein U	101.21	2.0E-02
LMRG_01039	penicillin binding protein 1A	95.06	1.9E-05
LMRG_01040	hypothetical protein	790.60	2.0E-05
LMRG_01041	endonuclease III	481.18	3.1E-05
LMRG_01043	asparaginyl-tRNA synthetase	447.08	1.6E-03

LMRG_01046	DnaQ family exonuclease/DinG family helicase	403.92	1.5E-02
LMRG_01048	pantoate-beta-alanine ligase	133.79	1.6E-04
LMRG_01049	3-methyl-2-oxobutanoate hydroxymethyltransferase	775.17	3.6E-04
LMRG_01053	methylglyoxal synthase	788.80	1.7E-04
LMRG_01058	hypothetical protein	553.16	3.9E-05
LMRG_01059	hypothetical protein	465.96	3.0E-04
LMRG_01064	formate acetyltransferase	347.03	1.7E-02
LMRG_01068	hypothetical protein	497.59	7.2E-06
LMRG_01070	3-phosphoshikimate 1-carboxyvinyltransferase	91.19	1.2E-04
LMRG_01074	3-dehydroquinate synthase	121.91	6.3E-07
LMRG_01075	chorismate synthase	81.16	4.3E-04
LMRG_01078	2-heptaprenyl-1,4-naphthoquinone methyltransferase	410.41	2.6E-02
LMRG_01082	protein-tyrosine phosphatase	716.85	7.9E-06
LMRG_01087	L-asparaginase	19.24	1.3E-04
LMRG_01091	ferredoxin	314.78	3.4E-02
LMRG_01099	diaminopimelate decarboxylase	286.59	1.1E-03
LMRG_01100	purine nucleoside phosphorylase I	821.14	1.5E-02
LMRG_01101	phosphopentomutase	174.98	4.5E-02
LMRG_01103	fur family transcriptional regulator	247.25	1.9E-04
LMRG_01106	iron complex transport system substrate-binding protein	596.20	2.6E-03
LMRG_01112	ADP-ribose pyrophosphatase	788.53	2.0E-05
LMRG_01114	hypothetical protein	151.15	1.1E-02
LMRG_01116	2-dehydro-3-deoxyphosphogluconate aldolase/4-hydroxy-2-oxoglutarate aldolase	576.21	3.7E-05
LMRG_01117	hypothetical protein	345.61	9.4E-05
LMRG_01118	ascorbate-specific PTS system IIC component	650.66	2.8E-05
LMRG_01129	hypothetical protein	522.32	2.4E-02
LMRG_01131	dihydroxy-acid dehydratase	628.68	2.3E-05
LMRG_01134	ketol-acid reductoisomerase	848.03	2.8E-06
LMRG_01136	3-isopropylmalate dehydrogenase	602.34	1.1E-02
LMRG_01137	3-isopropylmalate dehydratase large subunit	549.85	1.2E-02

LMRG_01140	alpha-acetolactate decarboxylase	597.23	2.1E-07
LMRG_01144	deoxyribonucleoside regulator	89.95	9.2E-05
LMRG_01146	sugar isomerase domain-containing protein	433.19	1.5E-02
LMRG_01148	mannose-specific PTS system IID component	452.24	1.6E-08
LMRG_01149	mannose-specific PTS system IIC component	809.79	6.2E-06
LMRG_01152	transcription regulator GntR family protein	130.05	5.3E-03
LMRG_01160	hypothetical protein	539.38	6.2E-05
LMRG_01169	cell division initiation protein	720.10	5.9E-04
LMRG_01176	internalin	740.87	2.5E-02
LMRG_01178	YggT family protein	461.92	4.5E-06
LMRG_01179	cell division protein sepF	869.84	1.9E-04
LMRG_01190	methylase MraW	281.76	4.5E-03
LMRG_01194	hypothetical protein	118.08	8.4E-03
LMRG_01195	2-dehydropantoate 2-reductase	625.58	5.9E-05
LMRG_01199	hypothetical protein	193.15	2.5E-04
LMRG_01204	hypothetical protein	983.28	1.2E-05
LMRG_01205	hypothetical protein	523.18	1.1E-03
LMRG_01207	protoheme IX farnesyltransferase	627.77	2.2E-02
LMRG_01208	heme A synthase	915.11	1.7E-03
LMRG_01215	hypothetical protein	2372.65	3.5E-02
LMRG_01216	hypothetical protein	311.63	1.5E-03
LMRG_01217	choloylglycine hydrolase	573.25	8.3E-07
LMRG_01222	hypothetical protein	2459.07	3.5E-04
LMRG_01227	ribosomal-protein-alanine acetyltransferase	77.91	9.2E-03
LMRG_01232	crcB protein	1797.89	1.9E-06
LMRG_01233	crcB protein	1223.63	8.2E-03
LMRG_01239	hypothetical protein	858.01	2.4E-07
LMRG_01241	argininosuccinate synthase	401.63	1.5E-04
LMRG_01242	argininosuccinate lyase	543.80	2.5E-04
LMRG_01243	glycine betaine transporter	1212.49	4.0E-02
LMRG_01244	hypothetical protein	1760.17	5.5E-06
LMRG_01246	1-phosphofructokinase	1358.88	1.4E-06
LMRG_01248	galactitol-specific PTS system IIB component	108.08	9.4E-04

LMRG_01250	hypothetical protein	261.44	2.0E-04
LMRG_01256	phosphate acetyltransferase	133.70	3.5E-03
LMRG_01259	hypothetical protein	1248.46	1.6E-04
LMRG_01277	maltose/maltodextrin transport system permease	1984.42	1.9E-08
LMRG_01279	maltose/maltodextrin transport system substrate-binding protein	685.03	4.1E-02
LMRG_01282	hypothetical protein	1185.49	3.5E-02
LMRG_01285	hypothetical protein	248.25	1.8E-05
LMRG_01286	5-methyltetrahydropteroyltriglutamate-homocysteine S-methyltransferase	102.17	4.7E-02
LMRG_01291	menaquinone-specific isochorismate synthase	66.82	5.0E-02
LMRG_01292	2-succinyl-5-enolpyruvyl-6-hydroxy-3-cyclohexene-1-carboxylate synthase	148.51	8.4E-05
LMRG_01295	O-succinylbenzoate-CoA ligase	182.08	5.0E-04
LMRG_01302	hypothetical protein	239.92	6.6E-05
LMRG_01321	exonuclease SbcC	175.43	2.7E-02
LMRG_01325	aconitate hydratase 1	284.44	4.9E-03
LMRG_01326	hypothetical protein	248.91	5.0E-04
LMRG_01328	hypothetical protein	329.92	4.8E-04
LMRG_01331	DNA binding 3-demethylubiquinone-9 3-methyltransferase domain-containing protein	196.98	1.3E-05
LMRG_01337	N-(5'phosphoribosyl)anthranilate isomerase	178.45	1.1E-03
LMRG_01338	tryptophan synthase	161.92	1.5E-05
LMRG_01339	tryptophan synthase subunit alpha	427.56	1.3E-04
LMRG_01345	7,8-dihydro-8-oxoguanine triphosphatase	216.13	1.0E-03
LMRG_01346	succinyl-diaminopimelate desuccinylase	112.57	1.9E-05
LMRG_01348	hypothetical protein	366.71	2.6E-05
LMRG_01351	tRNA (guanine-N(7)-)-methyltransferase	485.93	5.6E-07
LMRG_01352	hypothetical protein	437.62	8.6E-06
LMRG_01353	hypothetical protein	1455.94	2.0E-04
LMRG_01355	aminopeptidase	775.98	2.6E-05
LMRG_01356	hypothetical protein	700.36	1.9E-04

LMRG_01358	hypothetical protein	255.69	9.8E-07
LMRG_01363	peroxiredoxin	184.75	1.7E-03
LMRG_01366	hypothetical protein	311.90	8.1E-05
LMRG_01367	bifunctional 3-deoxy-7-phosphoheptulonate synthase/chorismate mutase	144.85	2.9E-06
LMRG_01368	catabolite control protein A	276.24	1.1E-03
LMRG_01375	thiamine biosynthesis/tRNA modification protein ThiI	884.41	2.0E-07
LMRG_01377	ArgJ family protein	272.12	3.0E-05
LMRG_01379	acetylornithine aminotransferase	309.42	6.0E-03
LMRG_01380	ornithine carbamoyltransferase	527.08	5.4E-07
LMRG_01384	thiol peroxidase	994.64	2.0E-02
LMRG_01386	acetate kinase	38.91	2.3E-03
LMRG_01387	universal stress protein	346.86	1.1E-04
LMRG_01401	isocitrate dehydrogenase	590.79	4.5E-05
LMRG_01419	leader peptidase /N-methyltransferase	161.31	3.3E-06
LMRG_01420	DNA repair protein RadC	246.14	2.3E-07
LMRG_01431	glycerol uptake facilitator protein	1603.07	1.3E-04
LMRG_01443	bifunctional preprotein translocase subunit SecD/SecF	42.42	3.8E-02
LMRG_01448	D-tyrosyl-tRNA(Tyr) deacylase	265.14	5.4E-04
LMRG_01455	HTH-type transcriptional regulator cymR	474.67	1.6E-02
LMRG_01460	hypothetical protein	555.44	3.9E-08
LMRG_01461	RecD/TraA family helicase	516.41	1.2E-07
LMRG_01467	hypothetical protein	814.24	2.5E-04
LMRG_01471	aminodeoxychorismate lyase	568.72	2.5E-03
LMRG_01475	hypothetical protein	132.50	3.0E-04
LMRG_01476	MTA/SAH nucleosidase	957.38	1.1E-04
LMRG_01479	glutamate decarboxylase	852.77	1.8E-02
LMRG_01481	Rrf2 family protein	327.35	8.2E-05
LMRG_01486	hypothetical protein	180.44	2.4E-06
LMRG_01491	HTH-type transcriptional regulator ytlI	309.71	1.0E-03
LMRG_01492	FMN reductase	212.20	2.3E-06
LMRG_01493	hypothetical protein	340.07	6.2E-06
LMRG_01495	polar amino acid transport system permease	173.68	1.2E-04
LMRG_01499	hypothetical protein	409.72	4.6E-06

LMRG_01501	ribosomal small subunit pseudouridine synthase A	755.97	2.5E-03
LMRG_01509	DNA-binding protein	352.63	4.5E-05
LMRG_01510	competence transcription factor ComK	341.27	3.3E-06
LMRG_01512	hypothetical protein	259.31	3.3E-03
LMRG_01513	hypothetical protein	662.30	3.3E-07
LMRG_01525	recombination protein RecT	938.22	2.1E-06
LMRG_01526	gp49	468.25	1.7E-05
LMRG_01527	gp32	1572.59	2.1E-03
LMRG_01529	gp66	1495.96	9.5E-03
LMRG_01531	terminase small subunit	179.63	2.3E-04
LMRG_01532	phage terminase large subunit	52.68	1.2E-04
LMRG_01533	phage portal protein	84.94	2.5E-04
LMRG_01535	scaffolding protein	303.61	1.7E-05
LMRG_01536	phage capsid protein	738.01	7.9E-07
LMRG_01538	gp9	2242.33	1.7E-02
LMRG_01540	gp11	923.04	2.1E-03
LMRG_01543	gp14	523.52	8.7E-06
LMRG_01547	tail or base plate protein gp18	1001.01	5.7E-07
LMRG_01548	tail or base plate protein gp19	132.90	3.8E-04
LMRG_01549	long tail fibre	73.99	2.7E-03
LMRG_01550	short tail fibre	881.22	4.2E-07
LMRG_01552	gp23	495.47	9.9E-05
LMRG_01553	phage holin	1620.14	2.4E-08
LMRG_01555	gp26	1046.66	4.0E-07
LMRG_01558	phage protein	320.88	5.8E-04
LMRG_01566	hypothetical protein	198.15	3.8E-04
LMRG_01569	hypothetical protein	740.99	2.4E-03
LMRG_01570	hypothetical protein	828.00	2.1E-05
LMRG_01575	protease I	223.54	9.5E-04
LMRG_01576	hypothetical protein	117.83	7.5E-03
LMRG_01580	polar amino acid transport system ATP-binding protein	602.36	5.3E-07
LMRG_01583	hypothetical protein	101.19	7.4E-03
LMRG_01584	hypothetical protein	363.59	8.7E-05
LMRG_01585	oxidoreductase	786.13	5.2E-05
LMRG_01587	hypothetical protein	268.97	1.1E-03
LMRG_01588	ribosomal large subunit pseudouridine synthase D	1425.73	2.2E-04

LMRG_01592	ABC-2 type transport system ATP-binding protein	747.71	2.7E-02
LMRG_01595	hypothetical protein	1809.66	5.0E-07
LMRG_01602	hypothetical protein	161.08	4.3E-04
LMRG_01603	hypothetical protein	475.45	1.3E-05
LMRG_01607	fumarate hydratase class II	731.41	3.8E-02
LMRG_01609	hypothetical protein	1100.54	6.3E-05
LMRG_01613	foldase prsA 2	438.86	3.2E-05
LMRG_01615	hypothetical protein	108.21	1.0E-02
LMRG_01616	hit-like protein	1379.20	1.1E-02
LMRG_01622	hypothetical protein	344.97	1.8E-05
LMRG_01628	hypothetical protein	2922.67	2.4E-04
LMRG_01632	MarR family transcriptional regulator	656.83	8.2E-05
LMRG_01637	peptide/nickel transport system permease	615.67	5.3E-05
LMRG_01638	peptide/nickel transport system permease	386.99	3.3E-05
LMRG_01646	heme uptake protein IsdC	648.47	7.7E-06
LMRG_01652	hypothetical protein	120.55	2.0E-05
LMRG_01656	hypothetical protein	546.24	2.9E-03
LMRG_01657	3-oxoacyl-[acyl-carrier protein] reductase	434.14	5.2E-04
LMRG_01658	hypothetical protein	122.51	2.3E-04
LMRG_01661	major facilitator family transporter	754.62	2.1E-02
LMRG_01668	hypothetical protein	296.58	4.4E-04
LMRG_01671	hypothetical protein	441.88	2.5E-02
LMRG_01674	hypothetical protein	491.66	1.3E-03
LMRG_01681	hypothetical protein	1038.95	3.1E-06
LMRG_01682	hypothetical protein	1058.14	3.3E-04
LMRG_01684	hypothetical protein	1037.38	6.0E-09
LMRG_01685	hypothetical protein	1266.47	2.2E-02
LMRG_01686	hypothetical protein	86.03	7.7E-08
LMRG_01687	nicotinate-regulated transporter	110.52	3.8E-04
LMRG_01688	hypothetical protein	890.85	1.1E-04
LMRG_01690	hypothetical protein	2028.28	1.3E-05
LMRG_01693	glycosyl transferase	208.92	1.9E-04
LMRG_01700	homoserine dehydrogenase	1426.22	3.3E-03
LMRG_01701	threonine synthase	1443.52	8.9E-08
LMRG_01702	homoserine kinase	1089.83	5.7E-07

LMRG_01705	protein-(glutamine-N5) methyltransferase	742.89	3.7E-05
LMRG_01707	protein-tyrosine phosphatase	107.40	3.5E-03
LMRG_01716	ATP synthase F1 delta subunit	232.89	7.6E-04
LMRG_01720	ATP synthase F1 epsilon subunit	134.32	2.5E-05
LMRG_01725	single-strand binding protein family	656.42	6.4E-06
LMRG_01728	O-succinylbenzoic acid synthetase	276.28	1.2E-06
LMRG_01729	undecaprenyl-phosphate alpha-N-acetylglucosaminyltransferase	1052.09	2.0E-03
LMRG_01730	transcriptional regulator LytR	280.77	4.5E-03
LMRG_01731	ribosomal-protein-alanine N-acetyltransferase	1663.26	3.9E-03
LMRG_01745	cardiolipin synthase	846.40	1.8E-02
LMRG_01746	hypothetical protein	461.78	1.2E-02
LMRG_01752	phosphate ABC transporter	461.40	7.8E-06
LMRG_01755	HTH-type transcriptional repressor czrA	1222.94	1.1E-04
LMRG_01756	hypothetical protein	1880.22	7.2E-04
LMRG_01763	PspC domain-containing protein	5389.25	5.7E-08
LMRG_01768	hexapeptide transferase	311.53	7.2E-05
LMRG_01771	UDP-glucose 4-epimerase	414.26	3.5E-03
LMRG_01775	hypothetical protein	1406.05	4.0E-06
LMRG_01777	NADPH dehydrogenase	551.65	1.1E-03
LMRG_01787	RNA polymerase sigma-54 factor	687.95	2.4E-02
LMRG_01788	transcriptional regulator	316.23	3.5E-05
LMRG_01792	2,3-bisphosphoglycerate-independent phosphoglycerate mutase	269.65	6.9E-05
LMRG_01794	hypothetical protein	707.40	1.2E-04
LMRG_01796	carboxylesterase	136.67	5.5E-03
LMRG_01797	preprotein translocase SecG subunit	2753.05	1.3E-05
LMRG_01799	ribonuclease R	355.05	2.7E-03
LMRG_01801	hypothetical protein	1312.92	3.1E-02
LMRG_01805	hypothetical protein	999.25	4.1E-11
LMRG_01808	hypothetical protein	1417.28	5.6E-07
LMRG_01813	hypothetical protein	368.93	5.2E-06
LMRG_01815	tributyrin esterase	1664.92	2.6E-04
LMRG_01817	iron complex transport system substrate-binding protein	314.60	6.3E-03
LMRG_01821	rod shape-determining protein RodA	682.19	1.6E-05
LMRG_01822	arsenate reductase	635.11	1.5E-04

LMRG_01823	glycine cleavage system H protein	716.91	1.7E-05
LMRG_01840	transcriptional regulator	1359.56	7.0E-05
LMRG_01844	hypothetical protein	2975.56	5.2E-05
LMRG_01845	hypothetical protein	1078.78	4.0E-02
LMRG_01847	hydrolase	557.44	1.6E-03
LMRG_01849	hypothetical protein	439.57	2.1E-04
LMRG_01850	phosphatidylglycerophosphatase A	846.02	2.2E-02
LMRG_01858	sucrose phosphorylase	131.33	2.4E-03
LMRG_01859	multiple sugar transport system substrate-binding protein	573.11	1.2E-02
LMRG_01862	hypothetical protein	1066.71	2.6E-03
LMRG_01864	hypothetical protein	1355.59	1.3E-06
LMRG_01875	hypothetical protein	1540.92	6.0E-07
LMRG_01878	amino-terminal domain-containing protein	722.18	1.0E-02
LMRG_01888	tRNA uridine 5-carboxymethylaminomethyl modification enzyme GidA	377.92	1.2E-03
LMRG_01890	hypothetical protein	38.22	9.2E-05
LMRG_01891	hypothetical protein	225.45	8.6E-04
LMRG_01895	16S rRNA methyltransferase GidB	776.38	3.9E-05
LMRG_01903	nucleoid occlusion protein	610.13	6.8E-06
LMRG_01904	lipoprotein	750.10	3.3E-02
LMRG_01906	chromosome partitioning protein	357.16	4.2E-02
LMRG_01909	beta-glucoside operon transcriptional antiterminator	573.68	5.5E-04
LMRG_01915	cellobiose-specific PTS system IIB component	3048.20	2.1E-07
LMRG_01917	cellobiose-specific PTS system IIA component	1972.54	9.6E-06
LMRG_01925	glutamate-cysteine ligase/gamma-glutamylcysteine synthetase	1159.54	1.2E-04
LMRG_01927	hypothetical protein	38.17	1.5E-02
LMRG_01928	hypothetical protein	3305.22	3.5E-07
LMRG_01929	RpiR family phosphosugar-binding transcriptional regulator	1151.30	5.4E-06
LMRG_01930	cellobiose-specific PTS system IIA component	1364.33	3.3E-06

LMRG_01933	cellobiose-specific PTS system IIB component	1349.52	7.5E-06
LMRG_01934	beta-glucosidase	1677.87	4.7E-03
LMRG_01936	ABC transporter ATP-binding protein	954.70	4.8E-02
LMRG_01937	hypothetical protein	520.01	4.0E-02
LMRG_01938	inosine-5'-monophosphate dehydrogenase	193.35	8.4E-04
LMRG_01943	hypothetical protein	2295.78	6.8E-08
LMRG_01946	hypothetical protein	2702.28	3.1E-06
LMRG_01947	anthranilate synthase component II	2790.42	3.5E-02
LMRG_01952	hypothetical protein	264.10	9.7E-06
LMRG_01953	transaldolase	1337.38	4.0E-06
LMRG_01959	catabolite control protein B	966.58	5.1E-05
LMRG_01965	hypothetical protein	759.52	2.7E-05
LMRG_01966	HAD-superfamily hydrolase	2682.26	6.4E-06
LMRG_01968	MerR family transcriptional regulator	1859.74	6.5E-07
LMRG_01970	MarR family transcriptional regulator	2070.69	3.0E-06
LMRG_01971	mate efflux family protein	637.54	2.3E-04
LMRG_01974	hypothetical protein	994.07	3.6E-02
LMRG_01978	cytochrome bd-I oxidase subunit I	217.26	3.5E-03
LMRG_01979	cytochrome d ubiquinol oxidase subunit II	177.84	1.6E-04
LMRG_01980	ABC transporter CydDC cysteine exporter CydD	97.90	4.4E-06
LMRG_01981	ABC transporter CydDC cysteine exporter CydC	143.23	3.8E-04
LMRG_01987	hypothetical protein	848.37	1.0E-02
LMRG_01991	hypothetical protein	3238.05	1.9E-02
LMRG_01996	hypothetical protein	1205.08	2.1E-06
LMRG_01997	aldo/keto reductase family oxidoreductase	1039.67	3.9E-04
LMRG_02000	dihydroxyacetone kinase	817.06	2.3E-05
LMRG_02002	dihydroxyacetone kinase DhaK subunit	1278.12	2.9E-03
LMRG_02009	hypothetical protein	700.82	1.5E-04
LMRG_02011	hypothetical protein	582.81	1.0E-07
LMRG_02013	succinate-semialdehyde dehydrogenase	801.03	4.7E-02
LMRG_02014	cellobiose-specific PTS system IIB component	1956.41	9.1E-06

LMRG_02016	cellobiose-specific PTS system IIA component	1287.45	3.7E-06
LMRG_02017	beta-glucosidase	312.24	1.8E-05
LMRG_02020	ABC transporter permease	738.73	6.6E-06
LMRG_02022	pantothenate kinase	615.14	1.5E-05
LMRG_02023	ABC-2 type transport system ATP-binding protein	573.32	1.1E-04
LMRG_02024	ABC-2 type transport system permease	245.41	6.2E-04
LMRG_02029	hypothetical protein	1513.28	8.0E-06
LMRG_02030	lipoate-protein ligase A	1633.19	5.5E-07
LMRG_02038	hypothetical protein	782.00	1.0E-02
LMRG_02041	starvation-inducible DNA-binding protein	497.41	3.6E-03
LMRG_02042	hypothetical protein	792.20	8.6E-05
LMRG_02046	MFS transporter	322.30	2.0E-04
LMRG_02047	hypothetical protein	1046.83	2.2E-02
LMRG_02050	hypothetical protein	489.23	3.5E-06
LMRG_02051	hypothetical protein	1103.11	6.8E-05
LMRG_02052	hypothetical protein	560.71	2.6E-04
LMRG_02053	hypothetical protein	1467.37	1.3E-03
LMRG_02054	hypothetical protein	228.34	3.2E-03
LMRG_02059	hypothetical protein	957.35	6.5E-03
LMRG_02064	adenylate cyclase	546.83	1.2E-04
LMRG_02066	GTP pyrophosphokinase	152.21	1.8E-04
LMRG_02071	D-alanine-poly(phosphoribitol) ligase subunit 2	64.85	1.6E-02
LMRG_02072	membrane protein	304.62	3.0E-05
LMRG_02073	D-alanine-poly(phosphoribitol) ligase subunit 1	227.35	4.1E-02
LMRG_02074	hypothetical protein	910.58	3.2E-05
LMRG_02076	hypothetical protein	511.38	9.2E-05
LMRG_02078	branched-chain amino acid aminotransferase	347.70	1.7E-05
LMRG_02079	antibiotic transport system ATP-binding protein	75.56	1.8E-06
LMRG_02083	glutathione peroxidase	879.45	1.1E-04
LMRG_02089	hypothetical protein	575.57	2.0E-03
LMRG_02090	hypothetical protein	508.17	5.0E-04
LMRG_02091	hypothetical protein	627.00	2.8E-04

LMRG_02094	hypothetical protein	1613.93	8.3E-05
LMRG_02095	YkrP protein	1014.56	1.9E-03
LMRG_02096	methylated-DNA-[protein]-cysteine S-methyltransferase	588.12	3.6E-03
LMRG_02097	ATP-dependent Clp protease ATP-binding subunit ClpE	212.06	1.7E-04
LMRG_02101	hypothetical protein	282.54	2.5E-04
LMRG_02104	hypothetical protein	1716.13	2.8E-06
LMRG_02105	3-hydroxyisobutyrate dehydrogenase	267.24	7.9E-04
LMRG_02107	hypothetical protein	1038.39	5.4E-05
LMRG_02108	hypothetical protein	640.73	4.8E-02
LMRG_02110	hypothetical protein	391.47	3.3E-06
LMRG_02114	glycine betaine/proline transport system ATP-binding protein	656.19	3.2E-04
LMRG_02118	copper homeostasis protein	93.36	2.4E-03
LMRG_02119	hypothetical protein	234.66	3.1E-04
LMRG_02121	two-component sensor histidine kinase	600.88	1.7E-05
LMRG_02122	response regulator LiaR	665.92	1.0E-02
LMRG_02123	ktr system potassium uptake protein C	643.32	1.2E-05
LMRG_02124	hypothetical protein	516.32	1.8E-04
LMRG_02130	ATP-binding protein	458.30	2.8E-04
LMRG_02133	transcription regulator	2640.53	2.8E-05
LMRG_02135	csn2 family CRISPR-associated protein	426.04	2.9E-06
LMRG_02136	CRISPR-associated protein cas2	554.34	1.8E-04
LMRG_02137	CRISPR-associated protein cas1	239.34	2.4E-08
LMRG_02142	tRNA pseudouridine synthase A	1162.24	8.1E-06
LMRG_02143	cobalt/nickel transport system permease	1021.39	1.3E-08
LMRG_02147	amidase	1630.27	3.7E-03
LMRG_02148	hypothetical protein	270.34	1.6E-03
LMRG_02153	50S ribosomal protein L36	267.38	1.2E-04
LMRG_02195	hypothetical protein	555.63	2.2E-04
LMRG_02196	mannitol-specific PTS system IIA component	503.17	6.6E-06
LMRG_02203	diamine N-acetyltransferase	3070.74	3.2E-02
LMRG_02211	galactitol-specific PTS system IIB component	83.04	1.3E-03
LMRG_02212	hypothetical protein	425.90	2.4E-04
LMRG_02216	hypothetical protein	1116.45	1.4E-05

LMRG_02218	universal stress protein	385.06	7.9E-05
LMRG_02220	hypothetical protein	2211.51	2.2E-05
LMRG_02222	alpha/beta fold family hydrolase	1716.79	7.8E-06
LMRG_02223	KDP operon response regulator KdpE	1107.55	6.4E-06
LMRG_02224	sensor histidine kinase KdpD	738.02	9.6E-06
LMRG_02227	K+-transporting ATPase A subunit	593.74	1.0E-07
LMRG_02229	cellobiose-specific PTS system IIC component	1354.96	5.5E-05
LMRG_02230	cellobiose-specific PTS system IIA component	2066.23	3.5E-02
LMRG_02244	hypothetical protein	395.35	3.8E-04
LMRG_02249	hypothetical protein	559.66	7.4E-06
LMRG_02255	transposase	1554.95	2.5E-02
LMRG_02263	MarR family transcriptional regulator	1485.41	1.5E-06
LMRG_02266	hypothetical protein	2403.94	2.0E-06
LMRG_02272	amidase	141.39	6.5E-04
LMRG_02273	hypothetical protein	126.04	8.2E-03
LMRG_02274	hypothetical protein	2515.97	9.0E-06
LMRG_02275	hypothetical protein	307.91	1.3E-03
LMRG_02284	multiple sugar transport system permease	1091.62	3.3E-06
LMRG_02287	hypothetical protein	384.99	1.0E-05
LMRG_02293	hypothetical protein	442.38	7.0E-04
LMRG_02294	hypothetical protein	696.85	8.2E-04
LMRG_02295	hypothetical protein	442.05	6.3E-03
LMRG_02301	hypothetical protein	266.57	3.6E-03
LMRG_02302	hypothetical protein	810.65	9.9E-06
LMRG_02306	hypothetical protein	399.15	3.1E-06
LMRG_02310	alanine racemase	227.70	3.7E-06
LMRG_02311	CopG family transcriptional regulator	611.04	3.2E-05
LMRG_02314	RsbT antagonist protein rsbS	920.27	2.5E-03
LMRG_02317	anti-sigma-B factor antagonist	2983.01	3.0E-05
LMRG_02319	RNA polymerase sigma-B factor	1501.83	1.6E-04
LMRG_02321	SulP family sulfate permease	185.29	1.6E-02
LMRG_02322	hypothetical protein	10.11	1.6E-02
LMRG_02326	transferase	1517.00	1.8E-02
LMRG_02327	hypothetical protein	759.80	2.0E-02
LMRG_02339	ATP synthase F1 alpha subunit	1299.35	4.6E-02
LMRG_02340	ATP synthase F1 gamma subunit	1042.40	4.4E-03

LMRG_02342	F-type H+-transporting ATPase subunit epsilon	2108.95	2.7E-02
LMRG_02348	hypothetical protein	3093.35	3.5E-06
LMRG_02349	hypothetical protein	2699.99	1.8E-05
LMRG_02351	hypothetical protein	2446.44	1.4E-06
LMRG_02360	hypothetical protein	26.11	1.6E-02
LMRG_02364	hypothetical protein	326.29	3.0E-04
LMRG_02367	antigen A	441.25	3.4E-04
LMRG_02369	hypothetical protein	1106.95	2.7E-07
LMRG_02373	hypothetical protein	644.94	6.6E-06
LMRG_02374	hypothetical protein	1492.09	2.1E-02
LMRG_02377	hypothetical protein	1438.71	5.2E-05
LMRG_02378	N-acetylmuramoyl-L-alanine amidase	1048.14	3.9E-04
LMRG_02382	hypothetical protein	4010.56	1.1E-06
LMRG_02393	hypothetical protein	1198.33	2.0E-02
LMRG_02411	endonuclease	2620.52	8.9E-05
LMRG_02419	L-rhamnose isomerase	1712.19	2.0E-06
LMRG_02423	hypothetical protein	2427.79	1.4E-08
LMRG_02427	50S ribosomal protein L34	830.40	3.9E-03
LMRG_02432	hypothetical protein	194.39	1.8E-02
LMRG_02433	DNA replication and repair protein recF	177.06	2.1E-03
LMRG_02448	hypothetical protein	736.39	1.7E-02
LMRG_02449	hypothetical protein	11.10	2.4E-02
LMRG_02453	mannose-specific PTS system IID component	241.41	2.5E-05
LMRG_02455	copper homeostasis protein	538.39	3.9E-06
LMRG_02459	hypothetical protein	776.95	4.0E-02
LMRG_02461	hypothetical protein	985.23	1.3E-03
LMRG_02467	agmatine deiminase	12.35	1.7E-02
LMRG_02468	carbamate kinase	1200.91	1.3E-06
LMRG_02470	RpiR family transcriptional regulator	230.23	1.0E-04
LMRG_02472	arginine deiminase	789.99	2.3E-02
LMRG_02473	30S ribosomal protein S6	103.99	7.5E-05
LMRG_02478	hypothetical protein	1882.47	1.0E-06
LMRG_02482	50S ribosomal protein L9	1067.98	9.2E-06
LMRG_02484	hypothetical protein	2806.18	2.4E-03
LMRG_02485	adenylosuccinate synthetase	2670.46	1.2E-06
LMRG_02487	hypothetical protein	293.24	7.7E-03
LMRG_02488	secretion system component EssA	255.75	9.6E-05

LMRG_02489	YukD protein	328.22	7.3E-06
LMRG_02492	hypothetical protein	553.39	1.5E-04
LMRG_02493	hypothetical protein	403.95	7.1E-06
LMRG_02494	hypothetical protein	546.78	2.2E-05
LMRG_02496	AIR carboxylase	563.61	4.5E-08
LMRG_02498	adenylosuccinate lyase	926.32	1.7E-08
LMRG_02499	phosphoribosylaminoimidazole-succinocarboxamide synthase	160.50	8.5E-04
LMRG_02500	phosphoribosylformylglycinamidine synthase	278.34	7.9E-04
LMRG_02501	phosphoribosylformylglycinamidine synthase I	493.88	1.4E-03
LMRG_02505	phosphoribosylglycinamide formyltransferase	636.99	5.7E-04
LMRG_02508	TrpR protein YerC/YecD	360.87	8.1E-06
LMRG_02514	hypothetical protein	295.30	1.1E-04
LMRG_02522	shikimate kinase	239.44	3.1E-04
LMRG_02524	hypothetical protein	328.21	1.2E-04
LMRG_02527	hypothetical protein	1508.70	3.1E-06
LMRG_02528	hypothetical protein	985.72	9.7E-04
LMRG_02531	polar amino acid transport system permease	231.36	4.6E-02
LMRG_02533	polar amino acid transport system substrate-binding protein	424.30	1.5E-07
LMRG_02539	lactose/L-arabinose transport system permease	418.18	2.3E-04
LMRG_02541	lactose/L-arabinose transport system substrate-binding protein	354.95	9.4E-03
LMRG_02542	beta-glucosidase	272.86	3.8E-02
LMRG_02544	LacI family transcriptional regulator	614.94	4.9E-02
LMRG_02548	hypothetical protein	818.56	1.9E-07
LMRG_02551	cellobiose-specific PTS system IIB component	910.16	4.8E-06
LMRG_02556	rod shape-determining protein MreB	332.92	2.3E-05
LMRG_02558	aminopeptidase	344.79	3.1E-05
LMRG_02559	flavodoxin	2199.16	2.0E-07
LMRG_02566	hypothetical protein	1513.90	1.6E-02
LMRG_02567	cellobiose-specific PTS system IIA component	352.43	2.7E-05

LMRG_02569	cellobiose-specific PTS system IIB component	50.59	4.3E-03
LMRG_02574	GNAT family acetyltransferase	2087.08	7.4E-05
LMRG_02578	hypothetical protein	1772.52	4.3E-05
LMRG_02580	ribonuclease Z	339.87	1.2E-02
LMRG_02581	hypothetical protein	4269.98	5.8E-03
LMRG_02582	YycH protein	2738.14	5.5E-03
LMRG_02583	sensor histidine kinase VicK	55.69	2.2E-05
LMRG_02586	D-methionine transport system substrate-binding protein	453.10	2.2E-02
LMRG_02588	D-methionine transport system permease	1527.19	2.8E-06
LMRG_02597	maltose/maltodextrin transport system ATP-binding protein	1682.52	7.0E-06
LMRG_02606	hypothetical protein	1116.20	5.1E-04
LMRG_02608	phosphoglycerate mutase	653.36	1.4E-02
LMRG_02610	hypothetical protein	1191.99	1.1E-06
LMRG_02616	lipoprotein-releasing system ATP-binding protein	974.23	1.7E-06
LMRG_02618	stage V sporulation protein G	713.54	5.3E-04
LMRG_02619	stage V sporulation protein G	1052.64	1.1E-05
LMRG_02622	listeriolysin regulatory protein	3463.46	1.1E-07
LMRG_02623	1-phosphatidylinositol phosphodiesterase	1781.77	8.4E-04
LMRG_02624	listeriolysin O	818.54	8.0E-06
LMRG_02626	actin-assembly inducing protein ActA	1037.36	6.9E-07
LMRG_02627	phospholipase C	1962.46	7.7E-03
LMRG_02628	hypothetical protein	782.22	1.7E-09
LMRG_02629	hypothetical protein	109.53	6.8E-03
LMRG_02632	L-lactate dehydrogenase	1293.73	3.1E-02
LMRG_02636	transcription-repair coupling factor	318.18	1.7E-02
LMRG_02638	ribosome-associated heat shock protein	2179.12	8.2E-04
LMRG_02640	S1 RNA binding domain-containing protein	495.62	5.0E-05
LMRG_02649	hydrolase	766.31	8.7E-08
LMRG_02652	hypothetical protein	1266.78	3.3E-04
LMRG_02662	50S ribosomal protein L33	1263.12	2.5E-02

LMRG_02663	RNA polymerase sporulation-specific sigma factor	723.72	3.9E-05
LMRG_02664	hypothetical protein	899.03	6.3E-04
LMRG_02665	TrmH family RNA methyltransferase group 3	387.33	7.6E-05
LMRG_02674	ATP-dependent Clp protease ATP-binding subunit ClpC	529.67	1.2E-03
LMRG_02675	ATP:guanido phosphotransferase	707.30	8.4E-04
LMRG_02686	hypothetical protein	750.99	2.0E-02
LMRG_02688	internalin H	3528.90	2.2E-05
LMRG_02689	hypothetical protein	328.38	2.9E-04
LMRG_02690	hypothetical protein	1481.75	3.6E-06
LMRG_02694	hypothetical protein	1330.69	6.9E-05
LMRG_02696	riboflavin biosynthesis protein RibD domain-containing protein	1746.34	3.7E-07
LMRG_02698	hypothetical protein	845.37	1.6E-04
LMRG_02699	peptide/nickel transport system substrate-binding protein	2607.51	2.0E-08
LMRG_02703	hypothetical protein	1433.51	4.4E-07
LMRG_02709	DNA-directed RNA polymerase delta subunit	479.52	8.6E-06
LMRG_02714	general stress protein 13	1205.65	3.3E-05
LMRG_02719	aspartate kinase	29.84	1.1E-06
LMRG_02729	monovalent cation/H+ antiporter subunit G	321.46	8.8E-06
LMRG_02730	ComA operon protein 2	208.81	4.7E-04
LMRG_02731	hypothetical protein	31.23	4.6E-02
LMRG_02734	hypothetical protein	1038.35	1.5E-03
LMRG_02736	hypothetical protein	313.12	7.0E-03
LMRG_02744	multiple sugar transport system permease	465.72	1.5E-05
LMRG_02752	primase	397.32	1.1E-03
LMRG_02753	dimethyladenosine transferase	1250.83	7.9E-05
LMRG_02755	4-(cytidine 5'-diphospho)-2-C-methyl-D-erythritol kinase	1001.92	4.9E-03
LMRG_02757	fur family transcriptional regulator	987.45	2.2E-05
LMRG_02761	hypothetical protein	171.55	1.1E-03
LMRG_02763	A/G-specific adenine glycosylase	536.95	3.7E-06
LMRG_02765	dUTP pyrophosphatase	398.08	2.1E-03

LMRG_02767	regulatory protein recX	14.09	1.5E-02
LMRG_02783	enoyl-[acyl carrier protein] reductase II	476.79	4.9E-07
LMRG_02784	fructokinase	1390.67	3.3E-06
LMRG_02792	hypothetical protein	793.84	8.7E-03
LMRG_02795	hypothetical protein	178.94	7.1E-04
LMRG_02799	hypothetical protein	718.47	4.0E-04
LMRG_02803	fructose-specific PTS system IIA component	849.21	1.6E-04
LMRG_02807	fructose-bisphosphate aldolase class II	959.26	1.5E-06
LMRG_02815	hypothetical protein	509.59	3.1E-05
LMRG_02818	hypothetical protein	673.15	7.2E-06
LMRG_02819	glutamine amidotransferase	309.41	1.6E-02
LMRG_02828	50S ribosomal protein L35	77.18	3.8E-03
LMRG_02831	hypothetical protein	1862.82	1.7E-05
LMRG_02835	hypothetical protein	436.80	3.6E-02
LMRG_02841	hypothetical protein	468.71	1.8E-05
LMRG_02843	hypothetical protein	756.38	9.9E-05
LMRG_02847	hypothetical protein	117.00	5.8E-05
LMRG_02849	hypothetical protein	540.59	9.5E-05
LMRG_02856	aluminum resistance protein	305.67	1.0E-02
LMRG_02861	hypothetical protein	1073.51	5.4E-06
LMRG_02863	hypothetical protein	216.98	1.0E-04
LMRG_02872	hypothetical protein	626.93	3.7E-04
LMRG_02874	flagellar motor switch protein FliN	1122.10	3.8E-05
LMRG_02879	hypothetical protein	508.81	6.6E-07
LMRG_02888	hypothetical protein	1745.90	1.6E-07
LMRG_02891	hypothetical protein	656.63	3.6E-07
LMRG_02892	hypothetical protein	1936.10	5.4E-09
LMRG_02895	hypothetical protein	663.89	3.3E-03
LMRG_02896	hypothetical protein	256.08	6.1E-05
LMRG_02899	hypothetical protein	627.84	4.0E-05
LMRG_02904	mannitol operon transcriptional antiterminator	1165.58	1.9E-06
LMRG_02920	anti-repressor protein	309.83	2.0E-04
LMRG_02921	hypothetical protein	1732.99	5.6E-06
LMRG_02946	hypothetical protein	258.42	2.3E-02
LMRG_02949	late competence protein ComEC	261.27	1.8E-03
LMRG_02963	hypothetical protein	1225.96	3.8E-07
LMRG_02967	hypothetical protein	1250.54	4.3E-07

LMRG_02982	hypothetical protein	916.02	2.7E-04
LMRG_02984	hypothetical protein	903.53	2.7E-04
LMRG_05001	Lys tRNA	278.98	6.2E-04
LMRG_05004	Lys tRNA	260.76	2.1E-04
LMRG_05006	Gly tRNA	131.45	3.5E-06
LMRG_05010	Ala tRNA	493.78	1.8E-04
LMRG_05013	Ser tRNA	168.00	8.0E-04
LMRG_05019	Ser tRNA	149.17	3.3E-03
LMRG_05021	Ile tRNA	947.11	6.6E-08
LMRG_05030	Ala tRNA	528.03	4.9E-05
LMRG_05034	Gly tRNA	126.43	4.3E-04
LMRG_05036	Lys tRNA	244.84	1.0E-05
LMRG_05039	Arg tRNA	763.62	2.4E-05
LMRG_05045	Lys tRNA	280.56	4.7E-04
LMRG_05060	Ala tRNA	500.77	1.2E-05
LMRG_05061	Ile tRNA	939.79	1.1E-05
LMRG_05065	Ala tRNA	554.75	2.3E-04
LMRG_05066	Ile tRNA	952.46	4.3E-05

Table S3.4 Primers used for transposon library PCR amplification for NovaSeq 6000 sequencing.

Primer name	Sequence
NovaSeq_Fwd	ACACTCTTTCCCTACACGACGCTCTTCCGATCTgTGGGGTACGCGTAATACGACTCactata
NovaSeq_Rev	GTGACTGGAGTTCAGACGTGTGCTCTTCCGATCTGGGGGGGGGGGGGGGGG

CHAPTER 4 – Summary, conclusions, and future directions

Authors and their contributions:

Simone Shen: Planned, organized, and wrote this manuscript.

Anna Huttenlocher: Supervised writing of this manuscript.

Overview

The innate immune system is a major host defense mechanism for protection against pathogens through pattern-recognition receptors (PRRs) (Mogensen, 2009; D. Li & Wu, 2021). PRRs detect pathogens through pathogen-associated molecular patterns (PAMPs), which further trigger downstream signaling resulting in inflammation (Mogensen, 2009). Inflammation is critical for eliminating bacterial infections. However, this response can become a double-edged sword due to its potential for collateral damage (Agrati et al., 2022). While inflammatory cytokines and chemokines recruit immune cells to the site of infection, they can also induce tissue damage and disrupt normal physiological functions if not tightly regulated (Sariol & Perlman, 2021; Agrati et al., 2022). Excessive or prolonged inflammation may lead to systemic complications such as septic shock or chronic inflammatory conditions (Cao et al., 2023). Therefore, while inflammation is essential for combating bacterial infections, maintaining an intricate balance in its amplitude and duration is crucial to avoid inadvertent systemic damage. Understanding the complex interplay between inflammation and host-pathogen interactions is crucial for advancing our knowledge of infectious diseases and developing efficient therapeutic approaches to improve outcomes of infection-associated inflammatory problems.

While immune-mediated inflammatory responses facilitate the clearance of bacteria, bacterial pathogens have evolved strategies to evade these immune responses. For example, many bacterial species alter their cell wall or cell surface components to avoid detection by PRRs, such as modification of peptidoglycan by *L. monocytogenes* to

escape Nod2 detection (Boneca et al., 2007) and remodeling of LPS by *Shigella flexneri* to evade inflammasome activation (Paciello et al., 2013). Modifying cell wall charges through aminoacylation of peptidoglycan to increase resistance to host produced antimicrobial peptides (AMPs) is another virulence mechanism demonstrated in many bacterial species, including *Clostridium perfringens*, *Enterococcus faecalis*, *Pseudomonas aeruginosa*, *Mycobacterium tuberculosis*, *Bacillus anthracis*, *Bacillus subtilis*, *Enterococcus faecium*, and *L. monocytogenes* (*Cole & Nizet, 2016; Nawrocki et al., 2014).* Other virulence determinants to promote spreading utilize strategies such as hijacking host cell actin to facilitate actin-based motility are also important factors for bacterial pathogenesis (Lamason & Welch, 2017; Goldberg & Theriot, 1995; Reed et al., 2014; Srinon et al., 2019). There are many other tactics that pathogens require to elude the complicated immune defenses of the host to allow for their survival and replication in the host. Identification of virulence factors employed by bacteria can enhance our understanding of the strategies by which bacteria cause diseases, which can further provide insight into potential antibiotic targets.

This dissertation combines two powerful models, zebrafish and *Listeria monocytogenes*, to understand the complex relationship between host-pathogen interactions. The genetic tractability of both zebrafish and *L. monocytogenes* makes them valuable models for understanding the mechanisms behind inflammation mediated by immune response during infection as well as mechanisms behind the strategies that bacterial pathogens utilize to evade the host immune-mediated responses. In **Chapter 2**, I utilized *L. monocytogenes* as a tool to stimulate different innate immune responses in

zebrafish and investigated how inflammation induced by bacteria impairs wound healing. Furthermore, in **Chapter 3**, I utilized zebrafish as a tool for a *L. monocytogenes* genome-wide genetic screen combining the techniques of transposon mutagenesis and next-generation sequencing to identify virulence determinants that pathogens employed to survive and replicate in the host.

Inflammasome signaling and wound healing

Bacterial infections can be detrimental to wound healing. While inflammation is required for the process of wound healing, when it is dysregulated, it can hinder wound repair (Nguyen & Soulika, 2019). However, how bacterial infections modulate inflammation in the context of wound healing is not very well understood. **Chapter 2** of this dissertation aimed to elucidate the effect of bacterial-derived inflammation on wound healing and dissect the mechanism behind the inhibition of wound healing during infections. I utilized genetically engineered *L. monocytogenes* and found that extensive inflammasome activation impaired wound healing despite an attenuation in bacterial virulence, suggesting that inflammasome-mediated inflammatory response triggered by bacteria impairs wound healing. Additionally, I demonstrated that blocking IL-1β signaling, downstream of inflammasome activation, either through genetic knockdown in zebrafish or treatment of anakinra, an IL-1 receptor antagonist, improved healing outcomes without affecting bacterial burden. *L. monocytogenes* is utilized as a model pathogen to model inflammatory responses stimulated by bacteria at the wound. Future work investigating if blocking IL-1β signaling by anakinra administration can also rescue wound healing in wounds infected with other wound-associated pathogens such as

Pseudomonas aeruginosa, *Staphylococcus aureus*, *Klebsiella pneumoniae*, *Enterococcus faecalis*, and *Acinetobacter baumannii* will provide better insight into the potential of targeting IL-1β as therapeutics for treating infection wounds (Puca et al., 2021).

Studies have shown that sustained inflammasome activation also impairs wound healing in diabetic wounds, which are often associated with persistent inflammation similar to infected wounds (Cavalcante-Silva & Koh, 2023; Y. Ding et al., 2022). Blocking inflammation signaling through caspase-1 inhibition has been shown to improve wound healing in diabetic mice models (X. Li et al., 2022; Mirza et al., 2014). Consistent with our findings, blocking IL-1β signaling with an IL-1 receptor antagonist or IL-1β-neutralizing antibody also improved wound healing in diabetic mice (Tan et al., 2021; Mirza et al., 2013). A question stemming from these findings is the mechanism by which IL-1β signaling inhibits wound healing. Studies in diabetic wounds have suggested that IL-1β acts as a positive feedback loop for sustained inflammasome activation (Mirza et al., 2013, 2014). Furthermore, inhibiting IL-1β downregulates the proinflammatory phenotype and upregulates the pro-healing phenotype in macrophages (Mirza et al., 2013). This corroborates our finding that anakinra treatment decreases TNFα expression in macrophages at the wound in the context of an infection. Future studies examining anti-inflammatory or pro-healing markers in macrophages, such as TGF-β and IL-10, at infected wounds using zebrafish transgenic reporter with or without anakinra treatment could provide a more comprehensive understanding of macrophage phenotypic switch by IL-1β. Additionally, investigating if IL-1β affects the proliferation of

epithelial cells will provide a better mechanistic understanding of how inflammatory responses driven by IL-1β may impair wound healing. We can utilize a dual Fucci zebrafish transgenic line (Bouldin & Kimelman, 2014), which allows *in vivo* imaging of the cell cycle state using tagged fluorescent proteins, and test if blocking IL-1β signaling affects cell proliferation.

Other studies have suggested that in diabetic wounds, ROS drives the persistent inflammasome activation and treatment with a ROS scavenger dampens inflammasome activation and improves wound healing (Dai et al., 2017; Mirza et al., 2014). It will be interesting to explore if ROS also drives prolonged inflammation through activation of the inflammasome and further impairs wound healing in the context of bacteria-infected wounds. To test this, we can treat wounded and infected TNFα/macrophage dual reporter zebrafish with antioxidant N-acetyl Cysteine (NAC) and quantify wound healing and proinflammatory macrophage at the wound site. Additionally, a combination of anakinra and NAC administrations could test if IL-1β and ROS act independently to impair wound healing. If the combination of the two drugs enhances the improvement of wound healing compared to anakinra or NAC alone, this would suggest that components other than IL-1β downstream of inflammasome signaling, such as pyroptosis, could be the driver for the defect in wound healing. To test if other signaling pathways downstream of inflammasome other than IL-1β may play a role in wound healing, we can target caspase-1, which is upstream of IL-1β. If blocking caspase-1 either through caspase-1 inhibitor YVAD or morpholino oligonucleotide (MO) *caspy2* genetic knockdown shows a bigger improvement in wound healing than blocking IL-1β,

this would suggest that other players downstream of caspase-1 also inhibit wound healing. To directly examine if pyroptosis impairs wound healing, we can treat zebrafish with Ac-FEID-CMK, a potent zebrafish-specific GSDMEb-derived peptide inhibitor, and test for the healing outcome of *L. monocytogenes* infected wounds.

Itaconate and wound healing

Neither anakinra treatment nor *il1b* knockdown in zebrafish fully rescued wound healing in zebrafish transected wounds infected with *L. monocytogenes.* This suggests that besides inflammasome signaling, other signaling pathways induced by infections could also influence wound healing. Our transcriptomic data suggested that *acod1*, aconitate decarboxylase 1 also known as immunoresponsive gene 1 (*irg1*), which encodes for itaconate is also highly upregulated by *L. monocytogenes* at the wound. Little is known about the effect of itaconate on wound healing. It has been suggested in a human blood monocyte-derived macrophages model that itaconate promotes pro-healing phenotype in macrophages (Maassen et al., 2023), which is contrary to what we would expect since *L. monocytogenes* infected zebrafish with upregulated expression of *acod1* displayed wound healing defects.

Irg1 expression has been demonstrated to be induced by many bacterial pathogen infections, including *L. monocytogenes*, *Staphylococcus aureus*, *Mycobacterium tuberculosis*, and *Salmonella Typhimurium* (Degrandi et al., 2009; Tomlinson et al., 2021; Bomfim et al., 2022; M. Chen et al., 2020; R. Wu et al., 2022). However, itaconate has been shown to play varying roles under infections by different pathogens. While

itaconate serves as a host defense mechanism against pathogens such as *Mycobacterium tuberculosis* and *Salmonella Typhimurium* (Nair et al., 2018; Ruetz et al., 2019; M. Chen et al., 2020), it can be utilized by other pathogens such as *Pseudomonas aeruginosa* and *Staphylococcus aureus* to facilitate biofilm formation and increase pathogenicity (Riquelme et al., 2019, 2020; Tomlinson et al., 2021; Peace & O'Neill, 2022). Although *L. monocytogenes* induces irg1 expression (Degrandi et al., 2009), it has been shown that irg1$^{-/-}$ mice did not have a difference in susceptibility to *L. monocytogenes* compared to WT mice (Nair et al., 2018). Interestingly, itaconate has been reported to dampen inflammasome signaling and regulate the level of IL-1β, which leads us to hypothesize that the elevated *acod1* expression may be a response due to sustained inflammasome activation (Lampropoulou et al., 2016; Bambouskova et al., 2021). To test this hypothesis, we can utilize *irg1* transgenic reporter zebrafish and test if blocking IL-1β signaling with anakinra affects the expression of ACOD1/IRG1 at *L. monocytogenes*-infected wounds (Sanderson et al., 2015). Furthermore, examining if the knockdown of *irg1* using MO affects *il1b* expression and wound healing by quantifying the *il1b* level through RT-qPCR would also reveal if *irg1* acts through the same signaling axis. If loss of *irg1* results in an increased *il1b* expression and further worsens wound healing, this would suggest that *irg1* most likely plays a protective role in regulating *il1b* signaling and is not the driver for the wound healing defect. On the other hand, if the loss of *irg1* improves wound healing, this would indicate a role in wound healing inhibition in the context of infected wounds. Future studies validating the impact of itaconate in bacteria-infected wounds are crucial to providing better insights into whether itaconate plays a protective or inhibitory role during wound healing.

Bacteria clearance and wound healing

Current treatment for bacteria-infected wounds focuses on clearing the bacteria from the wound through antibiotic and antiseptic therapy (Hurlow & Bowler, 2022; Liu et al., 2022; X. Ding et al., 2022). Importantly, in **Chapter 2**, I demonstrated that antibiotic administration at later time points post-infection (after 1 dpi) was not able to control the inflammation nor rescue wound healing despite effective clearance of the bacteria, suggesting that early eradication of infection is critical to prevent non-resolving inflammation and defect in wound healing. This also indicates that early signaling events activated by *L. monocytogenes* drive prolonged inflammation and inhibition in wound healing. Even though early elimination of bacteria at the wound prevents impaired wound healing, around 70% of infected wounds are colonized by bacteria that are resistant to at least one of the commonly used antibiotics (X. Ding et al., 2022). Therefore, there is a need to identify novel antimicrobial targets to develop new strategies for bacteria clearance by understanding the mechanisms by which bacterial pathogens infect and replicate in the host.

Virulence determinants required in *L. monocytogenes* for survival and replication in the host

To discover strategies that pathogens employ to survive in the host, in **Chapter 3**, we executed whole genome-wide genetic screens utilizing TIS technologies to identify genes in *L. monocytogenes* required to defend against cell-intrinsic immunity, inflammasome-mediated immunity, and intact innate immunity.

L. monocytogenes genes important for cell-intrinsic immune defense (Table 3.1)

To identify genes required for *L. monocytogenes* intracellular survival and replication, we performed a TIS screen using murine bone marrow-derived macrophages (BMDMs). We identified several genes that had been described previously as important during infection, including genes involved in menaquinone biosynthesis (*aroA, aroB, aroE, aroF, menB, menC, menD, menE, menF, menI*) (G. Y. Chen, McDougal, et al., 2017; Rivera-Lugo et al., 2022; H. B. Smith et al., 2021, 2023). All the genes we found that are involved in the menaquinone pathway are involved in the synthesis of the intermediate product, 1,4-dihydroxy-2-naphthoyl acid (DHNA), corroborating with previous findings (G. Y. Chen, McDougal, et al., 2017).

We also identified several genes associated with cell wall synthesis, including genes with putative functions in cell division (*secA2, ftsK, divIVA, sepF*) and PG biosynthesis (*pgdA, pbpA1*); all of which, except for *sepF* and *pbpA1*, have been demonstrated to contribute to virulence (Boneca et al., 2007; Fischer et al., 2022b; Halbedel et al., 2012; Lenz et al., 2003). Future work generating clean deletions of *sepF* and *pbpA1* in *L. monocytogenes* and validating their growth defect in BMDMs is necessary. In *Bacillus subtilis*, *sepF* has been shown to be required for a late stage of cell division and it interacts with *fstZ*, whose function is to assemble the Z-ring during cell division (Hamoen et al., 2006). *fstZ* had very low transposon insertions in our transposon library pool and was claimed to be essential in our screen. If Δ*sepF* is attenuated, further studies investigating if *sepF* plays a similar role in *L. monocytogenes* can provide a better understanding of the reason behind its importance in intracellular growth and

replication. To test for interaction between SepF and FstZ, we can utilize a bacterial two-hybrid system, Bacterial Adenylate Cyclase-Based Two-Hybrid (BACTH) by cloning SepF and FstZ into bacterial two-hybrid plasmids pU18 and pKT25 (Karimova et al., 2017). Additionally, we can fuse a fluorescent protein to SepF and visualize its localization through microscopy. To test for SepF's role in cell division, we can examine the shape of bacterial cells of Δ*sepF*. If Δ*sepF* exhibits long filaments compared to WT, this would suggest a role for SepF in cell division.

Additionally, other genes that have been demonstrated with putative functions in cell wall metabolism (*yycH, walk*/*yycG*) in other bacterial species were also found in our screen (Cameron et al., 2016; Dubrac et al., 2007; Szurmant et al., 2007). *walK* or *yycG* encodes for sensor histidine kinase and is part of the two-component system and YycH is an extracellular auxiliary protein. WalK/YycG is important for peptidoglycan synthesis in *Staphylococcus aureus* and *Bacillus subtilis* (Dubrac et al., 2007; Dobihal et al., 2022). YycH has been shown to interact with YycI in both *S. aureus* and *B. subtilis* but they play opposite roles in the two bacterial species. While YycH and YycI induce WalK's activity in *S. aureus* through phosphorylation, they suppress WalK's activity in *B. subtilis* and lead to non-diving cells (Gajdiss et al., 2020; Fukushima et al., 2011). Although we did not identify YycI to be important for survival and replication *ex vivo*, a closer examination of the result of our screen uncovered that there is an over 5-fold reduction in fitness for *yycI* but it is not statistically significant (p-value = 0.06). We, therefore, hypothesize that YycH and YycI act through similar mechanisms in *L. monocytogenes* as in the *S. aureus* model. To test this hypothesis, we need to validate

the importance of YycH and YycI for intracellular growth by generating clean deletion of *walK, yycH,* and *yycI* in *L. monocytogenes* and testing for their survival in BMDMs. Additionally, experiments testing for their role in cell division by examining the cell shape of these mutants through microscopy are needed. It is also important to test for interactions of YycH and YycI through the bacterial two-hybrid system. To further test for YycH and YycI regulation on walK, we can generate *L. monocytogenes ΔwalKΔyycH* and *ΔwalKΔyycI* double deletion mutants and *ΔwalKΔyycHΔyycI* triple mutant and examine if there is a difference in cell shape between these mutants. If all these mutants display similar levels of elongation phenotype, this would suggest their functions are interconnected. Furthermore, to test the hypothesis that YycH and YycI act through phosphorylation, we can investigate if there is a decreased level of phosphorylated WalK in *ΔyycH* and *ΔyycI* compared to WT utilizing Phos-tag SDS-PAGE (Gajdiss et al., 2017). Characterization of these genes in *L. monocytogenes* may aid our understanding of how *L. monocytogenes* survive and replicate in the host cell.

L. monocytogenes genes important for inflammasome-mediated immune defense (Table 3.2)

For cytosolic pathogens to survive and replicate in the cell, it is important for them to evade inflammasome-mediated immune defense. What virulence factors facilitate *L. monocytogenes'* defense against inflammasome signaling is unclear. To identify virulence factors that *L. monocytogenes* utilize to evade inflammasome immunity, we performed a TIS screen using caspase-1-deficient BMDMs (Chapter 3). We found that DHNA-deficient mutants with a negative fitness in WT BMDMs can survive in caspase-

1-deficient BMDMs. Future work needs to test for the growth of these mutants using primed WT BMDMs to activate the inflammasome and compare their growth in caspase-1 deficient macrophages to validate the link between inflammasome-mediated killing in DHNA-deficient mutants. Our findings suggest that DHNA is important for *L. monocytogenes* to evade inflammasome immune response, leading to a major question: How does DHNA play a role in inflammasome signaling?

Little is known about how DHNA affects inflammasome signaling. However, studies have found that DHNA acts as an agonist of the aryl hydrocarbon receptor (AhR) (Fukumoto et al., 2014; Y. Cheng et al., 2017). In addition, the activation of AhR has been demonstrated to suppress the transcription of NLRP3 and dampen NLRP3 inflammasome signaling (Huai et al., 2014). We therefore hypothesize that DHNA is important for inflammasome defense in *L. monocytogenes* by inhibiting NLRP3 inflammasome signaling through AhR. To test this hypothesis, future work investigating if WT *L. monocytogenes* leads to higher inflammasome activation compared to DHNA-deficient mutants if important to test the direct link between DHNA and inflammasome signaling. To test for inflammasome activation, we can utilize Western Blot to measure the activation of caspase-1, IL-1β, and IL-18. ELIZA can also be used to measure the level of IL-1β and IL-18. Lactate dehydrogenase (LDH) release assay can be used to quantify pyroptosis. An important control would be supplementing in DHNA for cells infected with DHNA-deficient mutants. If DHNA-deficient mutants trigger more inflammasome signaling compared to WT *L. monocytogenes* and supplementation of DHNA reverts inflammasome activation back to the level stimulated by WT *L.*

monocytogenes, this would suggest that DHNA can suppress inflammasome response. To further test if the reduction in inflammasome signaling by DHNA is through AhR signaling, we can utilize AhR-deficient BMDMs and evaluate if WT *L. monocytogenes* stimulate a higher level of inflammasome signaling and are less fit to survive in AhR-deficient BMDMs compared to WT BMDMs. It would also be interesting to see if DHNA-deficient mutants stimulate excessive inflammation through inflammasome signaling in the zebrafish transection wound model and investigate if DHNA supplementation could improve wound healing in zebrafish infected with WT *L. monocytogenes*.

Besides genes involved in DHNA synthesis, we also identified multiple genes involved in galactitol-specific PTS systems, including *LMRG_00184*, *LMRG_01248*, and *LMRG_02211*, that are negatively selected for fitness in WT BMDMs but are dispensable in caspase-1-deficient BMDMs. *L. monocytogenes* has 3 PTS galactitol families. *LMRG_00183* encodes for the IIA component and both *LMRG_01248* and *LMRG_02211* encode for the IIB component. The galactitol-specific PTS system is not very well studied. A genetic screen in *Salmonella Typhimurium* found the galactitol-specific PTS system to be important for virulence in chickens, cattle, mice, and pigs (Chaudhuri et al., 2013). However, how the galactitol-specific PTS system regulates virulence is unknown. It has been reported in *E. coli* that overexpression of galactitol transport factor GatA increases tolerance to acidic stress and enhances energy production under acidic stress (Yang et al., 2022). These are the only studies that have described the role of the galactitol PTS system during infection. Future work validating if clean deletion of the genes in the galactitol PTS systems is attenuated in WT BMDM is

crucial to confirm if these genes are indeed required for intracellular survival and replication. Additionally, verifying the growth of these mutants in caspase-1-deficient BMDMs is also needed. If these genes are validated to be indispensable in WT BMDM but dispensable in caspase-1-deficient BMDMs, this would suggest a novel role for galactitol uptake or utilization for evading the inflammasome. Since so little is known about the galactitol PTS system, utilizing transcriptomic approaches such as performing RNA-sequencing on these mutants and comparing gene expressions to WT *L. monocytogenes* may help shed light on the mechanisms by which galactitol-specific PTS systems may promote virulence. Examining the expression of known virulence genes in the Listeria Pathogenicity Island 1 (LIPI-1) could answer if galactitol may be used as a signal to turn on the expression of these other virulence factors.

Galactitol is a sugar alcohol derived from galactose. In the host, galactitol is formed when galactose is in excess through the polyol pathway by reduction. Galactitol poorly diffuses through the cell membrane; therefore, it accumulates in the cells. The build-up of galactitol in the cells induces hyperosmotic and oxidative stress (Succoio et al., 2022). Perhaps the purpose of the uptake of galactitol by *L. monocytogenes* is to reduce the accumulation of galactitol in the host cell to minimize osmotic or oxidative stress. The stress reduction may lead to fewer damage-associated molecular patterns (DAMPs) released in the host cells, which are potent inflammasome activators (Jo et al., 2016; Murao et al., 2021; D. Li & Wu, 2021). To test for this hypothesis, it is important to determine if *L. monocytogenes* reduces galactitol levels within host cells by infecting BMDMs with WT or mutant strains lacking the galactitol-specific PTS system through

high-performance liquid chromatography (HPLC) or mass spectrometry to quantify intracellular galactitol levels over time. Additionally, to assess osmotic stress, we can measure cell swelling and viability using cell size analysis and viability assays. To measure oxidative stress, we can quantify reactive oxygen species (ROS) through ELISA. ELISA can also help quantify DAMPs release by measuring extracellular DAMPs such as HMGB1, ATP, and mitochondrial DNA. These experiments can collectively provide a better understanding of whether galactitol uptake by *L. monocytogenes* is important for preventing stress in the host cell to further avoid inflammasome activation.

***L. monocytogenes* genes important for intact immune defense**

An animal host presents a much more stressful environment with defense mechanisms from an intact immune system compared to the environment in a single cell in ex vivo cell culture models (Shi et al., 2019). To further identify genes in *L. monocytogenes* that are important for survival and replication *in vivo*, we performed a TIS screen using zebrafish as our model organism. We identified 909 genes that are crucial for fitness in zebrafish, which is an overwhelming number of genes. Therefore, we further utilize a deep learning-based genome-wide prediction of protein-protein interactions (PPI) approach (Cong et al., 2019; Humphreys et al., 2021) to prioritize virulence candidates that we propose for further investigation in future studies. We identified PPI pairs with interactions between two *in vivo* virulence genes and further picked out the pairs whose gene expression has been shown to be upregulated *in vivo* (Camejo et al., 2009). This resulted in 9 putative PPI pairs (Table 3.4), including 3 PPI pairs (OppB/OppC,

DltA/DltC, and Fur/PerR) that are known to be involved in virulence. Future work generating clean deletion of these genes in the other 6 PPI pairs in *L. monocytogenes* is needed to further verify the importance of these genes *in vivo*. Additionally, confirming interactions between the two genes in each of these PPI pairs through the bacterial two-hybrid system is important to support the validity of our protein-protein interaction approach (Karimova et al., 2017). If a virulence defect is confirmed for these mutants, future studies further characterizing the function of these genes could be critical for enhancing our understanding of the mechanisms by which bacterial pathogens utilize to survive and replicate in the host.

Importantly, the two genes in each of these known virulence pairs are known to work through the same function to promote virulence. This suggests that future studies can identify PPI pairs consisting of a virulence gene of known function with another virulence gene of unknown function to further reveal the function of the hypothetical protein. For example, one of our final PPI candidates is made up of listeriolysin O (LLO) and another hypothetical protein (LMRG_02629). LLO is a very well-studied virulence factor in *L. monocytogenes* that is utilized for phagosomal escape (Schnupf & Portnoy, 2007). We, therefore, hypothesize that LMRG_02629 may also be involved in the process of escaping the stressful environment of the phagosome. To test for phagosomal escape, we can utilize plaque assay. If LMRG_02629 is important for escaping the phagosome, Δ*LMRG_02629* should have a plaquing defect compared to WT *L. monocytogenes.* However, mutants with a cell-to-cell spreading defect will also display a plaquing defect. Therefore, if there is a phenotype observed from the plaque

assay with Δ*LMRG_02629*, future experiments tagging WT *L. monocytogenes* and Δ*LMRG_02629* with a fluorescent protein and labeling the phagosome marker, lysosomal-associated membrane protein 1 (LAMP-1), with a different fluorescent protein and then examine if there is a higher colocalization for the mutant though fluorescent microscopy could more specifically answer the question if LMRG_02629 is involved in phagosomal escape.

MiaA /LMRG_02629, TrmB/RimP, and MsrA/LMRG_00459 are three other PPI pairs we identified as our final candidates that may play a potential role in regulating stress responses in *L. monocytogenes*. MiaA is a tRNA modifying enzyme that is important for resisting oxidative and nitrosative stress, as well as osmotic stress in ExPEC (B. A. Fleming et al., 2022). The tRNA methyltransferase TrmB has been demonstrated to be critical for oxidative and pH stress responses and *in vivo* virulence in *Acinetobacter baumannii* through post-translational upregulation of other proteins (McGuffey et al., 2023). In *Mycobacterium fortuitum*, ribosomal maturation factor (RimP) has also been reported to be important for survival in acidic stress (Poonam et al., 2019). Peptide-methionine (S)-S-oxide reductase (MsrA) also has a protective role in oxidative stress and contributes to virulence in *Haemophilus influenzae*, *Mycoplasma genitalium*, and *Staphylococcus aureus*, while its interacting partner, LMRG_00459, is a hypothetical protein (Nasreen et al., 2022; Dhandayuthapani et al., 2001; Singh et al., 2018). We hypothesize that these PPI pairs may play a similar role in *L. monocytogenes* and are crucial for regulating stress responses to allow for their survival in the harsh environment in the host. To test if these genes are important for regulating oxidative

stress, we can cultivate these mutants *in vitro* in BHI broth supplemented with paraquat or hydrogen peroxide and observe if there is a growth defect in these mutants compared to WT *L. monocytogenes*. To investigate if these genes regulate pH stress, we can lower the pH of the BHI broth by HCl and monitor the growth of these mutants compared to WT *L. monocytogenes* under low pH conditions. These proposed experiments will provide a better understanding of the regulation of stress responses by these genes in *L. monocytogenes.*

Our final candidate genes indicate that oxidative stress response may be a required defense for *L. monocytogenes in vivo*. To further identify other genes that may be critical for regulating oxidative stress, future studies can execute a TIS screen using zebrafish lacking phagocyte oxidase ($p22^{phox-/-}$) (Schoen et al., 2020). If a gene is important in WT zebrafish but becomes dispensable in $p22^{phox-/-}$ zebrafish, this would suggest that the gene may be essential for protecting *L. monocytogenes* from ROS stress. Additional TIS screens using other immunodeficient zebrafish could further facilitate the discovery of genes in *L. monocytogenes* with specific functions *in vivo*. For example, a TIS screen using Tg(*mpx:rac2*^{D57N}) zebrafish, a zebrafish mutant with a defect in neutrophil motility and thus unable to enter the site of infection, can reveal *L. monocytogenes* genes that are important to prevent killing by neutrophil (Deng et al., 2011). A TIS screen utilizing *irf8*-/- zebrafish, a zebrafish mutant with impaired macrophage development, can uncover genes required in *L. monocytogenes* for protection against macrophage immune defenses (Shiau et al., 2015).

Our zebrafish TIS screen yielded an overwhelming number of genes in *L. monocytogenes* that could be critical for virulence *in vivo* and it is not feasible to verify each gene for their importance. Future studies generating an ordered *L. monocytogenes* transposon library could be beneficial for further validations of virulence for the genes identified from our screen. To construct this ordered library, we can utilize the Knockout Sudoku method using combinatorial pooling, barcode labeling, next-generation sequencing, and a Bayesian inference algorithm to deconvolve the data set and enable mapping of individually sequenced transposon mutants to their corresponding positions in 96 well plates (Anzai et al., 2017; Baym et al., 2016).

In conclusion, this dissertation highlights the power of using zebrafish as a model organism to study host-pathogen interactions. Using zebrafish as a model provides the ease of genetic manipulation, the ability to administrate drugs through simple diffusion, and the capability to perform non-invasive imaging due to its transparency, which enabled us to discover that bacteria-induced inflammation derived from inflammasome signaling impairs wound healing (**Chapter 2**). Additionally, the high fecundity and cheap cost of zebrafish allowed us to perform one of the first *L. monocytogenes* TIS screens *in vivo* (**Chapter 3**).

Translation to Clinic

In **Chapter 2**, we demonstrated that blocking IL-1 signaling with anakinra improves wound healing without having a negative impact on the host immune defense against infections. Importantly, anakinra is already an FDA-approved drug. Our findings support

the potential of starting a clinical trial testing the use of anakinra for treating infected wounds. Additionally, if the genes identified in our TIS screens are validated to promote bacterial virulence, our findings from Chapter 3 can provide implications for potential antimicrobial targets to treat antibiotic-resistant infections in the clinic.

REFERENCES

Abachin, E., Poyart, C., Pellegrini, E., Milohanic, E., Fiedler, F., Berche, P., & Trieu-Cuot, P. (2002). Formation of D -alanyl-lipoteichoic acid is required for adhesion and virulence of *Listeria monocytogenes*. *Molecular Microbiology*, *43*(1), 1–14. https://doi.org/10.1046/j.1365-2958.2002.02723.x

Abel, S., Abel Zur Wiesch, P., Chang, H.-H., Davis, B. M., Lipsitch, M., & Waldor, M. K. (2015). Sequence tag–based analysis of microbial population dynamics. *Nature Methods*, *12*(3), 223–226. https://doi.org/10.1038/nmeth.3253

Adedeji, W. A. (2016). THE TREASURE CALLED ANTIBIOTICS. *Annals of Ibadan Postgraduate Medicine*, *14*(2), 56–57.

Agrati, C., Carsetti, R., Bordoni, V., Sacchi, A., Quintarelli, C., Locatelli, F., Ippolito, G., & Capobianchi, M. R. (2022). The immune response as a double-edged sword: The lesson learnt during the COVID -19 pandemic. *Immunology*, *167*(3), 287–302. https://doi.org/10.1111/imm.13564

Alexander, J. W. (1985). The Contributions of Infection Control to a Century of Surgical Progress: *Annals of Surgery*, *201*(4), 423–428. https://doi.org/10.1097/00000658-198504000-00004

Allerberger, F., & Wagner, M. (2010). Listeriosis: A resurgent foodborne infection. *Clinical Microbiology and Infection*, *16*(1), 16–23. https://doi.org/10.1111/j.1469-0691.2009.03109.x

Alves, P. M., Al-Badi, E., Withycombe, C., Jones, P. M., Purdy, K. J., & Maddocks, S. E. (2018). Interaction between Staphylococcus aureus and Pseudomonas aeruginosa is

beneficial for colonisation and pathogenicity in a mixed biofilm. *Pathogens and Disease*, *76*(1). https://doi.org/10.1093/femspd/fty003

Anzai, I. A., Shaket, L., Adesina, O., Baym, M., & Barstow, B. (2017). Rapid curation of gene disruption collections using Knockout Sudoku. *Nature Protocols*, *12*(10), 2110–2137. https://doi.org/10.1038/nprot.2017.073

Armstrong, D. G., Edmonds, M. E., & Serena, T. E. (2023). Point-of-care fluorescence imaging reveals extent of bacterial load in diabetic foot ulcers. *International Wound Journal*, *20*(2), 554–566. https://doi.org/10.1111/iwj.14080

Auvray, F., Chassaing, D., Duprat, C., & Carpentier, B. (2007). The Listeria monocytogenes homolog of the Escherichia coli era gene is involved in adhesion to inert surfaces. *Applied and Environmental Microbiology*, *73*(23), 7789–7792. https://doi.org/10.1128/AEM.01157-07

Bambouskova, M., Potuckova, L., Paulenda, T., Kerndl, M., Mogilenko, D. A., Lizotte, K., Swain, A., Hayes, S., Sheldon, R. D., Kim, H., Kapadnis, U., Ellis, A. E., Isaguirre, C., Burdess, S., Laha, A., Amarasinghe, G. K., Chubukov, V., Roddy, T. P., Diamond, M. S., … Artyomov, M. N. (2021). Itaconate confers tolerance to late NLRP3 inflammasome activation. *Cell Reports*, *34*(10), 108756. https://doi.org/10.1016/j.celrep.2021.108756

Barber, G. N. (2011). Innate immune DNA sensing pathways: STING, AIMII and the regulation of interferon production and inflammatory responses. *Current Opinion in Immunology*, *23*(1), 10–20. https://doi.org/10.1016/j.coi.2010.12.015

Barnes, P. D., Bergman, M. A., Mecsas, J., & Isberg, R. R. (2006). *Yersinia pseudotuberculosis* disseminates directly from a replicating bacterial pool in the intestine. *The Journal of Experimental Medicine*, *203*(6), 1591–1601. https://doi.org/10.1084/jem.20060905

Baym, M., Shaket, L., Anzai, I. A., Adesina, O., & Barstow, B. (2016). Rapid construction of a whole-genome transposon insertion collection for Shewanella oneidensis by Knockout Sudoku. *Nature Communications*, *7*(1), 13270. https://doi.org/10.1038/ncomms13270

Berude, J. C., Kennouche, P., Reniere, M. L., & Portnoy, D. A. (2024). *Listeria monocytogenes* utilizes glutathione and limited inorganic sulfur compounds as sources of essential cysteine. *Infection and Immunity*, *92*(3), e00422-23. https://doi.org/10.1128/iai.00422-23

Bessa, L. J., Fazii, P., Di Giulio, M., & Cellini, L. (2015). Bacterial isolates from infected wounds and their antibiotic susceptibility pattern: Some remarks about wound infection. *International Wound Journal*, *12*(1), 47–52. https://doi.org/10.1111/iwj.12049

Bojarczuk, A., Miller, K. A., Hotham, R., Lewis, A., Ogryzko, N. V., Kamuyango, A. A., Frost, H., Gibson, R. H., Stillman, E., May, R. C., Renshaw, S. A., & Johnston, S. A. (2016). Cryptococcus neoformans Intracellular Proliferation and Capsule Size Determines Early Macrophage Control of Infection. *Scientific Reports*, *6*(1), 21489. https://doi.org/10.1038/srep21489

Bomfim, C. C. B., Fisher, L., Amaral, E. P., Mittereder, L., McCann, K., Correa, A. A. S., Namasivayam, S., Swamydas, M., Moayeri, M., Weiss, J. M., Chari, R., McVicar, D. W., Costa, D. L., D'Império Lima, M. R., & Sher, A. (2022). Mycobacterium tuberculosis Induces Irg1 in Murine Macrophages by a Pathway Involving Both TLR-2 and STING/IFNAR Signaling and Requiring Bacterial Phagocytosis. *Frontiers in Cellular and Infection Microbiology*, *12*, 862582. https://doi.org/10.3389/fcimb.2022.862582

Boneca, I. G., Dussurget, O., Cabanes, D., Nahori, M.-A., Sousa, S., Lecuit, M., Psylinakis, E., Bouriotis, V., Hugot, J.-P., Giovannini, M., Coyle, A., Bertin, J., Namane, A., Rousselle, J.-C., Cayet, N., Prévost, M.-C., Balloy, V., Chignard, M., Philpott, D. J., … Girardin, S.

E. (2007). A critical role for peptidoglycan N-deacetylation in *Listeria* evasion from the host innate immune system. *Proceedings of the National Academy of Sciences*, *104*(3), 997–1002. https://doi.org/10.1073/pnas.0609672104

Borezee, E., Pellegrini, E., & Berche, P. (2000). OppA of *Listeria monocytogenes* , an Oligopeptide-Binding Protein Required for Bacterial Growth at Low Temperature and Involved in Intracellular Survival. *Infection and Immunity*, *68*(12), 7069–7077. https://doi.org/10.1128/IAI.68.12.7069-7077.2000

Bouldin, C. M., & Kimelman, D. (2014). Dual Fucci: A New Transgenic Line for Studying the Cell Cycle from Embryos to Adults. *Zebrafish*, *11*(2), 182–183. https://doi.org/10.1089/zeb.2014.0986

Brundage, R. A., Smith, G. A., Camilli, A., Theriot, J. A., & Portnoy, D. A. (1993). Expression and phosphorylation of the Listeria monocytogenes ActA protein in mammalian cells. *Proceedings of the National Academy of Sciences*, *90*(24), 11890–11894. https://doi.org/10.1073/pnas.90.24.11890

Cain, A. K., Barquist, L., Goodman, A. L., Paulsen, I. T., Parkhill, J., & Van Opijnen, T. (2020). A decade of advances in transposon-insertion sequencing. *Nature Reviews Genetics*, *21*(9), 526–540. https://doi.org/10.1038/s41576-020-0244-x

Caldwell, M. D. (2020). Bacteria and Antibiotics in Wound Healing. *Surgical Clinics of North America*, *100*(4), 757–776. https://doi.org/10.1016/j.suc.2020.05.007

Camejo, A., Buchrieser, C., Couvé, E., Carvalho, F., Reis, O., Ferreira, P., Sousa, S., Cossart, P., & Cabanes, D. (2009). In Vivo Transcriptional Profiling of Listeria monocytogenes and Mutagenesis Identify New Virulence Factors Involved in Infection. *PLoS Pathogens*, *5*(5), e1000449. https://doi.org/10.1371/journal.ppat.1000449

Cameron, D. R., Jiang, J.-H., Kostoulias, X., Foxwell, D. J., & Peleg, A. Y. (2016). Vancomycin susceptibility in methicillin-resistant Staphylococcus aureus is mediated by YycHI activation of the WalRK essential two-component regulatory system. *Scientific Reports*, *6*(1), 30823. https://doi.org/10.1038/srep30823

Camilli, A., Tilney, L. G., & Portnoy, D. A. (1993). Dual roles of *plcA* in *Listeria monocytogenes* pathogenesis. *Molecular Microbiology*, *8*(1), 143–157. https://doi.org/10.1111/j.1365-2958.1993.tb01211.x

Cañedo-Dorantes, L., & Cañedo-Ayala, M. (2019). Skin Acute Wound Healing: A Comprehensive Review. *International Journal of Inflammation*, *2019*, 1–15. https://doi.org/10.1155/2019/3706315

Cao, M., Wang, G., & Xie, J. (2023). Immune dysregulation in sepsis: Experiences, lessons and perspectives. *Cell Death Discovery*, *9*(1), 465. https://doi.org/10.1038/s41420-023-01766-7

Carter, M. J., DaVanzo, J., Haught, R., Nusgart, M., Cartwright, D., & Fife, C. E. (2023). Chronic wound prevalence and the associated cost of treatment in Medicare beneficiaries: Changes between 2014 and 2019. *Journal of Medical Economics*, *26*(1), 894–901. https://doi.org/10.1080/13696998.2023.2232256

Casadevall, A., & Pirofski, L. (2009). Virulence factors and their mechanisms of action: The view from a damage–response framework. *Journal of Water and Health*, *7*(S1), S2–S18. https://doi.org/10.2166/wh.2009.036

Cavalcante-Silva, J., & Koh, T. J. (2023). Targeting the NOD-Like Receptor Pyrin Domain Containing 3 Inflammasome to Improve Healing of Diabetic Wounds. *Advances in Wound Care*, *12*(11), 644–656. https://doi.org/10.1089/wound.2021.0148

Centers for Disease Control and Prevention (U.S.). (2019). *Antibiotic resistance threats in the United States, 2019*. Centers for Disease Control and Prevention (U.S.). https://doi.org/10.15620/cdc:82532

Chakraborty, T., Leimeister-Wächter, M., Domann, E., Hartl, M., Goebel, W., Nichterlein, T., & Notermans, S. (1992). Coordinate regulation of virulence genes in Listeria monocytogenes requires the product of the prfA gene. *Journal of Bacteriology*, *174*(2), 568–574. https://doi.org/10.1128/jb.174.2.568-574.1992

Chao, M. C., Abel, S., Davis, B. M., & Waldor, M. K. (2016). The design and analysis of transposon insertion sequencing experiments. *Nature Reviews Microbiology*, *14*(2), 119–128. https://doi.org/10.1038/nrmicro.2015.7

Chaudhuri, R. R., Morgan, E., Peters, S. E., Pleasance, S. J., Hudson, D. L., Davies, H. M., Wang, J., Van Diemen, P. M., Buckley, A. M., Bowen, A. J., Pullinger, G. D., Turner, D. J., Langridge, G. C., Turner, A. K., Parkhill, J., Charles, I. G., Maskell, D. J., & Stevens, M. P. (2013). Comprehensive Assignment of Roles for Salmonella Typhimurium Genes in Intestinal Colonization of Food-Producing Animals. *PLoS Genetics*, *9*(4), e1003456. https://doi.org/10.1371/journal.pgen.1003456

Chen, G. Y., McDougal, C. E., D'Antonio, M. A., Portman, J. L., & Sauer, J.-D. (2017). A Genetic Screen Reveals that Synthesis of 1,4-Dihydroxy-2-Naphthoate (DHNA), but Not Full-Length Menaquinone, Is Required for *Listeria monocytogenes* Cytosolic Survival. *mBio*, *8*(2), e00119-17. https://doi.org/10.1128/mBio.00119-17

Chen, G. Y., Pensinger, D. A., & Sauer, J.-D. (2017). *Listeria monocytogenes* cytosolic metabolism promotes replication, survival, and evasion of innate immunity. *Cellular Microbiology*, *19*(10), e12762. https://doi.org/10.1111/cmi.12762

Chen, M., Sun, H., Boot, M., Shao, L., Chang, S.-J., Wang, W., Lam, T. T., Lara-Tejero, M., Rego, E. H., & Galán, J. E. (2020). Itaconate is an effector of a Rab GTPase cell-autonomous host defense pathway against *Salmonella*. *Science*, *369*(6502), 450–455. https://doi.org/10.1126/science.aaz1333

Cheng, C., Han, X., Xu, J., Sun, J., Li, K., Han, Y., Chen, M., & Song, H. (2021). YjbH mediates the oxidative stress response and infection by regulating SpxA1 and the phosphoenolpyruvate-carbohydrate phosphotransferase system (PTS) in *Listeria monocytogenes*. *Gut Microbes*, *13*(1), 1884517. https://doi.org/10.1080/19490976.2021.1884517

Cheng, Y., Jin, U.-H., Davidson, L. A., Chapkin, R. S., Jayaraman, A., Tamamis, P., Orr, A., Allred, C., Denison, M. S., Soshilov, A., Weaver, E., & Safe, S. (2017). Editor's Highlight: Microbial-Derived 1,4-Dihydroxy-2-naphthoic Acid and Related Compounds as Aryl Hydrocarbon Receptor Agonists/Antagonists: Structure–Activity Relationships and Receptor Modeling. *Toxicological Sciences*, *155*(2), 458–473. https://doi.org/10.1093/toxsci/kfw230

Cole, J. N., & Nizet, V. (2016). Bacterial Evasion of Host Antimicrobial Peptide Defenses. *Microbiology Spectrum*, *4*(1), 4.1.04. https://doi.org/10.1128/microbiolspec.VMBF-0006-2015

Cong, Q., Anishchenko, I., Ovchinnikov, S., & Baker, D. (2019). Protein interaction networks revealed by proteome coevolution. *Science*, *365*(6449), 185–189. https://doi.org/10.1126/science.aaw6718

Cossart, P. (2007). Listeriology (1926–2007): The rise of a model pathogen. *Microbes and Infection*, *9*(10), 1143–1146. https://doi.org/10.1016/j.micinf.2007.05.001

Dai, J., Shen, J., Chai, Y., & Chen, H. (2021). IL-1β Impaired Diabetic Wound Healing by Regulating MMP-2 and MMP-9 through the p38 Pathway. *Mediators of Inflammation, 2021*, 1–10. https://doi.org/10.1155/2021/6645766

Dai, J., Zhang, X., Wang, Y., Chen, H., & Chai, Y. (2017). ROS-activated NLRP3 inflammasome initiates inflammation in delayed wound healing in diabetic rats. *International Journal of Clinical and Experimental Pathology*, *10*(9), 9902–9909.

Dasari, N., Jiang, A., Skochdopole, A., Chung, J., Reece, E. M., Vorstenbosch, J., & Winocour, S. (2021). Updates in Diabetic Wound Healing, Inflammation, and Scarring. *Seminars in Plastic Surgery*, *35*(03), 153–158. https://doi.org/10.1055/s-0041-1731460

Degrandi, D., Hoffmann, R., Beuter-Gunia, C., & Pfeffer, K. (2009). The Proinflammatory Cytokine-Induced IRG1 Protein Associates with Mitochondria. *Journal of Interferon & Cytokine Research*, *29*(1), 55–68. https://doi.org/10.1089/jir.2008.0013

Deng, Q., Yoo, S. K., Cavnar, P. J., Green, J. M., & Huttenlocher, A. (2011). Dual Roles for Rac2 in Neutrophil Motility and Active Retention in Zebrafish Hematopoietic Tissue. *Developmental Cell*, *21*(4), 735–745. https://doi.org/10.1016/j.devcel.2011.07.013

Dhandayuthapani, S., Blaylock, M. W., Bebear, C. M., Rasmussen, W. G., & Baseman, J. B. (2001). Peptide Methionine Sulfoxide Reductase (MsrA) Is a Virulence Determinant in *Mycoplasma genitalium*. *Journal of Bacteriology*, *183*(19), 5645–5650. https://doi.org/10.1128/JB.183.19.5645-5650.2001

Ding, X., Tang, Q., Xu, Z., Xu, Y., Zhang, H., Zheng, D., Wang, S., Tan, Q., Maitz, J., Maitz, P. K., Yin, S., Wang, Y., & Chen, J. (2022). Challenges and innovations in treating chronic and acute wound infections: From basic science to clinical practice. *Burns & Trauma*, *10*, tkac014. https://doi.org/10.1093/burnst/tkac014

Ding, Y., Ding, X., Zhang, H., Li, S., Yang, P., & Tan, Q. (2022). Relevance of NLRP3 Inflammasome-Related Pathways in the Pathology of Diabetic Wound Healing and Possible Therapeutic Targets. *Oxidative Medicine and Cellular Longevity*, *2022*, 1–15. https://doi.org/10.1155/2022/9687925

Disson, O., & Lecuit, M. (2013). In vitro and in vivo models to study human listeriosis: Mind the gap. *Microbes and Infection*, *15*(14–15), 971–980. https://doi.org/10.1016/j.micinf.2013.09.012

Dobihal, G. S., Flores-Kim, J., Roney, I. J., Wang, X., & Rudner, D. Z. (2022). The WalR-WalK Signaling Pathway Modulates the Activities of both CwlO and LytE through Control of the Peptidoglycan Deacetylase PdaC in Bacillus subtilis. *Journal of Bacteriology*, *204*(2), e00533-21. https://doi.org/10.1128/jb.00533-21

Dobin, A., Davis, C. A., Schlesinger, F., Drenkow, J., Zaleski, C., Jha, S., Batut, P., Chaisson, M., & Gingeras, T. R. (2013). STAR: Ultrafast universal RNA-seq aligner. *Bioinformatics*, *29*(1), 15–21. https://doi.org/10.1093/bioinformatics/bts635

D'Onofrio, F., Schirone, M., Paparella, A., Krasteva, I., Tittarelli, M., Pomilio, F., Iannetti, L., D'Alterio, N., & Luciani, M. (2023). Stress Adaptation Responses of a Listeria monocytogenes 1/2a Strain via Proteome Profiling. *Foods*, *12*(11), 2166. https://doi.org/10.3390/foods12112166

D'Orazio, S. E. F. (2019). Innate and Adaptive Immune Responses during *Listeria monocytogenes* Infection. *Microbiology Spectrum*, *7*(3), 7.3.12. https://doi.org/10.1128/microbiolspec.GPP3-0065-2019

Doron, S., & Gorbach, S. L. (2008). Bacterial Infections: Overview. In *International Encyclopedia of Public Health* (pp. 273–282). Elsevier. https://doi.org/10.1016/B978-012373960-5.00596-7

Dubrac, S., Boneca, I. G., Poupel, O., & Msadek, T. (2007). New Insights into the WalK/WalR (YycG/YycF) Essential Signal Transduction Pathway Reveal a Major Role in Controlling Cell Wall Metabolism and Biofilm Formation in *Staphylococcus aureus*. *Journal of Bacteriology*, *189*(22), 8257–8269. https://doi.org/10.1128/JB.00645-07

Durand, J. M., Björk, G. R., Kuwae, A., Yoshikawa, M., & Sasakawa, C. (1997). The modified nucleoside 2-methylthio-N6-isopentenyladenosine in tRNA of Shigella flexneri is required for expression of virulence genes. *Journal of Bacteriology*, *179*(18), 5777–5782. https://doi.org/10.1128/jb.179.18.5777-5782.1997

Dussurget, O. (2008). Chapter 1 New Insights into Determinants of Listeria Monocytogenes Virulence. In *International Review of Cell and Molecular Biology* (Vol. 270, pp. 1–38). Elsevier. https://doi.org/10.1016/S1937-6448(08)01401-9

Eddy, S. R. (2011). Accelerated Profile HMM Searches. *PLoS Computational Biology*, *7*(10), e1002195. https://doi.org/10.1371/journal.pcbi.1002195

Edelson, B. T., & Unanue, E. R. (2002). MyD88-Dependent but Toll-Like Receptor 2-Independent Innate Immunity to *Listeria*: No Role for Either in Macrophage Listericidal Activity. *The Journal of Immunology*, *169*(7), 3869–3875. https://doi.org/10.4049/jimmunol.169.7.3869

Edman, D. C., Pollock, M. B., & Hall, E. R. (1968). *Listeria monocytogenes* L Forms I. Induction, Maintenance, and Biological Characteristics. *Journal of Bacteriology*, *96*(2), 352–357. https://doi.org/10.1128/jb.96.2.352-357.1968

Eisenreich, W., Heesemann, J., Rudel, T., & Goebel, W. (2015). Metabolic Adaptations of Intracellullar Bacterial Pathogens and their Mammalian Host Cells during Infection ("Pathometabolism"). *Microbiology Spectrum*, *3*(3), 3.3.10. https://doi.org/10.1128/microbiolspec.MBP-0002-2014

Faith, N. G., Kim, J.-W., Azizoglu, R., Kathariou, S., & Czuprynski, C. (2012). Purine Biosynthesis Mutants (*purA* and *purB*) of Serotype 4b *Listeria monocytogenes* Are Severely Attenuated for Systemic Infection in Intragastrically Inoculated A/J Mice. *Foodborne Pathogens and Disease*, *9*(5), 480–486. https://doi.org/10.1089/fpd.2011.1013

Fajgenbaum, D. C., & June, C. H. (2020). Cytokine Storm. *New England Journal of Medicine*, *383*(23), 2255–2273. https://doi.org/10.1056/NEJMra2026131

Fischer, M. A., Engelgeh, T., Rothe, P., Fuchs, S., Thürmer, A., & Halbedel, S. (2022a). *Listeria monocytogenes* genes supporting growth under standard laboratory cultivation conditions and during macrophage infection. *Genome Research*, *32*(9), 1711–1726. https://doi.org/10.1101/gr.276747.122

Fischer, M. A., Engelgeh, T., Rothe, P., Fuchs, S., Thürmer, A., & Halbedel, S. (2022b). *Listeria monocytogenes* genes supporting growth under standard laboratory cultivation conditions and during macrophage infection. *Genome Research*, *32*(9), 1711–1726. https://doi.org/10.1101/gr.276747.122

Fleming, A. (n.d.). *ON THE ANTIBACTERIAL ACTION OF CULTURES OF A PENICILLIUM, WITH SPECIAL REFERENCE TO THEIR USE IN THE ISOLATION OF B. INFLUENZ?1E.*

Fleming, B. A., Blango, M. G., Rousek, A. A., Kincannon, W. M., Tran, A., Lewis, A. J., Russell, C. W., Zhou, Q., Baird, L. M., Barber, A. E., Brannon, J. R., Beebout, C. J., Bandarian, V., Hadjifrangiskou, M., Howard, M. T., & Mulvey, M. A. (2022). A tRNA modifying enzyme as a tunable regulatory nexus for bacterial stress responses and virulence. *Nucleic Acids Research*, *50*(13), 7570–7590. https://doi.org/10.1093/nar/gkac116

Flo, T. H., Halaas, Ø., Lien, E., Ryan, L., Teti, G., Golenbock, D. T., Sundan, A., & Espevik, T. (2000). Human Toll-Like Receptor 2 Mediates Monocyte Activation by *Listeria monocytogenes* , But Not by Group B Streptococci or Lipopolysaccharide. *The Journal of Immunology*, *164*(4), 2064–2069. https://doi.org/10.4049/jimmunol.164.4.2064

Forn-Cuní, G., Meijer, A. H., & Varela, M. (2019). Zebrafish in Inflammasome Research. *Cells*, *8*(8), 901. https://doi.org/10.3390/cells8080901

Freiberg, J. A. (2017). The mythos of laudable pus along with an explanation for its origin. *Journal of Community Hospital Internal Medicine Perspectives*, *7*(3), 196–198. https://doi.org/10.1080/20009666.2017.1343077

Freitag, N. E., Port, G. C., & Miner, M. D. (2009). Listeria monocytogenes—From saprophyte to intracellular pathogen. *Nature Reviews Microbiology*, *7*(9), 623–628. https://doi.org/10.1038/nrmicro2171

Freitag, N. E., Rong, L., & Portnoy, D. A. (1993). Regulation of the prfA transcriptional activator of Listeria monocytogenes: Multiple promoter elements contribute to intracellular growth and cell-to-cell spread. *Infection and Immunity*, *61*(6), 2537–2544. https://doi.org/10.1128/iai.61.6.2537-2544.1993

Fukumoto, S., Toshimitsu, T., Matsuoka, S., Maruyama, A., Oh-oka, K., Takamura, T., Nakamura, Y., Ishimaru, K., Fujii-Kuriyama, Y., Ikegami, S., Itou, H., & Nakao, A. (2014). Identification of a probiotic bacteria-derived activator of the aryl hydrocarbon receptor that inhibits colitis. *Immunology & Cell Biology*, *92*(5), 460–465. https://doi.org/10.1038/icb.2014.2

Fukushima, T., Furihata, I., Emmins, R., Daniel, R. A., Hoch, J. A., & Szurmant, H. (2011). A role for the essential YycG sensor histidine kinase in sensing cell division. *Molecular Microbiology*, *79*(2), 503–522. https://doi.org/10.1111/j.1365-2958.2010.07464.x

Gadar, K., & McCarthy, R. R. (2023). Using next generation antimicrobials to target the mechanisms of infection. *Npj Antimicrobials and Resistance*, *1*(1), 11. https://doi.org/10.1038/s44259-023-00011-6

Gajdiss, M., Monk, I. R., Bertsche, U., Kienemund, J., Funk, T., Dietrich, A., Hort, M., Sib, E., Stinear, T. P., & Bierbaum, G. (2020). YycH and YycI Regulate Expression of Staphylococcus aureus Autolysins by Activation of WalRK Phosphorylation. *Microorganisms*, *8*(6), 870. https://doi.org/10.3390/microorganisms8060870

Gajdiss, M., Türck, M., & Bierbaum, G. (2017). Bacterial Histidine Kinases: Overexpression, Purification, and Inhibitor Screen. In P. Sass (Ed.), *Antibiotics* (Vol. 1520, pp. 247–259). Springer New York. https://doi.org/10.1007/978-1-4939-6634-9_15

Goldberg, M. B., & Theriot, J. A. (1995). Shigella flexneri surface protein IcsA is sufficient to direct actin-based motility. *Proceedings of the National Academy of Sciences*, *92*(14), 6572–6576. https://doi.org/10.1073/pnas.92.14.6572

Gomes, M. C., & Mostowy, S. (2020). The Case for Modeling Human Infection in Zebrafish. *Trends in Microbiology*, *28*(1), 10–18. https://doi.org/10.1016/j.tim.2019.08.005

Gosain, A., & DiPietro, L. A. (2004). Aging and Wound Healing. *World Journal of Surgery*, *28*(3), 321–326. https://doi.org/10.1007/s00268-003-7397-6

Grada, A., Mervis, J., & Falanga, V. (2018). Research Techniques Made Simple: Animal Models of Wound Healing. *Journal of Investigative Dermatology*, *138*(10), 2095-2105.e1. https://doi.org/10.1016/j.jid.2018.08.005

GTEx Consortium. (2017). Genetic effects on gene expression across human tissues. *Nature*, *550*(7675), 204–213. https://doi.org/10.1038/nature24277

Guo, S., & DiPietro, L. A. (2010). Factors Affecting Wound Healing. *Journal of Dental Research*, *89*(3), 219–229. https://doi.org/10.1177/0022034509359125

Halbedel, S., Hahn, B., Daniel, R. A., & Flieger, A. (2012). DivIVA affects secretion of virulence-related autolysins in *Listeria monocytogenes*. *Molecular Microbiology*, *83*(4), 821–839. https://doi.org/10.1111/j.1365-2958.2012.07969.x

Hamoen, L. W., Meile, J., De Jong, W., Noirot, P., & Errington, J. (2006). SepF, a novel FtsZ-interacting protein required for a late step in cell division. *Molecular Microbiology*, *59*(3), 989–999. https://doi.org/10.1111/j.1365-2958.2005.04987.x

Hamon, M., Bierne, H., & Cossart, P. (2006). Listeria monocytogenes: A multifaceted model. *Nature Reviews Microbiology*, *4*(6), 423–434. https://doi.org/10.1038/nrmicro1413

Hayashi, F., Smith, K. D., Ozinsky, A., Hawn, T. R., Yi, E. C., Goodlett, D. R., Eng, J. K., Akira, S., Underhill, D. M., & Aderem, A. (2001). The innate immune response to bacterial flagellin is mediated by Toll-like receptor 5. *Nature*, *410*(6832), 1099–1103. https://doi.org/10.1038/35074106

Hensel, M., Shea, J. E., Gleeson, C., Jones, M. D., Dalton, E., & Holden, D. W. (1995). Simultaneous Identification of Bacterial Virulence Genes by Negative Selection. *Science*, *269*(5222), 400–403. https://doi.org/10.1126/science.7618105

Hesketh, M., Sahin, K. B., West, Z. E., & Murray, R. Z. (2017). Macrophage Phenotypes Regulate Scar Formation and Chronic Wound Healing. *International Journal of Molecular Sciences*, *18*(7), 1545. https://doi.org/10.3390/ijms18071545

Holl, J., Kowalewski, C., Zimek, Z., Fiedor, P., Kaminski, A., Oldak, T., Moniuszko, M., & Eljaszewicz, A. (2021). Chronic Diabetic Wounds and Their Treatment with Skin Substitutes. *Cells*, *10*(3), 655. https://doi.org/10.3390/cells10030655

Hornef, M. W., Wick, M. J., Rhen, M., & Normark, S. (2002). Bacterial strategies for overcoming host innate and adaptive immune responses. *Nature Immunology*, *3*(11), 1033–1040. https://doi.org/10.1038/ni1102-1033

Howe, K., Clark, M. D., Torroja, C. F., Torrance, J., Berthelot, C., Muffato, M., Collins, J. E., Humphray, S., McLaren, K., Matthews, L., McLaren, S., Sealy, I., Caccamo, M., Churcher, C., Scott, C., Barrett, J. C., Koch, R., Rauch, G.-J., White, S., … Stemple, D. L. (2013). The zebrafish reference genome sequence and its relationship to the human genome. *Nature*, *496*(7446), 498–503. https://doi.org/10.1038/nature12111

Huai, W., Zhao, R., Song, H., Zhao, J., Zhang, L., Zhang, L., Gao, C., Han, L., & Zhao, W. (2014). Aryl hydrocarbon receptor negatively regulates NLRP3 inflammasome activity by inhibiting NLRP3 transcription. *Nature Communications*, *5*(1), 4738. https://doi.org/10.1038/ncomms5738

Humphreys, I. R., Pei, J., Baek, M., Krishnakumar, A., Anishchenko, I., Ovchinnikov, S., Zhang, J., Ness, T. J., Banjade, S., Bagde, S. R., Stancheva, V. G., Li, X.-H., Liu, K., Zheng, Z.,

Barrero, D. J., Roy, U., Kuper, J., Fernández, I. S., Szakal, B., … Baker, D. (2021). Computed structures of core eukaryotic protein complexes. *Science*, *374*(6573), eabm4805. https://doi.org/10.1126/science.abm4805

Humphreys, I. R., Zhang, J., Baek, M., Wang, Y., Krishnakumar, A., Pei, J., Anishchenko, I., Tower, C. A., Jackson, B. A., Warrier, T., Hung, D. T., Peterson, S. B., Mougous, J. D., Cong, Q., & Baker, D. (2024). Essential and virulence-related protein interactions of pathogens revealed through deep learning. *bioRxiv: The Preprint Server for Biology*, 2024.04.12.589144. https://doi.org/10.1101/2024.04.12.589144

Hurlow, J., & Bowler, P. G. (2022). Acute and chronic wound infections: Microbiological, immunological, clinical and therapeutic distinctions. *Journal of Wound Care*, *31*(5), 436–445. https://doi.org/10.12968/jowc.2022.31.5.436

Hutchings, M. I., Truman, A. W., & Wilkinson, B. (2019). Antibiotics: Past, present and future. *Current Opinion in Microbiology*, *51*, 72–80. https://doi.org/10.1016/j.mib.2019.10.008

Ikuta, K. S., Swetschinski, L. R., Robles Aguilar, G., Sharara, F., Mestrovic, T., Gray, A. P., Davis Weaver, N., Wool, E. E., Han, C., Gershberg Hayoon, A., Aali, A., Abate, S. M., Abbasi-Kangevari, M., Abbasi-Kangevari, Z., Abd-Elsalam, S., Abebe, G., Abedi, A., Abhari, A. P., Abidi, H., … Naghavi, M. (2022). Global mortality associated with 33 bacterial pathogens in 2019: A systematic analysis for the Global Burden of Disease Study 2019. *The Lancet*, *400*(10369), 2221–2248. https://doi.org/10.1016/S0140-6736(22)02185-7

Janakiraman, A., & Lesser, C. F. (2017). How to manage stress: Lessons from an intracellular pathogen. *Virulence*, *8*(4), 359–361. https://doi.org/10.1080/21505594.2016.1256538

Jo, E.-K., Kim, J. K., Shin, D.-M., & Sasakawa, C. (2016). Molecular mechanisms regulating NLRP3 inflammasome activation. *Cellular & Molecular Immunology*, *13*(2), 148–159. https://doi.org/10.1038/cmi.2015.95

Jones, S., & Portnoy, D. A. (1994). Characterization of Listeria monocytogenes pathogenesis in a strain expressing perfringolysin O in place of listeriolysin O. *Infection and Immunity*, *62*(12), 5608–5613. https://doi.org/10.1128/iai.62.12.5608-5613.1994

Jumper, J., Evans, R., Pritzel, A., Green, T., Figurnov, M., Ronneberger, O., Tunyasuvunakool, K., Bates, R., Žídek, A., Potapenko, A., Bridgland, A., Meyer, C., Kohl, S. A. A., Ballard, A. J., Cowie, A., Romera-Paredes, B., Nikolov, S., Jain, R., Adler, J., … Hassabis, D. (2021). Highly accurate protein structure prediction with AlphaFold. *Nature*, *596*(7873), 583–589. https://doi.org/10.1038/s41586-021-03819-2

Kaiser, P., Slack, E., Grant, A. J., Hardt, W.-D., & Regoes, R. R. (2013). Lymph Node Colonization Dynamics after Oral Salmonella Typhimurium Infection in Mice. *PLoS Pathogens*, *9*(9), e1003532. https://doi.org/10.1371/journal.ppat.1003532

Kanther, M., Sun, X., Mühlbauer, M., Mackey, L. C., Flynn, E. J., Bagnat, M., Jobin, C., & Rawls, J. F. (2011). Microbial Colonization Induces Dynamic Temporal and Spatial Patterns of NF-κB Activation in the Zebrafish Digestive Tract. *Gastroenterology*, *141*(1), 197–207. https://doi.org/10.1053/j.gastro.2011.03.042

Karimova, G., Gauliard, E., Davi, M., Ouellette, S. P., & Ladant, D. (2017). Protein–Protein Interaction: Bacterial Two-Hybrid. In L. Journet & E. Cascales (Eds.), *Bacterial Protein Secretion Systems* (Vol. 1615, pp. 159–176). Springer New York. https://doi.org/10.1007/978-1-4939-7033-9_13

Kelliher, J. L., Grunenwald, C. M., Abrahams, R. R., Daanen, M. E., Lew, C. I., Rose, W. E., & Sauer, J.-D. (2021). PASTA kinase-dependent control of peptidoglycan synthesis via ReoM is required for cell wall stress responses, cytosolic survival, and virulence in Listeria monocytogenes. *PLOS Pathogens*, *17*(10), e1009881. https://doi.org/10.1371/journal.ppat.1009881

Kim, S., Bauernfeind, F., Ablasser, A., Hartmann, G., Fitzgerald, K. A., Latz, E., & Hornung, V. (2010). *Listeria monocytogenes* is sensed by the NLRP3 and AIM2 inflammasome. *European Journal of Immunology*, *40*(6), 1545–1551. https://doi.org/10.1002/eji.201040425

Kobayashi, K. S., Chamaillard, M., Ogura, Y., Henegariu, O., Inohara, N., Nuñez, G., & Flavell, R. A. (2005). Nod2-Dependent Regulation of Innate and Adaptive Immunity in the Intestinal Tract. *Science*, *307*(5710), 731–734. https://doi.org/10.1126/science.1104911

Kocks, C., Gouin, E., Tabouret, M., Berche, P., Ohayon, H., & Cossart, P. (1992). L. monocytogenes-induced actin assembly requires the actA gene product, a surface protein. *Cell*, *68*(3), 521–531. https://doi.org/10.1016/0092-8674(92)90188-I

Kraemer, P. S., Mitchell, A., Pelletier, M. R., Gallagher, L. A., Wasnick, M., Rohmer, L., Brittnacher, M. J., Manoil, C., Skerett, S. J., & Salama, N. R. (2009). Genome-Wide Screen in *Francisella novicida* for Genes Required for Pulmonary and Systemic Infection in Mice. *Infection and Immunity*, *77*(1), 232–244. https://doi.org/10.1128/IAI.00978-08

Krypotou, E., Scortti, M., Grundström, C., Oelker, M., Luisi, B. F., Sauer-Eriksson, A. E., & Vázquez-Boland, J. (2019). Control of Bacterial Virulence through the Peptide Signature of the Habitat. *Cell Reports*, *26*(7), 1815-1827.e5. https://doi.org/10.1016/j.celrep.2019.01.073

Lam, S. H., Chua, H. L., Gong, Z., Lam, T. J., & Sin, Y. M. (2004). Development and maturation of the immune system in zebrafish, Danio rerio: A gene expression profiling, in situ hybridization and immunological study. *Developmental & Comparative Immunology*, *28*(1), 9–28. https://doi.org/10.1016/S0145-305X(03)00103-4

Lamason, R. L., & Welch, M. D. (2017). Actin-based motility and cell-to-cell spread of bacterial pathogens. *Current Opinion in Microbiology*, *35*, 48–57. https://doi.org/10.1016/j.mib.2016.11.007

Lampropoulou, V., Sergushichev, A., Bambouskova, M., Nair, S., Vincent, E. E., Loginicheva, E., Cervantes-Barragan, L., Ma, X., Huang, S. C.-C., Griss, T., Weinheimer, C. J., Khader, S., Randolph, G. J., Pearce, E. J., Jones, R. G., Diwan, A., Diamond, M. S., & Artyomov, M. N. (2016). Itaconate Links Inhibition of Succinate Dehydrogenase with Macrophage Metabolic Remodeling and Regulation of Inflammation. *Cell Metabolism*, *24*(1), 158–166. https://doi.org/10.1016/j.cmet.2016.06.004

Lauer, P., Chow, M. Y. N., Loessner, M. J., Portnoy, D. A., & Calendar, R. (2002). Construction, Characterization, and Use of Two *Listeria monocytogenes* Site-Specific Phage Integration Vectors. *Journal of Bacteriology*, *184*(15), 4177–4186. https://doi.org/10.1128/JB.184.15.4177-4186.2002

Leaper, D., Assadian, O., & Edmiston, C. E. (2015). Approach to chronic wound infections. *British Journal of Dermatology*, *173*(2), 351–358. https://doi.org/10.1111/bjd.13677

LeBert, D., Squirrell, J. M., Freisinger, C., Rindy, J., Golenberg, N., Frecentese, G., Gibson, A., Eliceiri, K. W., & Huttenlocher, A. (2018). Damage-induced reactive oxygen species regulate vimentin and dynamic collagen-based projections to mediate wound repair. *eLife*, *7*, e30703. https://doi.org/10.7554/eLife.30703

Lee, M. H., Nuccio, S.-P., & Raffatellu, M. (2020). Pathogen Interference: Targeting Virulence Factors to Tackle Intracellular Microbes. *Cell Chemical Biology*, *27*(7), 765–767. https://doi.org/10.1016/j.chembiol.2020.06.017

Lenz, L. L., Mohammadi, S., Geissler, A., & Portnoy, D. A. (2003). SecA2-dependent secretion of autolytic enzymes promotes *Listeria monocytogenes* pathogenesis. *Proceedings of the National Academy of Sciences*, *100*(21), 12432–12437. https://doi.org/10.1073/pnas.2133653100

Li, B., & Dewey, C. N. (2011). RSEM: Accurate transcript quantification from RNA-Seq data with or without a reference genome. *BMC Bioinformatics*, *12*(1), 323. https://doi.org/10.1186/1471-2105-12-323

Li, D., & Wu, M. (2021). Pattern recognition receptors in health and diseases. *Signal Transduction and Targeted Therapy*, *6*(1), 291. https://doi.org/10.1038/s41392-021-00687-0

Li, X., Wang, T., Tao, Y., Wang, X., Li, L., & Liu, J. (2022). MF-094, a potent and selective USP30 inhibitor, accelerates diabetic wound healing by inhibiting the NLRP3 inflammasome. *Experimental Cell Research*, *410*(2), 112967. https://doi.org/10.1016/j.yexcr.2021.112967

Liu, Y.-F., Ni, P.-W., Huang, Y., & Xie, T. (2022). Therapeutic strategies for chronic wound infection. *Chinese Journal of Traumatology*, *25*(1), 11–16. https://doi.org/10.1016/j.cjtee.2021.07.004

López-Muñoz, A., Sepulcre, M. P., Roca, F. J., Figueras, A., Meseguer, J., & Mulero, V. (2011). Evolutionary conserved pro-inflammatory and antigen presentation functions of zebrafish

IFNγ revealed by transcriptomic and functional analysis. *Molecular Immunology*, *48*(9–10), 1073–1083. https://doi.org/10.1016/j.molimm.2011.01.015

Love, M. I., Huber, W., & Anders, S. (2014). Moderated estimation of fold change and dispersion for RNA-seq data with DESeq2. *Genome Biology*, *15*(12), 550. https://doi.org/10.1186/s13059-014-0550-8

Maassen, S., Coenen, B., Ioannidis, M., Harber, K., Grijpstra, P., Van Den Bossche, J., & Van Den Bogaart, G. (2023). Itaconate promotes a wound resolving phenotype in pro-inflammatory macrophages. *Redox Biology*, *59*, 102591. https://doi.org/10.1016/j.redox.2022.102591

Mariathasan, S., Weiss, D. S., Newton, K., McBride, J., O'Rourke, K., Roose-Girma, M., Lee, W. P., Weinrauch, Y., Monack, D. M., & Dixit, V. M. (2006). Cryopyrin activates the inflammasome in response to toxins and ATP. *Nature*, *440*(7081), 228–232. https://doi.org/10.1038/nature04515

Marjoram, L., Alvers, A., Deerhake, M. E., Bagwell, J., Mankiewicz, J., Cocchiaro, J. L., Beerman, R. W., Willer, J., Sumigray, K. D., Katsanis, N., Tobin, D. M., Rawls, J. F., Goll, M. G., & Bagnat, M. (2015). Epigenetic control of intestinal barrier function and inflammation in zebrafish. *Proceedings of the National Academy of Sciences*, *112*(9), 2770–2775. https://doi.org/10.1073/pnas.1424089112

Mathias, J. R., Perrin, B. J., Liu, T.-X., Kanki, J., Look, A. T., & Huttenlocher, A. (2006). Resolution of inflammation by retrograde chemotaxis of neutrophils in transgenic zebrafish. *Journal of Leukocyte Biology*, *80*(6), 1281–1288. https://doi.org/10.1189/jlb.0506346

McGuffey, J. C., Jackson-Litteken, C. D., Di Venanzio, G., Zimmer, A. A., Lewis, J. M., Distel, J. S., Kim, K. Q., Zaher, H. S., Alfonzo, J., Scott, N. E., & Feldman, M. F. (2023). The tRNA methyltransferase TrmB is critical for *Acinetobacter baumannii* stress responses and pulmonary infection. *mBio*, *14*(5), e01416-23. https://doi.org/10.1128/mbio.01416-23

Meeker, N. D., & Trede, N. S. (2008). Immunology and zebrafish: Spawning new models of human disease. *Developmental & Comparative Immunology*, *32*(7), 745–757. https://doi.org/10.1016/j.dci.2007.11.011

Meixenberger, K., Pache, F., Eitel, J., Schmeck, B., Hippenstiel, S., Slevogt, H., N'Guessan, P., Witzenrath, M., Netea, M. G., Chakraborty, T., Suttorp, N., & Opitz, B. (2010). *Listeria monocytogenes* -Infected Human Peripheral Blood Mononuclear Cells Produce IL-1β, Depending on Listeriolysin O and NLRP3. *The Journal of Immunology*, *184*(2), 922–930. https://doi.org/10.4049/jimmunol.0901346

Mengaud, J., Ohayon, H., Gounon, P., Mège, R.-M., & Cossart, P. (1996). E-Cadherin Is the Receptor for Internalin, a Surface Protein Required for Entry of L. monocytogenes into Epithelial Cells. *Cell*, *84*(6), 923–932. https://doi.org/10.1016/S0092-8674(00)81070-3

Mirhaj, M., Labbaf, S., Tavakoli, M., & Seifalian, A. (2022). An Overview on the Recent Advances in the Treatment of Infected Wounds: Antibacterial Wound Dressings. *Macromolecular Bioscience*, *22*(7), 2200014. https://doi.org/10.1002/mabi.202200014

Mirza, R. E., Fang, M. M., Ennis, W. J., & Koh, T. J. (2013). Blocking Interleukin-1β Induces a Healing-Associated Wound Macrophage Phenotype and Improves Healing in Type 2 Diabetes. *Diabetes*, *62*(7), 2579–2587. https://doi.org/10.2337/db12-1450

Mirza, R. E., Fang, M. M., Weinheimer-Haus, E. M., Ennis, W. J., & Koh, T. J. (2014). Sustained Inflammasome Activity in Macrophages Impairs Wound Healing in Type 2

Diabetic Humans and Mice. *Diabetes*, *63*(3), 1103–1114. https://doi.org/10.2337/db13-0927

Miskolci, V., Squirrell, J., Rindy, J., Vincent, W., Sauer, J. D., Gibson, A., Eliceiri, K. W., & Huttenlocher, A. (2019). Distinct inflammatory and wound healing responses to complex caudal fin injuries of larval zebrafish. *eLife*, *8*, e45976. https://doi.org/10.7554/eLife.45976

Miskolci, V., Tweed, K. E., Lasarev, M. R., Britt, E. C., Walsh, A. J., Zimmerman, L. J., McDougal, C. E., Cronan, M. R., Fan, J., Sauer, J.-D., Skala, M. C., & Huttenlocher, A. (2022). In vivo fluorescence lifetime imaging of macrophage intracellular metabolism during wound responses in zebrafish. *eLife*, *11*, e66080. https://doi.org/10.7554/eLife.66080

Mogensen, T. H. (2009). Pathogen Recognition and Inflammatory Signaling in Innate Immune Defenses. *Clinical Microbiology Reviews*, *22*(2), 240–273. https://doi.org/10.1128/CMR.00046-08

Monk, I. R., Gahan, C. G. M., & Hill, C. (2008). Tools for Functional Postgenomic Analysis of *Listeria monocytogenes*. *Applied and Environmental Microbiology*, *74*(13), 3921–3934. https://doi.org/10.1128/AEM.00314-08

Mostowy, S., Boucontet, L., Mazon Moya, M. J., Sirianni, A., Boudinot, P., Hollinshead, M., Cossart, P., Herbomel, P., Levraud, J.-P., & Colucci-Guyon, E. (2013). The Zebrafish as a New Model for the In Vivo Study of Shigella flexneri Interaction with Phagocytes and Bacterial Autophagy. *PLoS Pathogens*, *9*(9), e1003588. https://doi.org/10.1371/journal.ppat.1003588

Müller-Herbst, S., Wüstner, S., Mühlig, A., Eder, D., M Fuchs, T., Held, C., Ehrenreich, A., & Scherer, S. (2014). Identification of genes essential for anaerobic growth of Listeria monocytogenes. *Microbiology (Reading, England)*, *160*(Pt 4), 752–765. https://doi.org/10.1099/mic.0.075242-0

Murao, A., Aziz, M., Wang, H., Brenner, M., & Wang, P. (2021). Release mechanisms of major DAMPs. *Apoptosis*, *26*(3–4), 152–162. https://doi.org/10.1007/s10495-021-01663-3

Nair, S., Huynh, J. P., Lampropoulou, V., Loginicheva, E., Esaulova, E., Gounder, A. P., Boon, A. C. M., Schwarzkopf, E. A., Bradstreet, T. R., Edelson, B. T., Artyomov, M. N., Stallings, C. L., & Diamond, M. S. (2018). *Irg1* expression in myeloid cells prevents immunopathology during *M. tuberculosis* infection. *Journal of Experimental Medicine*, *215*(4), 1035–1045. https://doi.org/10.1084/jem.20180118

Naomi, R., Bahari, H., Yazid, M. D., Embong, H., & Othman, F. (2021). Zebrafish as a Model System to Study the Mechanism of Cutaneous Wound Healing and Drug Discovery: Advantages and Challenges. *Pharmaceuticals*, *14*(10), 1058. https://doi.org/10.3390/ph14101058

Nasreen, M., Nair, R. P., McEwan, A. G., & Kappler, U. (2022). The Peptide Methionine Sulfoxide Reductase (MsrAB) of Haemophilus influenzae Repairs Oxidatively Damaged Outer Membrane and Periplasmic Proteins Involved in Nutrient Acquisition and Virulence. *Antioxidants*, *11*(8), 1557. https://doi.org/10.3390/antiox11081557

Nawrocki, K., Crispell, E., & McBride, S. (2014). Antimicrobial Peptide Resistance Mechanisms of Gram-Positive Bacteria. *Antibiotics*, *3*(4), 461–492. https://doi.org/10.3390/antibiotics3040461

Negut, I., Grumezescu, V., & Grumezescu, A. M. (2018). Treatment Strategies for Infected Wounds. *Molecules*, *23*(9), 2392. https://doi.org/10.3390/molecules23092392

Nguyen, A. V., & Soulika, A. M. (2019). The Dynamics of the Skin's Immune System. *International Journal of Molecular Sciences*, *20*(8), 1811. https://doi.org/10.3390/ijms20081811

Nguyen-Chi, M., Laplace-Builhe, B., Travnickova, J., Luz-Crawford, P., Tejedor, G., Phan, Q. T., Duroux-Richard, I., Levraud, J.-P., Kissa, K., Lutfalla, G., Jorgensen, C., & Djouad, F. (2015). Identification of polarized macrophage subsets in zebrafish. *eLife*, *4*, e07288. https://doi.org/10.7554/eLife.07288

Opitz, B., Eitel, J., Meixenberger, K., & Suttorp, N. (2009). Role of Toll-like receptors, NOD-like receptors and RIG-I-like receptors in endothelial cells and systemic infections. *Thrombosis and Haemostasis*, *102*(12), 1103–1109. https://doi.org/10.1160/TH09-05-0323

Orazi, G., & O'Toole, G. A. (2019). "It Takes a Village": Mechanisms Underlying Antimicrobial Recalcitrance of Polymicrobial Biofilms. *Journal of Bacteriology*, *202*(1). https://doi.org/10.1128/JB.00530-19

Otoupal, P. B., Eller, K. A., Erickson, K. E., Campos, J., Aunins, T. R., & Chatterjee, A. (2021). Potentiating antibiotic efficacy via perturbation of non-essential gene expression. *Communications Biology*, *4*(1), 1267. https://doi.org/10.1038/s42003-021-02783-x

Ovington, L. (2003). Bacterial toxins and wound healing. *Ostomy/Wound Management*, *49*(7A Suppl), 8–12.

Özören, N., Masumoto, J., Franchi, L., Kanneganti, T.-D., Body-Malapel, M., Ertürk, İ., Jagirdar, R., Zhu, L., Inohara, N., Bertin, J., Coyle, A., Grant, E. P., & Núñez, G. (2006).

Distinct Roles of TLR2 and the Adaptor ASC in IL-1β/IL-18 Secretion in Response to *Listeria monocytogenes*. *The Journal of Immunology*, *176*(7), 4337–4342. https://doi.org/10.4049/jimmunol.176.7.4337

Paciello, I., Silipo, A., Lembo-Fazio, L., Curcurù, L., Zumsteg, A., Noël, G., Ciancarella, V., Sturiale, L., Molinaro, A., & Bernardini, M. L. (2013). Intracellular *Shigella* remodels its LPS to dampen the innate immune recognition and evade inflammasome activation. *Proceedings of the National Academy of Sciences*, *110*(46). https://doi.org/10.1073/pnas.1303641110

Park, S. F., & Stewart, G. S. A. B. (1990). High-efficiency transformation of Listeria monocytogenes by electroporation of penicillin-treated cells. *Gene*, *94*(1), 129–132. https://doi.org/10.1016/0378-1119(90)90479-B

Peace, C. G., & O'Neill, L. A. J. (2022). The role of itaconate in host defense and inflammation. *Journal of Clinical Investigation*, *132*(2), e148548. https://doi.org/10.1172/JCI148548

Pensinger, D. A., Gutierrez, K. V., Smith, H. B., Vincent, W. J. B., Stevenson, D. S., Black, K. A., Perez-Medina, K. M., Dillard, J. P., Rhee, K. Y., Amador-Noguez, D., Huynh, T. N., & Sauer, J.-D. (2023). Listeria monocytogenes GlmR Is an Accessory Uridyltransferase Essential for Cytosolic Survival and Virulence. *mBio*, *14*(2), e00073-23. https://doi.org/10.1128/mbio.00073-23

Poonam, Yennamalli, R. M., Bisht, G. S., & Shrivastava, R. (2019). Ribosomal maturation factor (RimP) is essential for survival of nontuberculous mycobacteria Mycobacterium fortuitum under in vitro acidic stress conditions. *3 Biotech*, *9*(4), 127. https://doi.org/10.1007/s13205-019-1659-y

Portnoy, D. A., Auerbuch, V., & Glomski, I. J. (2002). The cell biology of *Listeria monocytogenes* infection. *The Journal of Cell Biology*, *158*(3), 409–414. https://doi.org/10.1083/jcb.200205009

Portnoy, D. A., Jacks, P. S., & Hinrichs, D. J. (1988). Role of hemolysin for the intracellular growth of Listeria monocytogenes. *The Journal of Experimental Medicine*, *167*(4), 1459–1471. https://doi.org/10.1084/jem.167.4.1459

Puca, V., Marulli, R. Z., Grande, R., Vitale, I., Niro, A., Molinaro, G., Prezioso, S., Muraro, R., & Di Giovanni, P. (2021). Microbial Species Isolated from Infected Wounds and Antimicrobial Resistance Analysis: Data Emerging from a Three-Years Retrospective Study. *Antibiotics*, *10*(10), 1162. https://doi.org/10.3390/antibiotics10101162

Rădulescu, M., Holban, A., Mogoantă, L., Bălşeanu, T.-A., Mogoșanu, G., Savu, D., Popescu, R., Fufă, O., Grumezescu, A., Bezirtzoglou, E., Lazar, V., & Chifiriuc, M. (2016). Fabrication, Characterization, and Evaluation of Bionanocomposites Based on Natural Polymers and Antibiotics for Wound Healing Applications. *Molecules*, *21*(6), 761. https://doi.org/10.3390/molecules21060761

Ray, K., Marteyn, B., Sansonetti, P. J., & Tang, C. M. (2009). Life on the inside: The intracellular lifestyle of cytosolic bacteria. *Nature Reviews Microbiology*, *7*(5), 333–340. https://doi.org/10.1038/nrmicro2112

Rea, R. B., Gahan, C. G. M., & Hill, C. (2004). Disruption of Putative Regulatory Loci in *Listeria monocytogenes* Demonstrates a Significant Role for Fur and PerR in Virulence. *Infection and Immunity*, *72*(2), 717–727. https://doi.org/10.1128/IAI.72.2.717-727.2004

Rea, R., Hill, C., & Gahan, C. G. M. (2005). *Listeria monocytogenes* PerR Mutants Display a Small-Colony Phenotype, Increased Sensitivity to Hydrogen Peroxide, and Significantly

Reduced Murine Virulence. *Applied and Environmental Microbiology*, *71*(12), 8314–8322. https://doi.org/10.1128/AEM.71.12.8314-8322.2005

Reed, S. C. O., Lamason, R. L., Risca, V. I., Abernathy, E., & Welch, M. D. (2014). Rickettsia Actin-Based Motility Occurs in Distinct Phases Mediated by Different Actin Nucleators. *Current Biology*, *24*(1), 98–103. https://doi.org/10.1016/j.cub.2013.11.025

Reniere, M. L., Whiteley, A. T., Hamilton, K. L., John, S. M., Lauer, P., Brennan, R. G., & Portnoy, D. A. (2015). Glutathione activates virulence gene expression of an intracellular pathogen. *Nature*, *517*(7533), 170–173. https://doi.org/10.1038/nature14029

Ribet, D., & Cossart, P. (2015). How bacterial pathogens colonize their hosts and invade deeper tissues. *Microbes and Infection*, *17*(3), 173–183. https://doi.org/10.1016/j.micinf.2015.01.004

Richardson, R. J. (2018). Parallels between vertebrate cardiac and cutaneous wound healing and regeneration. *Npj Regenerative Medicine*, *3*(1), 21. https://doi.org/10.1038/s41536-018-0059-y

Riquelme, S. A., Liimatta, K., Wong Fok Lung, T., Fields, B., Ahn, D., Chen, D., Lozano, C., Sáenz, Y., Uhlemann, A.-C., Kahl, B. C., Britto, C. J., DiMango, E., & Prince, A. (2020). Pseudomonas aeruginosa Utilizes Host-Derived Itaconate to Redirect Its Metabolism to Promote Biofilm Formation. *Cell Metabolism*, *31*(6), 1091-1106.e6. https://doi.org/10.1016/j.cmet.2020.04.017

Riquelme, S. A., Lozano, C., Moustafa, A. M., Liimatta, K., Tomlinson, K. L., Britto, C., Khanal, S., Gill, S. K., Narechania, A., Azcona-Gutiérrez, J. M., DiMango, E., Saénz, Y., Planet, P., & Prince, A. (2019). CFTR-PTEN–dependent mitochondrial metabolic

dysfunction promotes *Pseudomonas aeruginosa* airway infection. *Science Translational Medicine*, *11*(499), eaav4634. https://doi.org/10.1126/scitranslmed.aav4634

Rivera-Lugo, R., Deng, D., Anaya-Sanchez, A., Tejedor-Sanz, S., Tang, E., Reyes Ruiz, V. M., Smith, H. B., Titov, D. V., Sauer, J.-D., Skaar, E. P., Ajo-Franklin, C. M., Portnoy, D. A., & Light, S. H. (2022). Listeria monocytogenes requires cellular respiration for NAD+ regeneration and pathogenesis. *eLife*, *11*, e75424. https://doi.org/10.7554/eLife.75424

Ruetz, M., Campanello, G. C., Purchal, M., Shen, H., McDevitt, L., Gouda, H., Wakabayashi, S., Zhu, J., Rubin, E. J., Warncke, K., Mootha, V. K., Koutmos, M., & Banerjee, R. (2019). Itaconyl-CoA forms a stable biradical in methylmalonyl-CoA mutase and derails its activity and repair. *Science*, *366*(6465), 589–593. https://doi.org/10.1126/science.aay0934

Sanderson, L. E., Chien, A.-T., Astin, J. W., Crosier, K. E., Crosier, P. S., & Hall, C. J. (2015). An inducible transgene reports activation of macrophages in live zebrafish larvae. *Developmental & Comparative Immunology*, *53*(1), 63–69. https://doi.org/10.1016/j.dci.2015.06.013

Sariol, A., & Perlman, S. (2021). SARS-CoV-2 takes its Toll. *Nature Immunology*, *22*(7), 801–802. https://doi.org/10.1038/s41590-021-00962-w

Sassetti, C. M., Boyd, D. H., & Rubin, E. J. (2001). Comprehensive identification of conditionally essential genes in mycobacteria. *Proceedings of the National Academy of Sciences*, *98*(22), 12712–12717. https://doi.org/10.1073/pnas.231275498

Sauer, J.-D., Pereyre, S., Archer, K. A., Burke, T. P., Hanson, B., Lauer, P., & Portnoy, D. A. (2011). *Listeria monocytogenes* engineered to activate the Nlrc4 inflammasome are severely attenuated and are poor inducers of protective immunity. *Proceedings of the*

National Academy of Sciences, *108*(30), 12419–12424. https://doi.org/10.1073/pnas.1019041108

Sauer, J.-D., Sotelo-Troha, K., Von Moltke, J., Monroe, K. M., Rae, C. S., Brubaker, S. W., Hyodo, M., Hayakawa, Y., Woodward, J. J., Portnoy, D. A., & Vance, R. E. (2011). The *N* -Ethyl- *N* -Nitrosourea-Induced *Goldenticket* Mouse Mutant Reveals an Essential Function of *Sting* in the *In Vivo* Interferon Response to *Listeria monocytogenes* and Cyclic Dinucleotides. *Infection and Immunity*, *79*(2), 688–694. https://doi.org/10.1128/IAI.00999-10

Sauer, J.-D., Witte, C. E., Zemansky, J., Hanson, B., Lauer, P., & Portnoy, D. A. (2010). Listeria monocytogenes Triggers AIM2-Mediated Pyroptosis upon Infrequent Bacteriolysis in the Macrophage Cytosol. *Cell Host & Microbe*, *7*(5), 412–419. https://doi.org/10.1016/j.chom.2010.04.004

Schauer, K., Geginat, G., Liang, C., Goebel, W., Dandekar, T., & Fuchs, T. M. (2010). Deciphering the intracellular metabolism of Listeria monocytogenes by mutant screening and modelling. *BMC Genomics*, *11*(1), 573. https://doi.org/10.1186/1471-2164-11-573

Schindelin, J., Arganda-Carreras, I., Frise, E., Kaynig, V., Longair, M., Pietzsch, T., Preibisch, S., Rueden, C., Saalfeld, S., Schmid, B., Tinevez, J.-Y., White, D. J., Hartenstein, V., Eliceiri, K., Tomancak, P., & Cardona, A. (2012). Fiji: An open-source platform for biological-image analysis. *Nature Methods*, *9*(7), 676–682. https://doi.org/10.1038/nmeth.2019

Schnupf, P., & Portnoy, D. A. (2007). Listeriolysin O: A phagosome-specific lysin. *Microbes and Infection*, *9*(10), 1176–1187. https://doi.org/10.1016/j.micinf.2007.05.005

Schoen, T. J., Rosowski, E. E., Knox, B. P., Bennin, D., Keller, N. P., & Huttenlocher, A. (2020). Neutrophil phagocyte oxidase activity controls invasive fungal growth and inflammation in zebrafish. *Journal of Cell Science*, *133*(5), jcs236539. https://doi.org/10.1242/jcs.236539

Seidelman, J., & Anderson, D. J. (2021). Surgical Site Infections. *Infectious Disease Clinics of North America*, *35*(4), 901–929. https://doi.org/10.1016/j.idc.2021.07.006

Shen, S., Miskolci, V., Dewey, C. N., Sauer, J.-D., & Huttenlocher, A. (2024). Infection induced inflammation impairs wound healing through IL-1β signaling. *iScience*, *27*(4), 109532. https://doi.org/10.1016/j.isci.2024.109532

Shen, Y., Naujokas, M., Park, M., & Ireton, K. (2000). InlB-Dependent Internalization of Listeria Is Mediated by the Met Receptor Tyrosine Kinase. *Cell*, *103*(3), 501–510. https://doi.org/10.1016/S0092-8674(00)00141-0

Shi, D., Mi, G., Wang, M., & Webster, T. J. (2019). In vitro and ex vivo systems at the forefront of infection modeling and drug discovery. *Biomaterials*, *198*, 228–249. https://doi.org/10.1016/j.biomaterials.2018.10.030

Shiau, C. E., Kaufman, Z., Meireles, A. M., & Talbot, W. S. (2015). Differential Requirement for irf8 in Formation of Embryonic and Adult Macrophages in Zebrafish. *PLOS ONE*, *10*(1), e0117513. https://doi.org/10.1371/journal.pone.0117513

Shumba, P., Mairpady Shambat, S., & Siemens, N. (2019). The Role of Streptococcal and Staphylococcal Exotoxins and Proteases in Human Necrotizing Soft Tissue Infections. *Toxins*, *11*(6), 332. https://doi.org/10.3390/toxins11060332

Singh, V. K., Singh, K., & Baum, K. (2018). The Role of Methionine Sulfoxide Reductases in Oxidative Stress Tolerance and Virulence of Staphylococcus aureus and Other Bacteria. *Antioxidants*, *7*(10), 128. https://doi.org/10.3390/antiox7100128

Smith, G. A., Marquis, H., Jones, S., Johnston, N. C., Portnoy, D. A., & Goldfine, H. (1995). The two distinct phospholipases C of Listeria monocytogenes have overlapping roles in escape from a vacuole and cell-to-cell spread. *Infection and Immunity*, *63*(11), 4231–4237. https://doi.org/10.1128/iai.63.11.4231-4237.1995

Smith, H. B., Lee, K., Freeman, M. J., Stevenson, D. M., Amador-Noguez, D., & Sauer, J.-D. (2023). *Listeria monocytogenes* requires DHNA-dependent intracellular redox homeostasis facilitated by Ndh2 for survival and virulence. *Infection and Immunity*, *91*(10), e00022-23. https://doi.org/10.1128/iai.00022-23

Smith, H. B., Li, T. L., Liao, M. K., Chen, G. Y., Guo, Z., & Sauer, J.-D. (2021). Listeria monocytogenes MenI Encodes a DHNA-CoA Thioesterase Necessary for Menaquinone Biosynthesis, Cytosolic Survival, and Virulence. *Infection and Immunity*, *89*(5), e00792-20. https://doi.org/10.1128/IAI.00792-20

Solaimanpour, S., Sarmiento, F., & Mrázek, J. (2015). Tn-Seq Explorer: A Tool for Analysis of High-Throughput Sequencing Data of Transposon Mutant Libraries. *PLOS ONE*, *10*(5), e0126070. https://doi.org/10.1371/journal.pone.0126070

Srinon, V., Chaiwattanarungruengpaisan, S., Korbsrisate, S., & Stevens, J. M. (2019). Burkholderia pseudomallei BimC Is Required for Actin-Based Motility, Intracellular Survival, and Virulence. *Frontiers in Cellular and Infection Microbiology*, *9*, 63. https://doi.org/10.3389/fcimb.2019.00063

Stamm, C. E., McFarland, A. P., Locke, M. N., Tabakh, H., Tang, Q., Thomason, M. K., & Woodward, J. J. (2024). *RECON gene disruption enhances host resistance to enable genome-wide evaluation of intracellular pathogen fitness during infection*. https://doi.org/10.1101/2024.01.15.575726

Stein, C., Caccamo, M., Laird, G., & Leptin, M. (2007). Conservation and divergence of gene families encoding components of innate immune response systems in zebrafish. *Genome Biology*, *8*(11), R251. https://doi.org/10.1186/gb-2007-8-11-r251

Stoop, E. J. M., Schipper, T., Rosendahl Huber, S. K., Nezhinsky, A. E., Verbeek, F. J., Gurcha, S. S., Besra, G. S., Vandenbroucke-Grauls, C. M. J. E., Bitter, W., & Van Der Sar, A. M. (2011). Zebrafish embryo screen for mycobacterial genes involved in the initiation of granuloma formation reveals a newly identified ESX-1 component. *Disease Models & Mechanisms*, *4*(4), 526–536. https://doi.org/10.1242/dmm.006676

Stritzker, J., Janda, J., Schoen, C., Taupp, M., Pilgrim, S., Gentschev, I., Schreier, P., Geginat, G., & Goebel, W. (2004). Growth, Virulence, and Immunogenicity of *Listeria monocytogenes aro* Mutants. *Infection and Immunity*, *72*(10), 5622–5629. https://doi.org/10.1128/IAI.72.10.5622-5629.2004

Succoio, M., Sacchettini, R., Rossi, A., Parenti, G., & Ruoppolo, M. (2022). Galactosemia: Biochemistry, Molecular Genetics, Newborn Screening, and Treatment. *Biomolecules*, *12*(7), 968. https://doi.org/10.3390/biom12070968

Szurmant, H., Mohan, M. A., Imus, P. M., & Hoch, J. A. (2007). YycH and YycI Interact To Regulate the Essential YycFG Two-Component System in *Bacillus subtilis*. *Journal of Bacteriology, 189*(8), 3280–3289. https://doi.org/10.1128/JB.01936-06

Takeuchi, O., & Akira, S. (2010). Pattern Recognition Receptors and Inflammation. *Cell*, *140*(6), 805–820. https://doi.org/10.1016/j.cell.2010.01.022

Tan, J. L., Lash, B., Karami, R., Nayer, B., Lu, Y.-Z., Piotto, C., Julier, Z., & Martino, M. M. (2021). Restoration of the healing microenvironment in diabetic wounds with matrix-binding IL-1 receptor antagonist. *Communications Biology*, *4*(1), 422. https://doi.org/10.1038/s42003-021-01913-9

Teame, T., Zhang, Z., Ran, C., Zhang, H., Yang, Y., Ding, Q., Xie, M., Gao, C., Ye, Y., Duan, M., & Zhou, Z. (2019). The use of zebrafish (Danio rerio) as biomedical models. *Animal Frontiers*, *9*(3), 68–77. https://doi.org/10.1093/af/vfz020

The Galaxy Community, Afgan, E., Nekrutenko, A., Grüning, B. A., Blankenberg, D., Goecks, J., Schatz, M. C., Ostrovsky, A. E., Mahmoud, A., Lonie, A. J., Syme, A., Fouilloux, A., Bretaudeau, A., Nekrutenko, A., Kumar, A., Eschenlauer, A. C., DeSanto, A. D., Guerler, A., Serrano-Solano, B., … Briggs, P. J. (2022). The Galaxy platform for accessible, reproducible and collaborative biomedical analyses: 2022 update. *Nucleic Acids Research*, *50*(W1), W345–W351. https://doi.org/10.1093/nar/gkac247

Theisen, E., & Sauer, J.-D. (2016). Listeria monocytogenes and the Inflammasome: From Cytosolic Bacteriolysis to Tumor Immunotherapy. In S. Backert (Ed.), *Inflammasome Signaling and Bacterial Infections* (Vol. 397, pp. 133–160). Springer International Publishing. https://doi.org/10.1007/978-3-319-41171-2_7

Theisen, E., & Sauer, J.-D. (2017). Listeria monocytogenes-Induced Cell Death Inhibits the Generation of Cell-Mediated Immunity. *Infection and Immunity*, *85*(1), e00733-16. https://doi.org/10.1128/IAI.00733-16

Thongdee, N., Jaroensuk, J., Atichartpongkul, S., Chittrakanwong, J., Chooyoung, K., Srimahaeak, T., Chaiyen, P., Vattanaviboon, P., Mongkolsuk, S., & Fuangthong, M. (2019). TrmB, a tRNA m7G46 methyltransferase, plays a role in hydrogen peroxide resistance and positively modulates the translation of katA and katB mRNAs in Pseudomonas aeruginosa. *Nucleic Acids Research*, *47*(17), 9271–9281. https://doi.org/10.1093/nar/gkz702

Tilney, L. G., & Portnoy, D. A. (1989). Actin filaments and the growth, movement, and spread of the intracellular bacterial parasite, Listeria monocytogenes. *The Journal of Cell Biology*, *109*(4), 1597–1608. https://doi.org/10.1083/jcb.109.4.1597

Tomlinson, K. L., Lung, T. W. F., Dach, F., Annavajhala, M. K., Gabryszewski, S. J., Groves, R. A., Drikic, M., Francoeur, N. J., Sridhar, S. H., Smith, M. L., Khanal, S., Britto, C. J., Sebra, R., Lewis, I., Uhlemann, A.-C., Kahl, B. C., Prince, A. S., & Riquelme, S. A. (2021). Staphylococcus aureus induces an itaconate-dominated immunometabolic response that drives biofilm formation. *Nature Communications*, *12*(1), 1399. https://doi.org/10.1038/s41467-021-21718-y

Tomlinson, K. L., Riquelme, S. A., Baskota, S. U., Drikic, M., Monk, I. R., Stinear, T. P., Lewis, I. A., & Prince, A. S. (2023). Staphylococcus aureus stimulates neutrophil itaconate production that suppresses the oxidative burst. *Cell Reports*, *42*(2), 112064. https://doi.org/10.1016/j.celrep.2023.112064

Torraca, V., & Mostowy, S. (2018). Zebrafish Infection: From Pathogenesis to Cell Biology. *Trends in Cell Biology*, *28*(2), 143–156. https://doi.org/10.1016/j.tcb.2017.10.002

Torres, D., Barrier, M., Bihl, F., Quesniaux, V. J. F., Maillet, I., Akira, S., Ryffel, B., & Erard, F. (2004). Toll-Like Receptor 2 Is Required for Optimal Control of *Listeria monocytogenes*

Infection. *Infection and Immunity*, *72*(4), 2131–2139. https://doi.org/10.1128/IAI.72.4.2131-2139.2004

Tuttle, M. S. (2015). Association Between Microbial Bioburden and Healing Outcomes in Venous Leg Ulcers: A Review of the Evidence. *Advances in Wound Care*, *4*(1), 1–11. https://doi.org/10.1089/wound.2014.0535

Uberoi, A., McCready-Vangi, A., & Grice, E. A. (2024). The wound microbiota: Microbial mechanisms of impaired wound healing and infection. *Nature Reviews Microbiology*. https://doi.org/10.1038/s41579-024-01035-z

Van Avondt, K., Sorge, N. M. V., & Meyaard, L. (2015). Bacterial Immune Evasion through Manipulation of Host Inhibitory Immune Signaling. *PLOS Pathogens*, *11*(3), e1004644. https://doi.org/10.1371/journal.ppat.1004644

Van Der Vaart, M., Spaink, H. P., & Meijer, A. H. (2012). Pathogen Recognition and Activation of the Innate Immune Response in Zebrafish. *Advances in Hematology*, *2012*, 1–19. https://doi.org/10.1155/2012/159807

van der Veen, S., Abee, T., de Vos, W. M., & Wells-Bennik, M. H. J. (2009). Genome-wide screen for Listeria monocytogenes genes important for growth at high temperatures. *FEMS Microbiology Letters*, *295*(2), 195–203. https://doi.org/10.1111/j.1574-6968.2009.01586.x

Varshney, G. K., Sood, R., & Burgess, S. M. (2015). Understanding and Editing the Zebrafish Genome. In *Advances in Genetics* (Vol. 92, pp. 1–52). Elsevier. https://doi.org/10.1016/bs.adgen.2015.09.002

Vázquez-Boland, J. A., Kuhn, M., Berche, P., Chakraborty, T., Domínguez-Bernal, G., Goebel, W., González-Zorn, B., Wehland, J., & Kreft, J. (2001). *Listeria* Pathogenesis and

Molecular Virulence Determinants. *Clinical Microbiology Reviews*, *14*(3), 584–640. https://doi.org/10.1128/CMR.14.3.584-640.2001

Vincent, W. J. B., Freisinger, C. M., Lam, P., Huttenlocher, A., & Sauer, J.-D. (2016). Macrophages mediate flagellin induced inflammasome activation and host defense in zebrafish: Zebrafish inflammasome-mediated immunity. *Cellular Microbiology*, *18*(4), 591–604. https://doi.org/10.1111/cmi.12536

Wall, D. P., Fraser, H. B., & Hirsh, A. E. (2003). Detecting putative orthologs. *Bioinformatics (Oxford, England)*, *19*(13), 1710–1711. https://doi.org/10.1093/bioinformatics/btg213

Wang, J., Hossain, M., Thanabalasuriar, A., Gunzer, M., Meininger, C., & Kubes, P. (2017). Visualizing the function and fate of neutrophils in sterile injury and repair. *Science*, *358*(6359), 111–116. https://doi.org/10.1126/science.aam9690

Wang, Y., Wang, Y., Liu, B., Wang, S., Li, J., Gong, S., Sun, L., & Yi, L. (2019). *Pdh* modulate virulence through reducing stress tolerance and biofilm formation of *Streptococcus suis* serotype 2. *Virulence*, *10*(1), 588–599. https://doi.org/10.1080/21505594.2019.1631661

Warren, S. E., Mao, D. P., Rodriguez, A. E., Miao, E. A., & Aderem, A. (2008). Multiple Nod-Like Receptors Activate Caspase 1 during *Listeria monocytogenes* Infection. *The Journal of Immunology*, *180*(11), 7558–7564. https://doi.org/10.4049/jimmunol.180.11.7558

Way, S. S., Kollmann, T. R., Hajjar, A. M., & Wilson, C. B. (2003). Cutting Edge: Protective Cell-Mediated Immunity to *Listeria monocytogenes* in the Absence of Myeloid Differentiation Factor 88. *The Journal of Immunology*, *171*(2), 533–537. https://doi.org/10.4049/jimmunol.171.2.533

Welch, D. F., Sword, C. P., Brehm, S., & Dusanic, D. (1979). Relationship between superoxide dismutase and pathogenic mechanisms of Listeria monocytogenes. *Infection and Immunity*, *23*(3), 863–872. https://doi.org/10.1128/iai.23.3.863-872.1979

Wiles, T. J., Norton, J. P., Russell, C. W., Dalley, B. K., Fischer, K. F., & Mulvey, M. A. (2013). Combining Quantitative Genetic Footprinting and Trait Enrichment Analysis to Identify Fitness Determinants of a Bacterial Pathogen. *PLoS Genetics*, *9*(8), e1003716. https://doi.org/10.1371/journal.pgen.1003716

Wilson, J. W., Schurr, M. J., LeBlanc, C. L., Ramamurthy, R., Buchanan, K. L., & Nickerson, C. A. (2002). Mechanisms of bacterial pathogenicity. *Postgraduate Medical Journal*, *78*(918), 216–224. https://doi.org/10.1136/pmj.78.918.216

Witte, C. E., Archer, K. A., Rae, C. S., Sauer, J.-D., Woodward, J. J., & Portnoy, D. A. (2012). Innate Immune Pathways Triggered by Listeria monocytogenes and Their Role in the Induction of Cell-Mediated Immunity. In *Advances in Immunology* (Vol. 113, pp. 135–156). Elsevier. https://doi.org/10.1016/B978-0-12-394590-7.00002-6

Woodward, J. J., Iavarone, A. T., & Portnoy, D. A. (2010). C-di-AMP Secreted by Intracellular *Listeria monocytogenes* Activates a Host Type I Interferon Response. *Science*, *328*(5986), 1703–1705. https://doi.org/10.1126/science.1189801

Wu, J., Fernandes-Alnemri, T., & Alnemri, E. S. (2010). Involvement of the AIM2, NLRC4, and NLRP3 Inflammasomes in Caspase-1 Activation by Listeria monocytogenes. *Journal of Clinical Immunology*, *30*(5), 693–702. https://doi.org/10.1007/s10875-010-9425-2

Wu, R., Kang, R., & Tang, D. (2022). Mitochondrial ACOD1/IRG1 in infection and sterile inflammation. *Journal of Intensive Medicine*, *2*(2), 78–88. https://doi.org/10.1016/j.jointm.2022.01.001

Yang, J., Peng, Z., Ji, X., Zhang, J., & Du, G. (2022). Galactitol Transport Factor GatA Relieves ATP Supply Restriction to Enhance Acid Tolerance of Escherichia coli in the Two-Stage Fermentation Production of D-Lactate. *Fermentation*, *8*(12), 665. https://doi.org/10.3390/fermentation8120665

Ye, S., Jiang, L., Wu, J., Su, C., Huang, C., Liu, X., & Shao, W. (2018). Flexible Amoxicillin-Grafted Bacterial Cellulose Sponges for Wound Dressing: In Vitro and in Vivo Evaluation. *ACS Applied Materials & Interfaces*, *10*(6), 5862–5870. https://doi.org/10.1021/acsami.7b16680

Yesilkaya, H., Spissu, F., Carvalho, S. M., Terra, V. S., Homer, K. A., Benisty, R., Porat, N., Neves, A. R., & Andrew, P. W. (2009). Pyruvate Formate Lyase Is Required for Pneumococcal Fermentative Metabolism and Virulence. *Infection and Immunity*, *77*(12), 5418–5427. https://doi.org/10.1128/IAI.00178-09

Zemansky, J., Kline, B. C., Woodward, J. J., Leber, J. H., Marquis, H., & Portnoy, D. A. (2009). Development of a *mariner* -Based Transposon and Identification of *Listeria monocytogenes* Determinants, Including the Peptidyl-Prolyl Isomerase PrsA2, That Contribute to Its Hemolytic Phenotype. *Journal of Bacteriology*, *191*(12), 3950–3964. https://doi.org/10.1128/JB.00016-09

Zhang, T., Abel, S., Abel Zur Wiesch, P., Sasabe, J., Davis, B. M., Higgins, D. E., & Waldor, M. K. (2017). Deciphering the landscape of host barriers to *Listeria monocytogenes* infection. *Proceedings of the National Academy of Sciences*, *114*(24), 6334–6339. https://doi.org/10.1073/pnas.1702077114

Zhao, R., Liang, H., Clarke, E., Jackson, C., & Xue, M. (2016). Inflammation in Chronic Wounds. *International Journal of Molecular Sciences*, *17*(12), 2085. https://doi.org/10.3390/ijms17122085